

Dissecting the Nucleosome: Single-Molecule Studies of Subnucleosomal Structure and Dynamics

Ordu, Orikide

DOI

[10.4233/uuid:c7127c0f-0a4d-4857-a0c2-d99ac839a342](https://doi.org/10.4233/uuid:c7127c0f-0a4d-4857-a0c2-d99ac839a342)

Publication date

2018

Document Version

Final published version

Citation (APA)

Ordu, O. (2018). *Dissecting the Nucleosome: Single-Molecule Studies of Subnucleosomal Structure and Dynamics*. [Dissertation (TU Delft), Delft University of Technology]. <https://doi.org/10.4233/uuid:c7127c0f-0a4d-4857-a0c2-d99ac839a342>

Important note

To cite this publication, please use the final published version (if applicable).
Please check the document version above.

Copyright

Other than for strictly personal use, it is not permitted to download, forward or distribute the text or part of it, without the consent of the author(s) and/or copyright holder(s), unless the work is under an open content license such as Creative Commons.

Takedown policy

Please contact us and provide details if you believe this document breaches copyrights.
We will remove access to the work immediately and investigate your claim.

Dissecting the Nucleosome: Single-Molecule Studies of Subnucleosomal Structure and Dynamics

PROEFSCHRIFT

ter verkrijging van de graad van doctor
aan de Technische Universiteit Delft,
op gezag van de Rector Magnificus prof. dr. ir. T.H.J.J. van der Hagen,
voorzitter van het College voor Promoties,
in het openbaar te verdedigen op
donderdag 27 september 2018 om 12:30 uur

DOOR

Orkide ORDU

Diplom-Physikerin, Karlsruher Institut für Technologie, Duitsland
geboren te Heilbronn-Neckargartach, Duitsland

Dit proefschrift is goedgekeurd door de promotor.

Samenstelling promotiecommissie bestaat uit:

Rector Magnificus	voorzitter
Prof. dr. N.H. Dekker	Technische Universiteit Delft, <i>promotor</i>

Onafhankelijke leden:

Prof. dr. M. Dogterom	Technische Universiteit Delft
Prof. dr. ir. S.J.T. van Noort	Universiteit Leiden
Prof. dr. J. Michaelis	Universität Ulm, Duitsland
Dr. S.M. Depken	Technische Universiteit Delft
Dr. F. Mattioli	Hubrecht Instituut
Prof. dr. B. Rieger	Technische Universiteit Delft, <i>reserve lid</i>

Overig lid:

Dr. A. Lusser	Medizinische Universität Innsbruck, Oostenrijk
---------------	---



Keywords: Single-Molecule Techniques, Magnetic Tweezers, Chromatin, Nucleosomes, Tetrasomes

Printed by: Gildeprint

Cover: Artistic representation of magnetic tweezers dissecting a nucleosome. The protein images were created by modifying the structural data with the identification code 1AOI from the RCSB PDB using PyMOL, Version 1.8 Schrödinger, LLC.

Copyright ©2018 by Orkide Ordu
Casimir PhD series, Delft-Leiden 2018-33
ISBN 978-90-8593-362-5

An electronic version of this dissertation is available at
<http://repository.tudelft.nl/>

To Paul and my parents.

Contents

List of Recurring Abbreviations and Symbols	1
1 Introduction	5
1.1 Nucleosome Structure and Dynamics	6
1.2 Single-Molecule Techniques in Nucleosome Research . . .	7
1.2.1 Fluorescence microscopy and fluorescence spectroscopy	8
1.2.2 Force spectroscopy	11
1.2.3 Atomic force microscopy	13
1.3 This Thesis	15
1.4 References	16
2 Magnetic Tweezers for the Measurement of Twist and Torque	25
2.1 Introduction	26
2.2 Materials and Methods	28
2.2.1 Preparation and incubation of a DNA sample . . .	28
2.2.2 Measurements on single DNA molecules in the conventional MT	31
2.2.3 Measurements of DNA twist using FOMT	32
2.2.4 Measurements of DNA torque using MTT	33
2.3 Representative Results	35
2.4 Discussion	42
2.4.1 Considerations prior to start of FOMT and MTT experiments	42
2.4.2 The alignment of FOMT and MTT experiments .	43
2.4.3 Critical steps and considerations for tracking during FOMT and MTT experiments	45
2.4.4 Significance of the FOMT and MTT approaches compared to existing methods and applications . .	47
2.5 References	47
3 Recent Insights from <i>In Vitro</i> Single-Molecule Studies into Nucleosome Structure and Dynamics	51
3.1 Introduction	52

3.2	Nucleosome Structure and Dynamics	52
3.2.1	Intrinsic nucleosome dynamics	52
3.2.2	The sequence of the nucleosomal DNA	54
3.2.3	Post-translational modification of histones	54
3.2.4	ATP-Dependent remodeling	55
3.2.5	Genome-processing enzymes	56
3.3	Subnucleosomal Structures and Dynamics	57
3.4	The Nucleosome as a Barrier	61
3.5	Conclusions and Future Perspectives	65
3.6	References	67
4	Comparing the Assembly and Handedness Dynamics of (H3.3-H4)₂ Tetrasomes to Canonical Tetrasomes	73
4.1	Introduction	74
4.2	Materials and Methods	77
4.2.1	Single-molecule instrumentation	77
4.2.2	Protein expression and purification	77
4.2.3	Flow cell passivation and buffer conditions	77
4.2.4	DNA constructs	78
4.3	Results and Discussion	78
4.3.1	NAP1-assisted assembly of (H3.3-H4) ₂ tetrasomes	78
4.3.2	Spontaneous changes in the linking number of (H3.3-H4) ₂ tetrasomes	79
4.3.3	Structural transitions within (H3.3-H4) ₂ tetrasomes by minute torques	85
4.4	Discussion and Conclusion	88
4.5	Supplementary Information	90
4.6	References	92
5	Modification of the Histone Tetramer at the H3-H3 Interface Impacts Tetrasome Conformations and Dynamics	95
5.1	Introduction	96
5.2	Materials and Methods	99
5.2.1	Preparation of DNA constructs	99
5.2.2	Protein expression and purification	99
5.2.3	Histone treatment with IA	99
5.2.4	MS analysis of IA-treated histones	100
5.2.5	Tetrasome reconstitution via salt-dialysis	100
5.2.6	Sample preparation for tetrasome assembly in single-molecule experiments	100
5.2.7	MT instrumentation	101

5.2.8	Data analysis	101
5.3	Results	102
5.3.1	NAP1-mediated assembly of IA-treated tetrasomes results in proper complexes	102
5.3.2	IA-treated tetrasomes have reduced tendency to- wards handedness flipping	107
5.3.3	IA-treatment impacts the conformational plasticity of tetrasomes	110
5.4	Discussion and Conclusion	114
5.5	Supplementary Information	118
5.6	References	138
6	Structural Dynamics of Tetrasomes Depend on the Un- derlying DNA Sequence and Ambient Conditions	143
6.1	Introduction	144
6.2	Materials and Methods	145
6.2.1	Preparation of DNA molecules	145
6.2.2	Expression and purification of proteins	146
6.2.3	Preparation of histones and tetrasome assembly . .	146
6.2.4	MT instrumentation	147
6.2.5	Data analysis	147
6.3	Results and Discussion	149
6.3.1	The structural properties of tetrasomes are unaf- fected by the underlying DNA sequence and ambient conditions	149
6.3.2	The kinetics of the flipping in tetrasome handedness are altered by the underlying DNA sequence and ambient conditions	154
6.3.3	The effects of the underlying DNA sequence and ambient conditions is revealed in the energetics of tetrasomes	158
6.4	Conclusion	163
6.5	Supplementary Information	164
6.6	References	188
	Summary	195
	Samenvatting	199
	Acknowledgments	203

Contents

Curriculum Vitae	207
List of Publications	209

List of Recurring Abbreviations and Symbols

Chemical Compounds

ATP	adenosine triphosphate
Tris	tris(hydroxymethyl)aminomethane
EDTA	ethylenediaminetetraacetic acid
HEPES	4-(2-hydroxyethyl)-1-piperazineethanesulfonic acid
PBS	phosphate buffered saline
PEG	polyethylene glycol
PVA	polyvinyl alcohol
IA	iodoacetamide

Biomolecules

DNA	deoxyribonucleic acid
ssDNA	single-stranded DNA
dsDNA	double-stranded DNA
RNA	ribonucleic acid
RNAP	RNA polymerase
BSA	bovine serum albumin
NAP1	nucleosome assembly protein-1
ACF	ATP-dependent chromatin assembly and remodeling factor
ISWI	imitation switch
CAF1	chromatin assembly factor-1
CHD1	chromodomain helicase DNA binding protein-1

Units

m	meter
mm	millimeter (10^{-3} meter)
μm	micrometer (10^{-6} meter)
nm	nanometer (10^{-9} meter)
bp	base pair (~ 0.34 nanometer)
kbp	kilo-base pair (10^3 base pairs)
N	newton
pN	piconewton (10^{-12} newton)
fN	femtonewton (10^{-15} newton)
M	molar
mM	millimolar (10^{-3} molar)
μM	micromolar (10^{-6} molar)
nM	nanomolar (10^{-9} molar)
l	liter
ml	milliliter (10^{-3} liter)
μl	microliter (10^{-6} liter)
pl	picoliter (10^{-12} liter)
h	hour
min	minute
s	second
ms	millisecond (10^{-3} second)
μs	microsecond (10^{-6} second)
Hz	hertz (1/second)
kHz	kilohertz (10^3 Hertz)
RT	room temperature
Pa	pascal
$k_{\text{B}}T$	scale factor of thermal energy
k_{B}	Boltzmann constant
T	temperature

Techniques and Methods

TIRF(M)	Total Internal Reflection Fluorescence (Microscopy)
(sm)FRET	(single-molecule) Förster or Fluorescence Resonance Energy Transfer
FCS	Fluorescence Correlation Spectroscopy
OT	Optical Tweezers
MT	Magnetic Tweezers
(HS-)AFM	(High-Speed) Atomic Force Microscopy
FOMT	Freely-Orbiting Magnetic Tweezers
MTT	Magnetic Torque Tweezers
eMTT	electro-Magnetic Torque Tweezers
PCR	Polymerase Chain Reaction
SDS-PAGE	Sodium Dodecyl Sulfate Polyacrylamide Gel Electrophoresis
MS	Mass Spectrometry
HPLC	High-Performance Liquid Chromatography

Other

RCSB PDB	Research Collaboratory for Structural Bioinformatics Protein Data Bank
NA	Numerical Aperture
CCD	charge-coupled device
CMOS	complementary-metal-oxide semiconductor
PTM	post-translational modification
STD	standard deviation
SEM	standard error of the mean
w/v	weight-to-volume ratio
<i>E. coli</i>	<i>Escherichia coli</i>
e.g.	for example
i.e.	that is
<i>et al.</i>	<i>et alii</i> ('and others')

1 Introduction

The genome of eukaryotic organisms ranges from millions to hundreds of billions of base pairs for different species and can be stretched accordingly to millimeters or meters [1–3]. These lengths are several orders of magnitude larger than the cell nucleus with an average diameter of roughly 5 μm and must be tightly packed in order to fit in. To achieve an appropriate compaction level, eukaryotic organisms organize their genome in hierarchical protein-DNA assemblies termed chromatin that inevitably influence DNA accessibility during key cellular processes. Hence, revealing the details of chromatin structure is essential for understanding the regulation of the genome. As the basic component of chromatin, the nucleosome has therefore been a central subject of research for about four decades.

Bulk studies based on traditional biochemical approaches from molecular and structural biology have provided invaluable insight into nucleosome structure and function [4–9]. However, these methods only reflect collective properties of samples due to ensemble and time averaging. Partial features, such as rare or transient events, and especially the intrinsic dynamics of usually heterogeneous biological samples cannot be resolved.

When many identical biomolecules are present in a solution, each one can occupy any one of a number of different conformational states with similar energies. Assuming for simplicity that each state corresponds to a distinct, visible color, the whole solution will at any given time display a color that reflects the average of all the individual molecules, which will each occupy different states with their corresponding distinct colors. Likewise, the observation of a single molecule on a long timescale, during which the molecule can convert between all states with the corresponding colors, will also yield an average color. The heterogeneity arising from both static differences between single biomolecules and individual dynamic changes in, e.g., their structure, function or chemical modification remains therefore hidden.

Except for Section 1.3, this chapter has been published in O. Ordu, A. Lusser, and N. H. Dekker. *Biophys. Rev.* **8**, 33 (2016).

1 Introduction

Details of molecular properties can be revealed by directly studying single molecules over time. However, the insights that can be obtained here strongly depend on the characteristics of the experimental system in use and the spatial and temporal resolution of the applied technique. During the observation within a certain time frame, the molecule might convert between barely different states at such high speed that intermediates would be averaged out and obscured. Hence, since the 1990s the development of single-molecule studies has not only included the interrogation of different biological systems but also the continued improvement of their accuracy and sensitivity [10–19]. Single-molecule techniques have become a highly suitable tool for investigating DNA-protein interactions at molecular level [20–22].

This chapter introduces the basic properties of nucleosomes, as well as the most commonly used single-molecule techniques in chromatin research and presents the pioneering insights they have provided into nucleosome structure, function and dynamics.

1.1 Nucleosome Structure and Dynamics

The nucleosome consists of 147 bp of DNA wrapped ~ 1.7 times in a left-handed superhelix around a discoidal protein structure of ~ 5 nm in height and ~ 7 nm in diameter formed by eight histones [23–25] (Figure 1.1). This histone octamer contains two copies of each of the so-called core histones H2A, H2B, H3 and H4 that are assembled into four heterodimers, i.e. two H2A/H2B and two H3-H4 dimers, by short-range interactions between the central α -helical histone-fold domains in a ‘handshake’ manner [26, 27]. The two H3-H4 dimers join to form a tetramer through the four-helix bundles of the H3 histones centered on the pseudo-twofold symmetry (dyad) axis, while the two H2A/H2B dimers attach to the tetramer via similar four-helix bundle interactions between the H2B and H4 histones. Each core histone further features a flexible N-terminal tail, while the histone H2A additionally exhibits a C-terminal tail. All of the histones are highly positively charged, and as such they balance the negative charge of the DNA. Hence, the histone octamer is only found to be stable in the presence of DNA or at high salt concentrations (~ 2 M), and it dissociates into the $(\text{H3-H4})_2$ tetramer and the two H2A/H2B dimers at physiological conditions [28]. Likewise, the nucleosome is assembled in a stepwise manner by the initial binding of the $(\text{H3-H4})_2$ tetramer to the DNA and the subsequent incorporation of the H2A/H2B dimers [29]. However, the nucleosome complex resulting from this well-defined assembly pathway is

not static, but a highly dynamic entity. Its inter-dependent structural, mechanical, chemical and functional properties are continuously altered by different mechanisms such as intrinsic dynamics, chemical modifications of the DNA and histones, ATP-dependent remodeling, as well as by forces and torques exerted by genome processing enzymes. The concerted action of all of these mechanisms makes it very difficult to study this complex system as a whole using single-molecule techniques. Such methods can, however, provide invaluable insights into the different individual mechanisms and their impact on nucleosome structure, dynamics and function [30, 31]. The pioneering findings using the most common single-molecule techniques are highlighted in the following section, while recently obtained insights are described in Chapter 3.

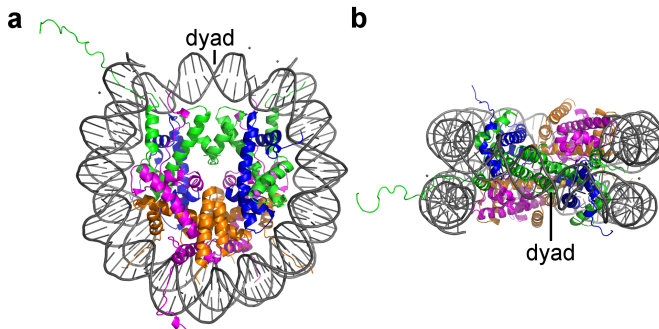


Figure 1.1: Structure of the nucleosome. A total of 147 bp of DNA (gray) are wrapped around a discoidal protein structure containing two copies of the four core histones H2A (magenta), H2B (orange), H3 (green) and H4 (blue) in a left-handed superhelix. **a** Top view. **b** Side view along the pseudo-twofold symmetry (dyad) axis. The images were created from the structural data in the RCSB PDB with the identification code 1AOI [24] using the PyMOL Molecular Graphics System, Version 1.7.2.1 Schrödinger, LLC.

1.2 Single-Molecule Techniques in Nucleosome Research

Over the past two decades, time-resolved observation and manipulation of single molecules have become very powerful means to investigate biological systems. The major single-molecule techniques enable the researchers to either directly visualize or influence individual molecules to reveal molec-

1 Introduction

ular details of their structure, function and dynamics on the nanometer scale. Substantial technical advances in optical microscopy and fluorescent probes have made fluorescence microscopy and fluorescence spectroscopy routine methods for directly visualizing and observing single molecules over time [32, 33]. The manipulation of individual molecules using force spectroscopy has become possible by the development of trapping methods with different types of force transducers [34]. Among these techniques, Atomic Force Microscopy (AFM) is a unique method that enables either the direct observation or the manipulation of single molecules by imaging or trapping, respectively [35, 36]. The most commonly employed single-molecule techniques and their associated specific experimental approaches are described in this section.

1.2.1 Fluorescence microscopy and fluorescence spectroscopy

Fluorescence microscopy essentially relies on the detection of light emitted at a specific wavelength by specific molecules (fluorophores) that are fused to the biomolecule of interest following their excitation at an initial, typically shorter, wavelength. The type and precise characteristics of these fluorophores will ultimately determine the efficiency and applicability of this technique to a specific study [37, 38]. Fluorescent samples can be excited either in a large or a small area depending on the design of the microscope. In wide-field microscopy, the sample is illuminated by a nearly collimated light beam, resulting in the simultaneous excitation of numerous fluorophores at different depths of focus and therefore in considerable background noise [39, 40]. This out-of-focus fluorescence is substantially decreased in Total Internal Reflection Fluorescence Microscopy (TIRFM), which restricts the illumination depth to about 100 nm via a highly localized, quickly decaying electromagnetic field (evanescent field) that is generated at the sample surface [41, 42]. Confocal microscopy reduces the excitation volume and almost entirely eliminates out-of-focus light by using a focused laser beam and a spatial pinhole just before the detector [43, 44]. These excitation methods are used in combination with different fluorescence spectroscopy techniques depending on the research question. Förster or Fluorescence Resonance Energy Transfer (FRET) is a well-established method to study the structural dynamics of single molecules. It is based on the non-radiative energy transfer between two fluorescent probes in very close proximity [45, 46]. An excited fluorophore (donor) can non-radiatively transfer its energy to another, sufficiently close fluorophore (acceptor) which then emits fluorescent light (Figure 1.2a). By monitoring

this energy transfer and its efficiency in real-time, the dynamics and distances of inter- and intramolecular interactions involved in conformational changes can be revealed on the scale of 1–10 nm. This method was first applied to nucleosomes for studying their structural dynamics [47]. The efficiency of FRET between a donor and an acceptor fluorophore each located on the nucleosomal DNA ~ 45 bp from its entry and exit sites showed fast dynamic changes in nucleosome structure between a long-lived, fully wrapped state (2–5 s) and a transient, substantially unwrapped conformation (100–200 ms). This work represents the first attempt to directly investigate the dynamic nature of nucleosomes, and the results suggest a potential mechanism by which DNA accessibility for DNA-binding proteins can be regulated. However, the observed dynamics was highly affected by fluorophore blinking, which influenced the results and was corrected for in a later publication by the authors [48]. Different FRET-based assays have subsequently been developed and used, enabling more accurate, robust and reliable insights into nucleosome structure and dynamics [49–52].

Another frequently used single-molecule fluorescence technique is Fluorescence Correlation Spectroscopy (FCS), which allows the study of the dynamics of individual molecules as they freely diffuse in solution [53–56]. FCS is based on the correlation analysis of fluctuations in the time-resolved fluorescence signal that arises from very few molecules diffusing through the tiny excitation volume ($\sim 10^{-3}$ pl) generated in a confocal microscope (Figure 1.2b). Essentially, the fluorescence signal is compared to its replicas calculated at different lag times to check their similarity and reveal repetitive patterns due to the underlying physical processes, such as free diffusion, chemical reaction or conformational changes. The resulting mathematical expression (the autocorrelation function) yields the characteristic parameters of these processes, such as diffusion constants, concentrations, hydrodynamic radii or reaction rates. FCS was first used to investigate the structural dynamics of nucleosomes in combination with FRET [57]. The un- and rewinding rates of the nucleosome were initially determined indirectly via FRET by trapping the open conformation using a site-specific DNA-binding protein. FCS measurements were then performed on nucleosomes labeled with either donor only or a donor-acceptor pair to directly observe conformational changes for a more reliable interpretation of the kinetics. The results obtained from both approaches led to the conclusion that nucleosomal DNA unwraps on a timescale of ~ 250 ms and rewinds more rapidly within 10–50 ms. Subsequent efforts using this technique have provided additional insights into nucleosome structure and dynamics [58–62].

1 Introduction

These studies convincingly demonstrate the great power of the most commonly used single-molecule fluorescence techniques to visualize DNA-protein interactions. When used in combination, they can yield complementary insights that allow the researchers to draw more reliable conclusions. However, the data acquisition, analysis and interpretation in fluorescence microscopy studies must always take into account the many factors related to the photophysics of the fluorophores [63]. This issue is entirely eliminated in force spectroscopy techniques which rely on the detection of light scattered by micron-sized massive particles. The most common approaches of these manipulation methods are presented in the following subsection.

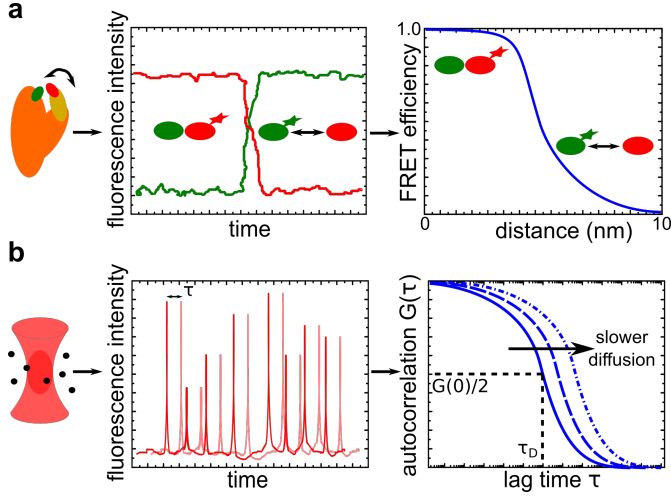


Figure 1.2: Sketched examples of fluorescence spectroscopy techniques. **a** Single-Molecule Fluorescence Resonance Energy Transfer (smFRET). A dynamic molecule (*orange/yellow*) is labelled with a donor (*green*) and an acceptor (*red*) fluorophore. When the fluorophores are close together within 10 nm, the excited donor will transfer its energy to the acceptor for fluorescence emission. For distances >10 nm, only the donor will fluoresce. The recorded time-resolved fluorescence signals of the donor (*green*) and acceptor (*red*) are used to calculate the efficiency of FRET. **b** Fluorescence correlation spectroscopy (FCS). Very few molecules (*black*) diffusing through the tiny excitation volume generated in a confocal microscope are excited for fluorescence emission. The time-resolved fluorescence signal is recorded and analyzed by autocorrelation, i.e. checking its similarity to its replicas shifted by lag times τ . The resulting autocorrelation function $G(\tau)$ yields the characteristic parameters of the underlying process, such as the diffusion time τ_D at about half of the amplitude ($G(0)/2$).

1.2.2 Force spectroscopy

The basis of force spectroscopy techniques is the specific attachment of single molecules between a substrate and a force transducer by interacting proteins or organic or engineered compounds. This tethering enables manipulation of the molecules by the application of forces and, in some cases, torques. The readouts provided by the force transducers are tracked in real-time, allowing for the investigation of primarily mechanical properties of the sample. Depending on the biological question of interest, different force transducers are used together with distinct methods for trapping and monitoring them.

In Optical Tweezers (OT) dielectric micron-sized particles are captured in the focus of an intense laser beam exerting a force due to the light gradient [64–66]. In biological applications, OT typically involve a nucleic acid molecule tethered between an optically trapped bead and a substrate, which can either be the surface of the sample holder or another, fixed bead held by a micropipette or even a second optical trap (Figure 1.3a). The underlying mechanism is based on controlling the position of the trapped bead and, thereby, the molecule’s extension. Therefore, this type of trapping is referred to as an extension clamp. Moving the focused laser beam with the trapped bead allows the manipulation of the molecule by inducing a concomitant change in its extension, which concurrently affects the molecule’s tension that is related to the applied forces ranging between 0.1 and 100 pN. The bead’s position is recorded indirectly by detecting the laser signal on a position-sensitive device, which enables the simultaneous measurement of force and extension, the two key quantities of force spectroscopy. This method was first used in chromatin research to study the structure of native chromatin fibers extracted from chicken erythrocytes [67]. The mechanical stretch-release manipulation revealed a reversible decondensation of the fibers at low forces (<6 pN), which was attributed to internucleosomal interactions. Specifically, the fibers showed a pronounced transition between condensation and decondensation at 5–6 pN under physiological salt concentrations, indicating strong internucleosomal interactions with energies comparable to the thermal energy. Upon pulling at high forces (>20 pN), the fibers were observed to undergo irreversible changes in their extension, which was explained by the possible eviction of the histone proteins during this mechanical unfolding. The results of this study led to the first insights into the energy landscape of chromatin structure and also suggested a considerable dynamic nature due to thermal fluctuations. It was followed by many other OT-based assays that shed more light on the structure and dynamics of nucleosomes

1 Introduction

[68–79].

Another very common technique used for mechanical manipulation of single molecules is Magnetic Tweezers (MT). In this method, magnetic beads are trapped by permanent or electrical magnets that exert a force as result of a magnetic field gradient [80–85]. In the most common designs a nucleic acid molecule is tethered between a magnetic bead and the surface of the sample holder at its two extremities and manipulated using permanent magnets (Figure 1.3b). Vertical movement of the magnets results in a corresponding change of the applied force, ranging from 10^{-3} pN to 100 pN, and a concomitant change of the bead’s position which is directly recorded by video microscopy with a CCD or CMOS camera. As the applied force is the parameter that is precisely controlled in this technique, the underlying mechanism is also referred to as force clamp. However, besides forces, MT can also apply torques by rotating the magnets. MT were first used in chromatin research to study the time- and force-dependence of the assembly and disassembly of chromatin fibers [86]. Fibers were found to assemble only at forces up to 10 pN, while assemblies at the higher forces within this range were observed to be reversible. These results revealed a strong dependency of chromatin assembly on the force applied to the DNA and illustrated the dynamic equilibrium of this process. Translated to a possible scenario in the cell, these experiments allow conclusions to be drawn on the potential fate of chromatin/nucleosomes under forces exerted by enzymes during DNA-templated processes. For example, the forces generated by the *E. coli* RNAP were shown to be in the piconewton range [87]. Subsequent MT studies confirmed and further refined these results to a more detailed picture of the structure and dynamics of chromatin and nucleosomes [52, 88–91]. The specific function of the nucleosome in higher-order folding of chromatin based on inter-nucleosomal interactions has also been assessed using single-molecule force and torque spectroscopy, but it still remains elusive due to additional restrictions on the electrostatics, topology and elasticity of the complex [92, 93]. While MT and OT have become the routine approaches for force spectroscopy due to their simple yet robust principles, they are, however, limited to mechanical manipulation of samples and do not allow direct observation.

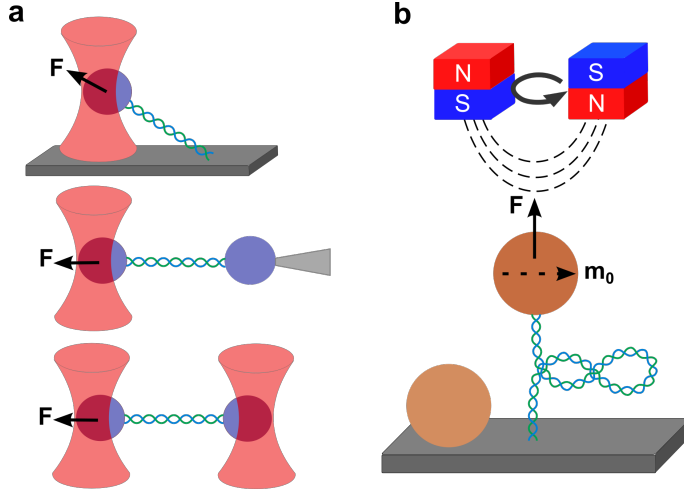


Figure 1.3: Overview of force spectroscopy techniques. **a** Optical Tweezers (OT). A DNA molecule (*blue/green*) is tethered between an optically trapped dielectric microsphere (*violet*) and either the glass coverslip (top) or another bead fixed using a micropipette (middle) or a second optical trap (bottom). Moving the optical trap will change the tether's extension and tension related to the applied forces (F) ranging between 0.1 pN and 100 pN (extension clamp). **b** Magnetic Tweezers (MT). A DNA molecule (*blue/green*) is tethered between the glass coverslip and a magnetic bead (*dark brown*) that is trapped using a pair of cubic permanent magnets (*red/blue*) which accurately exert forces ranging between 10^{-3} pN and 100 pN due to the magnetic field gradient (force clamp). Due to an induced horizontal magnetic moment (m_0), the bead is also torsionally trapped, which allows the application of torques by rotating the permanent magnets. Torque application leads to supercoiling of the DNA molecule and the formation of plectonemes (*circles of DNA*). Non-magnetic reference beads (*light brown*) adhered to the surface are used to correct for drift.

1.2.3 Atomic force microscopy

Atomic Force Microscopy (AFM), also called Scanning Force Microscopy (SFM), is a technique that is capable of either observing or manipulating single molecules on the same instrument by imaging or force spectroscopy, respectively [94, 95]. Both principles are based on the use of a cantilever as the force transducer. This cantilever is either scanned over a sample to obtain a topographical image by means of atomic interactions or tethered to one extremity of an individual molecule for its mechanical manipulation. Its interaction with the sample involving forces ranging between 10 pN

1 Introduction

and 10^4 pN leads to the bending of the cantilever, which is tracked by the use of a laser beam directed on the cantilever and reflected onto a position-sensitive device (Figure 1.4). In this way, either the topology of a sample or the extension of a molecule can be indirectly read out with near atomic resolution (≤ 1 nm) by controlling the position of the cantilever. Hence, like OT, AFM also operates primarily as an extension clamp in force spectroscopy. In nucleosome research, this technique is mainly used for imaging, as the applied forces are in the higher range of the molecular scale and the distinct structures of chromatin, such as mono- and polynucleosomes, or higher-order foldings into fibers are very suitable to study using this specific approach. The first AFM study was performed on nucleosome arrays in order to directly observe and characterize their structural details [96]. This work convincingly illustrated the applicability of AFM imaging for high-resolution studies on nucleosome structure and was followed up by many researchers investigating the dynamics, as well as the role of nucleosomes in DNA accessibility [97–102]. Therefore, AFM represents another widely used technique in nucleosome research in addition to fluorescence and force spectroscopy. Chapter 3 will highlight recent insights into (sub)nucleosomal structure and dynamics from studies using most of the specific single-molecule approaches presented here.

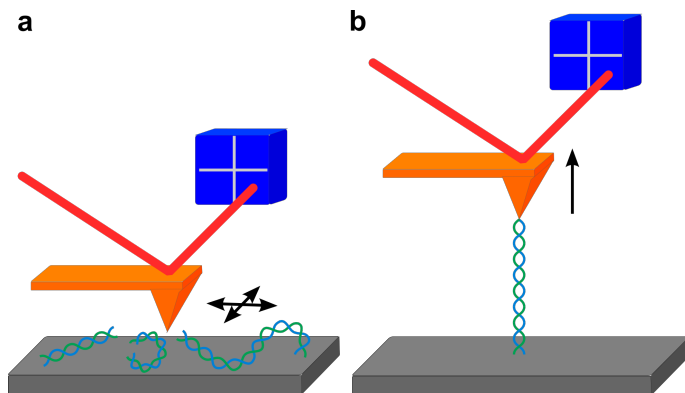


Figure 1.4: Principles of Atomic Force Microscopy (AFM). A cantilever (*orange*) is used to exert atomic forces on the sample. Their interaction leads to distortions of the cantilever which is recorded using a laser beam (*red*) that is reflected onto a position-sensitive device such as a quadrant photodiode (*blue*). **a** The cantilever can scan the sample to obtain a topographical image. **b** A DNA molecule (*blue/green*) is tethered between the glass coverslip and the cantilever to exert forces between 10 pN and 10^4 pN for force spectroscopy.

1.3 This Thesis

The research presented in this thesis comprises investigations of chromatin structure and dynamics on the molecular scale at the subnucleosomal level. Based on previous studies reporting on the stable complex of the $(\text{H3-H4})_2$ tetramer and DNA [28, 58, 71, 72, 90, 103–114], these so-called *tetrasomes* have been studied here at the single-molecule level in real time. Novel MT techniques allowing the measurement of twist and torque [115–117] in addition to the length of the DNA molecules and the applied force have been used to characterize the structure, stability, and dynamics of tetrasomes.

The technical basis for the presented research is set in **Chapter 2**. Here, the principles of the employed MT techniques are detailed in mutual comparison, together with the basic experimental procedures. Therefore, this chapter may also serve as a guideline to researchers for implementing and performing MT measurements.

In **Chapter 3**, the motivation and relevance of the presented research is described in the context of recent insights that single-molecule studies have provided into nucleosome structure and dynamics. Here, subnucleosomal structures and dynamics are introduced as important intermediates formed in different chemical conditions or mechanical processes. By this means, this chapter also provides the basis for the presented research on tetrasomes from a non-technical perspective.

Following up on our previous study on canonical *Drosophila* tetrasomes [118], **Chapter 4** presents our work on the structure and dynamics of tetrasomes containing the variant histone H3.3. Interestingly, these variant tetrasomes exhibited the same features as the canonical tetrasomes in terms of their overall structure and spontaneous dynamics in the handedness of DNA wrapping. This key finding indicates that their different functions likely arise from more subtle differences resulting in distinct interactions within the environment of the nucleus. Furthermore, the repeated observation of spontaneous flipping in tetrasome handedness suggests the intrinsic and key nature of this novel mechanism of chromatin for gene regulation.

Previous studies have suggested that the handedness dynamics of tetrasomes may derive from the structural rearrangement of the $(\text{H3-H4})_2$ at their H3-H3 interface [110–112, 114]. Based on this hypothesis, we have investigated the structure and dynamics of tetrasomes chemically modified at their H3-H3 interface, which is described in **Chapter 5**. Such tetrasomes exhibited the same structural features as unmodified tetrasomes with a reduced overall tendency towards handedness flipping. This key

1 Introduction

result suggests that a structural rearrangement of the histone tetramer plays a critical role in the spontaneous handedness dynamics of tetrasomes. In addition, the findings confirm the intrinsic nature of this mechanism and indicate that it may additionally be tuned by external effects, such as histone modifications.

Inspired by the potential impact of external effects on the structural dynamics of tetrasomes, we have also performed studies on tetrasomes assembled on the high-affinity 601-sequence [119] in different buffer conditions, which are presented in **Chapter 6**. Overall, the tetrasomes exhibited the same structural features, but their conformational plasticity varied with the chemical environment. The key results indicate a critical role of the underlying DNA sequence and ambient conditions for tetrasome dynamics. The findings further reconfirm the intrinsic and tunable nature of this potential key mechanism of chromatin to regulate the genome in eukaryotic organisms. Moreover, this study demonstrates that results obtained from measurements using specific nucleosome-positioning sequences and ambient conditions have to be considered and interpreted carefully.

In summary, this thesis gives an overview of fundamental research directed to advance our understanding of the structure, function and dynamics of chromatin in eukaryotes. The studies provide new insights into a novel mechanism that depicts a potential key feature of chromatin for gene regulation at the subnucleosomal level. The detailed knowledge of genome organization in all levels is essential to understand the viability and functioning of cells and, hence, all living organisms.

1.4 References

- [1] M. G. Kidwell. *Genetica* **115**, 49 (2002).
- [2] V. Merhej and D. Raoult. *Front Cell Infect. Microbiol.* **2**, 17 (2012).
- [3] C. Zimmer. *Science* **315**, 1358 (2007).
- [4] R. D. Kornberg. *Annu. Rev. Biochem.* **46**, 931 (1977).
- [5] R. D. Kornberg and Y. L. Lorch. *Cell* **98**, 285 (1999).
- [6] B. Li, M. Carey, and J. L. Workman. *Cell* **128**, 707 (2007).
- [7] J. D. McGhee and G. Felsenfeld. *Annu. Rev. Biochem.* **49**, 1115 (1980).

- [8] J. L. Workman and R. E. Kingston. *Annu. Rev. Biochem.* **67**, 545 (1998).
- [9] G. E. Zentner and S. Henikoff. *Nat. Struct. Mol. Biol.* **20**, 259 (2013).
- [10] D. Dulin, J. Lipfert, M. C. Moolman, and N.H. Dekker. *Nat. Rev. Genet.* **14**, 9 (2013).
- [11] M. Eigen and R. Rigler. *Proc. Natl. Acad. Sci. U.S.A.* **91**, 5740 (1994).
- [12] S. W. Hell. *Nat. Methods* **6**, 24 (2009).
- [13] B. Huang, M. Bates, X. W. Zhuang. *Annu. Rev. Biochem.* **78**, 993 (2009).
- [14] E. A. Jares-Erijman and T. M. Jovin. *Nat. Biotechnol.* **21**, 1387 (2003).
- [15] C. Joo, H. Balci, Y. Ishitsuka, C. Buranachai, and T. Ha. *Annu. Rev. Biochem.* **77**, 51 (2008).
- [16] W. E. Moerner. *Proc. Natl. Acad. Sci. U.S.A.* **104**, 12596 (2007).
- [17] K. C. Neuman and A. Nagy. *Nat. Methods* **5**, 491 (2008).
- [18] I. Tinoco and R. L. Gonzalez. *Genes Dev.* **25**, 1205 (2011).
- [19] S. Weiss. *Science* **283**, 1676 (1999).
- [20] D. Duzdevich, S. Redding, and E. C. Greene. *Chem. Rev.* **114**, 3072 (2014).
- [21] I. Heller, T. P. Hoekstra, G. A. King, E. J. G. Peterman, and G. J. L. Wuite. *Chem. Rev.* **114**, 3087 (2014).
- [22] C. Monico, M. Capitanio, G. Belcastro, F. Vanzi, and F. S. Pavone. *Int. J. Mol. Sci.* **14**, 3961 (2013).
- [23] T. J. Richmond, J. T. Finch, B. Rushton, D. Rhodes, and A. Klug. *Nature* **311**, 532 (1984).
- [24] K. Luger, A. W. Mäder, R. K. Richmond, D. F. Sargent, and T. J. Richmond. *Nature* **389**, 251 (1997).
- [25] C. A. Davey, D. F. Sargent, K. Luger, A. W. Mäder, and T. J. Richmond. *J. Mol. Biol.* **319**, 1097 (2002).

1 Introduction

- [26] G. Arents, R. W. Burlingame, B. C. Wang, W. E. Love, and E. N. Moudrianakis. *Proc. Natl. Acad. Sci. U.S.A.* **88**, 10148 (1991).
- [27] A. Klug, D. Rhodes, J. Smith, J. T. Finch, and J. O. Thomas. *Nature* **287**, 509 (1980).
- [28] T. H. Eickbush and E. N. Moudrianakis. *Biochemistry* **17**, 4955 (1978).
- [29] S. E. Polo and G. Almouzni. *Curr. Opin. Genet. Dev.* **16**, 104 (2006).
- [30] J. L. Killian, M. Li, M. Y. Sheinin, M. D. Wang. *Curr. Opin. Struct. Biol.* **22**, 80 (2012).
- [31] J. S. Choy and T. H. Lee. *Trends Biochem. Sci.* **37**, 425 (2012).
- [32] B. N. G Giepmans, S. R. Adams, M. H. Ellisman, and R. Y. Tsien. *Science* **312**, 217 (2006).
- [33] W. E. Moerner and D. P. Fromm. *Rev. Sci. Instrum.* **74**, 3597 (2003).
- [34] K. C. Neuman, T. Lionnet, and J. F. Allemand. *Annu. Rev. Mater. Res.* **37**, 33 (2007).
- [35] H. J. Butt, B. Cappella, and M. Kappl. *Surf. Sci. Rep.* **59**, 1 (2005).
- [36] H. G. Hansma and J. H. Hoh. *Annu. Rev. Biophys. Biomol. Struct.* **23**, 115 (1994).
- [37] J. E. Berlier, A. Rothe, G. Buller, J. Bradford, D. R. Gray, B. J. Filanoski, W. G. Telford, S. Yue, J. Liu, C. Y. Cheung, W. Chang, J. D. Hirsch, J. M. Beechem, R. P. Haugland, and R. P. Haugland. *J. Histochem. Cytochem.* **51**, 1699 (2003).
- [38] N. C. Shaner, P. A. Steinbach, R. Y. Tsien. *Nat. Methods* **2**, 905 (2005).
- [39] T. Funatsu, Y. Harada, M. Tokunaga, K. Saito, and T. Yanagida. *Nature* **374**, 555 (1995).
- [40] T. Schmidt, G. J. Schütz, W. Baumgartner, H. J. Gruber, H. Schindler. *Proc. Natl. Acad. Sci. U.S.A.* **93**, 2926 (1996).
- [41] D. Axelrod. *J. Cell Biol.* **89**, 141 (1981).
- [42] D. Axelrod. *Traffic* **2**, 764 (2001).

- [43] M. Minsky. *Scanning* **10**, 128 (1988).
- [44] S. M. Nie, D. T. Chiu, and R. N. Zare. *Science* **266**, 1018 (1994).
- [45] T. Förster. *Ann. Phys.* **2**, 55 (1948).
- [46] T. Ha, T. Enderle, D. F. Ogletree, D. S. Chemla, P. R. Selvin, and S. Weiss. *Proc. Natl. Acad. Sci. U.S.A.* **93**, 6264 (1996).
- [47] M. Tomschick, H. C. Zheng, K. van Holde, J. Zlatanova, and S. H. Leuba. *Proc. Natl. Acad. Sci. U.S.A.* **102**, 3278 (2005).
- [48] M. Tomschick, K. van Holde, and J. Zlatanova. *J. Fluoresc.* **19**, 53 (2009).
- [49] T. R. Blosser, J. G. Yang, M. D. Stone, G. J. Narlikar, and X. Zhuang. *Nature* **462**, 1022 (2009).
- [50] W. J. A. Koopmans, A. Brehm, C. Logie, T. Schmidt, and J. van Noort. *J. Fluoresc.* **17**, 785 (2007).
- [51] J. A. North, J. C. Shimko, S. Javaid, A. M. Mooney, M.A. Shoffner, S. D. Rose, R. Bundschuh, R. Fishel, J. J. Ottesen, and M. G. Poirier. *Nucleic Acids Res.* **40**, 10215 (2012).
- [52] M. Simon, J. A. North, J. C. Shimko, R. A. Forties, M. B. Ferdinand, M. Manohar, M. Zhang, R. Fishel, J. J. Ottesen, and M. G. Poirier. *Proc. Natl. Acad. Sci. U.S.A.* **108**, 12711 (2011).
- [53] E. L. Elson and D. Magde. *Biopolymers* **13**, 1 (1974).
- [54] D. Magde, E. Elson, and W. W. Webb. *Phys. Rev. Lett.* **29**, 705 (1972).
- [55] D. Magde, E. L. Elson, and W. W. Webb. *Biopolymers* **13**, 29 (1974).
- [56] M. Rigler, Ü. Mets, J. Widengren, and P. Kask. *Eur. Biophys. J.* **22**, 169 (1993).
- [57] G. Li, M. Levitus, C. Bustamante, and J. Widom. *Nat. Struct. Mol. Biol.* **12**, 46 (2005).
- [58] V. Böhm, A. R. Hieb, A. J. Andrews, A. Gansen, A. Rocker, K. Toth, K. Luger, and J. Langowski. *Nucleic Acids Res.* **39**, 3093 (2011).

1 Introduction

- [59] A. Gansen, A. Valeri, F. Hauger, S. Felekyan, S. Kalinin, K. Toth, J. Langowski, and C. A. Seidel. *Proc. Natl. Acad. Sci. U.S.A.* **106**, 15308 (2009).
- [60] W. J. Koopmans, R. Buning, T. Schmidt, and J. van Noort. *Biophys. J.* **97**, 195 (2009).
- [61] M. G. Poirier, E. Oh, H. S. Tims, and J. Widom. *Nat. Struct. Mol. Biol.* **16**, 938 (2009).
- [62] H. S. Tims, K. Gurunathan, M. Levitus, and J. Widom. *J. Mol. Biol.* **411**, 430 (2011).
- [63] T. Ha and P. Tinnefeld. *Annu. Rev. Phys. Chem.* **63**, 595 (2012).
- [64] A. Ashkin, J. M. Dziedzic, J. E. Bjorkholm, and S. Chu. *Opt. Lett.* **11**, 288 (1986).
- [65] A. Ashkin. *Biophys. J.* **61**, 569 (1992).
- [66] S. B. Smith, Y. J. Cui, and C. Bustamante. *Science* **271**, 795 (1996).
- [67] Y. Cui and C. Bustamante. *Proc. Natl. Acad. Sci. U.S.A.* **97**, 127 (2000).
- [68] M. L. Bennink, S. H. Leuba, G. H. Leno, J. Zlatanova, B. G. de Grooth, and J. Greve. *Nat. Struct. Biol.* **8**, 606 (2001).
- [69] L. Bintu, T. Ishibashi, M. Dangkulwanich, Y. Y. Wu, L. Lubkowska, M. Kashlev, and C. Bustamante. *Cell* **151**, 738 (2012).
- [70] B. Brower-Toland, D. A. Wacker, R. M. Fulbright, J. T. Lis, W. L. Kraus, and M. D. Wang. *J. Mol. Biol.* **346**, 135 (2005).
- [71] G. J. Gemmen, R. Sim, K. A. Haushalter, P. C. Ke, J. T. Kadonaga, and D. E. Smith. *J. Mol. Biol.* **351**, 89 (2005).
- [72] M. A. Hall, A. Shundrovsky, L. Bai, R. M. Fulbright, J. T. Lis, and M. D. Wang. *Nat. Struct. Mol. Biol.* **16**, 124 (2009).
- [73] C. Hodges, L. Bintu, L. Lubkowska, M. Kashlev, and C. Bustamante. *Science* **325**, 626 (2009).
- [74] J. Jin, L. Bai, D. S. Johnson, R. M. Fulbright, M. L. Kireeva, M. Kashlev, and M. D. Wang. *Nat. Struct. Mol. Biol.* **17**, 745 (2010).

- [75] A. H. Mack, D. J. Schlingman, R. P. Ilagan, L. Regan, and S. G. J. Mochrie. *J. Mol. Biol.* **423**, 687 (2012).
- [76] L. H. Pope, M. L. Bennink, K. A. van Leijenhorst-Groener, D. Nikova, J. Greve, and J. F. Marko. *Biophys. J.* **88**, 3572 (2005).
- [77] A. Shundrovsky, C. L. Smith, J. T. Lis, C. L. Peterson, and M. D. Wang. *Nat. Struct. Mol. Biol.* **13**, 549 (2006).
- [78] G. Sirinakis, C. R. Clapier, Y. Gao, R. Viswanathan, B. R. Cairns, and Y. L. Zhang. *EMBO J.* **30**, 2364 (2011).
- [79] Y. L. Zhang, C. L. Smith, A. Saha, S. W. Grill, S. Mihardja, S. B. Smith, B. R. Cairns, C. L. Peterson, and C. Bustamante. *Mol. Cell* **24**, 559 (2006).
- [80] F. Amblard, B. Yurke, A. Pargellis, and S. Leibler. *Rev. Sci. Instrum.* **67**, 818 (1996).
- [81] F. H. C. Crick and A. F. W. Hughes. *Exp. Cell Res.* **1**, 37 (1950).
- [82] S. B. Smith, L. Finzi, and C. Bustamante. *Science* **258**, 1122 (1992).
- [83] T. R. Strick, J. F. Allemand, D. Bensimon, A. Bensimon, and V. Croquette. *Science* **271**, 1835 (1996).
- [84] T. R. Strick, J. F. Allemand, D. Bensimon, and V. Croquette. *Biophys. J.* **74**, 2016 (1998).
- [85] F. Ziemann, J. Radler, and E. Sackmann. *Biophys. J.* **66**, 2210 (1994).
- [86] S. H. Leuba, M. A. Karymov, M. Tomschick, R. Ramjit, P. Smith, and J. Zlatanova. *Proc. Natl. Acad. Sci. U.S.A.* **100**, 495 (2003).
- [87] M. D. Wang, M. J. Schnitzer, H. Yin, R. Landick, J. Gelles, and S. M. Block. *Science* **282**, 902 (1998).
- [88] M. Kruithof, F. T. Chien, A. Routh, C. Logie, D. Rhodes, and J. van Noort. *Nat. Struct. Mol. Biol.* **16**, 534 (2009).
- [89] G. Lia, E. Praly, H. Ferreira, C. Stockdale, Y. C. Tse-Dinh, D. Dunlap, V. Croquette, D. Bensimon, and T. Owen-Hughes. *Mol. Cell* **21**, 417 (2006).
- [90] R. Vlijm, J. S. J. Smitshuijzen, A. Lusser, and C. Dekker. *PLoS One* **7**, e46306 (2012).

1 Introduction

- [91] J. Yan, T. J. Maresca, D. Shoko, C. D. Adams, B. T. Xiao, M. O. Christensen, R. Heald, and J. F. Marko. *Mol. Biol. Cell* **18**, 464 (2007).
- [92] F. T. Chien and J. van Noort. *Curr. Pharm. Biotechnol.* **10**, 474 (2009).
- [93] C. Lavelle, J. M. Victor, and J. Zlatanova. *Int. J. Mol. Sci.* **11**, 1557 (2010).
- [94] G. Binnig, C. F. Quate, and C. Gerber. *Phys. Rev. Lett.* **56**, 930 (1986).
- [95] E. L. Florin, V. T. Moy, and H. E. Gaub. *Science* **264**, 415 (1994).
- [96] M. J. Allen, X. F. Dong, T. E. Oneill, P. Yau, S. C. Kowalczykowski, J. Gatewood, R. Balhorn, and E. M. Bradbury. *Biochemistry* **32**, 8390 (1993).
- [97] L. Bintu, M. Kopaczynska, C. Hodges, L. Lubkowska, M. Kashlev, and C. Bustamante. *Nat. Struct. Mol. Biol.* **18**, 1394 (2011).
- [98] Y. Dalal, H. Wang, S. Lindsay, and S. Henikoff. *PLoS Biol.* **5**, 1798 (2007).
- [99] E. K. Dimitriadis, C. Weber, R. K. Gill, S. Diekmann, and Y. Dalal. *Proc. Natl. Acad. Sci. U.S.A.* **107**, 20317 (2010).
- [100] A. Miyagi, T. Ando, and Y. L. Lyubchenko. *Biochemistry* **50**, 7901 (2011).
- [101] L. S. Shlyakhtenko, A. Y. Lushnikov, and Y. L. Lyubchenko. *Biochemistry* **48**, 7842 (2009).
- [102] K. Yoda, S. Ando, S. Morishita, K. Houmura, K. Hashimoto, K. Takeyasu, and T. Okazaki. *Proc. Natl. Acad. Sci. U.S.A.* **97**, 7266 (2000).
- [103] B. Sollner-Webb, R. D. Camerini-Otero, and G. Felsenfeld. *Cell* **9**, 179 (1976).
- [104] M. Bina-Stein and R. T. Simpson. *Cell* **11**, 609 (1977).
- [105] F. Dong and K. E. van Holde. *Proc. Natl. Acad. Sci. U.S.A.* **88**, 10596 (1991).

- [106] S. Jackson, W. Brooks, and V. Jackson. *Biochemistry* **33**, 5392 (1994).
- [107] B. D. Brower-Toland, C. L. Smith, R. C. Yeh, J. T. Lis, C. L. Peterson, and M. D. Wang. *Proc. Natl. Acad. Sci. U.S.A.* **99**, 1960 (2002).
- [108] S. Mihardja, A. J. Spakowitz, Y. L. Zhang, and C. Bustamante. *Proc. Natl. Acad. Sci. U.S.A.* **103**, 15871 (2006).
- [109] V. Jackson. *Biochemistry* **34**, 10607 (1995).
- [110] A. Hamiche, V. Carot, M. Alilat, F. De Lucia, M. F. O'Donohue, B. Revet, and A. Prunell. *Proc. Natl. Acad. Sci. U.S.A.* **93**, 7588 (1996).
- [111] A. Hamiche, and H. Richard-Foy. *J. Biol. Chem.* **273**, 9261 (1998).
- [112] M. Alilat, A. Sivolob, B. Revet, and A. Prunell. *J. Mol. Biol.* **291**, 815 (1999).
- [113] A. Sivolob and A. Prunell. *J. Mol. Biol.* **295**, 41 (2000).
- [114] A. Sivolob, F. De Lucia, M. Alilat, and A. Prunell. *J. Mol. Biol.* **295**, 55 (2000).
- [115] J. Lipfert, J. W. J. Kerssemakers, T. Jager, and N. H. Dekker. *Nat. Methods* **7**, 977 (2010).
- [116] J. Lipfert, M. Wiggin, J. W. J. Kerssemakers, F. Pedaci, and N. H. Dekker. *Nat. Commun.* **2**, 439 (2011).
- [117] X. J. A. Janssen, J. Lipfert, T. Jager, R. Daudey, J. Beekman, and N. H. Dekker. *Nano Lett.* **12**, 3634 (2012).
- [118] R. Vlijm, M. Lee, J. Lipfert, A. Lusser, C. Dekker, and N. H. Dekker. *Cell Rep.* **10**, 216 (2015).
- [119] P. T. Lowary and J. Widom. *J. Mol. Biol.* **276**, 19 (1998).

2 Magnetic Tweezers for the Measurement of Twist and Torque

Single-molecule techniques make it possible to investigate the behavior of individual biological molecules in solution in real time. These techniques include so-called force spectroscopy approaches such as atomic force microscopy, optical tweezers, flow stretching, and magnetic tweezers. Amongst these approaches, magnetic tweezers have distinguished themselves by their ability to apply torque while maintaining a constant stretching force. Here, it is illustrated how such a “conventional” magnetic tweezers experimental configuration can, through a straightforward modification of its field configuration to minimize the magnitude of the transverse field, be adapted to measure the degree of twist in a biological molecule. The resulting configuration is termed the freely-orbiting magnetic tweezers. Additionally, it is shown how further modification of the field configuration can yield a transverse field with a magnitude intermediate between that of the “conventional” magnetic tweezers and the freely-orbiting magnetic tweezers, which makes it possible to directly measure the torque stored in a biological molecule. This configuration is termed the magnetic torque tweezers. An associated video explains in detail how the conversion of conventional magnetic tweezers into freely-orbiting magnetic tweezers and magnetic torque tweezers can be accomplished, and demonstrates the use of these techniques. These adaptations maintain all the strengths of conventional magnetic tweezers while greatly expanding the versatility of this powerful instrument.

This chapter has been published as J. Lipfert, M. Lee, O. Ordu, J. W. J. Kerssemakers, and N. H. Dekker. *J. Vis. Exp.* **87**, e51503 (2014). The associated video is located at <https://www.jove.com/video/51503/>.

2.1 Introduction

In recent years, single-molecule techniques have proven their wide applicability in the study of processive motor proteins and other enzymes, yielding insight into their kinetics and the underlying mechanochemistry. In the context of force spectroscopy, important contributions have been made by atomic force microscopy flow stretching, and OT and MT. OT and MT have notably succeeded in combining great flexibility in terms of molecular manipulation with high spatial and temporal resolution. Here, we focus on MT, which can apply both stretching forces and torques to biological molecules tethered between a surface and superparamagnetic beads [1–3]. MT (Figure 2.1a) are a very versatile single-molecule technique that has been used to monitor both the mechanical properties of nucleic acids as well as their interactions with proteins. MT have many strengths, including overall simplicity and robustness of the experimental implementation, facile application of torque, natural operation and straightforward calibration in constant force mode [4], extension to parallel measurements [5, 6], and absence of sample heating and photodamage. Compared to other single-molecule approaches, MT provide a way to perform force-dependence measurements at forces as low as ~ 10 fN and have the ability to straightforwardly control the degree of supercoiling. While MTs have predominantly been used as an experimental tool to investigate biological processes involving nucleic acids [7, 8], they have also found application in studies of the mechanical properties of proteins [9–13] or cells [10, 14–17]. Numerous useful references are available that describe how to build and run a MT [4, 18–20].

However, conventional MT (Figure 2.1a, left) do not track rotational motion directly, and, while they apply torque, they do not measure torque directly. In addition, they constrain the free rotation of the nucleic acid tether. Here, we present two extensions of magnet tweezers. The first, termed Freely-Orbiting Magnetic Tweezers (FOMT; Figure 2.1a, center [21]), allows the measurements of equilibrium angle fluctuations and changes in the twist of tethered nucleic acid molecules, without constraining the rotational motion around the tether axis. The second, termed Magnetic Torque Tweezers (MTT; Figure 2.1a, right), which has the capability to apply and directly measure both forces and torques to single biomolecules [22–27].

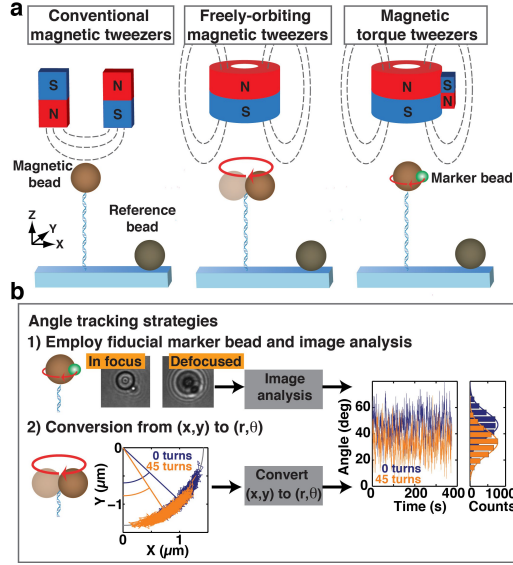


Figure 2.1: Schematics of conventional MT, FOMT, MTT, and two strategies for tracking rotation angle. **a** In all three implementations of MT, magnetic beads are tethered to a flow cell surface by functionalized macromolecules, e.g., the dsDNA molecules shown schematically. Reference beads are attached to the flow cell surface and tracked for drift correction. All three MT setups employ magnets to apply an upward stretching force on the magnetic bead and, therefore, DNA tether. In conventional MT, a pair of magnets exerts a magnetic field that is oriented transversely relative to the tether axis, tightly constraining rotation of the bead around the DNA-tether axis. In FOMT, a cylindrically-shaped magnet provides a magnetic field that oriented along the tether direction. When the tether is aligned to the center of the cylindrically-shaped magnet, any remaining transverse fields are minimized, allowing free rotation about the tether axis. In MTT, a side magnet is added to the cylindrically-shaped magnet used in FOMT in order to provide a small transverse field (reduced in magnitude compared to MT). This small transverse field enables the application of torque as well as its measurement. **b** Two strategies to measure the rotation angle of a magnetic bead about the DNA-tether axis are shown. 1): a marker bead (*green*) attached to the magnetic bead (*brown*) gives an asymmetric image that enables angle tracking by image analysis. Two CCD images of a 1.4- μ m-radius magnetic bead with a 0.5- μ m-radius fiducial marker are shown, in focus and out-of-focus. 2): when the DNA is tethered to the magnetic bead at a position away from the bead's south pole, the center of the bead fluctuates along an arc whose center defines an angular position. Either strategy can be used to track rotation angle and to monitor shifts in the angle position as the tether is torsionally strained (traces on the right), thus enabling measurements of single molecule torque.

In the following protocol, we presume that the reader has at his/her disposition a ‘conventional’ MT instrument. We refer the reader to Section 2.4 for references on how to build and run a MT setup, as well as considerations that must be taken into account in the selection of magnetic beads, magnets, and tracking routines. In addition, Subsections 2.2.1 and 2.2.2 describe how we typically prepare and incubate a DNA sample for use in the MT as well as the preliminary measurements that can be performed on a single DNA in the conventional MT. Subsections 2.2.3 and 2.2.4 illustrate how an MT instrument can be readily adapted and used for FOMT and MTT measurements.

2.2 Materials and Methods

2.2.1 Preparation and incubation of a DNA sample

1. Prepare DNA constructs that are ligated to duplex ends (typically employ ~ 600 bp DNA PCR fragments) that are functionalized with multiple biotin and digoxigenin groups, respectively [18]. To start, a DNA tether length $> 1 \mu\text{m}$, e.g., 7.9 kbp corresponding to a stretched length of $\sim 2.7 \mu\text{m}$ as employed here, is recommended for ease of use; in particular, using a DNA length that is similar to or shorter than the bead radius is problematic due to the attachment geometry in the MTT and FOMT. See Section 2.4 for a description of how DNA length influences temporal response in the angular domain.
2. Assemble the flow cells for single-molecule experiments. For the flow cells, use two glass microscope coverslips separated by a double-layer parafilm spacer. The top microscope coverslip should have two holes for the fluid in- and outlets to the cell. It is convenient to use a sandblaster to drill the holes. The bottom coverslip is coated with nitrocellulose (0.1% w/v in amyl acetate). Place the Parafilm spacers on the nitrocellulose-coated side of the bottom slides and close the top with clean top slides.
3. Seal the flow cells. Using physical tweezers, place the assembled flow cell on a heater plate set to 80 - 100 °C for ~ 1 min. Pay attention that the flow cell is well sealed, that the parafilm does not close off the holes that connect to the in- and outlet, and that the glass slides are well aligned.

Note: To ensure a good seal, it is recommended to stroke out bubbles in the parafilm using a large cotton swab. The flow cell can then be mounted on the MT instrument.

4. Prepare buffers. Prepare TE tethering buffer (10mM Tris-HCl (pH 8.0), 1 mM EDTA, and 200 mM NaCl). Alternatively, one can use PBS buffer (137 mM NaCl, 2.7 mM KCl, 10 mM phosphate buffer (pH 7.4)) supplemented with 100 μ g/ml BSA, 0.1% Tween and 5 mM sodium azide (PBS+) as tethering buffer. Flush 2-3 cell volumes TE tethering buffer into the flow cell.
5. Incubate 0.5 or 1.5- μ m-radius non-magnetic latex beads in the flow cell for \sim 30 min. These beads will act as reference beads during MT measurements that allow one to minimize the effect of drift between the objective and the sample holder (i.e. the flow cell). Flush out unattached non-magnetic beads by rinsing with 2-3 cell volumes of TE tethering buffer.
6. Functionalize the bottom surface of the flow cell by incubation with 100 μ g/ml anti-digoxigenin in PBS for at least 1 h (preferably longer; incubation can be carried out overnight), to provide for DNA attachment. Rinse with 2-3 cell volumes of TE tethering buffer. Finally incubate the flow cell with 2 mg/ml bovine serum albumin (BSA) in TE tethering buffer for 30 min for surface passivation.
7. Take an aliquot of 2 ml streptavidin-coated superparamagnetic MyOne beads (see Section 2.4 and Table 2.1 with the materials) and dilute with 10 ml TE tethering buffer. Wash twice with 10 ml TE tethering buffer using a magnetic particle concentrator, and resuspend in 10 ml TE tethering buffer. Attach \sim 1 ml of the DNA molecules (\sim 1 ng) to these beads by incubation in TE tethering buffer for 30 min.
8. Dilute the solution of the DNA-tethered superparamagnetic beads ten-fold by adding 90 ml TE tethering buffer. Finally, inject the solution into the flow cell and incubate for \sim 1 h to allow for DNA attachment to the anti-digoxigenin-coated surface. Wash the flow cell thoroughly with TE tethering buffer. After incubation of the DNA-tether constructs, flush extensively with experimental buffer (this can be TE tethering buffer) to remove all non-attached beads.
9. For measurements that employ an angular tracking protocol that requires fiducial marker beads attached to the magnetic beads [23] (see Section 2.4), incubate the flow cell with 1,000-fold diluted stock of marker beads in TE tethering buffer for at least 30 min and rinse with the buffer thoroughly.

Table 2.1: Specifications of the materials.

Name	Company	Catalogue Number
Sandblaster	Great Lake Orthodontics	190-070 Microetcher II
Nitrocellulose	Life Technologies	LC2001
Magnetic Particle Concentrator	Life Technologies	12002D
Non-magnetic latex beads (0.5 μm radius)	Polysciences	17010
Non-magnetic latex beads (1.5 μm radius)	Sanbio	PV05N/2179
Antidigoxigenin	Roche	11 214 667 001
Streptavidin-coated superparamagnetic beads (0.25 μm radius)	Ademtech	3150
Streptavidin-coated superparamagnetic beads (0.5 μm radius, “MyOne”)	Life Technologies	650.01
Streptavidin-coated superparamagnetic beads (1.4 μm radius, “M270”)	Life Technologies	653.05
Biotin-coated latex beads (0.5 μm radius)	Life Technologies	F-8786
cubic magnets for conventional MT	Supermagnete	W-05-N50-G
cylindrical magnets for FOMT and MTT	Supermagnete	R-06-02-02G
Side magnet for MTT	Supermagnete	S-04-07-N
Linear stage	Physik Instrumente	M-126.PD
Rotary stage	Physik Instrumente	C-150
High-resolution automated sample stage	Physik Instrumente	C-733
Software for coding analysis routines	The Mathworks	MATLAB

2.2.2 Measurements on single DNA molecules in the conventional MT

1. Using a conventional MT (see Section 2.4) with appropriate field configuration (Figure 2.1a, left) and both translational and rotational control of the magnet position, search for rotationally constrained DNA molecules in the flow cell. At pulling forces of ≥ 1 pN (consult references [4, 19, 20, 28, 29] regarding force calibration in MT), tethered beads can easily be distinguished from beads stuck to the surface of the bottom slide by their different heights in the focus. Whether a DNA molecule is rotationally constrained can be assessed by introducing 20-30 turns of the magnets at a force of ~ 0.25 pN: here, the tether length should decrease by 0.4 - 0.5 μm .

Note: To run MT experiments, image processing is used to determine the x, y , and z position of DNA-tethered beads.

2. Verify that the bead is attached by a single DNA tether. This can be done by comparing the behavior under positive and negative turns at forces of > 1 pN (Figure 2.2a). In this force regime, the presence of multiple DNA tethers will give rise to an approximately symmetric decrease in the extension upon introducing positive and negative turns, whereas single DNA tethers will give rise to an asymmetric response.
3. Search for appropriate fixed beads stuck to the bottom surface in the vicinity of the tether of interest that can serve as reference beads.
4. Calibrate the length of the DNA, l . The position of the flowcell surface can be determined by bringing the tethered bead in contact with the surface (e.g., by rotating the magnet by ~ 60 turns at a force below 0.2 pN). Measurements of the tethered bead's vertical position with respect to this surface then report on absolute value of l .

Note: To minimize subsequent effects of drift, it is advised to perform measurements of l relative to the position of a reference bead affixed to the surface.

5. Record a rotation curve (i.e. a measurement of the DNA extension as a function of the number of turns) at a stretching force of ~ 0.25 pN (Figure 2.2a).
6. Determine the number of turns at which the extension is maximal, as this corresponds to the state at which the DNA molecule is torsionally relaxed. To do so, it is useful to fit the rotation curve locally with a

parabolic or a Gaussian function to determine the center position. Define this point as “zero turns”.

7. For a series of ~ 20 magnet positions, determine the average extension of the torsionally-relaxed molecule (i.e. at “zero turns”, see step 6) from the z -trace.
8. For each measurement point in step 7, precisely determine the stretching force from the fluctuations in the x or y position [20, 28, 29], or, provided the magnetization of the bead is well-known, using knowledge of the local field gradient [4]. Plotting the stretching force versus the average extension results in a force-extension curve (Figure 2.2b).
9. Fit the resulting force-extension data to the worm-like chain equation using the polynomial approximation by Bouchiat *et al.* [30].
10. If preparing for subsequent FOMT measurements, slowly rotate the magnets while recording the magnetic bead’s (x,y) -excursions.
Note: The smaller the radius of the resulting annulus in the conventional MT configuration, the more closely the DNA molecule is tethered closer to the “south pole” of the magnetic bead. When one switches to the FOMT configuration, such a DNA molecule will be tethered closely to the “equator” of the magnetic bead, which enables reliable tracking of the rotation angle from the (x,y) -position (see Section 2.4).

2.2.3 Measurements of DNA twist using FOMT

1. Manually replace the square magnets of the conventional MT by a cylindrical magnet that is used for FOMT (Figure 2.1a, center). This operation should be performed in such a way that the selected DNA tether remains within the field of view. This can be accomplished in less than 1 min by simply unscrewing the complete magnet head that holds the magnets for the conventional tweezers configuration and replacing it by a magnet head that holds a cylindrical magnet for FOMT.
2. The (x,y) -excursion of a magnetic bead tethered by a single dsDNA tether depend strongly on the position of the tether with respect to the axis of the cylindrical magnet (Figure 2.1b, Figure 2.3a). Record the (x,y) -excursions in order to determine the corresponding location within the characteristic fluctuation pattern (Figure 2.3a, Section 2.4).

3. Perform coarse alignment of the magnet in the FOMT. This can be achieved by moving the cylindrical magnet above the flow-cell using (x,y) -translation stages. If the (x,y) -excursions follow an arc, the cylindrical magnet is not properly aligned and needs to be moved in the appropriate direction (Figure 2.3b). Coarse alignment can be accomplished within 15 min for the case of MyOne beads with 7.9 kbp tethers, and is complete when measurement of the (x,y) -excursions results in the observation of circular motion (Figure 2.3b, center).

Note: Coarse alignment is typically sufficient to observe the changes in twist occasioned by protein binding to single DNAs tethered in the FOMT configuration [21, 31] (see Section 2.3, Figure 2.5), despite the fact the accompanying two-dimensional histogram may not have its counts absolutely uniformly distributed along the circular annulus (Figure 2.3c).

4. If required for further experiments, perform fine alignment in the FOMT. This can be achieved using high-resolution micrometer screws or a high-resolution automated stage to either move the magnet or the flow cell to center the cylindrical magnet onto the bead to within $\sim 10 \mu\text{m}$. In the fine alignment stage, the magnet is carefully positioned such that the fluctuations on the circle annulus are nearly uniform, corresponding to a situation where the energy barrier to full rotation due to the magnet is $k_B T$ (Figure 2.4). Fine alignment can be accomplished within 45 min for the case of MyOne beads with 7.9 kbp tethers, and in reduced time frames for smaller beads and shorter tethers are employed (see Section 2.4).

Note: Fine alignment is typically required to perform measurements of the torsional stiffness of bare or protein-coated DNA (see Section 2.3, Figure 2.4).

5. If required for analysis, calibrate the force in the FOMT. This can be carried in a manner analogous to MT, using either the bead's radial fluctuations $\langle r^2 \rangle$ (where the angled brackets denote the time average) as shown in the associated video and detailed in Lipfert *et al.* [21], or, provided the magnetization of the bead is well-known, using knowledge of the local field gradient [21].

2.2.4 Measurements of DNA torque using MTT

1. Manually replace the cylindrical magnet that is used for FOMT by a cylindrical magnet plus a side (permanent) magnet for the MTT (Figure 2.1a, right). This operation should be performed in such a way that the selected DNA tether remains within the field of view.

2 Magnetic Tweezers for the Measurement of Twist and Torque

The most straightforward way to achieve this is to manually add the side magnet at its proper location, which can be accomplished within 1 min. No further realignment is necessary.

Note: An alternative to a side magnet is the use of electromagnets [32].

2. If required for analysis, calibrate the force in a manner analogous to MT, using either the bead's x or y fluctuations or, provided the magnetization of the bead is well-known, using knowledge of the local field gradient [21].
3. Track the angular fluctuations as a function of time $\theta(t)$ using either the fiducial based tracking protocol [23] or the angular tracking protocol based on monitoring the (x,y) -position (see Section 2.4). In the former case, record full images of the bead as a function of time for subsequent image processing. In the latter case, it is sufficient to record the bead's (x,y) -fluctuations at this step.
4. As described in Section 2.4, for the angular tracking protocol based on monitoring the (x,y) -position it is also advisable to record a time trace where the magnets are slowly (typically at 0.1 Hz) rotated by several turns. This will allow one to accurately convert Cartesian (x,y) -coordinates into polar coordinates (r, θ) using Equations 2.3-2.5 in Section 2.4.

Note: The measurement time depends mostly on the desired torque resolution. A detailed argument is given in Lipfert *et al.* [24]. For MyOne beads and 8 kbp DNA tethers, measuring for 30-100 s should be sufficient to give a torque resolution in the range of ~ 1 pN·nm.

5. Determine the stiffness of the torsional trap from the variance of the angular fluctuations (σ_θ^2 , in radians) using:

$$k_\theta = \frac{k_B T}{\sigma_\theta^2} \quad (2.1)$$

Note: Typical rotational trap stiffnesses achieved in the MTT are in the range of 10-1,000 pN·nm/rad, lower than for conventional MT.

6. In addition, record the z -position of the bead and use this to determine the tether length l (see also steps 4-10 in Subsection 2.2.2).
7. Rotate N turns and again record $\theta(t)$ and $l(t)$.

Note: The reduced rotational trap stiffness of the MTT compared to MT renders it suitable for measurements of single molecule torque, but implies

that the maximum torque that can be exerted is reduced. This implies that the MTT may not be able to counterbalance high drag torques caused by rapid rotation. Care must therefore be taken not to exceed the maximum speed; typically rotate at rates close to 0.1 Hz.

8. Determine the torque accumulated in the nucleic acid tether after N turns using:

$$\Gamma = -k_\theta \langle \theta_N - \theta_0 \rangle \quad (2.2)$$

Where $\langle \dots \rangle$ denotes the average and θ_0 and θ_N are the angle at zero turns (corresponding to a torsionally relaxed tether, cf. step 4 of Subsection 2.2.2 and N turns, respectively).

9. Repeat steps 6 and 7 as necessary in order to fully determine a molecule's torque response in a single measurement run (see Section 2.3, Figure 2.6).

2.3 Representative Results

Representative results from the MT (Figure 2.1a) are shown in Figure 2.2. Figure 2.2a shows rotation-extension curves for a 7.9 kb DNA taken at $F = 0.25$ pN, 0.5 pN, and 2.0 pN. The response of a single DNA to rotation should be symmetric at the lowest forces (0.25 pN), with the extension of the DNA decreasing as a result of the formation of positive or negative plectonemic supercoils. Qualitative knowledge of this response is useful when initially searching for a rotationally constrained DNA tether (see step 1 in Subsection 2.2.2). Note that additional inspection of the tether is required to verify that it consists of a single DNA molecule: here, the asymmetric response of a single DNA to rotation at forces exceeding 0.5 pN helps to distinguish it from multiple DNAs (see step 2 in Subsection 2.2.2). Once this has been verified, one returns to the rotational response at 0.25 pN in order to determine the exact number of magnet turns at which the single DNA is torsionally relaxed, where one takes a force-extension curve, which should resemble Figure 2.2b. For this particular measurement, a fit of the data to the worm-like chain model (solid line) yielded a fitted contour length $L_C = 2.71 \mu\text{m}$ and bending persistence length $L_P = 45$ nm. For dsDNA, the fitted values of the persistence length should lie in the range 40-55 nm, depending on the buffer conditions [33], and the fitted contour length should be close (typically within 10%) to the value expected for the DNA construct that is used in the measurements, using the relationship $L_{DNA} = 0.34 \text{ nm/bp} \cdot \text{number of base pairs}$.

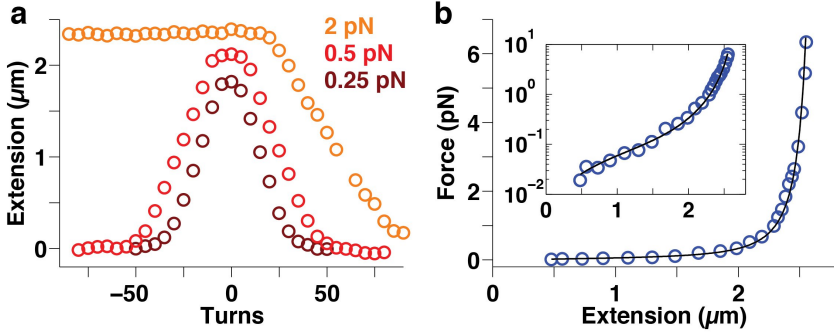


Figure 2.2: DNA calibration measurements in the conventional MT. **a** Rotation-extension curves for a 7.9 kbp DNA taken at $F = 0.25$ pN, 0.5 pN, and 2.0 pN. The asymmetric response under rotation to positive and negative turns of single dsDNA tethers can be used as a convenient test of the tether attachment. **b** Force-extension curve for a 7.9 kbp DNA, together with a fit to the worm-like chain model (*solid line*), yielding a fitted contour length $L_C = 2.71$ μm and bending persistence length $L_P = 45$ nm. All measurements were performed in PBS buffer.

Figure 2.3 shows the procedures and results of alignment in the FOMT (Figure 2.1b). The initial (x, y) -excursions recorded in step 2 in Subsection 2.2.3 can be compared to the overall view of fluctuations as a function of the transverse magnet position shown in Figure 2.3a, which shows a “vortex” pattern that can be used to guide subsequent relative displacement between the magnet and DNA-tethered bead held in the FOMT. When subsequent coarse alignment is complete, the bead’s (x, y) -fluctuations trace out a circular trajectory, as is also shown by the black trace in Figure 2.3b. At this point, the torque from the magnets about the z -axis is reduced to the point that thermal fluctuations suffice to rotate the bead around its attachment point. The radius R_{circle} of the resulting circular annulus (fitted circle is shown in red) represents the radial distance between the DNA attachment point and the bead’s center (Figure 2.1b). As shown in Figure 2.3c, however, a histogram of the data in Figure 2.3b shows that coarse alignment does not guarantee uniform coverage of all possible positions along the circular annulus. Even though thermal fluctuations are sufficient to explore all rotations angle on the circle, there remains a small energy barrier (of the order of the thermal energy $k_B T$) to free rotation.

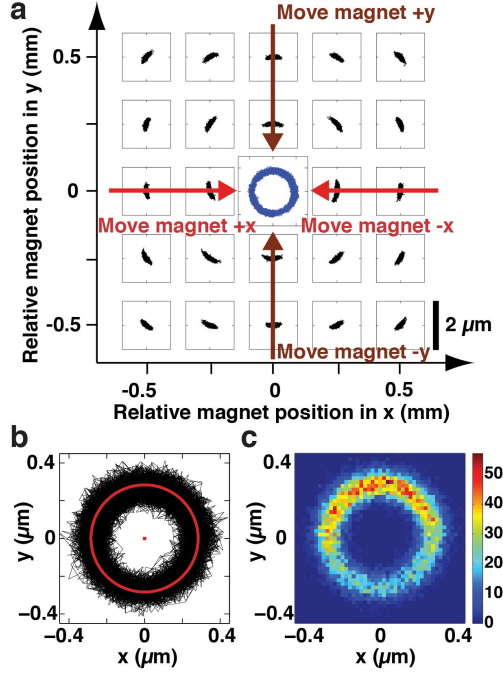


Figure 2.3: Alignment in the FOMT. **a** (x,y) -fluctuations of DNA-tethered bead held in the FOMT as a function of magnet position. The position of the cylindrical magnet was scanned at a constant height of 3 mm across the flow cell surface in steps of $250\ \mu\text{m}$ in x and y and is indicated on the outer plot axes. At each (x,y) -position of the magnet, fluctuations of the same DNA-tethered bead were recorded and are plotted in the small coordinate systems (the scale bar on the bottom right applies to all sub-coordinate systems). Systematic variations of the bead's (x,y) -fluctuation pattern with magnet position resembling a cyclone or vortex are apparent. This “vortex” pattern can be used to guide the displacement of the magnet (or alternatively the tether while keeping the magnet fixed) in x and y (indicated by the *large arrows*) to achieve alignment. When coarse alignment is complete, the bead's (x,y) -fluctuations trace out a circular trajectory (*blue trace* in the center of the plot). This trace was recorded in a separate experiment after aligning the magnets in smaller steps about the center and is shown for illustration in this plot. **b** (x,y) -fluctuations of a DNA-tethered bead held in the FOMT after successful coarse-alignment of the magnet (*black trace*). The fluctuations lie on a circular annulus and thermal fluctuations are sufficient to explore all rotations angles on the circle. A fitted circle is shown in *red*. **c** A histogram corresponding to the data in (b), showing that coarse alignment does not guarantee uniform coverage of all possible positions along the circular annulus. Even though thermal fluctuations are sufficient to explore all rotations angle on the circle, there remains an energy barrier (of the order of the thermal energy $k_B T$) to free rotation.

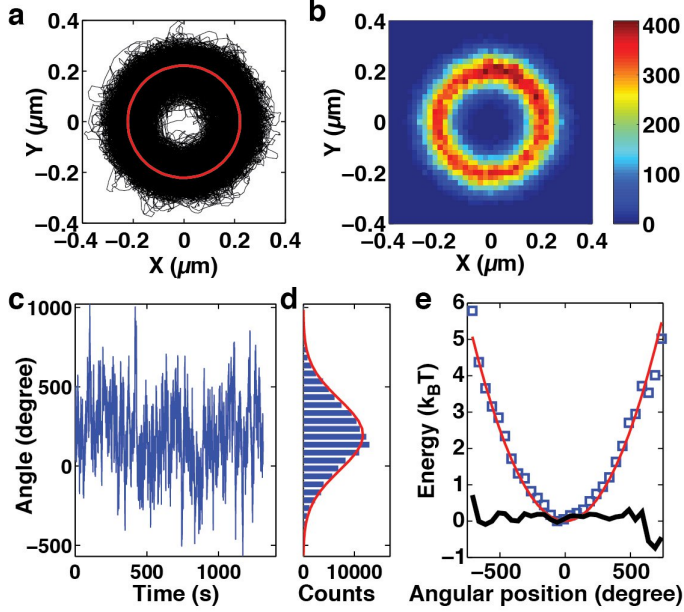


Figure 2.4: Measurement of DNA torsional stiffness using FOMT. **a** (x, y) -trajectory and **b** histogram of a DNA-tethered bead's fluctuations after fine alignment of the relative magnet-tether position in the FOMT. Under these circumstances, the histogram reveals essentially uniform coverage of the positions on the circle. **c** Rotational fluctuations of the bead determined from the (x, y) -positions. **d** Histogram of the rotational fluctuations. The *red line* is a Gaussian fit with $\sigma_\theta = 223^\circ$. **e** The energy landscape implied by the rotational fluctuation density from (c) and (d). The difference between the energy landscape implied by the rotational fluctuations and an harmonic approximation (with $k_\theta = k_B T / \sigma_\theta^2 = 0.27 \text{ pN}\cdot\text{nm}/\text{rad}$) is much smaller than the thermal energy $k_B T$ over several turns. Data are offset for clarity such that $\theta_0 = 0$. The width of the fluctuations can be used to determine the torsional stiffness of DNA, see main text. The measurement was carried out in PBS buffer at a stretching force of $\sim 1 \text{ pN}$. Data are adapted from Lipfert *et al.* [21].

When finer alignment is carried out in the FOMT (step 4 in Subsection 2.2.3), the instrument can be used to determine the torsional modulus of DNA (Figure 2.4). First, fine alignment of the sample is used to obtain circular motion (Figure 2.4a) whose two-dimensional histogram should now show uniform coverage (Figure 2.4b). The corresponding time trace $q(t)$ of angular fluctuations (obtained from conversion of the (x, y) -positions, see below) shows no periodicity corresponding to 360° (Figure 2.4c) and

reveals large excursions corresponding to several full turns (Figure 2.4d). The implied energy landscape is harmonic over a range of $>1,000^\circ$ (Figure 2.4e). The STD of the fluctuations is $\sigma_\theta = 223^\circ$, corresponding to an angular trap stiffness of $k_\theta = k_B T / \sigma_\theta^2 = 0.27 \text{ pN}\cdot\text{nm}/\text{rad}$, which in turn gives an estimate of the effective torsional persistence length of DNA equal to $C = L_C / \sigma_\theta^2 \sim 76 \text{ nm}$ ($L_C = 1,150 \text{ nm}$ for the 3.4 kbp DNA used in this measurement) at the measured force.

An example of how FOMT can be used to measure the change in twist induced into the tethered DNA molecule through the binding of proteins [21, 31] is shown in Figure 2.5. Here, we have monitored the binding of RAD51 protein to dsDNA; RAD51 is known to both lengthen and unwind DNA as it forms a nucleoprotein filament [31]. Upon flushing RAD51 into the flow-cell, we observe that the bead undergoes a spiraling trajectory in the FOMT (Figure 2.5a). By converting trace of (x,y) -motion as a function of time to $q(t)$ as described above, we can co-plot the effect that RAD51 has on the DNA tether length and its degree of unwinding (Figure 2.5b,c).

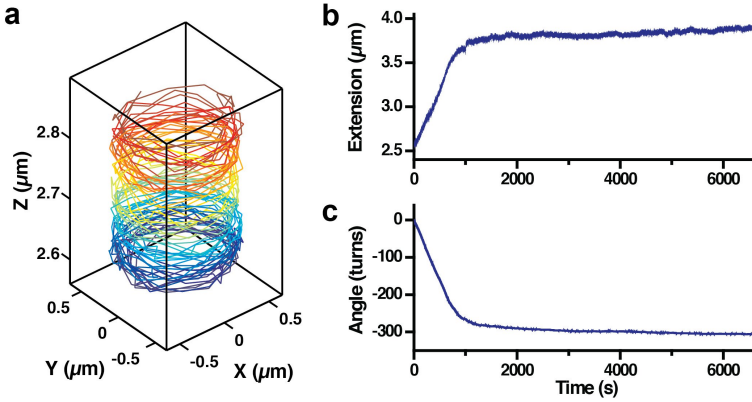
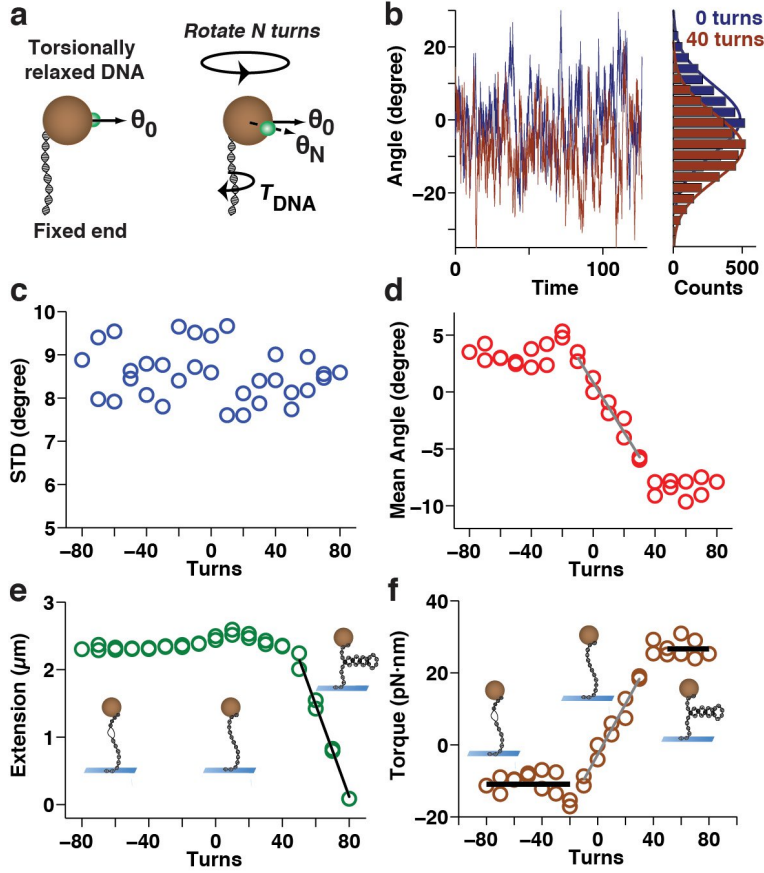


Figure 2.5: The binding of RAD51 protein to DNA measured using FOMT. **a** Assembly of RAD51 protein onto a tethered 7.9 kbp dsDNA monitored at 3.5 pN. The (x,y,z) -trajectory executed by the magnetic bead (diameter 1.0 μm) during the first 200 s of the assembly is shown, with time color-coded from *blue* to *red*. **b** The extension of the dsDNA deduced from the z -component of the bead trajectory in (a) as a function of time. **c** The rotational angle about the dsDNA tether axis deduced from the x,y components of the bead trajectory in (a) as a function of time.

2 Magnetic Tweezers for the Measurement of Twist and Torque



An alternative approach to measuring the torsional properties of DNA are the MTT (Figure 2.1, right; Figure 2.6). The schematic in Figure 2.6a illustrates the principle of the measurement: after overwinding (or underwinding) the DNA tether by N turns, the DNA exerts a restoring torque on the bead that leads to a shift in the equilibrium angular position from θ_0 to θ_N . In the MTT the transverse component of magnetic field is reduced compared to the MT, which facilitates measurement of such angular shifts while still permitting bead rotation (Figure 2.1). The magnitude of the angular shift measured after applying $N = 45$ turns to a 7.9 kbp DNA is shown in Figure 2.6b. The complete sequence of the MTT measurement protocol and the resulting outcome of a torque versus rota-

Figure 2.6: Torque measurements on a single DNA tether in the MTT. **a** Schematic showing the principle of the torque measurement. After over- (or under-) winding the DNA tether by N turns, the DNA exerts a restoring torque on the bead that leads to a shift in the equilibrium angular position from θ_0 to θ_N . **b** Example of angle traces used to measure torque: angular fluctuations of a bead tethered to a torsionally relaxed 7.9 kbp DNA molecule before (*blue*) and after introducing 40 turns (*dark red*). **c-f** Torque measurement on a 7.9 kbp DNA molecule in PBS buffer held at a stretching force of ~ 3 pN using the fiducial marker bead based angular tracking protocol. Angular fluctuations as shown in (b) were recorded as a function of the number of applied turns. **c** The STD of the angular fluctuations as a function of applied turns. The width of the fluctuations is approximately constant, indicating constant angular trap stiffness. **d** The shift in the mean rotation angle as a function of applied turns. Systematic shifts of the mean angle upon over- and underwinding are apparent. **e** The simultaneously monitored DNA tether extension as a function of applied turns. **f** The torque exerted by the DNA tether determined from the mean angle shown in (d), see main text. Over- and underwinding around zero turns gives rise to a linear torque vs. turns response of the DNA-tether (fitted grey slopes in (d) and (f)) that can be used to determine the effective torsional persistence length (~ 77 nm for this data set). Further overwinding leads to buckling and formation of plectonemic supercoils (schematically shown in the insets), corresponding to a torque plateau (*black line* at positive turns in (f) at ~ 26 pN·nm) and a linear decrease of the tether extension with number of turns (*black slope* in (e)). Unwinding beyond the linear regime causes the DNA to locally melt (shown in the insets on the left), marked by a torque plateau equal to the melting torque (*black line* at negative turns in (f) at ~ -11 pN·nm).

tion curve for DNA are shown in Figure 2.6c-f. Here, measurements of the STD (Figure 2.6c) and the mean (Figure 2.6d) of the angular coordinate are shown as a function of over- and underwinding, with the STD being inversely proportional to the angular trap stiffness (Equation 2.1). Taken together, these quantities allow one to construct a torque versus rotation curve for DNA (Figure 2.6f), which should show a linear response region centered about 0 turns and two plateaus at which the torque saturates, at positive and negative rotations, respectively. Such a torque versus rotation curve complements the information in an extension versus rotation curve (Figure 2.6e), thereby quantifying the transitions that accompany the buckling and denaturation of DNA.

2.4 Discussion

When running experiments using the MTT or the FOMT, a number of choices need to be made regarding beads, magnets, tracking protocols, etc. The best choices to be made will depend on the experiment of interest. Below, we describe the trade-offs that accompany different choices, which should facilitate selection for a particular experiment. Next, we describe several critical steps that accompany the alignment and running of MTT and FOMT experiments. Lastly, we discuss the significance of the MTT and FOMT with respect to existing methods as well as future applications.

2.4.1 Considerations prior to start of FOMT and MTT experiments

Any experiment requires one to select a type of magnetic bead for use. One can select between several commercially-available streptavidin-coated superparamagnetic beads, e.g., 0.25- μm -radius beads, 0.5- μm -radius beads, or 1.4- μm -radius beads (see Table 2.1 with the materials). Larger beads will have an increased magnetic moment compared to smaller beads (roughly scaling as the volume) and therefore their use will facilitate the application of higher forces (for typical forces achieved in our instruments, see Table 2.2). When angular tracking using marker beads is desired, we typically work with 1.4- μm -radius and use 0.5- μm -radius non-magnetic biotinylated beads as marker beads (see step 10 in Subsection 2.2.1 for the corresponding attachment protocol). The use of smaller beads is particularly recommended for the FOMT, as the characteristic timescale for bead rotation τ_C equals the ratio of the system's drag over its spring constant γ/k_θ ; importantly, the rotational drag coefficient relevant for the angular measurement time scale scales as $\sim R_{\text{bead}}^3$, i.e. with the third power of the radius (see Table 2.3 for the characteristic time scales for several bead-DNA combinations in FOMT and MTT measurements). Accompanying reductions in the maximum force that can be applied can be addressed by using a flipped stack of cylindrical magnets [27]. Nonetheless, in FOMT measurements it may sometimes be necessary to compromise between the best achievable temporal resolution and the maximum applied force.

Additionally, an experiment requires the selection of a magnet configuration. In the conventional MT configuration (Figure 2.1a, left), we typically use a pair of 5 mm \times 5 mm \times 5 mm cubic magnets in vertical orientation with a 0.5 mm or 1 mm gap between the magnets [4]. When the magnets are spaced along the x (y) axis, this yields a magnetic field that is primarily directed along the x (y) axis. For FOMT experiments, a cylindrically-

shaped magnet is selected at whose center the magnetic field is primarily directed along the z axis (Figure 2.1, center). In practice, we use a stack of three such cylindrically-shaped magnets, each with a diameter of 6 mm and a 2 mm diameter central hole, for a total thickness of 6 mm. When higher pulling forces are desired, a “flipped stack” magnet configuration in which the bottom magnet is stacked with opposite magnetization is preferred. To achieve the MTT configuration (Figure 2.1a, right), we add an additional magnet to the side of the main magnet stack of the FOMT configuration, typically a solid cylinder with 4 mm diameter and a height of 7 mm. To see how the maximal forces achieved in our instruments depend on the magnet configuration, see Table 2.2.

Table 2.2: Maximum forces typically achieved for different magnet configurations and bead types.

MT configuration	M270 ($R_{bead} = 1.4 \mu\text{m}$)	MyOne ($R_{bead} = 0.5 \mu\text{m}$)	Ademtech ($R_{bead} = 0.25 \mu\text{m}$)
Conventional MT (pair of cubic $5 \times 5 \times 5 \text{ mm}^3$, 1 mm gap, vertical alignment)	70 pN	8 pN	1.6 pN
FOMT or MTT* (stack of three cylindrical magnets, 6 mm diameter, 2 mm diameter gap)	9 pN	1 pN	0.2 pN
FOMT or MTT* (stack of three cylindrical magnets, 6 mm diameter, 1 mm diameter gap)	18 pN	2 pN	0.4 pN
FOMT or MTT* (stack of three cylindrical magnets, last one flipped, 1 mm diameter gap)	~ 50 pN	9 pN	1.8 pN

*The presence of the small side magnet in the MTT has a negligible effect on the stretching force

2.4.2 The alignment of FOMT and MTT experiments

Since magnetic beads have an (approximately) uniformly functionalized surface (typically streptavidin) and since the attachment of both the functionalized nucleic acid tethers and marker beads (in case the marker bead-based angular tracking is employed) occurs via simple incubation in solution, one does not control where the tether and/or marker bead attach

to the magnetic bead. The magnetic beads have a preferred magnetization axis that tends to align along the direction of the external field. If we denote the points where the preferred magnetization axis intersects the bead's surface as the north and south poles, then beads where the DNA-tether is attached close to the equator will trace out a circular annulus with a radius close to or slightly larger than the bead radius in the FOMT; in contrast, beads that are attached close to the south pole will fluctuate on a circular annulus with very small radius in the FOMT, which can preclude fitting of the circle using Equations 2.3-2.5. We note that by simple spherical geometry, the probability of attaching near the equator is much larger than an attachment exactly at the poles; therefore, most beads will be tethered such that the (x,y) -based angular tracking can be carried out successfully.

A similar argument holds for the attachment of the marker beads for the fiducial marker based angular tracking. The marker bead is used to create an asymmetry in the image of the magnetic bead that enables angle tracking. If the marker bead is attached exactly at the north or south pole of the bead (i.e. directly on top or on the bottom), the resulting image is still rotationally symmetric and the angular tracking protocol fails. However, by the same spherical geometry argument, the chance for a marker bead to attach directly at one of the poles is relatively small; we find that in practice most marker beads give a sufficient asymmetry to enable angular tracking. Finally, we note that in the conventional MT the field direction is in the (x,y) -plane; therefore, the preferred magnetization axis of the bead will align in the (x,y) -plane and the north and south poles, as defined above, are going to be at the sides of the bead, unlikely the situation in the FOMT or MTT, where the poles are at the top and bottom.

In FOMT experiments, a critical step is the alignment of the cylindrical magnet such that the radial magnetic field is negligible in proximity to the bead. This alignment is performed for a single bead at a time. To judge whether bead motion in the FOMT is evenly distributed over a circular annulus, the measurement time should exceed $20 \cdot \tau_C$. As τ_C equals ~ 45 s for 8 kbp DNA and a $0.5\text{-}\mu\text{m}$ -radius bead, the measurement time is ~ 900 s in the final stages of alignment. For comparison, use of 1.9 kbp DNA and $0.25\text{-}\mu\text{m}$ -radius beads reduces τ_C twenty-fold to ~ 2 s (see also Table 2.3).

Table 2.3: Friction coefficients and characteristic time scales for FOMT and MTT.

Characteristic quantity	M270 $R_{bead} = 1.4 \mu\text{m}$	MyOne $R_{bead} = 0.5 \mu\text{m}$	Ademtech $R_{bead} = 0.25 \mu\text{m}$
Friction coefficient*	120 pN·nm·s	5.5 pN·nm·s	0.7 pN·nm·s
Characteristic time scale FOMT, 10 kbp DNA**	1200 s	55 s	7 s
Characteristic time scale FOMT, 1 kbp DNA	120 s	5.5 s	0.7 s
Characteristic time scale MTT, $k_{q,DNA} = 100 \text{ pN}\cdot\text{nm}/\text{rad}$	1.2 s	0.06 s	0.007 s = 7 ms
Characteristic time scale MTT, $k_{q,DNA} = 1000 \text{ pN}\cdot\text{nm}/\text{rad}$	0.12 s	0.006 s = 6 ms	0.0007 s = 0.7 ms

*Friction coefficient for rotation about an axis through the “equator” (i.e. the situation shown in Figure 2.1b), given by $14\pi\eta R_{bead}^3$, where η is the viscosity of the buffer.

**In the FOMT, the rotational trap stiffness is given by the torsional stiffness of the DNA, $k_{q,DNA} = Ck_BT/L_C$, where C is the effective torsional persistence length, assumed to be 80 nm here (which is characteristic of an intermediate force regime, $F \sim 1 \text{ pN}$) and L_C is the contour length of DNA, 0.34 nm per base pair.

2.4.3 Critical steps and considerations for tracking during FOMT and MTT experiments

To track the bead’s in-plane fluctuations, i.e. its (x,y) -position, we employ a cross-correlation analysis of the intensity profiles displayed by a bead at subsequent time intervals [34, 35]. This can be carried out at sub-pixel resolution to an accuracy of a few nanometers [20]. To track the bead’s motion in z , we typically use a method first designed by Gosse and Croquette, in which the objective’s focal plane (OFP) is accurately shifted in the vertical direction while imaging the diffraction rings of the bead attached to the nucleic acid [20]. In this manner, a calibration profile is generated correlating the diffraction pattern of the bead to the distance between the bead and the OFP [19]. When this calibration profile is interpolated, the vertical displacements of the bead can be also measured with an accuracy of up to a few nanometers [20]. We refer the reader

to additional references that describe more refined tracking algorithms [36, 37] as well as their application to parallel tracking of multiple beads [5, 6, 36].

When using angular tracking that relies on the conversion of (x, y) -positions into angular coordinates, we advise to proceed as follows. From a time trace in which the bead traces out a circular annulus, use the (x_i, y_i) -positions (where the index i denotes subsequent measurement points) to fit the circle center (x_0, y_0) and radius R_{circle} (Figure 2.2a) by minimizing:

$$\min_{x_0, y_0, R_{circle}} (x_i, y_i) = \sum_i \left((x_i - x_0)^2 + (y_i - y_0)^2 - R_{circle}^2 \right)^2, \quad (2.3)$$

where the sum runs over all data points. After fitting x_0, y_0 , and R_{circle} , determine the polar coordinates (r_i, θ_i) of each data point in the time trace using:

$$r_i = \sqrt{(x_i - x_0)^2 + (y_i - y_0)^2} \quad (2.4)$$

$$\theta_i = \arctan \left(\frac{y_i - y_0}{x_i - x_0} \right) \quad (2.5)$$

Note that one should take care to “unwrap” the angle θ , i.e. to add phase jumps of $\pm\pi$ where appropriate. In the FOMT, a time trace in which the bead traces out a circular annulus can be obtained by achieving coarse alignment (cf. step 3 in Subsection 2.2.3) and recording the thermal fluctuations of the bead. In the MTT, thermal fluctuations are insufficient to trace out the circular annulus; instead, use a time trace where the magnets are slowly (typically at 0.1 Hz) rotated by several turns to fit the circle using Equations 2.3-2.5.

We note that for the MTT, it is important to choose the proper angular tracking approach, i.e. via an angular tracking marker (Figure 2.1b-1); Figure 2.3a) or via the conversion of (x, y) -positions into angular coordinates (Figure 2.1b-2); Figure 2.2b). While typically the accuracies of the angular tracking from (x, y) -positions and the use of marker beads are comparable, it is important to realize that crosstalk occurs between a bead’s (x, y) - and in angle-fluctuations, as described in Janssen *et al.* [32]: thus, angular tracking from (x, y) -positions is only valid provided that the Brownian fluctuations in the (x, y) -positions contribute only negligibly to the uncertainty in the angular coordinate, and its proper use of (x, y) -tracking may require tuning of the rotational trap stiffness via adjustment of the position of the side magnet. Typically, the use of higher trap stiffness requires the use of angular tracking using marker beads. The use of marker beads requires an additional attachment step, which may

reduce the number of usable tethers (see the attachment protocol in step 10 in Subsection 2.2.1). When using the marker bead-based tracking, it is important to select magnetic beads which have a marker bead is attached near the equator for best results.

2.4.4 Significance of the FOMT and MTT approaches compared to existing methods and applications

In the above, we have shown how one can, starting from conventional MT, easily modify the magnet configurations to convert the instrument into MTT or FOMT. This straightforward modification, which may be accompanied by the introduction of angular tracking when the use of an angular tracking marker is desired, is an immediate strong point of both configurations, as it permits the user to apply torque, measure torque, or measure twist depending on the experiment at hand. As mentioned in the Introduction, both FOMT and MTT benefit from many of the existing strengths of MT, notably their simplicity, with the MTT in particular also benefiting from the capability of parallel measurements [5, 6] (these are not as easily achieved in FOMT given the requirement of alignment of the tether with respect to the center of the cylindrical magnet). Notably, MTT and FOMT do not require, in contrast with other techniques, specially nano-fabricated particles [22, 38, 39], complex optical design [40], or the introduction of additional beads within the tethered (DNA) molecule [41]. Such other techniques may nonetheless provide other advantages such as higher temporal resolution [27, 42, 43]. Both FOMT and MTT should find future applications in the study of genome processing, as the behavior of molecular motors on DNA is both influenced by and has consequences for the local twist and torque. Additional applications can be found in the emerging field of DNA nanotechnology [27] or in the wider field of rotary motors active in biological processing [7, 44].

2.5 References

- [1] T. R. Strick, J. F. Allemand, D. Bensimon, A. Bensimon, and V. Croquette. *Science* **271**, 1835 (1996).
- [2] C. Bustamante, Z. Bryant, and S. B. Smith. *Nature* **421**, 423 (2003).
- [3] K. C. Neuman and A. Nagy. *Nat. Methods* **5**, 491 (2008).
- [4] J. Lipfert, X. Hao, and N. H. Dekker. *Biophys. J.* **96**, 5040 (2009).

- [5] N. Ribeck and O. A. Saleh. *Rev. Sci. Instrum.* **79**, 094301 (2008).
- [6] I. De Vlaminck, T. Henighan, M. T. J. van Loenhout, I. Pfeiffer, J. Huijts, J. W. J. Kerssemakers, A. J. Katan, A. van Langen-Suurling, E. van der Drift, C. Wyman, and C. Dekker. *Nano Lett.* **11**, 5489 (2011).
- [7] D. A. Koster, A. Crut, S. Shuman, M. A. Bjornsti, and N. H. Dekker. *Cell* **142**, 519 (2010).
- [8] D. Dulin, J. Lipfert, M. C. Moolman, and N.H. Dekker. *Nat. Rev. Genet.* **14**, 9 (2013).
- [9] R. Ajjan, B. C. B. Lim, K. F. Standeven, R. Harrand, S. Dolling, F. Phoenix, R. Greaves, R. H. Abou-Saleh, S. Connell, D. A. M. Smith, J. W. Weisel, P. J. Grant, and R. A. S. Ariëns. *Blood* **111**, 643 (2008).
- [10] C. T. Mierke, P. Kollmannsberger, D. P. Zitterbart, J. Smith, B. Fabry, and W. H. Goldmann. *Biophys. J.* **94**, 661 (2008).
- [11] H. Shang and G. U. Lee. *J. Am. Chem. Soc.* **129**, 6640 (2007).
- [12] H. Shang, P. M. Kirkham, T. M. Myers, and G. H. Cassell, and G. U. Lee. *J. Magn. Magn. Mater.* **293**, 382 (2005).
- [13] G. U. Lee, S. Metzger, M. Natesan, C. Yanavich, and Y. F. Dufrêne. *Anal. Biochem.* **287**, 261 (2000).
- [14] A. S. Smith, K. Sengupta, S. Goennenwein, U. Seifert, and E. Sackmann. *Proc. Natl. Acad. Sci. U.S.A.* **105**, 6906 (2008).
- [15] J. S. Kanger, V. Subramaniam, and R. van Driel. *Chromosome Res.* **16**, 511 (2008).
- [16] M. Tanase, N. Biais, and M. Sheetz. *Methods Cell Biol.* **83**, 473 (2007).
- [17] A. R. Bausch, W. Möller, and E. Sackmann. *Biophys. J.* **76**, 573 (1999).
- [18] J. Lipfert, D. A. Koster, I. D. Vilfan, S. Hage, and N. H. Dekker. *Methods Mol. Biol.* **582**, 71 (2009).
- [19] I. D. Vilfan, J. Lipfert, D. A. Koster, S. G. Lemay, and N. H. Dekker. In: Hintendorfer, P., van Oijen, A. *Handbook of Single-Molecule Biophysics*. Springer, New York, NY (2009)

- [20] C. Gosse and V. Croquette. *Biophys. J.* **82**, 3314 (2002).
- [21] J. Lipfert, M. Wiggin, J. W. J. Kerssemakers, F. Pedaci, and N. H. Dekker. *Nat. Commun.* **2**, 439 (2011).
- [22] A. Celedon, I. M. Nodelman, B. Wildt, R. Dewan, P. Searson, D. Wirtz, G. D. Bowman, and S. X. Sun. *Nano Lett.* **9**, 1720 (2009).
- [23] J. Lipfert, J. W. J. Kerssemakers, M. Rojer, and N. H. Dekker. *Rev. Sci. Instrum.* **82**, 103707 (2011).
- [24] J. Lipfert, J. W. J. Kerssemakers, T. Jager, and N. H. Dekker. *Nat. Methods* **7**, 977 (2010).
- [25] F. Mosconi, J. F. Allemand, D. Bensimon, and V. Croquette. *Phys. Rev. Lett.* **102**, 078301 (2009).
- [26] F. Mosconi, J. F. Allemand, and V. Croquette. *Rev. Sci. Instrum.* **82**, 034302 (2011).
- [27] D. J. Kauert, T. Kurth, T. Liedl, and R. Seidel. *Nano Lett.* **11**, 5558 (2011).
- [28] A. J. te Velthuis, J. W. J. Kerssemakers, J. Lipfert, and N. H. Dekker. *Biophys. J.* **99** 1292 (2010).
- [29] B. M. Lansdorp and O. A. Saleh. *Rev. Sci. Instrum.* **83**, 025115 (2012).
- [30] C. Bouchiat, M. D. Wang, J. F. Allemand, T. Strick, S. M. Block, and V. Croquette. *Biophys. J.* **76**, 409 (1999).
- [31] M. Lee, J. Lipfert, H. Sanchez, C. Wyman, and N. H. Dekker. *Nucleic Acids Res.* **41**, 7023 (2013).
- [32] X. J. A. Janssen, J. Lipfert, T. Jager, R. Daudey, J. Beekman, and N. H. Dekker. *Nano Lett.* **12**, 3634 (2012).
- [33] C. G. Baumann, S. B. Smith, V. A. Bloomfield, and C. Bustamante. *Proc. Natl. Acad. Sci. U.S.A.* **94**, 6185 (1997).
- [34] M. K. Cheezum, W. F. Walker, and W. H. Guilford. *Biophys. J.* **81**, 2378 (2001).
- [35] J. Gelles, B. J. Schnapp, and M. P. Sheetz. *Nature* **331**, 450 (1988).

- [36] M. T. J. van Loenhout, J. W. J. Kerssemakers, I. De Vlaminck, and C. Dekker. *Biophys. J.* **102**, 2362 (2012).
- [37] K. Kim and O. A. Saleh. *Nucleic Acids Res.* **37**, e136 (2009).
- [38] C. Deufel, S. Forth, C. R. Simmons, S. Dejgosha, and M. D. Wang. *Nat. Methods* **4**, 223 (2007).
- [39] Z. Huang, F. Pedaci, M. M. van Oene, M. J. Wiggins, and N. H. Dekker. *ACS Nano* **5**, 1418 (2011).
- [40] A. La Porta and M. D. Wang. *Phys. Rev. Lett.* **92**, 190801 (2004).
- [41] J. Gore, Z. Bryant, M. Nöllmann, M. U. Le, N. R. Cozzarelli, and C. Bustamante. *Nature* **442**, 836 (2006).
- [42] Z. Bryant, F. C. Oberstrass, and A. Basu. *Curr. Opin. Struct. Biol.* **22**, 304 (2012).
- [43] F. C. Oberstrass, L. E. Fernandes, and Z. Bryant. *Proc. Natl. Acad. Sci. U.S.A.* **109**, 6106 (2012).
- [44] S. Forth, M. Y. Sheinin, J. Inman, and M. D. Wang. *Annu. Rev. Biophys.* **42**, 583 (2013).

3 Recent Insights from *In Vitro* Single-Molecule Studies into Nucleosome Structure and Dynamics

Eukaryotic DNA is tightly packed into a hierarchically ordered structure called chromatin in order to fit into the micron-scaled nucleus. The basic unit of chromatin is the nucleosome, which consists of a short piece of DNA wrapped around a core of eight histone proteins. In addition to their role in packaging DNA, nucleosomes impact the regulation of essential nuclear processes such as replication, transcription, and repair by controlling the accessibility of DNA. Thus, knowledge of this fundamental DNA-protein complex is crucial for understanding the mechanisms of gene control. While structural and biochemical studies over the past few decades have provided key insights into both the molecular composition and functional aspects of nucleosomes, these approaches necessarily average over large populations and times. In contrast, single-molecule methods are capable of revealing features of subpopulations and dynamic changes in the structure or function of biomolecules, rendering them a powerful complementary tool for probing mechanistic aspects of DNA-protein interactions. In this chapter, recent insights into nucleosomal and subnucleosomal structures and dynamics from single-molecule studies are presented.

This chapter has been published in O. Ordu, A. Lusser, and N. H. Dekker. *Biophys. Rev.* **8**, 33 (2016).

3.1 Introduction

A major milestone in chromatin research was set about forty years ago, when chromatin was first reported to comprise a repeating unit of ~ 200 bp DNA wrapped around a core of histone proteins [1–3]. This basic component of chromatin, termed the nucleosome, has been a central subject of research ever since. Since their implementation in the 1990s, single-molecule techniques have yielded new, complementary findings on the structure, function and especially dynamics of chromatin and nucleosomes [4–9]. This chapter gives an overview of the recent insights that single-molecule studies have provided into nucleosomal and subnucleosomal structures and dynamics.

3.2 Nucleosome Structure and Dynamics

The basic properties of the nucleosome, as well as the principles of the most commonly used single-molecule techniques and their early results in chromatin research were introduced in Chapter 1. This section concerns major findings on nucleosome structure and dynamics, which were recently made in *in vitro* single-molecule studies.

3.2.1 Intrinsic nucleosome dynamics

The observation of nucleosomes at the single-molecule level have revealed that their structure is intrinsically dynamic. About 30 bp at the entry and exit sites of the nucleosomal DNA were reported to spontaneously unwrap and rewrap on a timescale between 10–300 ms [10–12] (Figure 3.1a). However, until recently this phenomenon of DNA breathing was studied either indirectly with assays using DNA-binding proteins to trap the open nucleosome conformation or directly using methods limited in their specific time resolution for technical reasons. Very recently, the transient unwrapping and rewinding of nucleosomal DNA ends has been identified on a timescale of 1–10 ms using a novel single-molecule technique combining smFRET and FCS with stochastic data analysis based on maximum likelihood estimation (MLE) [13]. This approach enables the study of the structural dynamics of biomolecules on the sub-microsecond timescale considering the photophysical properties of the fluorophores. By this means, this study provided the first direct evidence that DNA breathing is a very fast process. In another recent work, the first experimental evidence for a novel spontaneous transition of nucleosome structure, called

gaping, was reported using smFRET [14]. This phenomenon refers to the transient opening of the two turns of nucleosomal DNA with respect to each other along the superhelical axis (Figure 3.1b). Different labeling schemes were used to study this conformational change associated with an estimated distance change of 0.5–1 nm and a timescale of 1–10 min (Figure 3.1c,d). However, due to technical limitations in terms of resolution owing to the use of FRET and the labeling strategy based on the use of a linker, further high-resolution studies are needed to reveal the details of this phenomenon, including potential structural changes in the histone octamer. Further evidence supporting these recent findings will certainly have strong implications for the role of the intrinsic structural dynamics of nucleosomes as a major mechanism for regulating DNA accessibility in the context of genomic processes.

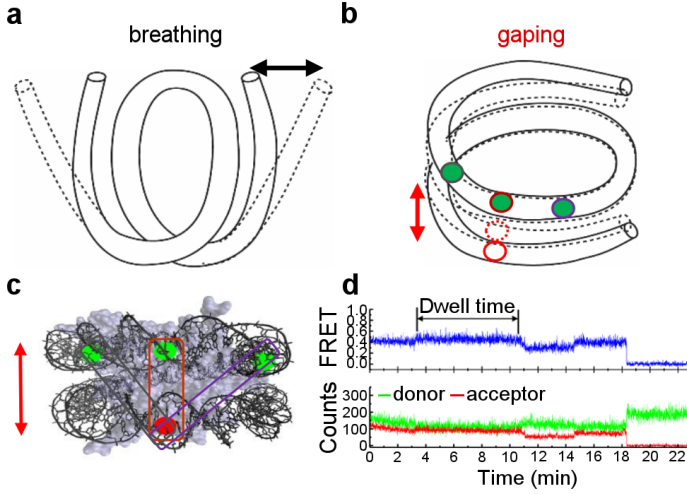


Figure 3.1: Intrinsic nucleosome dynamics. **a** The nucleosomal DNA ends transiently wrap and unwrap from the histone octamer (breathing), indicated by the *black arrow*. **b** The two turns of nucleosomal DNA transiently open with respect to each other along the superhelical axis (gaping), depicted by the *red arrow*. **c** Different labeling schemes to identify the gaping transition which is best characterized by the FRET-pair encircled in *red*. **d** Time-resolved fluorescence signals of the donor (*green*) and acceptor (*red*) fluorophore from the best characterizing FRET-pair are recorded and yield the FRET-efficiency, showing a slight increase over several minutes due to gaping. All panels (a-d) are figures reprinted with minor changes from Ngo and Ha [14], Copyright (2015), used under a [CC BY 4.0 license](#).

3.2.2 The sequence of the nucleosomal DNA

The structural, mechanical and functional properties of nucleosomes have also been suggested to depend on the underlying DNA sequence due to its influence on nucleosome positioning [15]. This notion has provoked high interest in investigating nucleosomal DNA sequences to identify weak and strong nucleosomes and has led to the development of different artificial sequences which have become widely used in *in vitro* studies [16]. Recently, the influence of DNA sequence on nucleosome structure was studied using a single-molecule approach combining smFRET and OT [17]. This assay allowed the simultaneous manipulation and observation of the nucleosome to probe force-induced local conformational changes. Nucleosomes were found to disassemble by asymmetric and directional unwrapping under force, whereby the relative stiffness of different regions of the nucleosomal DNA dictated the unwrapping direction, with a preference for starting from the stiffer side. When the DNA exhibited similar flexibility on both sides, nucleosomes unwrapped stochastically from either side. Both ends further showed an interplay in which the opening of one end stabilized the other, indicating that even small differences in DNA flexibility on either side could lead to an asymmetric stability of the nucleosome. These findings clearly demonstrate the influence of local DNA flexibility, caused by its sequence composition, on nucleosome stability and DNA accessibility. In a more general context, they suggest a new mechanism contributing to the regulation of DNA accessibility by the nucleosomal DNA sequence and its modifications. However, if and to what extent sequence-dependent effects on nucleosomal DNA dynamics play a role for *in vivo* processes awaits future investigation, which will likely be challenging, as many different mechanisms cooperate to influence nucleosome (re)organization in the cell.

3.2.3 Post-translational modification of histones

One well-established mechanism that substantially influences nucleosome structure and dynamics is the post-translational modification (PTM) of the unstructured histone tails protruding from the nucleosome core complex at specific positions [18]. This form of dynamic chemical alteration of the histones mediated by a great number of dedicated enzymes has been shown to change the structural and dynamic properties of nucleosomes by affecting histone-DNA or histone-histone interactions. The best-studied chemical modifications include histone acetylation and phosphorylation. Their effects on nucleosome structural dynamics were studied recently by complementing different biochemical assays with smFRET [19]. Phos-

phorylation of tyrosine 41 and threonine 45 of histone H3 located in the nucleosomal core near the DNA entry-exit sites were found to enhance DNA accessibility by three-fold, as did histone acetylation of lysine 56 in the same region. Remarkably, simultaneous phosphorylation and acetylation were observed to increase DNA accessibility by an order of magnitude. Although DNA accessibility was tested indirectly by a protein-binding assay, which does not allow direct quantification the intrinsic dynamics of nucleosomes, the study still clearly demonstrates the significant effect of PTMs on DNA unwrapping dynamics. In a broader context, these results suggest that particularly PTMs of the globular domains of the histones have the ability to directly affect nucleosome stability by impacting histone-DNA interactions while modulating the ability of the nucleosome to bind regulatory factors. A large and increasing number of identified PTMs awaits further study at the single-molecule level to advance our understanding of nucleosome structure and dynamics [20].

3.2.4 ATP-Dependent remodeling

Complementary to the chemical modification of histones, another mechanism that affects the stability and dynamics of nucleosomes is mediated by enzymes that actively reorganize nucleosome structure. These ATP-dependent chromatin remodelers catalyze changes in nucleosome position and composition by inducing nucleosome sliding or (partial) disassembly/assembly of histones upon ATP-hydrolysis [21]. The nucleosome remodeling process by ACF that contains a catalytic subunit belonging to the ISWI-family and generates uniformly spaced nucleosomal arrays was recently studied in molecular detail using smFRET [22]. This approach allowed for the time-dependent observation of DNA translocation upon remodeling by ACF. Both the linker DNA and the histone H4 tail were found to affect DNA translocation by increasing the pause durations in the remodeling process. The catalytic and accessory subunit of ACF, Snfh2 and Acf1, respectively, were observed to cooperate in detecting the linker DNA with the help of the histone H4 tail. For short linker DNA lengths, Acf1 preferably bound to the N-terminal region of the histone H4 tail, which resulted in autoinhibition of the ATPase activity of Snfh2 while possibly increasing pause durations. With increasing linker DNA lengths, however, Acf1 changed its binding preference towards the linker DNA by releasing the histone H4 tail, which in turn relieved the autorepression mechanism and resulted in activation of the Snf2h ATPase. These results indicate that DNA linker length and the histone H4 tail are important components of nucleosome remodeling by enzymes of the ISWI-family and

suggest a potential regulatory mechanism to direct nucleosome spacing. Many chromatin remodelers of different families have been identified, and the details of their remodeling mechanism still need to be studied [23]. As demonstrated by the results of this study, single-molecule techniques are highly suitable for this purpose. The bigger challenge seems to be the investigation of all mechanisms affecting nucleosome structure and dynamics in combination.

3.2.5 Genome-processing enzymes

In addition to the mechanisms presented above that specifically target nucleosomes, non-specific external events mediated by other factors influence nucleosome structure and dynamics. Certain enzymes have to exert forces and torques in order to perform their tasks in processing the genome. In a recent study, the effect of force and torque on nucleosome structure was investigated using an angular optical trapping method called the Optical Torque Wrench (OTW) [24]. In addition to allowing the manipulation of biomolecules by means of force, this OT-based technique allows the application and measurement of torque [25]. Qualitatively, torque was found to only have a modest effect on nucleosome disassembly. The unwrapping of nucleosomes always followed a distinct two-step pattern, namely, a sudden release of nucleosomal DNA at lower forces (<6 pN) attributed to the outer turns around the H2A/H2B dimers, and another release at higher forces (≥ 6 pN) assigned to the inner turn around the (H3-H4)₂ tetramer. This interpretation and the details of nucleosome unwrapping, however, might need to be reconsidered after the recent observation of asymmetric unwrapping reported above. Quantitatively, however, torque was observed to significantly affect the disruption forces by stabilizing the outer turns and destabilizing the inner turn. Remarkably, the application of positive torque additionally led to a striking loss of H2A/H2B dimers, whereas the (H3-H4)₂ tetramer remains stably bound to the DNA. These findings suggest a potential role of torque and supercoiling in regulating DNA-templated processes by facilitating the removal of the H2A/H2B dimers. More recently, the effect of supercoiling on nucleosome structure was investigated using AFM and FCS [26]. The architecture of the nucleosomes was revealed by AFM imaging, while their stability was studied by measuring the diffusion constants upon salt-induced destabilization using FCS. Nucleosome structure was found to be dependent on the sign and density of superhelical turns. Negative supercoiling resulted in more compact and stable nucleosomes that were resistant to changes in salt concentration. In contrast, nucleosomes reconstituted on either relaxed

or positively supercoiled DNA were observed to be more open and prone to salt-induced disassembly. Destabilization of these nucleosomes, leading to the enhanced eviction of the H2A/H2B dimers, was observed to start at $\sim 600\text{--}800\text{ mM}$ monovalent salt concentration. The $(\text{H3-H4})_2$ tetramer, however, was found to dissociate later at salt concentrations of $>1000\text{ mM}$. These results from the combined approach of imaging and fluorescence spectroscopy clearly demonstrate the significant impact of DNA topology on nucleosome structure and stability and further support the notion of DNA supercoiling as a potential mechanism for regulating the genome by facilitating histone eviction. Investigating structural transitions in the histone octamer itself under torque appears to be a logical next step to reveal more details of the force- and torque-induced disassembly of nucleosomes. The single-molecule approaches, however, need to take into account the biological relevance of all components, such as the range of the applied forces and torques, as well as the salt concentrations used. The regular observation of distinct behavior for the H2A/H2B dimers and the $(\text{H3-H4})_2$ tetramer raises more questions about the architecture and dynamics of subnucleosomal structures which will be discussed in the next section.

3.3 Subnucleosomal Structures and Dynamics

As mentioned above, nucleosomes have been observed to lose their outer H2A/H2B dimers under force, torque or changes in salt concentration, while $(\text{H3-H4})_2$ tetramers remain bound to the DNA. These findings indicate the existence of intermediate nucleosome states, several of which have in fact been reported in different studies [27–30]. The assembly of nucleosomes happens in a stepwise manner through the initial binding of the $(\text{H3-H4})_2$ tetramer to the DNA, followed by the incorporation of the two H2A/H2B dimers [31]. In the absence of DNA but under otherwise physiological conditions, the histone octamer itself dissociates into the $(\text{H3-H4})_2$ tetramer and H2A/H2B dimers [32]. Specific proteins called histone chaperones exist to bind and stabilize histones and to control their interactions for the assembly or disassembly of nucleosomes [33]. These proteins can also alter the composition of nucleosomes by being involved in the replacement of core histones with histone variants which differ in the protein sequence and can affect both histone-DNA and histone-histone interactions to specifically change nucleosome structure and dynamics

[34]. In addition, some histone chaperones contribute to the removal of H2A/H2B dimers during transcription, such as the facilitates chromatin transcription (FACT) complex [35]. Therefore, a reorganization of nucleosomes into substructures seems plausible, even crucial, in the context of chromatin dynamics for regulating DNA-templated processes. Thus, investigating subnucleosomal particles can provide further insight into the structure and dynamics of full nucleosomes.

As a whole, nucleosomes have been found to undergo a conformational transition upon positive torsional stress by changing their ‘chirality’ from a left-handed to a right-handed DNA-wrapping into a reversed nucleosomal structure called reversome [36]. Another nucleosome conformation termed the split nucleosome was recently observed in the form of partial splitting of the H2A/H2B dimers from the (H3-H4)₂ tetramer while remaining bound to the DNA during salt-induced disassembly, with an eventual stepwise release of the H2A/H2B dimers and the (H3-H4)₂ tetramer [37]. Also, passage of the transcription enzyme RNAP II through the nucleosome was found to produce a hexameric subcomplex missing one H2A/H2B dimer, termed a hexasome [38, 39]. The subnucleosomal structure that only contains the (H3-H4)₂ tetramer is called a tetrasome [40]. Tetrasomes were then also found to have the additional, remarkable feature of intrinsically switching between a left-handed and a right-handed ‘chirality’. Thus, tetrasomes constitute an important subnucleosomal structure to study.

The NAP1-mediated assembly of full nucleosomes or tetrasomes was recently investigated in real-time using FOMT and eMTT [41]. These novel MT techniques enable the study of the dynamics and the impact of small, and well-controlled torques on biomolecules [42, 43]. In this study, a bare dsDNA molecule was tethered between the glass coverslip and a magnetic bead that was trapped by a permanent magnet of cylindrical form, with the bead allowed to freely rotate on a circular trajectory (Figure 3.2a). Upon injection of the histones with NAP1, nucleosome assembly occurred instantaneously in steps that were reflected both in the tether’s extension as well as the rotation angle, corresponding to the tether’s twist and writhe (linking number). Nucleosome formation was also achieved by first assembling tetrasomes followed by the incorporation of the H2A/H2B dimers. Interaction with the DNA was not observed for H2A/H2B dimers, whereas they readily bound to previously formed tetrasomes. This observation again confirms the necessity of tetramer binding before the additional incorporation of H2A/H2B dimers. (H3-H4)₂ tetramers assembled instantaneously onto the DNA and remained stably bound for long times, indicating that tetrasomes are viable nucleosomal substructures (Figure 3.2b). Remarkably, tetrasomes were further found

3.3 Subnucleosomal Structures and Dynamics

to spontaneously switch their ‘chirality’ between a preferred left-handed and a less frequently occurring right-handed DNA wrapping, which is referred to as ‘handedness flipping’ (Figure 3.2c). These structural dynamics may explain the significantly delayed accumulation of torque in the DNA tether containing tetrasomes in torque measurements (Figure 3.2d,e). The conversion of tetrasomes from one chirality state to the other by applying weak torques was suggested as the underlying mechanism for this phenomenon. In contrast, this sort of structural dynamics and behavior was not observed for nucleosomes. On the whole, this study provides new insights into the structural dynamics of nucleosomes in the context of substructures, suggesting a potential mechanism to regulate supercoiling during DNA-templated processes by absorbing the generated torque. Very similar results were obtained in a more recent follow-up study with the histone variant H3.3 [44]. Comparable details of the nucleosome assembly and the structural dynamics of tetrasomes containing H3.3 indicate that the incorporation of this variant histone, which in the cell occurs upon histone loss in processes such as transcription, does not give rise to changes in nucleosomal structure and dynamics, but rather may affect other processes such as the recruitment of specific histone chaperones or remodelers.

The dynamics of (sub)nucleosomal structures were also investigated using HS-AFM [45]. This novel technique enables the visualization of the structure and dynamics of biomolecules at acquisition rates of up to 10 Hz or higher [46]. The histone-DNA complexes were either reconstituted by salt-dialysis or assembled using NAP1 and deposited onto a mica substrate for incubation prior to imaging in liquid. Nucleosomes were found to spontaneously disassemble in a fast process on a timescale of 1 s, while tetrasomes underwent several different dynamic changes, such as sliding, hopping between two stable positions involving a change in the ‘handedness’ of the DNA-wrapping and disassembly with the concomitant formation of a DNA-loop that remains stable for minutes. In addition to illustrating the suitability of HS-AFM for probing DNA-protein interactions, this study reveals the highly dynamic nature of (sub)nucleosomal structures which may add an additional layer of flexibility in the accommodation and control of processes such as transcription, replication and repair.

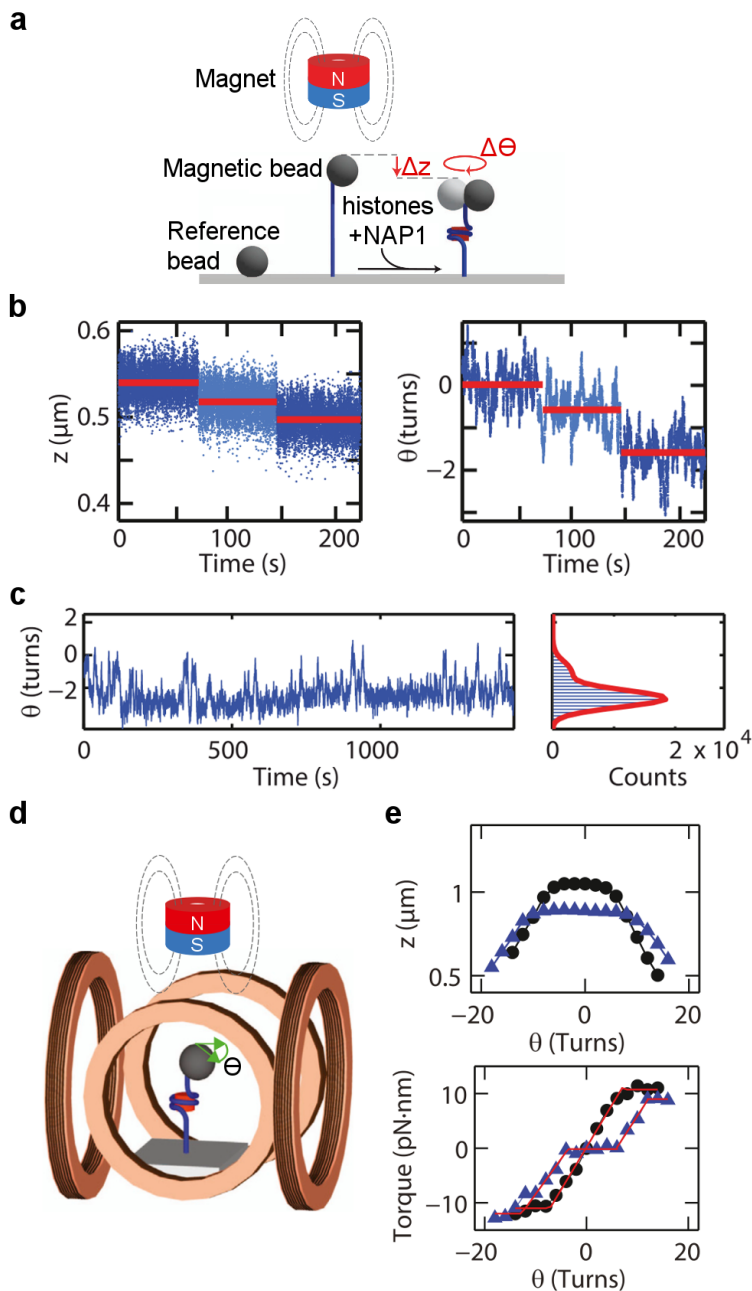


Figure 3.2: Real-time assembly and structural dynamics of tetrasomes.

a A DNA molecule is tethered between a glass coverslip and a magnetic bead trapped by a cylindrical magnet, thereby allowing its free rotation. The injection of histones together with NAP1 yields histone assembly reflected by a decrease in the tether's extension (z , in μm) and the rotation angle (θ , in turns) which is related to the tether's twist and writhe (linking number). **b** The extension and angle time traces show instantaneous changes in a stepwise manner upon tetrasome assembly. **c** The angle time traces of assembled tetrasomes reveal frequent transitions between two distinct linking numbers corresponding to a structural change in their handedness. **d** Two pairs of Helmholtz-coils are used to generate a horizontal magnetic field that is rotated by alternating the applied current to generate precisely controlled torques. **e** The rotation-extension traces of DNA molecules containing tetrasomes (*blue triangles*) show smaller extensions and broadening compared to the traces obtained with bare DNA (*black circles*), indicating assembled tethers and torque absorption, respectively. Torque absorption is verified by the rotation-torque curves revealing an additional plateau for small torques (pN·nm) applied to tetrasomes (*blue triangles*) that is absent with bare DNA (*black circles*). All panels (**a-e**) are figures reprinted or adapted from Vlijm *et al.* [41], Copyright (2015), with permission from Elsevier.

Overall, all nucleosomal (sub)structures and their properties carry significant biological potential in the context of gene regulation during essential cellular processes. There are still many questions left to be answered on their function which could also be explained in the context of other nucleosome-related mechanisms. Single-molecule techniques are a promising tool to advance the research on this topic by the development and application of more complex assays, as described in the next section.

3.4 The Nucleosome as a Barrier

As mentioned above, nucleosomes can act as dynamic mechanical barriers to related DNA-binding proteins and DNA-processing enzymes. Many different processes that influence nucleosome structure, such as intrinsic dynamics and remodeling involving histone chaperones, chromatin remodeling enzymes as well as post-translational modifications, possibly facilitate the overcoming of the barrier. However, the exact mechanisms underlying genome processing through nucleosomes that reveal the fate of colliding enzymes and histones still remain unclear. As the first step of gene expression and one of the crucial processes to maintain cell viability and function, transcription has become a topic of great interest in the

context of nucleosome research at the single-molecule level as well [47, 48]. Mimicking genome processing by unzipping dsDNA molecules containing single nucleosomes using OT revealed the locations and features of histone-DNA interactions at ~ 1 -bp resolution [49]. The 5-bp periodicity of these strong interactions within three broad regions indicates that nucleosomes actually represent a considerable energy barrier to DNA-processing enzymes. This conclusion was further confirmed by several direct studies of transcription through nucleosomes using purified RNAP II in different assays based on the common single-molecule techniques [38, 50–52]. Nucleosomes were found to have a significant effect on the dynamics of RNAP II by locally increasing the density and duration of its pausing, as well as by decreasing their actual (pause-free) velocity [51]. The authors concluded that the changes in polymerase dynamics are governed by fluctuations in nucleosome unwrapping, which would either deny or give the polymerase access to nucleosomal DNA in the closed or open nucleosome conformation, respectively. In addition to increasing the pause density and duration, nucleosomes were also observed to induce backtracking of polymerases. A successive RNAP was, however, found to release the preceding polymerase from backtracking to restart and even continue with elongation at a higher rate [52]. This finding suggests that multiple RNAP II enzymes could cooperatively increase transcription efficiency. The nucleosomal barrier to transcription was further shown to be highly controlled by specific structural elements of the nucleosome [50]. Elimination of the histone tails and destabilization of specific histone-DNA interactions enabled transcription to overcome the nucleosomal barrier more easily. The greater efficiency of transcription observed for weakened histone-DNA interactions shows their essential role in nucleosome stability, while, alternatively, the histone tails could have a significant function in the recruitment and mode of action of specific remodelers. Some details of nucleosomal fate during transcription were revealed by simultaneous imaging of RNAP and nucleosomes at different stages of transcription using AFM [38]. While some nucleosomes did not change their position upon transcription, others were found upstream of their initial location, which was explained by a DNA-looping mechanism for histone transfer. In addition, some of the transcribed nucleosomes showed a smaller size depending on the elongation rate, which was ascribed to the loss of one H2A/H2B dimer during transcription resulting in the formation of a hexamer. These studies have convincingly illustrated how transcription through nucleosomes both requires and causes structural changes that may occur by RNAP-mediated changes in supercoiling and/or the action of the accessory factors, such as histone chaperones, chromatin remodelers and other transcription factors.

Single-molecule research on transcription of nucleosome substrates is now moving towards more complex systems involving additional factors. The effect of nucleosomes on the binding and dissociation of transcription factors (TF) was recently studied using fluorescence microscopy, including smFRET [53]. In this study, dsDNA molecules containing a binding site for either the TF LexA or the TF Gal4 were used to reconstitute nucleosomes which remained intact or were trapped in an open conformation upon TF binding. Monitoring the FRET efficiency allowed the TF binding and dissociation rates to be determined. Nucleosomes were not only found to decrease the binding rate of the TFs by ~ 500 -fold, but also to significantly increase their dissociation rate by ~ 1000 -fold compared to bare dsDNA molecules. These results show that nucleosomes regulate TF access to DNA and propose a possible mechanism for facilitating TF exchange. This regulatory function of the nucleosome may also apply to other DNA-binding proteins.

In another study, the effect of two general transcription elongation factors, TFIIS and TFIIF, on the transcription process of both bare and nucleosomal DNA was investigated using OT [54]. The specific assay comprised a dsDNA molecule directly attached to one bead at its downstream end and tethered to another bead through an RNAP II complex (Figure 3.3a). Depending on the orientation of the DNA molecule, either an opposing or an assisting force could be applied to the RNAP, allowing for complementary insights into the transcription dynamics. Both TFs were added independently or together and were not found to significantly influence the actual (pause-free) elongation rate. However, the TFs did affect the pausing dynamics of the RNAP in a distinct manner (Figure 3.3b). TFIIS reduced the pause duration, while TFIIF decreased both the pause density and duration depending on the force. The same effects also enhanced the progression of RNAP through the nucleosomal barrier (Figure 3.3c). These single-molecule experiments thus helped to pin down the details on the dynamics and the biophysical mechanisms by which TFIIS and TFIIF enact their known positive effects on RNAP II elongation efficiency.

In a very recent study, the effects of nucleosome remodeling by either yeast SWI/SNF or ISW1a on the bound TF Gal4DBD and vice versa were investigated using the above-mentioned OT-based unzipping technique [55]. In this assay, the ssDNA segments of an already partially unzipped dsDNA molecule containing a single nucleosome and a bound TF were tethered between the glass coverslip and a microsphere. The molecules were further unzipped by moving the glass coverslip away from the bead, and the strengths and locations of the nucleosome and the bound TF were simultaneously reflected as peaks in the force-extension traces at

~1 bp resolution. Unzipping molecules after finalized remodeling reactions with either remodeler revealed that a TF represents a considerable barrier to remodeling by ISW1a for nucleosome repositioning. However, the SWI/SNF remodeler could generate nucleosome sliding accompanied by removal of the TF without a significant effect on nucleosome positioning. Interestingly, the nucleosomes were located in opposite directions after remodeling, indicating that both remodelers have distinct roles in nucleosome positioning in the presence of TFs. This study demonstrates a potential mechanism for the regulation of nucleosome remodeling by TFs and vice versa, which could further have a major role in the regulation of transcription in general.

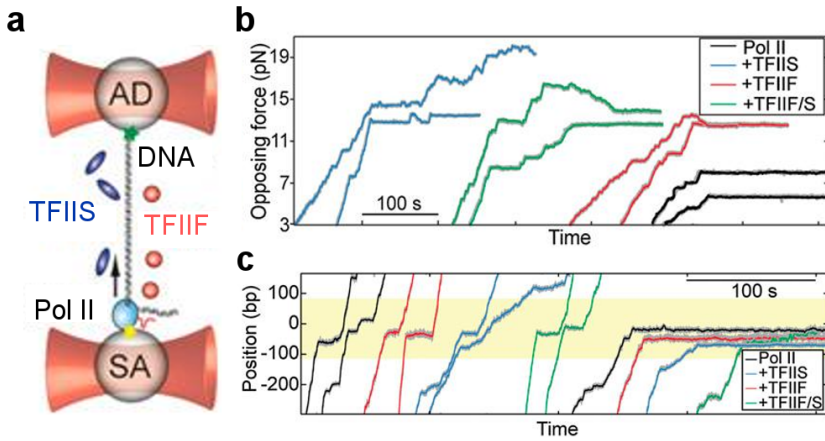


Figure 3.3: Real-time dynamics of RNAP II (Pol II) elongation activity in the presence of transcription elongation factors (TFs). **a** A DNA molecule is attached to an anti-digoxigenin (AD)-coated bead at its downstream end and tethered to another streptavidin (SA)-coated bead through an RNAP II complex with two optical traps. Two different TFs (TFIIS, blue; TFIIF, red) are injected to investigate their effect on transcription dynamics. **b** Time traces of the opposing force (in pN) to the transcribing RNAP II complex reveal facilitated elongation by the TFs individually (TFIIS, blue; TFIIF, red) or together (TFIIF/TFIIS, green) compared to RNAP II alone (black). **c** Time traces of the RNAP position (in bp) along a DNA molecule containing an initially well-positioned single nucleosome (yellow-shaded band) show stimulation of RNAP II processivity (black) through nucleosomes by the TFs individually (TFIIS, blue; TFIIF, red) or together (TFIIF/S, green). All panels (a-c) are figures reprinted with minor changes from Ishibashi *et al.* [54], with permission from PNAS.

In summary, the latest advances of *in vitro* single-molecule research on transcription involving nucleosomes represent a successful next step towards understanding more details of this complex process. The combination of multiple proteins and mechanisms in a crowded environment seems a promising approach to elucidate additional details of this complex fundamental process. The further development of this kind of assays is expected to also finally explain the still striking feature of transcription through chromatin *in vivo* occurring at similar rates to *in vitro* transcription of bare DNA [56].

3.5 Conclusions and Future Perspectives

As the basic packaging unit of chromatin, the nucleosome represents a fundamental DNA-protein complex whose study is required for understanding the organization and regulation of the genome during essential cellular processes. In this context, nucleosomes are not static, but highly ordered and dynamic entities. Their structure and dynamics are continuously altered by different mechanisms involving spontaneous conformational changes, the properties of the underlying DNA, post-translational modifications of the histones, ATP-dependent remodelers, external forces and torques, the incorporation of histone variants, and interactions with histone chaperones and other related proteins.

In this chapter, recent insights were presented, which single-molecule techniques have provided into nucleosome structure, function and dynamics. Studies of individual nucleosomes in a time-resolved manner have revealed transient conformational states on fast timescales, such as breathing and possibly gaping. The structural and chemical properties of the nucleosomal DNA are suggested to influence nucleosome structure and dynamics. Post-translational modifications of histones have been found to significantly affect the intrinsic dynamics and the stability of nucleosomes by altering DNA-histone or histone-histone interactions. More assays have been developed and extended by using other nucleosome-related components, such as histone chaperones and remodeling enzymes, to study their underlying molecular mechanisms and impact on nucleosome (dis)assembly, architecture and dynamics. Various subnucleosomal structures have been identified both *in vivo* and *in vitro* and are believed to play an important role in the regulation of the genome during nuclear processes. Some great insights into the function and fate of the nucleosome as a barrier during DNA-templated processes have been provided by the incorporation of genome processing machineries. Single-molecule studies in the context of histone variants and

replication could provide more insights into (sub)nucleosomal structure and dynamics and possibly reveal new mechanisms to complement current knowledge.

However, as several different mechanisms involving various proteins simultaneously act on nucleosomes in a concerted manner, many questions remain to be answered regarding the details of their interplay (Figure 3.4). A powerful approach seems to be the combination of fluorescence and force spectroscopy techniques, which has already been used to probe various DNA-protein interactions [57]. Further advances in microscopy and sample preparation techniques at the single-molecule level will enable measurements in crowded conditions involving several different components and mechanisms. This will allow the recapitulation of actual biological processes in an environment that approaches *in vivo* conditions. In the vast majority of single-molecule methods for studying nucleosomes, specifically designed and immobilized DNA constructs containing strong nucleosome-positioning sequences, purified, engineered or labeled proteins and non-physiological buffers are used. This allows for a better control of the biological system, but in the end does not reflect the native situation. On the other hand, *in vivo* single-molecule studies that are mainly based on fluorescence microscopy have been very challenging due to specific treatments of live cells and in particular the low spatial resolution. However, recent developments in live cell microscopy towards super-resolution microscopy with highly improved spatial resolution hold great promise for studies of chromatin structure and dynamics *in vivo* [58]. Collectively, the complementary insights from different techniques and assays will allow researchers to put individual parts of the huge puzzle on chromatin structure and dynamics together to advance our understanding of one of the fundamental aspects of life.

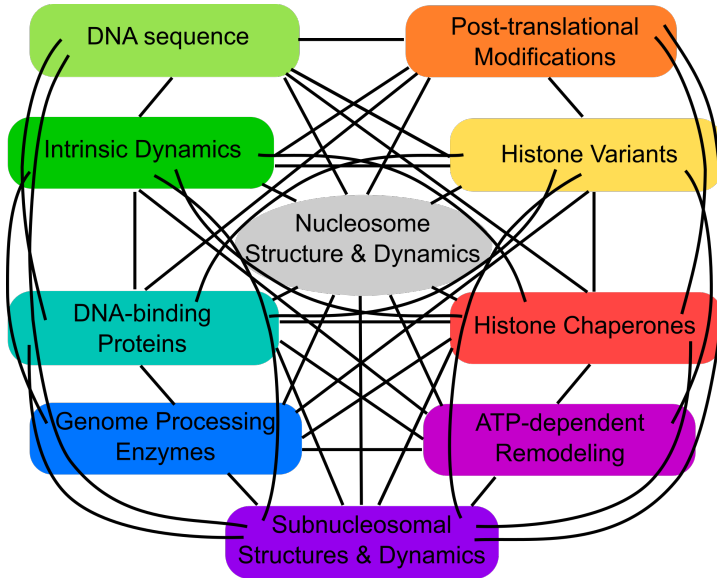


Figure 3.4: Overview of mechanisms influencing nucleosome structure and dynamics. Nucleosomes are intrinsically dynamic (*dark green*) entities, and their structure and dynamics are additionally affected by many different mechanisms, such as sequence and chemical properties of the underlying DNA (*light green*), post-translational modifications of histones (*orange*), the incorporation of histone variants (*yellow*), the interactions with histone chaperones (*red*), ATP-dependent remodelling (*magenta*), the reorganization in subnucleosomal substructures (*violet*) and non-specific external factors like genome processing machineries (*dark blue*) and DNA-binding proteins (*blue/green*). All these mechanisms are coherent and act in a concerted manner (*black lines*).

3.6 References

- [1] R. D. Kornberg. *Science* **184**, 868 (1974).
- [2] A. L. Olins and D. E. Olins. *Science* **183**, 330 (1974).
- [3] P. Oudet, M. Gross-Bellard, and P. Chambon. *Cell* **4**, 281 (1975).
- [4] R. Buning and J. van Noort. *Biochimie* **92**, 1729 (2010).
- [5] J. S. Choy and T. H. Lee. *Trends Biochem. Sci.* **37**, 425 (2012).

- [6] J. L. Killian, M. Li, M. Y. Sheinin, and M. D. Wang. *Curr. Opin. Struct. Biol.* **22**, 80 (2012).
- [7] C. Lavelle, E. Praly, D. Bensimon, E. le Cam, and V. Croquette. *FEBS J.* **278**, 3596 (2011).
- [8] S. J. Petesch and J. T. Lis. *Trends Genet.* **28**, 285 (2012).
- [9] J. Zlatanova and S. H. Leuba. *J. Mol. Biol.* **331**, 1 (2003).
- [10] W. J. A. Koopmans, A. Brehm, C. Logie, T. Schmidt, and J. van Noort. *J. Fluoresc.* **17**, 785 (2007).
- [11] G. Li, M. Levitus, C. Bustamante, and J. Widom. *Nat. Struct. Mol. Biol.* **12**, 46 (2005).
- [12] A. Miyagi, T. Ando, and Y. L. Lyubchenko. *Biochemistry* **50**, 7901 (2011).
- [13] S. Wei, S. J. Falk, B. E. Black, and T. H. Lee. *Nucleic Acids Res.* **43**, e111 (2015).
- [14] T. T. Ngo and T. Ha. *Nucleic Acids Res.* **43**, 3964 (2015).
- [15] J. Widom. *Q. Rev. Biophys.* **34**, 269 (2001).
- [16] E. N. Trifonov and R. Nibhani. *Biopolymers* **103**, 432 (2015).
- [17] T. T. Ngo, Q. Zhang, R. Zhou, J. G. Yodh, and T. Ha. *Cell* **160**, 1135 (2015).
- [18] G. D. Bowman and M. G. Poirier. *Chem. Rev.* **115**, 2274 (2015).
- [19] M. Brehove, T. Wang, J. North, Y. Luo, S. J. Dreher, J. C. Shimko, J. J. Ottesen, K. Luger, and M. G. Poirier. *J. Biol. Chem.* **290**, 22612 (2015).
- [20] A. M. Arnaudo and B. A. Garcia. *Epigenetics Chromatin* **6**, 24 (2013).
- [21] C. R. Clapier and B. R. Cairns. *Annu. Rev. Biochem.* **78**, 273 (2009).
- [22] W. L. Hwang, S. Deindl, B. T. Harada, X. Zhuang. *Nature* **512**, 213 (2014).
- [23] S. K. Hota and B. Bartholomew. *Biochim. Biophys. Acta.* **1809**, 476 (2011).

- [24] M. Y. Sheinin, M. Li, M. Soltani, K. Luger, and M. D. Wang. *Nat. Commun.* **4**, 2579 (2013).
- [25] A. La Porta and M. D. Wang. *Phys. Rev. Lett.* **92**, 190108 (2004).
- [26] T. Elbel and J. Langowski. *J. Phys. Condens. Matter* **27**, 064105 (2015).
- [27] A. J. Andrews and K. Luger. *Annu. Rev. Biophys.* **40**, 99 (2011).
- [28] C. Lavelle and A. Prunell. *Cell Cycle* **6**, 2113 (2007).
- [29] K. Luger, M. L. Dechessa, and D. J. Tremethick. *Nat. Rev. Mol. Cell Biol.* **13**, 436 (2012).
- [30] J. Zlatanova, T. C. Bishop, J. M. Victor, V. Jackson, and K. van Holde. *Structure* **17**, 160 (2009).
- [31] S. E. Polo and G. Almouzni. *Curr. Opin. Genet. Dev.* **16**, 104 (2006).
- [32] K. Luger. In: eLS. John Wiley & Sons Ltd, Chichester (2001).
- [33] Z. A. Gurard-Levin, J. P. Quivy, and G. Almouzni. *Annu. Rev. Biochem.* **83**, 487 (2014).
- [34] P. B. Talbert and S. Henikoff. *Nat. Rev. Mol. Cell Biol.* **11**, 264 (2010).
- [35] D. Reinberg and R. J. Sims. *J. Biol. Chem.* **281**, 23297 (2006).
- [36] A. Bancaud, G. Wagner, N. Conde e Silva, C. Lavelle, H. Wong, J. Mozziconacci, M. Barbi, A. Sivolob, E. Le Cam, L. Mouawad, J. L. Viovy, J. M. Victor, and A. Prunell. *Mol. Cell* **27**, 135 (2007).
- [37] V. Böhm, A. R. Hieb, A. J. Andrews, A. Gansen, A. Rocker, K. Toth, K. Luger, and J. Langowski. *Nucleic Acids Res.* **39**, 3093 (2011).
- [38] L. Bintu, M. Kopaczynska, C. Hodges, L. Lubkowska, M. Kashlev, and C. Bustamante. *Nat. Struct. Mol. Biol.* **18**, 1394 (2011).
- [39] M. L. Kireeva, W. Walter, V. Tchernajenko, V. Bondarenko, M. Kashlev, and V. M. Studitsky. *Mol. Cell* **9**, 541 (2002).
- [40] M. Alilat, A. Sivolob, B. Revet, and A. Prunell. *J. Mol. Biol.* **291**, 815 (1999).

- [41] R. Vlijm, M. Lee, J. Lipfert, A. Lusser, C. Dekker, and N. H. Dekker. *Cell Rep.* **10**, 216 (2015).
- [42] X. J. A. Janssen, J. Lipfert, T. Jager, R. Daudey, J. Beekman, and N. H. Dekker. *Nano Lett.* **12**, 3634 (2012).
- [43] J. Lipfert, M. Wiggin, J. W. J. Kerssemakers, F. Pedaci, and N. H. Dekker. *Nat. Commun.* **2**, 439 (2011).
- [44] R. Vlijm, M. Lee, O. Ordu, A. Boltengagen, A. Lusser, N. H. Dekker, and C. Dekker. *PLoS One* **10**, e0141267 (2015).
- [45] A. J. Katan, R. Vlijm, A. Lusser, and C. Dekker. *Small* **11**, 976 (2015).
- [46] T. Ando, T. Uchihashi, and N. Kodera. *Annu. Rev. Biophys.* **42**, 393 (2013).
- [47] M. Dangkulwanich, T. Ishibashi, L. Bintu, and C. Bustamante. *Chem. Rev.* **114**, 3203 (2014).
- [48] S. S. Teves, C. M. Weber, and S. Henikoff. *Trends Biochem. Sci.* **39**, 577 (2014).
- [49] M. A. Hall, A. Shundrovsky, L. Bai, R. M. Fulbright, J. T. Lis, and M. D. Wang. *Nat. Struct. Mol. Biol.* **16**, 124 (2009).
- [50] L. Bintu, T. Ishibashi, M. Dangkulwanich, Y. Y. Wu, L. Lubkowska, M. Kashlev, and C. Bustamante. *Cell* **151**, 738 (2012).
- [51] C. Hodges, L. Bintu, L. Lubkowska, M. Kashlev, and C. Bustamante. *Science* **325**, 626 (2009).
- [52] J. Jin, L. Bai, D. S. Johnson, R. M. Fulbright, M. L. Kireeva, M. Kashlev, and M. D. Wang. *Nat. Struct. Mol. Biol.* **17**, 745 (2010).
- [53] Y. Luo, J. A. North, S. D. Rose, and M. G. Poirier. *Nucleic Acids Res.* **42**, 3017 (2014).
- [54] T. Ishibashi, M. Dangkulwanich, Y. Coello, T. A. Lionberger, L. Lubkowska, A. S. Ponticelli, M. Kashlev, and C. Bustamante. *Proc. Natl. Acad. Sci. U.S.A.* **111**, 3419 (2014).
- [55] M. Li, A. Hada, P. Sen, L. Olufemi, M. A. Hall, B. Y. Smith, S. Forth, J. N. McKnight, A. Patel, G. D. Bowman, B. Bartholomew, and M. D. Wang. *Elife* **4** e06249 (2015).

- [56] M. G. Izban and D. S. Luse. *J. Biol. Chem.* **267**, 13647 (1992).
- [57] J. C. Cordova, D. K. Das, H. W. Manning, and M. J. Lang. *Curr. Opin. Struct. Biol.* **28**, 142 (2014).
- [58] M. Lakadamyali and M. P. Cosma. *FEBS Lett.* **589**, 3023 (2015).

4 Comparing the Assembly and Handedness Dynamics of (H3.3-H4)₂ Tetrasomes to Canonical Tetrasomes

Eukaryotic nucleosomes consist of an (H3-H4)₂ tetramer and two H2A-H2B dimers, around which 147 bp of DNA are wrapped in 1.7 left-handed helical turns. During chromatin assembly, the (H3-H4)₂ tetramer binds first, forming a tetrasome that likely constitutes an important intermediate during ongoing transcription. We recently showed that (H3-H4)₂ tetrasomes spontaneously switch between a left-handed and right-handed wrapped state of the DNA, a phenomenon that may serve to buffer changes in DNA torque induced by RNAP in transcription. Within nucleosomes of actively transcribed genes, however, canonical H3 is progressively replaced by its variant H3.3. Consequently, one may ask if and how the DNA chirality dynamics of tetrasomes is altered by H3.3. Here we report real-time single-molecule studies of (H3.3-H4)₂ tetrasome dynamics using FOMT and eMTT. We find that the assembly of H3.3-containing tetrasomes and nucleosomes by the histone chaperone NAP1 occurs in an identical manner to that of H3-containing tetrasomes and nucleosomes. Likewise, the flipping behavior of DNA handedness in tetrasomes is not impacted by the presence of H3.3. These data demonstrate that the incorporation of H3.3 does not alter the structural dynamics of tetrasomes, and hence that the preferred incorporation of this histone variant in transcriptionally active regions does not result from its enhanced ability to accommodate torsional stress, but rather may be linked to specific chaperone or remodeler requirements or communication with the nuclear environment.

This chapter has been published as R. Vlijm, M. Lee, O. Ordu, A. Boltengagen, A. Lusser, N. H. Dekker, and C. Dekker. *PLoS One* **10**, e0141267 (2015).

4.1 Introduction

The DNA in eukaryotic nuclei is substantially compacted by histone-induced packaging. The basic unit of compaction is the nucleosome: 147 bp of DNA that are wrapped 1.7 times around a histone octamer [1, 2]. The octamer is built up of two copies each of the core histones H2A, H2B, H3 and H4. All four families of core histones are highly positively charged with a conserved C-terminal histone fold domain and unique N-terminal tails [3]. The histone fold domains interact strongly with the other core histones within the nucleosome, and with the nucleosomal DNA. The tails do not display significant intra-nucleosomal contacts, but instead interact with neighboring nucleosomes and other proteins (e.g. remodelers). Nucleosomes are stabilized by the opposite charges of the histones and DNA backbone, but do not spontaneously assemble at physiological salt conditions [4]. Binding of histones to DNA occurs in a prescribed order, with each step being facilitated by a chaperone loading protein: first the (H3-H4)₂ tetramer binds to the DNA to form a tetrasome, and then two H2A-H2B dimers are added to form the complete nucleosome. The (H3-H4)₂ tetramer, also relevant in the biological context e.g. as a result of H2A-H2B dimer loss during transcription [5–9], has a horseshoe-shaped structure that includes an H3-H3 interface at its center [1, 10].

Packaging of DNA into nucleosomes affects the accessibility of DNA in important processes like transcription and replication. As such, the structure, number, position, and stability of nucleosomes impact multiple nuclear processes. To regulate DNA accessibility, chromatin remodeling proteins can assemble and evict nucleosomes, alter nucleosome position, or induce structural changes to histones or histone replacement [11]. Additionally, there exist many histone variants, which, play specific roles either through their unique positioning on the genome [3, 12–14] or by acting during specific phases of the cell cycle, serve as a ‘toolbox for genome regulation’. The *Drosophila melanogaster* genome encodes three H3 histone variants. These are the canonical H3 (H3.2 [15]) histone, which is only expressed during S phase when the DNA is replicated; the main replacement histone H3.3 [16, 17], which differs from H3 by only four amino acids; and the CENP-A (CID) variant, which is only located in centromeric regions and structurally deviates more from the other H3 histone variants [18]. Focusing specifically on the differences between H3.3 and canonical H3, three of the differing amino acids lie in α -helix 2 of the histone fold domain, while the fourth lies in the N-terminal region (Figure 4.1; [3]). Unlike H3, H3.3 is not restricted to S phase but is instead expressed and loaded onto chro-

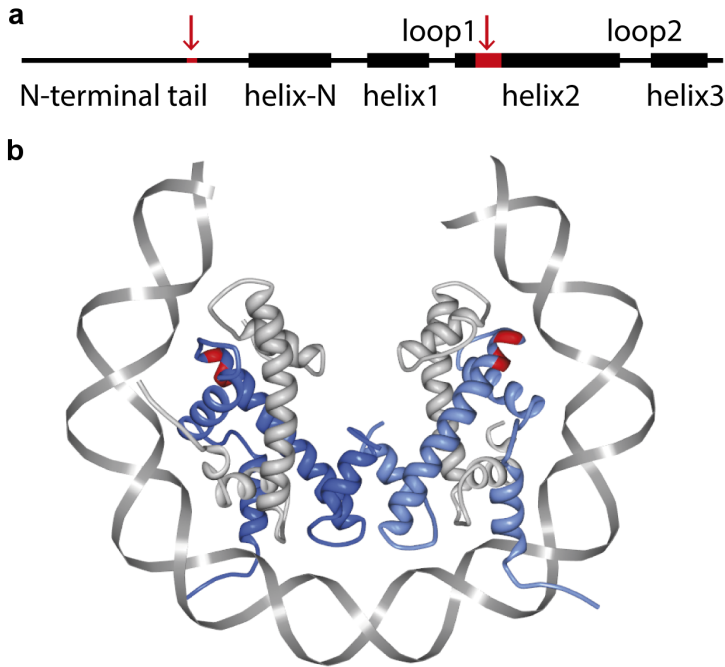


Figure 4.1: Domains and illustration of the (H3.3-H4)₂ tetrasome. **a** The *Drosophila* H3 and H3.3 vary by only four amino acids that are marked in red. One is located in the N-terminal tail domain and three are located in the α -helix 2 domain, at locations 87, 89 and 90 (after [3]). **b** The crystal structures for H3-H4 and H3.3-H4 tetrasomes are not known, but to illustrate the most likely configuration, we here show a visual rendering of the structure of the human nucleosome containing the histone variant H3.3 (3AV2 from PDB). Only histones H3.3 (*blue*) and H4 (*gray*) are shown, as well as part of the nucleosomal DNA (*gray*). The amino acid locations 87, 89 and 90 are marked in red to indicate the region that deviates from the canonical histone H3 in the histone fold domain. The amino acid variant in the N-terminal tail is not marked, since it is outside of this region. This image was created using the software described in Ref. [19].

matin throughout the entire cell cycle, predominantly at transcriptionally active regions [20]. Additionally, H3.3 has recently been located at silent chromatin loci such as telomeres and centromeres [21], and it appears to be required for male fertility [22]. It has been shown that replacement of any one of the three different amino acids in the histone-fold domain of H3 by the corresponding H3.3 counterpart results in replication-independent

deposition of the histone [20]. Since the three histone-fold domain amino acids are located at the surface of the α -helix 2 domain that is responsible for the formation of H3-H4 dimers and accessible in prenucleosomal complexes [23, 24], it has been suggested that the specificity associated with these amino acid positions derives from interactions with different assembly or post-translational-modification machineries. From a structural perspective, however, nucleosomes that contain canonical H3 or H3.3, appear to be very similar [24]. These findings highlight the importance of subtle differences between H3 and H3.3 and call for studies of potential underlying mechanistic differences.

We recently demonstrated that canonical (H3-H4)₂ tetrasomes are highly dynamic [7], finding that they exhibit spontaneous flipping between a preferentially occupied left-handed DNA wrapping and a less favored right-handed wrapping. Only upon addition of H2A/H2B is the left-handed state locked in and are full nucleosomes formed [7]. The handedness-flipping mechanism was proposed to involve a rotation of the two H3/H4 dimers with respect to each other at the H3-H3 interface, thus making H3 one of the key players in this process [10]. The remarkable torsional flexibility of tetrasomes led us to propose that tetrasomes might function as a twist reservoir under conditions of torsional stress, such as during transcription and replication [9].

During transcription, histone H3.3 (as opposed to H3) is incorporated into nucleosomes. To support transcription, chromatin fibers containing H3.3 nucleosomes tend to be less condensed [20, 25–27]. We aim to investigate whether tetrasomes and nucleosomes containing H3.3 have a different structure and structural stability compared to canonical tetrasomes/nucleosomes. Possibly, H3.3 tetrasomes/nucleosomes are less compacted, and any significant energy barrier between the left-handed and right-handed tetrasome states or an increased overall preference for a right-handed state could hinder the formation of left-handed nucleosomes. Using FOMT [28] we directly monitored both the real-time NAP1-mediated assembly of individual (H3.3-H4)₂ tetrasomes onto bare DNA and the subsequent dynamics. For further characterization, we also investigated the torsional response of tetrasomes using eMTT [29]. We find that the changes in DNA compaction and chirality upon assembly of H3.3-H4 containing tetrasomes and nucleosomes by the histone chaperone NAP1 occur in a manner identical to that of H3-containing tetrasomes and nucleosomes. Likewise, the flipping behavior of H3.3-containing nucleosomes is similar to that of canonical tetrasomes. Flushing out free NAP1 and histones in solution only slightly enhanced the positively wrapped state of the tetrasome.

4.2 Materials and Methods

4.2.1 Single-molecule instrumentation

The traces monitoring NAP1-assisted nucleosome and tetrasome assembly in real time via changes in extension and linking number, as well as any subsequent dynamics in linking number, were measured using FOMT [28]. The torque measurements were carried out using the eMTT [29]. All measurements were performed at 21°C and acquired at an acquisition frequency of 100 Hz.

4.2.2 Protein expression and purification

Recombinant *Drosophila* core histones were expressed in *E. coli* BL21(DE3) Rosetta (Novagen) and purified as described in Ref. [30], with the distinction that the purification procedure for the H3.3-H4 tetramers was identical to that of the H2A/H2B dimers. Expression plasmids were a kind gift of J. Kadonaga. Concentrations of core histones were determined by SDS-PAGE and Coomassie staining as well as calculated from A280 measurements and the H3-H4 extinction coefficient (Figure 4.S1 in the Supplementary Information). Recombinant *Drosophila* NAP1 was purified according to Ref. [31].

4.2.3 Flow cell passivation and buffer conditions

In all experiments, we employed a buffer consisting of 50 mM KCl, 25 mM Hepes-KOH (pH 7.6), 0.1 mM EDTA, 0.025% PEG and 0.025% PVA as crowding agents, and 0.1 mg/ml BSA both as crowding agent and for the prevention of nonspecific binding of histones to the surface. For the tetrasome assembly we used the histone chaperone NAP1. Although *in vivo* NAP1 is known as a histone chaperone for H2A and H2B, *in vitro* it has been shown that NAP1 assembles complete nucleosomes [7, 32–36]. The used protein concentrations were: 200 nM NAP1, 67 nM H3.3 and 67 nM H4 were preincubated for 30 min on ice. The pre-incubation buffer contained 50 mM KCl, 25 mM Hepes-KOH (pH 7.6), 0.1 mM EDTA, 0.25% PEG, 0.25% PVA and 1 mg/ml BSA. Just prior to flushing in, the protein concentration was reduced ~4000-fold. To achieve nucleosome assembly following tetrasome formation, 270 nM NAP1, 268 nM H2A, 268 nM H2B were preincubated for 30 min on ice. Just before flushing in, the protein concentration was reduced ~300-fold.

4.2.4 DNA constructs

We used 1.9 kbp dsDNA molecules in the FOMT experiments and 3.4 kbp DNA molecules in the eMTT experiments, both without positioning sequences (see Figures 4.S2 and 4.S3 in Supplementary Information). To attach the DNA molecules to the glass surface and the bead, their extremities contained multiple digoxigenin molecules at one end and multiple biotin molecules at the other end. The DNA molecules did not contain any nucleosome-positioning sequences. In the FOMT experiments, we used 0.5- μ m-diameter beads (Ademtech) and in the eMTT experiments we used 0.7- μ m-diameter beads (MagSense).

4.3 Results and Discussion

4.3.1 NAP1-assisted assembly of (H3.3-H4)₂ tetrasomes

We directly monitored tetrasome formation upon flushing in H3.3 and H4 pre-incubated with the histone chaperone NAP1 into the flow cell using FOMT, a technique that allows one to simultaneously measure dynamical changes in the end-to-end length and linking number of single tethered DNA molecules. In this approach, a vertically oriented magnetic field is used to apply a stretching force, without constraining the free rotation of the DNA molecule (Figure 4.2a). The DNA molecules employed (1.9 kbp in length) did not contain specific nucleosome-positioning sequences. We limited the applied stretching force to 0.8 pN, well below the 3 pN above which DNA begins to peel off from the nucleosome [37]. Upon flushing in NAP1/histone complexes, this experimental configuration allowed us to observe a distinct, stepwise decrease in the end-to-end length z of the DNA, indicating compaction, accompanied by a clockwise rotation θ of the bead, reflecting a decrease in the linking number of the DNA tether (left panels in Figures 4.2b and 4.2c). From several independent (H3.3-H4)₂ assembly experiments, we obtained an average extension change $\langle \Delta z \rangle = -25 \pm 6$ nm (Figure 4.2b, right) and linking number change $\langle \Delta \theta_{assembly} \rangle = -0.8 \pm 0.2$ turns (Figure 4.2c, right). By changing the histone concentration, we assembled varying numbers of tetrasomes per DNA molecule. The total degree of compaction Δz and the overall change in linking number $\Delta \theta_{assembly}$ following assembly were found to be linearly correlated with a slope $\Delta z / \Delta \theta_{assembly}$ of 32 ± 2 nm/turn (Figure 4.2d). These single-molecule assembly experiments revealed that NAP1 is capable of assembling (H3.3-H4)₂ tetrasomes. The obtained average exten-

sion change $\langle \Delta z \rangle = -25 \pm 6$ nm for assembly of $(\text{H3.3-H4})_2$ tetrasomes agrees well with previous results on canonical tetrasomes and nucleosomes [7, 36, 37], indicating that the alterations in the histone fold domain of H3.3 do not affect the overall tetrasome structure formed. The linear correlation between the total degree of compaction Δz and the overall change in linking number $\Delta \theta_{\text{assembly}}$ following assembly indicated that the conformation of the tetrasomes on the DNA is independent of the number of protein complexes assembled, excluding large effects of inter-tetrasomal interactions.

4.3.2 Spontaneous changes in the linking number of $(\text{H3.3-H4})_2$ tetrasomes

We also carried out a separate set of experiments to determine whether there were further dynamics to be observed on the single-molecule tethers following assembly. For reference, bare DNA has a constant length z and linking number θ , apart from Brownian fluctuations (Figures 4.3a and 4.3b). Following the assembly of a single $(\text{H3.3-H4})_2$ tetrasome (which compacted the DNA by 22 ± 1 nm), the resulting reduced DNA length z stayed constant (Figures 4.3a and 4.3c, left panels). Concomitant with the step in z , a step in the linking number of -0.81 ± 0.25 turns occurred (Figures 4.3a and 4.3c, right panels). However, subsequently the linking number did not stay constant but was rather observed to change between -0.80 ± 0.05 and $+0.86 \pm 0.39$ turns (Figures 4.3a and 4.3c, right panels). From this, we concluded that $(\text{H3.3-H4})_2$ tetrasomes exhibited spontaneous flipping between a preferentially occupied left-handed state and a right-handed state in a manner that left the DNA extension unchanged. On average, the $(\text{H3.3-H4})_2$ tetrasome showed spontaneous fluctuations in the linking number with a typical $\Delta L_k = 1.68 \pm 0.14$ turns, a mean change in linking number very similar to that observed for the canonical tetrasome [7].

To determine whether this flipping tetrasome could accommodate the assembly of a complete nucleosome, we subsequently added histones H2A-H2B (see Section 4.2). This led to a decrease in the mean linking number by 0.55 ± 0.25 turns in a single step, together with an arrest of the flipping behavior (Figure 4.3d, right). The total amount of compaction due to the assembly of the H2A-H2B was 31 nm. Adding histones H2A-H2B thus led to the assembly of a left-handed nucleosome with a total linking number of -1.36 ± 0.2 turns and total compaction of 54 ± 7 nm. We find that the handedness of nucleosomes containing only H3.3 remained stable.

4 Assembly and Handedness Dynamics of $(H3.3-H4)_2$ Tetrasomes

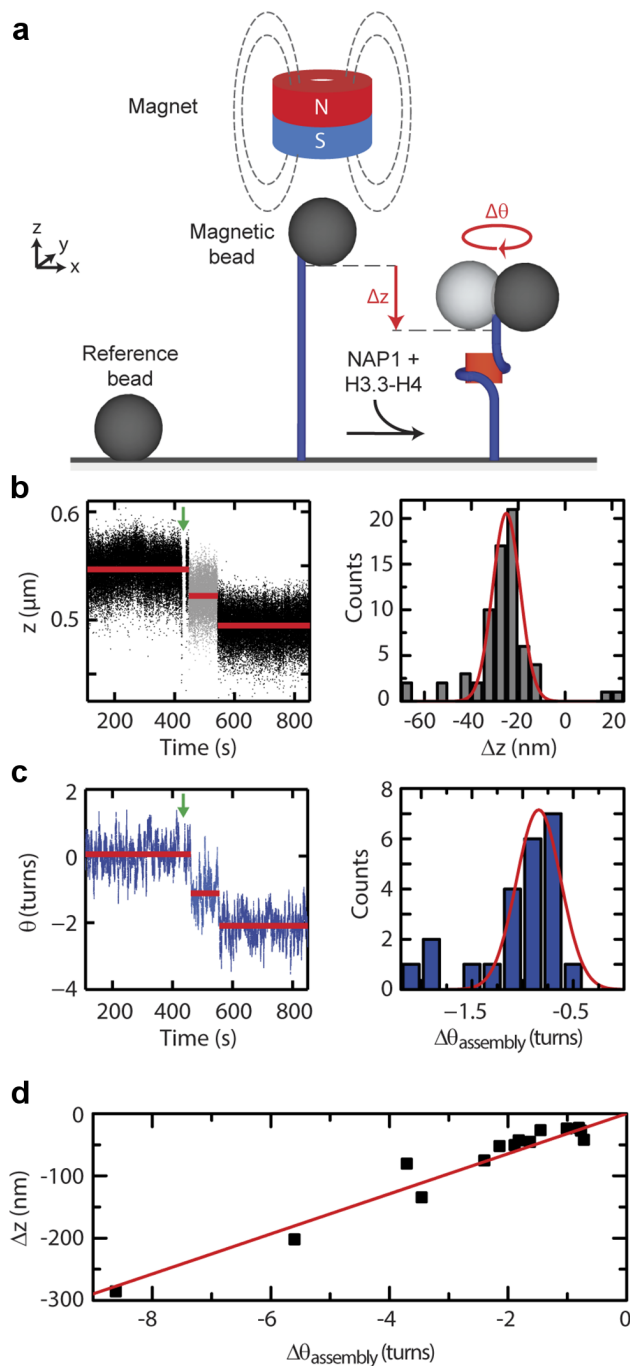
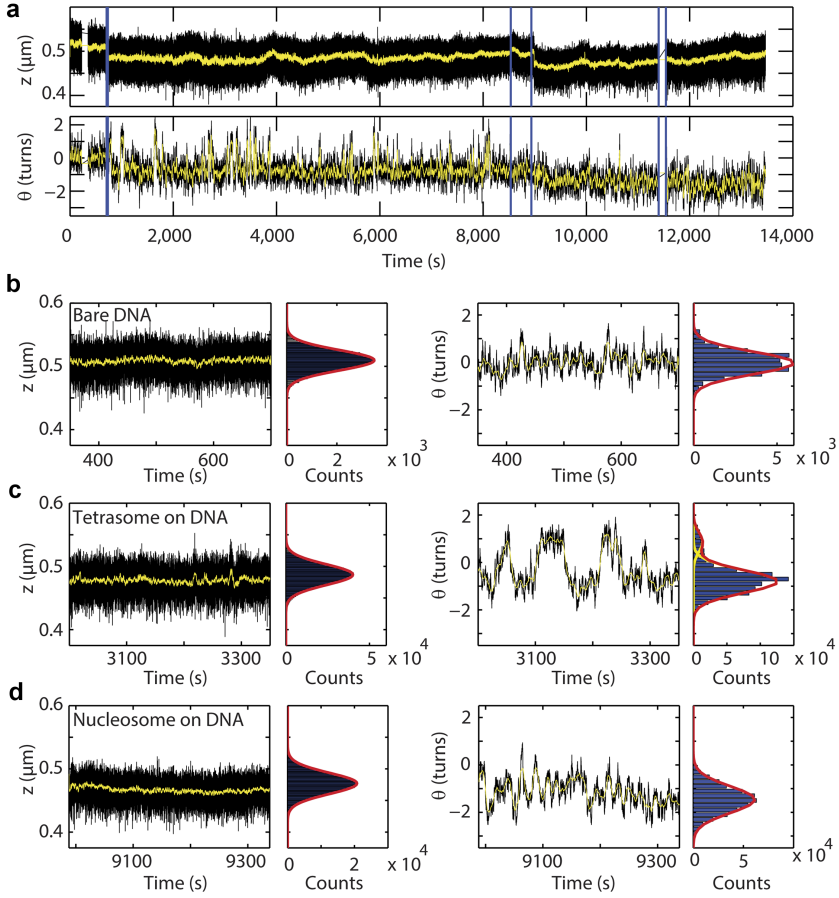


Figure 4.2: NAP1-assisted (H3.3-H4)₂ tetrasome assembly. **a** Schematic of the *in vitro* assay showing a single DNA molecule (*blue*) tethered between a glass surface and a paramagnetic bead. The circular magnet above the bead applies a stretching force to the bead (and hence to the DNA), but leaves it free to rotate about the DNA-tether axis. A non-magnetic reference bead is fixed to the surface to allow for drift correction. After flushing in NAP1 preincubated with histones H3.3-H4, tetrasomes are loaded onto the DNA. **b** Time-dependence of the end-to-end length z (in μm) (left) of a single DNA tether during the assembly of two (H3.3-H4)₂ tetrasomes. The step sizes are -25 and -27 ± 5 nm. The *green arrow* at $t = 420$ s indicates the flushing in of the proteins. Data was acquired at 100 Hz, and *red lines* indicate the mean values of each assembly step. The histogram on the right derives from 19 independent assembly experiments (69 steps). A Gaussian fit shows that the average step in z during tetramer assembly is -25 ± 6 nm. **c** Time-dependence of bead rotations θ (in turns) (left) of the same DNA tether as in (b). Compaction of the DNA (shown in (b)) occurs concurrently with a change in linking number (θ). The step sizes in θ are -1.17 ± 0.24 and -0.97 ± 0.24 turns. The *green arrow* at $t = 420$ s indicates the flushing in of the proteins. Data was acquired at 100 Hz, and *red lines* indicate the mean values of each assembly step. The histogram on the right derives from 15 independent assembly experiments (23 steps). It can be fitted to Gaussian peaks. The most likely step in θ during tetramer assembly is -0.8 ± 0.1 turns. A small number of steps appears to result from the simultaneous assembly of two tetramers, with a mean step size in θ of -1.9 ± 0.1 turns. **d** The total degree of compaction (Δz) plotted versus the total change in linking number ($\Delta\theta_{\text{assembly}}$) on 25 individual DNA molecules following the assembly of tetrasomes (*black squares*). Fits to a linear relationship yield $\Delta z / \Delta\theta_{\text{assembly}} = 32 \pm 2$ nm (*solid red line*).

We observed flipping signatures in the linking number for every DNA molecule that was loaded with H3.3-containing tetrasomes (but never for bare DNA nor for nucleosome-loaded DNA). A second example of a single tetrasome is shown in Figure 4.4a, whereas the behavior of four assembled tetrasomes, together with cartoons illustrating the number of tetrasomes in the left-handed and right-handed configuration, is shown in Figure 4.4b. To exclude any potential effect of NAP1 on the dynamics of (H3.3-H4)₂ tetrasomes, we also performed an experiment in which we removed the free proteins. Under these conditions, DNA molecules with tetrasomes, both for conditions with (*black*) and without (*gray*) free proteins in solution, displayed similar-sized angular steps between the discrete levels, $\langle \Delta\theta_{\text{flipping}} \rangle = 1.6 \pm 0.1$ turns (Figure 4.4c). These results, taken together with a similar independence of flipping dynamics on NAP1

4 Assembly and Handedness Dynamics of $(H3.3-H4)_2$ Tetrasomes

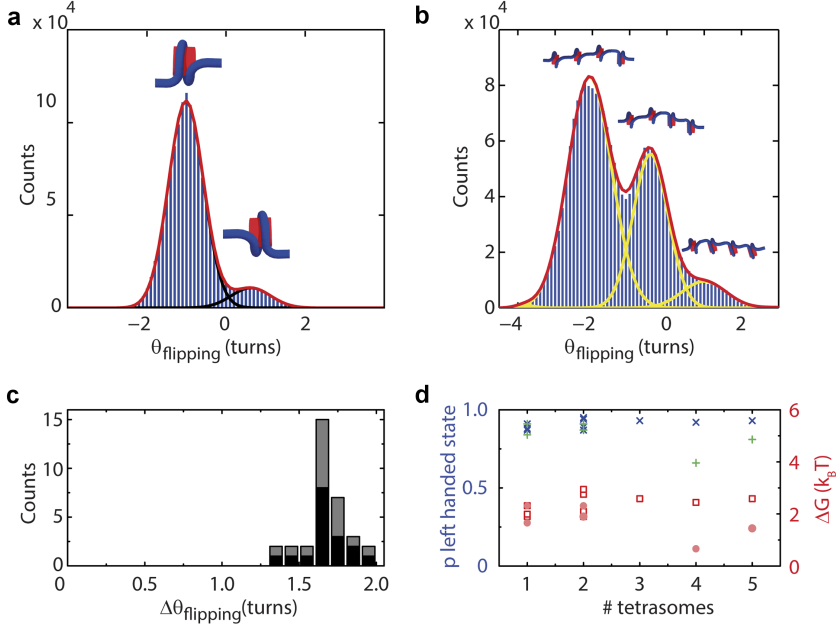


observed for canonical tetrasomes assembled by salt dialysis [7], leads us to conclude that NAP1 does not induce the change in handedness of the $(H3.3-H4)_2$ tetrasomes. Collectively, these experiments show that the inherent flipping behavior of the handedness of tetrasomes is not limited to H3-containing tetrasomes, but also applies to tetrasomes that contain H3.3. Moreover, they demonstrate that the dynamically flipping $(H3.3-H4)_2$ tetrasome is a viable intermediate in the assembly of stable, left-handed, nucleosomes. The flipping of the canonical tetrasomes loaded onto DNA by NAP1 can be analyzed in the framework of a binomial model in which a single tetrasome occupies either the left-handed or right-handed state with probabilities p and $(1 - p)$, respectively [7].

Figure 4.3: (H3.3-H4)₂ tetrasomes undergo dynamic changes in linking number and form a viable intermediate for nucleosomes. a Assembly of a single complete nucleosome from a single assembled tetrasome. By flushing in H3.3-H4 preincubated with NAP1 at $t = 708$ s, we assembled one tetrasome ($\Delta z = 23 \pm 5$ nm, $\Delta\theta_{assembly} = -0.81 \pm 0.25$ turns). Dynamic changes in the linking number were observed immediately following assembly and continued for ~ 8000 s. When we then flushed in histones H2A and H2B preincubated with NAP1 at 8536 s and 8935 s, we observed an additional assembly step ($\Delta z = 31 \pm 5$ nm and $\Delta\theta = -0.55 \pm 0.25$ turns). Subsequently, the linking number remained stable (i.e. the flipping behavior of the handedness ceased). *Blue lines* mark flushing in of NAP1 and core histones H3.3-H4 at $t = 708$ s and of H2A-H2B at $t = 8536$ s and $t = 8935$ s. All proteins are flushed out at $t = 11400$ s. Parts of the data shown in (a) are highlighted in panels (b)–(d). The left panels show a typical segment (350 s) of the end-to-end length z (left) and the angular coordinate θ (right). Side panels show histograms with fits to Gaussian functions (*red lines*) that are derived from the full portion of the trace acquired under the indicated conditions. **b** Bare DNA, before the proteins are flushed in. **c** DNA loaded with a single tetrasome. The centers of the Gaussian fits are at -0.80 and 0.86 turns. **d** DNA loaded with a single nucleosome. In (b)–(d), the mean extension, z , remains constant in time, with fluctuations merely arising from Brownian motion (STDs of $\sigma_{bare\ DNA}$, $\sigma_{tetrasome}$, and $\sigma_{nucleosome}$ are 23 nm). Both bare DNA and DNA loaded with nucleosomes exhibit a fixed mean linking number in time, with comparable fluctuations about the mean ($\sigma = 0.66$ turns and 0.77 turns, respectively). However, tetrasomes exhibit clear fluctuations in the linking number over time.

A value of p close to 1 indicates that tetrasomes are much more likely to occupy the left-handed state over the right-handed state, whereas a shift towards lower values of p indicates a more positively wrapped tetrasome. For each experiment, we determined the relative occupancies of each state from the ratios of the respective peak areas in the linking number histograms. We fitted p for distinct DNA molecules loaded with different numbers of tetrasomes resulted in a $\langle p \rangle = 0.91 \pm 0.03$ ($N = 12$) in the presence of free proteins (Figure 4.4d, *dark blue crosses*). Using $\Delta G = -k_B T \ln(1/p - 1)$ to compute the free energy difference between the left-handed and right-handed states, we deduced a free energy difference between the left-handed and right-handed states of $2.3 \pm 0.4 k_B T$ (Figure

4 Assembly and Handedness Dynamics of $(H3.3-H4)_2$ Tetrasomes



4.4d, *dark red squares*), similar to the $2.3 k_B T$ value found for canonical tetrasomes and the $2.5 k_B T$ value determined via electrophoretic mobility analysis of nucleosome populations [5, 7]. We note that that we measured a slightly reduced probability for the occupancy of the left-handed state $\langle p \rangle = 0.84 \pm 0.09$ ($N = 7$) after flushing out free proteins (Figure 4.4d, *green plus signs*), corresponding to a decreased free energy difference between the states of $1.6 \pm 0.8 k_B T$ (Figure 4.4d, *filled pink circles*). Flushing out of the proteins thus mildly increases the probability to occupy the right-handed state of the $(H3.3-H4)_2$ tetrasome. This finding, together with the observation that $\Delta\theta_{\text{flipping}}$ is unaffected by the removal of free proteins, suggests that NAP1 may stimulate the left-handed wrapping slightly while leaving the linking number of the left-handed and right-handed states unchanged.

Figure 4.4: Analysis of changes in linking number of (H3.3-H4)₂ tetrasomes. **a** A single (H3.3-H4)₂ tetrasome (for a different molecule than that of Figure 4.3, to emphasize repeatability). The histogram of $\theta_{flipping}$, the difference in angle between the left-handed and right-handed states from a single (H3.3-H4)₂ tetrasome, shows two peaks. The peak has a maximum at $\theta = -1.011 \pm 0.003$ turns. The positively wrapped state has a peak at $\theta = 0.63 (\pm 0.03)$ turns. **b** Histogram of $\theta_{flipping}$ of a DNA molecule loaded with four tetrasomes. Data are collected after flushing out free proteins. The most pronounced peaks are for 1 ($\theta = -2.1$ turns), 2 ($\theta = -0.44$ turns) and 3 ($\theta = 1.0$ turns) tetrasomes in the right-handed state (values extracted from Gaussian fitting to the histogram). When any one tetrasome flipped to the right-handed state, the linking number increased on average by 1.7 ± 0.2 turns. **c** Histogram of dynamical linking number steps observed following assembly of tetrasomes on distinct DNA molecules ($N = 10$) before (*black*) and after (*gray*) flushing out free proteins ($N = 33$), which yields a mean value of $\langle \Delta\theta_{flipping} \rangle = 1.7 \pm 0.1$ turns both before and after flushing out of free proteins. **d** Determination of the probability p of finding a tetrasome in the left-handed state in the presence ($N = 12$, *dark blue crosses*, $\langle p \rangle = 0.91 \pm 0.03$) and absence ($N = 7$, *green plusses*, $\langle p \rangle = 0.84 \pm 0.09$) of free proteins. Using the formula $\Delta G = -k_B T \ln((1/p) - 1)$, the difference in the free energy between the two states can be computed (*red datapoints*). We deduce $\Delta G = 2.3 \pm 0.4 k_B T$ prior to flushing out free proteins (*red open squares*) and $\Delta G = 1.6 \pm 0.8 k_B T$ following the flushing out of free proteins (*red filled circles*).

4.3.3 Structural transitions within (H3.3-H4)₂ tetrasomes by minute torques

We next studied the response of (H3.3-H4)₂ tetrasomes to physiologically relevant applied torques [38] at an applied stretching force of 0.8 pN by using eMTT [29] (Figure 4.5a). For these experiments, we utilized 3.4 kbp DNA (again without specific nucleosome-positioning sequences) loaded with tetrasomes by NAP1. Reference measurements on bare DNA showed that the application of turns to torsionally relaxed bare DNA initially left the DNA extension unchanged as the DNA twist increased, resulting in a linear build-up of torque (Figure 4.5b, *black squares*). At a critical buckling torque, a decrease in the DNA extension z was observed as DNA buckled to form plectonemic supercoils, and beyond this, no further torque build-up occurred (plateau in black squares for >6 turns and <-6 turns in Figure 4.5b). The torque response following NAP1-mediated assembly of ~ 5 (H3.3-H4)₂ tetrasomes (deduced from the total length decrease of 135 nm given the average length decrease of 25 nm per tetrasome, Figure 4.2b) is shown

in Figure 4.5b. Starting at positively induced supercoiling, the torque response was first measured from +17 turns to -17 turns (red triangles). Consecutively, the measurement direction was reversed (*green diamonds*). At the center of both torque response curves, a plateau at nearly zero torque was clearly visible. In this region, the induced turns did not lead to build up of twist (and hence torque) in the tethered molecule; instead, changes in the tetrasome conformation likely occurred that prevented such build-up. Alternately stated, a negligibly low torque could be used to drive a tetrasome into a left-handed configuration (when negative turns were imposed) or into a right-handed configuration (when positive turns were imposed). The widths of the near-zero torque plateaus for the negative (*red*) and positive (*green*) rotation directions were 7.5 ± 1.0 and 5.9 ± 1.0 turns, respectively (Figure 4.5b). Therefore the $\Delta L_k/\text{tetrasome}$ in the plateaus is 1.5 and 1.2 for the negative and positive rotation direction respectively. Once a sufficient number of turns was applied to force all tetrasomes to occupy either left- or right-handed states, torque build-up ensued as in the case of bare DNA. Finally, saturation of torque build-up occurred beyond a torque of +10 (-12) pN·nm (accompanied by a concomitant decrease in extension, consistent with plectoneme formation), also similar to the case of bare DNA.

We briefly examine the regions in which torque is built up for DNA loaded with tetrasomes (Figure 4.5b). In all cases, these slopes are shallower than those measured for bare DNA; this could reflect gradual changes in the conformation of the loaded tetrasomes. An example of this would be a change in the angle of the tetrasome's entry and exit DNA. Additionally, the torque response curves display hysteresis: neither the slopes of the torque response nor the widths of the plateaus around zero rotations are identical upon reversal of the direction of rotation. From the constant length of the molecule (data not shown), we can conclude that this hysteresis is not induced by tetrasome dissociation/rebinding events. Instead, it appears that the induced conformational changes from right-handed to left-handed tetrasomes is more gradual than vice versa.

For example, for the molecule shown in Figure 4.5 we expect that ~ 5 tetrasomes have been assembled as deduced from the length decrease upon assembly. We therefore expect the width of the zero-torque plateau to comprise $5 \times (\theta_{\text{flipping}} =) 1.7 = 8.5$ turns (Figure 4.4c). Given the measured plateau widths of 7.5 turns (from negative to positive rotations) and 5.9 turns (from positive to negative rotations), it appears that 0.2–0.5 turns per tetrasome are absorbed by more gradual conformational changes that occur as the magnitude of the torque in the tetrasome-loaded DNA is decreased. Summing up, these experiments directly demonstrate that the

application of only very weak positive torques can drive tetrasomes from left-handed into right-handed states. Furthermore, the torque response displays hysteresis as a function of the direction of rotation, indicating that the sudden conformational changes as shown by handedness flipping at low torques (e.g., conformational change at the H3.3-H3.3 interface as suggested in Ref. [18]) are accompanied by more gradual conformational changes (e.g., due to slight changes in direction of the entry and exit DNA) under the influence of torque at increased levels of torque.

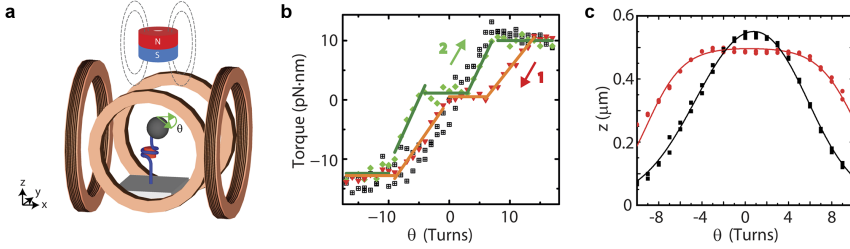


Figure 4.5: Torque response of DNA loaded with $(\text{H3.3-H4})_2$ tetrasomes. **a** Diagram of the eMTT configuration used in these experiments. The eMTT resembles the FOMT configuration, but additionally has two pairs of Helmholtz coils placed around the flow cell to permit the application of torque in the horizontal plane. **b** The torque stored in DNA loaded with 5 tetrasomes plotted as a function of the number of applied rotations, θ . The *black squares* represent the data for a bare DNA molecule, prior to assembly. Following assembly, the torque response of DNA loaded with tetrasomes is measured by decreasing the number of applied turns from +17 to -17 (*red triangles*, labeled by ‘1’). Consecutively, the torque response of DNA loaded with tetrasomes is measured in the opposite direction by increasing the number of applied turns -17 to +17 (*green diamonds*, labeled by ‘2’). The *solid lines* are segmented fits to the plateau regions (with slope 0) and to the sloped regions in which torque is built up. The widths of the plateaus for positive (*red*) and negative (*green*) rotation directions are 7.5 ± 1 turns and 5.9 ± 1 turns, respectively, as determined from the intersections between the segmented fits. The applied force is ~ 0.8 pN. **c** The DNA end-to-end length plotted as a function of the number of rotations, θ . The applied stretching force is 0.3 pN. The *black squares* show the data for a bare DNA molecule, prior to any tetrasome assembly. Following tetrasome assembly, a broad plateau (of $\sim 8 \pm 1$ turns) is observed surrounding 0 turns (*red circles*). The *solid lines* are linear fits to the data (5 per trace).

4.4 Discussion and Conclusion

The influence of DNA topology, specifically transcription-induced supercoiling, on gene regulation is an emerging topic of interest. It has been suggested that nucleosome assembly and disassembly processes, through their modification of the local degree of supercoiling, can play important roles in gene regulation on distances exceeding several kilo-base pairs [39–43]. In this research, we have found that canonical (H3.1-H4)₂ and variant (H3.3-H4)₂ tetrasomes exhibit similar behavior in both their assembly and subsequent dynamical changes in linking number. A comparison of all measured parameters for these two types of tetrasomes is shown in Table 4.1. Furthermore, both types of tetrasomes are viable intermediates for nucleosomes. We find that the overall number of assembled (H3.3-H4)₂ tetrasomes does not affect the change in linking number per tetrasome under our experimental conditions, from which we conclude that the assembly is not affected by inter-nucleosomal interactions. Once assembled, (H3.3-H4)₂ tetrasomes exhibit flipping in their chirality under the influence of thermal fluctuations that is similarly independent of the number of assembled tetrasomes and comparable to the case of canonical tetrasomes. The ease of flipping tetrasome handedness is also displayed by the appearance of a near-zero torque plateau in the torque response of DNA assembled with tetrasomes, similar to the previously studied (H3-H4)₂ tetrasomes. The additional hysteresis in the torque-turns curve indicates that mild gradual changes to the tetrasome structure also occur. The collective similarity with the results obtained for canonical (H3-H4)₂ tetrasomes demonstrates that the incorporation of H3.3 does not change the biophysical properties of tetrasomes. Therefore, the presence of H3.3 in transcriptionally active regions does not signal an enhanced ability to accommodate torsional stress, but may rather be linked to specific chaperone or remodeler requirements or communication with the nuclear environment.

Table 4.1: Comparison of the key physical properties measured for tetrasomes composed of (H3-H4)₂ (left; Ref. [7]) versus (H3.3-H4)₂ (right; this work).

Quantity	(H3-H4) ₂ tetrasomes	(H3.3-H4) ₂ tetrasomes
Δz	-24 ± 3 nm	-25 ± 7 nm
$\Delta\theta_{assembly}$	-0.73 ± 0.05 turns	-0.8 ± 0.1 turns
Δz (total)	34 ± 1 nm/turn	32 ± 2 nm/turn
$\Delta\theta_{assembly}$ (total)		
$\Delta\theta_{flipping}$	1.7 ± 0.1 turns	1.7 ± 0.1 turns
p before flush out	0.90 ± 0.08	0.91 ± 0.03
p after flush out	-	0.84 ± 0.09
Binomial distribution	Yes	Yes
Viable nucleosome intermediate	Yes	Yes
Structural transition under minute torques	Yes	Yes

4.5 Supplementary Information

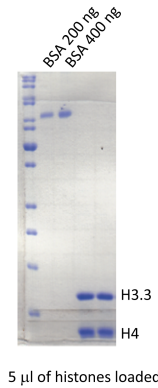


Figure 4.S1. Protein gel of the used H3.3 and H4 histones. The gel indicates 140 µg/ml of each histone.

TGCCGTTGTAACCGGTTCATCCCGAGTACGGCTGCAGCGCCCGCTCCGGCTGACCAGCGTGCCGGA
CACCGGCAGCAGCGCGATGCCGTTTCATGACCTGATAACTGCGGGCTGTCTGGTCCGTCATCATCA
CCGGATAATGCCAGCGTCGCGAGTGCCTCCTGGGCAGTCAGGCTGTCGCCGGACACCGCATCCGTCA
GGCTGTGATCCCAAGCTGGCCTGCAAGCGCACAAAAGAAAACCCGCGCATAGCGGGTTCAAGCA
TCAGCGGCTCATTAAGGCCATGCTGGCAATATGCGGGAGATTACGCAGCTCTGTGCTCACTTTCTC
CTCCTCTGTTGATTGTCGAGCCCGGATTCAAATGCTGCAGCCGCCAGCGGGCGGTTTAAAGACCG
GCTGCACGGCGCTCCATCGTTTCACGGACCTGCTGGGCAAAATTTCTGATAGTCGTACCCGCGTTT
TGGGCACTCTTTCTCGTAGGTACTCAGTCCGGCTTCTATCAGCATACCGGCTTCTGAACTCTTTCAG
ACCATCGATGGCCATACGACCGGAGCCTATCCAGTGCAGTTCCCCAGGCACTGCGGGCTTCTGGA
AACTGAAGCGCGCTTTTGAAGGTAACGTCACACGCGGCGAACGATGGCCTTTCCAGCCAGCACA
GAAACATCTGGCTCGCTGACGGGATGCGACGAATTTTCGCCGCCCATAAAGTACGCCACGACTC
GTTTCGCACTGGCCGTGCCGTGGAGTAGCTCATCTGGGCGTAATTCGGGAAAGCTGCTCATACGAG
ACACCCAGCCCGGCGAGCGATATACCGCAGCAGTGAAGTCTCAAACACGGAGTAGCCGTTATCCGAT
CCTGAGCCGTCTGCAGGTTCACTGAGTCACCGGCATCAGGTGCGGTACTTTTGCAGCTCCAGCGG
GACCGCGCTGCGGCGTAATACGCGGCAATTTACCAATCCAGCGGTCAGCCTTTCCCGCTGCTCCT
GACTGTTGCGGCCAGATAAAATCCATCGTGAAGTCTGCTGATCCAGTCACTCTCAATGGTGGCGGC
ATACATCGCCTTCACAATGGCGCTCTGCAGTGCCTGTTCTGCAGCGTGTGAGCATCTTCATCTGCT
CCATCAGCTGTAAACACATTTGCACCGGAGTCTGCCGCTCTCCAGGGTTCAAAACGTGAATG
AACGAGGCGCGCCCGCGGTAACCTACCGGGTATCCATGTCCATTTCTGCGGCATCCAGCCAGGAT
ACCGCTCTCGTGACGTAATATCCAGCGCCGACCGCTGTCTTAATCTGCACACCGGCACGGCA
GTTCCGGCTGTGCGCGGATTTGTTGGGTTGCTGATGCGCTTCCGGCTGACCATCCGGAAGTGTGTC
CGGAAAGCCGCGACGAACTGGTATCCAGGTGGCCTGAACGAACAGTTACCGGTTAAAGGCGTGC
ATGGCCACACCTTCCGAATCATCATGTTAAACGTGCGTTTTCGCTCAACGTCAATGCAGCAGCAGTC
ATCCTCGGCAAACTCTTTCATGCCGCTTCAACCTGCGGGGAAAGGACGCGGCTTCTTCTCCCCGA
TGCCAGATAGCGCCAGCTTGGGCGATGACTGAGCCGGAAAAAGACCCGACGATATGATCCTGAT
GCAGCTGGATGGCGTTGGCGCATAGCGTTATTGCGTACCAGATCGTCTGCGCGGCGATTGCCAC
GGGTAAAGTTGGGCAACAGGGGTGCATCCACACTTCACTCGGTGGGTTCCACGACCGCAACTGCC
TCCAAATCCGTGCCACCGCGTGATAACCGCATATTGCGCAGCGATGTATGCCGCTCCGGCCCC
AGAAGGGTGGGAATGGTGGCGTTTTATACATAAAATCCTGCAAGTCCCTGCGTCTGCTGAGG

Figure 4.S2. Sequence of the used 1.9 kbp DNA fragment.

CAGGTGGCACTTTTCGGGGAAATGTGCGCGGAACCCCTATTTGTTATTTTCTAAATACATTCAAAT
 ATGTATCCGCTCATGAGACAATAACCTGATAAATGCTTCAATAATATTGAAAAAGGAAGATATGA
 GTATTCAACATTTCCGTGTCGCCCTTATCCCTTTTTGCGGCATTTGCCTTCCTGTTTTGCTCACCCA
 GAAACGCTGGTGAAGTAAAAAGATGCTGAAGATCAGTTGGGTGCACGAGTGGGTACATCGAACTG
 GATCTCAACAGCGGTAAAGTCCTTGAGAGTTTTGCCCCGAAGAAGCTTTTCCAATGATGAGCACTTT
 TAAAGTTCTGCTATGTGGCGCGGTATTATCCCGTATTGACGCGGGCAAGAGCAACTCGGTCCGCCG
 ATACACTATTCTCAGAATGACTTGGTTGAGTACTCACCAGTCACAGAAAAGCATCTTACGGATGGCAT
 GACAGTAAGAGAATTATGCACTGCTGCCATAACCATGAGTGATAACACTGCGGCCAACTTACTTCTG
 ACAACGATCGGAGGACCGAAGGAGCTAACCGCTTTTTGCACAACATGGGGATCATGTAACTCGCC
 TTGATCGTTGGGAACCGGAGCTGAATGAAGCCATACCAACGACGAGCGTGACACACGATGCCTG
 TAGCAATGGCAACAACGTTGCGCAAACTATTAACCTGGCGAACTACTTACTAGCTTCCCGCAACAA
 GGTTTATTGCTGATAAATCTGGAGCCGGTGAGCGTGGGTCTCGCGGTATCATTGCAGCACTGGGGCC
 AGATGGTAAGCCCTCCCGTATCGTAGTTATCTACACGACGGGAGTCAGGCAACTATGGATGAACG
 AAATAGACAGATCGCTGAGATAGGTGCCTCACTGATTAAAGCATTGGTAAGTGTACAGACCAAGTTTAC
 TCATATATCTTTAGATTGATTTAAACCTTCATTTTAAATTTAAAGGATCTAGGTGAAGATCCTTTTT
 GATAATCTCATGACCAAAATCCCTTAACGTGAGTTTTCTGTTCCACTGAGCGTCAGACCCCGTAGAAAA
 GATCAAAAGGATCTTCTTGAGATCCTTTTTTCTGCGCGTAATCTGCTGCTTGCACCAAAAAAACAC
 CGCTACAGCGGTGTTGTTGCCGGATCAAGAGCTACCAACTCTTTTTCCGAAGGTAAGTGGCTTC
 AGCAGAGCGCAGATACCAAACTAGTGTCTTCTAGTGAGCCGTAGTTAGGCCACCACTTCAAGAACTC
 TGTAGCACCCTACATACCTCGCTCTGCTAATCCTGTTACCAGTGGCTGCTGCCAGTGGCGATAAGT
 CGTGCTTACCGGTTGGACTCAAGACGATAGTTACCGGATAAGGCGCAGCGTTCGGGTGAACGG
 GGGGTTCTGTGCACACAGCCAGCTTGAGCGAACGACCTACACCGAACTGAGATACCTACAGCGTG
 AGCTATGAGAAAGCGCCACGCTTCCGAAGGGAGAAAGGCGGACAGGTATCCGTAAGCGGCAGG
 GTCGGAACAGGAGAGCGCACGAGGGAGCTTCCAGGGGGAACGCTGGTATCTTTATAGTCTCTG
 GGGTTTCCGCACCTCTGACTTGAGCGTCGATTTTGTGATGCTGTCAGGGGGGCGGAGCCTATGGA
 AAAACGCCAGCAACGCGGCTTTTTACGGTTCCTGGCCTTTTGTGGCCTTTTGTCTACATGGCTCGA
 CAGATCTGCGCAGCACCATGGCCTGAAATAACCTCTGAAAGAGGAAGTGGTAGGTACCTTCTGAG
 GCGGAAAGAACAGCTGTGGAATGTGTGTCAGTTAGGGTGTGAAAGTCCCCAGGCTCCCCAGCAG
 GCAGAAGTATGCAAAGCATGCATCTCAATTAGTCAGCAACCAAGGTGTGAAAGTCCCCAGGCTCCCC
 AGCAGGCAGAAATGCAAGCATGCATCTCAATTAGTCAGCAACCATAGTCCCGCCCTAACTCCG
 CCCATCCGCCCCTAACTCCGCCCAGTTCCGCCATTCTCCGCCCATGGCTGACTAATTTTTTTTATTT
 ATGCAGAGGCGGAGGCCCTCGGCTCTGAGCTATTCAGAAGTAGTGAGGAGGCTTTTTTGGAG
 GCCTAGGCTTTTGCAAAAGCTTGATTCTTCTGACACAACAGTCTCGAACTTAAGCTGCAGAAAGTTGG
 TCGTGAGGCACTGGGCAGGTAAGTATCAAGGTTACAAGACAGGTTTAAGGAGACCAATAGAAACTG
 GGCTTGTGCAGACAGAGAAGACTTTGCGTTTCTGATAGGCACCTATTGGTCTTACTGACATCCACTT
 TGCTTTCTCTCCACAGGTGTCCACTCCAGTTCAATTACAGCTCTTAAGGCTAGAGTACTTAATACGA
 CTCCTATAGGCTAGCCACCATGACTTCGAAAGTTTATGATCCAGAACAAAGGAAACGGATGATAAC
 TGGTCCGCACTGGTGGGCCAGATGTAACAAATGAATGTTCTTGATTCATTTATTAATTTATGATT
 CAGAAAAACATGCAGAAAATGCTGTTATTTTTTACATGGTAACGCGGCTCTTCTTATTTATGGCGA
 CATGTTGTGCCACATATTGAGCCAGTAGCGCGGTATTATACCAGACCTATTGGTATGGGCAAAATC
 AGGCAAACTCGGTAATGGTTCTATAGGTTACTTGATCATTACAAATATCTTACTGCATGGTTGAACT
 TCTTAATTTACCAAGAAAGATCATTTTTGTCGGCCATGATTGGGGTGCTTTTGGCATTTCTATTATAG
 CTATGAGCATCAAGATAAGATCAAAGCAATAGTTACGCTGAAAGGTAGTAGATGTGATTGAATCA
 TGGGATGAATGGCCTGATATTGAAGAAGATATTGCGTTGATCAAACTGGAAGAAGGAGAAAAAATG
 GTTTTGAGAGATAACTTCTCTGTTGAAACCATGTTGCCATCAAAAAATCATGAGAAATTAGAACCCAG
 AAGAATTTGACGATATCTTTGAACCATCAAAGAGAAAAGTGAAGTTCTGTCGTCAACCAATATCATG
 GCCTCGTGAATCCCGTTAGTAAAGGTGGTAAACCTGACGTTGTACAAATTTGTAGGAATTTATAAT
 GCTTATCTACGTGCAAGTGATGATTACCAAAAATGTTTATTGAATCGGACCCAGGATCTTTTCCAAT
 GCTATTGTTGAAGGTGCCAAGGTTTCTAATACTGAATTTGTCAAAGTAAAGGTCCTCATTTTTTC
 GCAAGAAGATGCACCTGATGAAATGGGAAAATATATCAAATCGTTGTTGAGCGAGTTCTCAAAAAT
 GAACAATAATCTAG

Figure 4.S3. Sequence of the used 3.4 kbp DNA fragment.

4.6 References

- [1] K. Luger, A. W. Mäder, R. K. Richmond, D. F. Sargent, and T. J. Richmond. *Nature* **389**, 251 (1997).
- [2] K. Luger. *Curr. Opin. Genetics Dev.* **13**, 127 (2003).
- [3] R. T. Kamakaka and S. Biggins. *Genes Dev.* **19**, 295 (2005).
- [4] J. R. Daban and C. R. Cantor. *J. Mol. Biol.* **156**, 749 (1982).
- [5] A. Hamiche, V. Carot, M. Alilat, F. De Lucia, M. F. O'Donohue, B. Revet, and A. Prunell. *Proc. Natl. Acad. Sci. U.S.A.* **93**, 7588 (1996).
- [6] A. J. Katan, R. Vlijm, A. Lusser, and C. Dekker. *Small* **11**, 976 (2015).
- [7] R. Vlijm, M. Lee, J. Lipfert, A. Lusser, C. Dekker, and N. H. Dekker. *Cell Rep.* **10**, 216 (2015).
- [8] A. Bancaud, G. Wagner, N. Conde e Silva, C. Lavelle, H. Wong, J. Mozziconacci, M. Barbi, A. Sivolob, E. Le Cam, L. Mouawad, J. L. Viovy, J. M. Victor, and A. Prunell. *Mol. Cell* **27**, 135 (2007).
- [9] V. Levchenko, B. Jackson, and V. Jackson. *Biochemistry* **44**, 5357 (2005).
- [10] A. Hamiche, and H. Richard-Foy. *J. Biol. Chem.* **273**, 9261 (1998).
- [11] C. R. Clapier and B. R. Cairns. *Annu. Rev. Biochem.* **78**, 273 (2009).
- [12] J. Ausio and D. W. Abbott. *Biochemistry* **41**, 5945 (2002).
- [13] P. B. Talbert and S. Henikoff. *Nat. Rev. Mol. Cell Biol.* **11**, 264 (2010).
- [14] G. E. Zentner and S. Henikoff. *Nat. Struct. Mol. Biol.* **20**, 259 (2013).
- [15] H. Kurumizaka, N. Horikoshi, H. Tachiwana, and W. Kagawa. *Curr. Opin. Struct. Biol.* **23**, 109 (2013).
- [16] S. Fretzin, B. D. Allan, A. van Daal, S. C. Elgin. *Gene* **107**, 341 (1991).
- [17] A. S. Akhmanova, P. C. Bindels, J. Xu, K. Miedema, H. Kremer, and W. Hennig. *Genome* **38**, 586 (1995).

- [18] S. Henikoff, K. Ahmad, J. S. Platero, and B. van Steensel. *Proc. Natl. Acad. Sci. U.S.A.* **97**, 716 (2000).
- [19] J. L. Moreland, A. Gramada, O. V. Buzko, Q. Zhang, and P. E. Bourne. *BMC Bioinformatics* **6**, 21 (2005).
- [20] K. Ahmad and S. Henikoff. *Mol. Cell* **9**, 1191 (2002).
- [21] E. Szenker, D. Ray-Gallet, and G. Almouzni. *Cell Res.* **21**, 421 (2011).
- [22] A. Sakai, B. E. Schwartz, S. Goldstein, and K. Ahmad. *Curr. Biol.* **19**, 1816 (2009).
- [23] A. Y. Konev, M. Tribus, S. Y. Park, V. Podhraski, C. Y. Lim, A. V. Emelyanov, E. Vershilova, V. Pirrotta, J. T. Kadonaga, A. Lusser, and D. V. Fyodorov. *Science* **317**, 1087 (2007).
- [24] H. Tachiwana, A. Osakabe, T. Shiga, Y. Miya, H. Kimura, W. Kagawa, and H. Kurumizaka. *Acta Crystallogr. D. Biol. Crystallogr.* **67**, 578 (2011).
- [25] A. Thakar, P. Gupta, T. Ishibashi, R. Finn, B. Silva-Moreno, S. Uchiyama, K. Fukui, M. Tomschik, J. Ausio, and J. Zlatanova. *Biochemistry* **48**, 10852 (2009).
- [26] C. Jin and G. Felsenfeld. *Genes Dev.* **21**, 1519 (2007).
- [27] P. Chen, J. Zhao, Y. Wang, M. Wang, H. Long, D. Liang, L. Huang, Z. Wen, W. Li, X. Li, H. Feng, H. Zhao, P. Zhu, M. Li, Q. F. Wang, and G. Li. *Genes Dev.* **27**, 2109 (2013).
- [28] J. Lipfert, M. Wiggin, J. W. J. Kerssemakers, F. Pedaci, and N. H. Dekker. *Nat. Commun.* **2**, 439 (2011).
- [29] X. J. A. Janssen, J. Lipfert, T. Jager, R. Daudey, J. Beekman, and N. H. Dekker. *Nano Lett.* **12**, 3634 (2012).
- [30] M. E. Levenstein and J. T. Kadonaga. *J. Biol. Chem.* **277**, 8749 (2002).
- [31] A. Lusser, D. L. Urwin, and J. T. Kadonaga. *Nat. Struct. Mol. Biol.* **12**, 160 (2005).
- [32] J. Mazurkiewicz, J. F. Kepert, and K. Rippe. *J. Biol. Chem.* **281**, 16462 (2006).

- [33] T. Nakagawa, M. Bulger, M. Muramatsu, and T. Ito. *J. Biol. Chem.* **276**, 27384 (2001).
- [34] A. J. Andrews, X. Chen, A. Zevin, L. A. Stargell, and K. Luger. *Mol. Cell* **37**, 834 (2010).
- [35] T. Fujii-Nakata, Y. Ishimi, A. Okuda, and A. Kikuchi. *J. Biol. Chem.* **267**, 20980 (1992).
- [36] R. Vlijm, J. S. J. Smitshuijzen, A. Lusser, and C. Dekker. *PLoS One* **7**, e46306 (2012).
- [37] F. T. Chien and J. van Noort. *Curr. Pharm. Biotechnol.* **10**, 474 (2009).
- [38] J. Lipfert, J. W. J. Kerssemakers, T. Jager, and N. H. Dekker. *Nat. Methods* **7**, 977 (2010).
- [39] F. Kouzine, A. Gupta, L. Baranello, D. Wojtowicz, K. Ben-Aissa, J. Liu, T. M. Przytycka, and D. Levens. *Nat. Struct. Mol. Biol.* **20**, 396 (2013).
- [40] S. Chong, C. Chen, H. Ge, and X. S. Xie. *Cell* **158**, 314 (2014).
- [41] J. Ma, L. Bai, and M. D. Wang. *Science* **340**, 1580 (2013).
- [42] N. Gilbert and J. Allan. *Curr. Opin. Genetics Dev.* **25**, 15 (2014).
- [43] S. Meyer and G. Beslon. *PLoS Comput. Biol.* **10**, e1003785 (2014).

5 Modification of the Histone Tetramer at the H3-H3 Interface Impacts Tetrasome Conformations and Dynamics

Nucleosomes consisting of a short piece of DNA wrapped around an octamer of histone proteins form the fundamental unit of chromatin in eukaryotes. Their role in DNA compaction comes with regulatory functions that impact essential genomic processes such as replication, transcription, and repair. The assembly of nucleosomes obeys a precise pathway in which tetramers of histones H3 and H4 bind to the DNA first to form tetrasomes, and two dimers of histones H2A and H2B are subsequently incorporated to complete the complex. As viable intermediates, we previously showed that tetrasomes can spontaneously flip between a left-handed and right-handed conformation of DNA-wrapping. To pinpoint the underlying mechanism, here we investigated the role of the H3-H3 interface for tetramer flexibility in the flipping process at the single-molecule level. Using FOMT, we studied the assembly and structural dynamics of individual tetrasomes modified at the cysteines close to this interaction interface by iodoacetamide in real time. While such modification did not affect the structural properties of the tetrasomes, it caused a 3-fold change in their flipping kinetics. The results indicate that the IA-modification enhances the conformational plasticity of tetrasomes. Our findings suggest that subnucleosomal dynamics may be employed by chromatin as an intrinsic and adjustable mechanism to regulate DNA supercoiling.

This chapter has been published as O. Ordu, L. Kremser, A. Lusser, and N. H. Dekker. *J. Chem. Phys.* **148**, 123323 (2018).

5.1 Introduction

The genome of eukaryotic organisms is tightly packed into chromatin, a hierarchical DNA-protein assembly with a repeating basic unit termed the nucleosome [1–3]. This fundamental complex consists of 147 bp of DNA wrapped around a discoidal core of eight histone proteins by 1.7 turns in a left-handed superhelix [4–6]. The histone octamer comprises two copies of each of the core histones H2A, H2B, H3, and H4, which group into two types of heterodimers by the pairing of histones H2A and H2B, and histones H3 and H4, respectively [7, 8]. Via the four-helix region formed by both H3 histones, the two H3-H4 dimers form a tetramer to which H2A/H2B dimers attach through similar interactions between histones H2B and H4. In the presence of DNA, the (H3-H4)₂ tetramer assembles first into a tetrasome, after which two H2A/H2B dimers bind to form the full nucleosome [9]. In cells, nucleosome assembly is promoted by histone chaperones such as NAP1 or CAF1, and energy dependent chromatin assembly factors such as ACF or CHD1 [10, 11]. *In vitro*, nucleosomes are reconstituted via salt-dialysis or using purified recombinant enzymes [12]. This first level of DNA compaction already highly affects and thereby regulates the accessibility of the genome during vital processes such as replication, transcription, and repair. Therefore, detailed knowledge of nucleosome structure and dynamics is crucial for understanding cell function and viability.

Over four decades of research, structural and biochemical approaches have provided profound insights into the structure and function of nucleosomes [13–17]. More recently, such knowledge has been complemented by single-molecule studies which especially yielded substantial information concerning the dynamics of nucleosomes on the molecular scale [18]. It is now known that nucleosomes are intrinsically dynamic by partially un- and rewrapping their DNA ends (breathing [19–22]) and transiently opening the two turns of DNA along the axis of the superhelix (gaping [23]). In addition, nucleosome composition, stability, and dynamics are altered by chemical modification of the histones (post-translational modifications [24]) and by active remodeling enzymes (ATP-dependent remodelers [25]). Furthermore, changes in nucleosome structure and dynamics are induced and regulated by the incorporation of histone variants with DNA-sequence or cell-cycle dependent expression, deposition, and specific functions [26, 27]. Under extraneous causes in the form of force, torque or changes in buffer conditions, nucleosomes undergo structural rearrangements resulting in different conformations [28]. In agreement with the stepwise assembly of nucleosomes, tetrasomes – consisting of 80 bp DNA wrapped

around the $(\text{H3-H4})_2$ tetramer (Figure 5.1a,b) – have been observed as stable intermediates in various studies [29–41]. Remarkably, tetrasomes have further been found to wrap DNA either in a left-handed or right-handed superhelix [42–47] (Figure 5.1c). Recently, we have investigated this phenomenon by examining the dynamics of individual tetrasomes containing either the canonical *Drosophila* histone H3.1 [48] or its main replacement variant H3.3 [49]. By directly measuring the DNA linking number, we observed spontaneous flipping of such tetrasomes between a predominant state of left-handed superhelix, like in the full nucleosome, and a less occupied right-handed conformation of DNA-wrapping. The transition between the two states has been suggested to arise from the spontaneous reorientation of the $(\text{H3-H4})_2$ tetramer at the H3-H3 interface. However, experiments directed at pinpointing the mechanism underlying the handedness dynamics of tetrasomes via real-time measurements have been lacking.

In this work, we investigated the potential role of flexibility at the H3-H3 interface of the histone tetramers in the handedness flipping of tetrasomes at the single-molecule level. Using FOMT ([50]), we studied the assembly and structural dynamics of individual NAP1-loaded, chemically modified $(\text{H3.1-H4})_2$ and $(\text{H3.3-H4})_2$ tetrasomes in real time. The $(\text{H3-H4})_2$ tetramers were treated with IA, which covalently binds to the sulphur atom of the single cysteine at position 110 of the H3 histones (Figure 5.1d). In a previous bulk study, this modification was found to form inherently left-handed tetrasomes and to block their transition to the right-handed conformation, potentially by generating a steric hindrance at the H3-H3 interface of the $(\text{H3-H4})_2$ tetramers [44]. While IA-treated tetrasomes assembled with a very similar structure to untreated tetrasomes, we surprisingly found that the IA-treatment did not fully prevent the handedness flipping. However, the kinetics of IA-treated tetrasomes differed by 1.5-fold altered dwell times in the states of left-handed and right-handed DNA wrapping and by a 3-fold decrease of their ratio. These results indicate that the IA-treatment impacts the conformational flexibility and dynamics of tetrasomes. Our findings further suggest subnucleosomal dynamics as an intrinsic and tunable mechanism of chromatin to facilitate and regulate the impact of forces and torques on the genome. In the cell, such a mechanism could assist the corresponding activities by genome-processing enzymes such as the RNAP [51], and could be adjusted by histone core modifications that alter histone-DNA or histone-histone interactions [52].

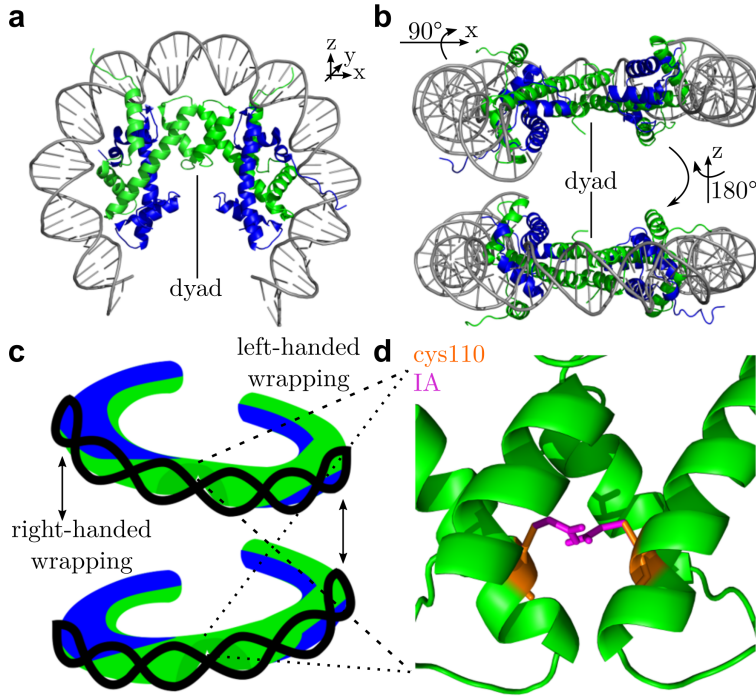


Figure 5.1: Schematics of the tetrasome structure and associated changes in handedness. **a** Top view of 80 bp of DNA (gray) wrapped around a horseshoe-shaped protein complex containing the core histones H3 (green) and H4 (blue) in a left-handed superhelix. Two H3-H4 heterodimers form a tetramer through the central four-helix domain of the H3 histones. This image was generated by modifying the structural data of the *Drosophila* nucleosome from the RCSB PDB with the identification code 2PYO [53] using the PyMOL Molecular Graphics System, Version 1.8.0.0 Schrödinger, LLC. **b** Side views of the structure in (a) along the pseudo-twofold symmetry (dyad) axis. **c** Illustration of the two possible ways of DNA-wrapping, left-handed or right-handed, around the tetramer. Flipping between these two tetrasome conformations may result from spontaneous reorientation of the heterodimers at the H3-H3 interface [43–45, 47–49]. **d** Zoomed-in structure in (a) at the H3-H3 interface that separates the H3-H4 heterodimers. IA-treatment of the histones results in derivatization (magenta) of the cysteine at position 110 (orange) of both histones H3. This image was generated by further modifying the structural data of the *Drosophila* nucleosome with two copies of the IA molecule extracted from the structure with PDB identification code 4QDT [54] using PyMOL.

5.2 Materials and Methods

5.2.1 Preparation of DNA constructs

Linear dsDNA fragments of 1.97 kbp length were used as templates for tetrasome assembly in all experiments. This DNA fragment was generated by PCR from plasmid pBluescript (pBlue) 2,3 using primers 1 and 2 (Table 5.S1 of the Supplementary Information). Subsequently, shorter fragments (handles) of 643 bp length containing nucleotides modified by either multiple biotin (Roche Diagnostics, Basel, Switzerland) or multiple digoxigenin (Roche Diagnostics) linkages were ligated to either end of the main DNA fragment at BsaI restriction sites. These handles were amplified by PCR from pBlueSKII+ (Stratagene/Agilent Technologies, Santa Clara, CA, United States) using primers 3 and 5 or 4 and 5 (Table 5.S1 of the Supplementary Information) in the presence of biotin-16-dUTP (Roche Diagnostics) or digoxigenin-11-dUTP (Roche Diagnostics) in a ratio of 1:5 with dTTP (Promega, Madison, WI, United States). The resulting DNA molecules contained no nucleosome-positioning sequences (Figure 5.S1 of the Supplementary Information).

5.2.2 Protein expression and purification

Expression and purification of recombinant *Drosophila* NAP1, histones H3.1-H4 and H3.3-H4 were performed as described in the respective previous studies [48, 49]. Example gel images of the histones after SDS-PAGE are shown in Figure 5.S2a,b of the Supplementary Information.

5.2.3 Histone treatment with IA

Purified H3.1-H4 and H3.3-H4 histones were dialyzed overnight against a buffer containing 10 mM Hepes-KOH (pH 7.6), 10 mM KCl, 1 mM EDTA, and 10% (v/v) glycerol (buffer A) with two buffer changes to remove dithiothreitol (DTT). Subsequently, the samples were incubated with 1 mM IA in buffer A for 3 h in the dark at RT. Afterwards, IA was removed by overnight dialysis against buffer A with 1 mM DTT at 4 °C with two changes of buffer. Aliquots of H3-H4 solutions at the different steps of treatment were analyzed by SDS-PAGE (Figure 5.S2a,b of the Supplementary Information). IA was our reagent of choice because it allows for a robust and quantitative modification of histone H3 in a technically straightforward manner [43–45].

5.2.4 MS analysis of IA-treated histones

The degree of derivatization of the core histones by incorporation of IA was quantified by MS. The experimental procedure is detailed in the Supplementary Information, together with the results shown in Figure 5.S2c,d. We found that all H3.1 histones (100%) and virtually all H3.3 histones (99.3%) were derivatized upon IA-treatment. The underlying chromatograms from HPLC and MS2-spectra are shown in Figures 5.S3 and 5.S4 of the Supplementary Information, respectively.

5.2.5 Tetrasome reconstitution via salt-dialysis

The capability of the histones to successfully load onto the DNA constructs designed for use in the single-molecule experiments was confirmed by reconstituting tetrasomes with both untreated and IA-treated tetrasomes using salt-gradient dialysis [55, 56]. The details of the employed protocol can be found in the Supplementary Information together with the results shown in Figure 5.S5.

5.2.6 Sample preparation for tetrasome assembly in single-molecule experiments

In single-molecule experiments, tetrasome assembly was performed in flow cells consisting of a channel cut into a double-layer of parafilm that was sandwiched between two cover glasses (24×60 mm/# 1, Menzel-Gläser, Braunschweig, Germany). The details of the assembly and preparation of the flow cells are described in the Supplementary Information.

For the experiments with histones, the buffer was changed to the measurement buffer containing 50 mM KCl (Merck, Darmstadt, Germany), 25 mM Hepes-KOH (pH 7.5; Sigma-Aldrich, St. Louis, MO, United States), 0.1 mM EDTA, 0.1 mg/ml BSA (Sigma Aldrich) for passivation, 0.25% PEG (Sigma-Aldrich) and 0.25% PVA (Sigma-Aldrich) as crowding agents. These buffer conditions with a 10-fold higher concentration of crowding agents compared to our previous studies [48, 49] were employed in most of the experiments ($n=13$ out of $N=15$) to increase tetrasome stability since tetrasomes had been observed to disassemble in the course of the first two experiments. For the NAP1-mediated assembly of tetrasomes, either 51 nM of an equimolar solution of H3.1_{IA}-H4 histones or 54 nM of an equimolar solution of H3.3_{IA}-H4 histones were incubated with 192 nM NAP1 for 30 min on ice in a buffer containing 50 mM KCl, 25 mM Hepes-KOH, 0.1 mM EDTA, 1 mg/ml BSA, 0.25% PEG, and 0.25% PVA. The incubated

protein solution was then diluted at least 1:100 and 100 μl of the diluted solution was flushed into the flow cell to achieve the controlled assembly of a few tetrasomes. Free proteins were not flushed out in most measurements due to the enhancing effect on tetrasome disassembly observed in the first two experiments. In our previous studies, the presence of NAP1 was found to affect neither the stability of tetrasomes nor the flipping dynamics for (H3.1-H4)₂ tetrasomes, but to slightly increase the flipping probability of (H3.3-H4)₂ tetrasomes [48, 49].

5.2.7 MT instrumentation

The NAP1-mediated assembly of tetrasomes was measured by directly monitoring the length and linking number of single DNA molecules using FOMT [50]. The hardware of the MT setup used in this study is described in the Supplementary Information. The exerted force was calibrated for each experiment and amounted to values between 0.6 pN and 0.7 pN. All experiments were performed at RT (22 °C).

5.2.8 Data analysis

The acquired data were analyzed using custom-written scripts in Matlab (Mathworks, Natick, MA, United States) and its built-in functions. The traces were analyzed for stepwise changes (steps) in DNA length and linking number using a custom-written step-fitting algorithm that improves upon its previous version described in Ref. [57]. In a subsequent analysis, steps coinciding in both time traces, and hence indicating assembly or disassembly of tetrasomes, were identified using these fits. The sizes of the coinciding steps in DNA length ($N = 71$) and linking number ($N = 71$) upon assembly and disassembly were then extracted as key quantities describing the structure of the tetrasomes.

The handedness dynamics was only analyzed in those parts of the time traces that had stable DNA length and linking number baseline, reflecting stably bound tetrasomes ($N = 34$). By fitting a corresponding number of Gaussian functions to the linking number data between two subsequent coinciding steps (Figure 5.4b), the handedness flipping was characterized in terms of the associated alteration in tetrasome structure ($n = 22$). The differences between the mean values of these fits were used to determine the change in linking number upon flipping ($N = 26$). The relative peak area ratios of the individual Gaussian fits yielded the probabilities for the tetrasomes to occupy the corresponding states.

For a more detailed picture of the handedness dynamics, the times a single

assembled and flipping $(\text{H3.1}_{\text{IA}}\text{-H4})_2$ tetrasome spent in the left-handed or right-handed state of DNA wrapping (dwell times) were analyzed using a custom-written algorithm based on Ref. [58]. Smoothed linking number data from the corresponding time traces ($N = 4$) were assigned to the two states with the help of a threshold zone set by the midpoint of the mean values and their STD obtained from the Gaussian fits to the unfiltered data (Figure 5.4b). The times between subsequent transitions from one state to the other, i.e., intersections with the midpoint, were considered as the dwell times in the corresponding states. All data sets assigned to the left-handed state ($N = 195$ for 3.4 s or $N = 76$ for 18.4 s time averaging by filtering) and right-handed state ($N = 199$ for 3.4 s or $N = 81$ for 18.4 s time averaging) were combined and fitted by an exponential function to determine the mean dwell time in each conformation (Figure 5.5a,b). For comparison, dwell times in these traces were also determined using the recorded dwell times in the plateaus of the steps fitted by the step-fitting algorithm in a separate analysis ($N = 65$ for the left-handed state, $N = 64$ for the right-handed state). For a direct comparison to the behavior of untreated tetrasomes, we further re-analyzed the dwell times in the partial time traces ($N = 6$) of one of our earlier experiments with untreated $(\text{H3.1-H4})_2$ tetrasomes published in the related article [48], using the same custom-written algorithm and settings ($N = 158$ for 3.4 s or $N = 69$ for 18.4 s time averaging for the left-handed state, $N = 160$ for 3.4 s and $N = 71$ for 18.4 s time averaging for the right-handed state).

Further details of the data analysis are described in the Supplementary Information, together with the complementing results shown in Figures 5.S6 and 5.S7. Overall, it should be noted that the values of the results obtained here for the dynamics and kinetics of the tetrasomes are an upper boundary due to the finite bead response time. The errors stated on the mean values determined in this study correspond to 1 STD based on the underlying distributions, unless indicated otherwise. The errors of computed quantities were calculated by error propagation.

5.3 Results

5.3.1 NAP1-mediated assembly of IA-treated tetrasomes results in proper complexes

Modified tetrasomes were assembled by flushing IA-treated histone $((\text{H3}_{\text{IA}}\text{-H4})_2)$ tetramers pre-incubated with NAP1 chaperones into a flow cell containing individually tethered DNA molecules without specific nucleosome-

positioning sequences. The formation of tetrasomes was monitored in real-time by measuring the length and the linking number of a single DNA molecule using FOMT [50]. A magnetic bead-tethered DNA molecule is precisely aligned with the axis of the vertically oriented magnetic field generated by a cylindrical permanent magnet allowing controlled application of force without constraining the bead's rotational motion (Figure 5.2a). In this study, constant stretching forces of 0.6-0.7 pN were applied, comparable to our previous studies with untreated tetrasomes [48, 49]. The assembly of tetrasomes upon flushing in histone/chaperone-complexes was reflected in stepwise decreases in both DNA length z (in μm) (Figure 5.2b) and linking number θ (in turns) (Figure 5.2c) simultaneously. Histone tetramers or NAP1 alone did not interact with the DNA molecule under identical conditions (Figure 5.S8 of the Supplementary Information).

For improved statistics, different numbers of tetrasomes were assembled in several experiments ($N = 15$) by changing the protein concentration. For the same purpose, the results obtained for $(\text{H3.1}_{\text{IA}}\text{-H4})_2$ and $(\text{H3.3}_{\text{IA}}\text{-H4})_2$ tetrasomes were combined, as we previously found the properties of untreated $(\text{H3.1-H4})_2$ and $(\text{H3.3-H4})_2$ tetrasomes to be very similar [48, 49]. The total, simultaneous changes in DNA length Δz_{tot} and linking number $\Delta \theta_{\text{tot}}$ upon assembly of different numbers of tetrasomes in several experiments follow a linear relation with a slope of $\Delta z_{\text{tot}}/\Delta \theta_{\text{tot}} = 33 \pm 6 \text{ nm/turn}$ (95% confidence interval for estimated values from a linear fit) (Figure 5.3a). Interestingly, some of the total changes in DNA linking number were smaller than the value expected from their corresponding change in DNA length, suggesting the assembly of right-handed tetrasomes. Therefore, such results ($n = 5$) were excluded from the fit. From the total changes, we determined that 11% ($n = 8$) of all modified tetrasomes ($N = 74$) assembled in the right-handed conformation. In contrast to untreated tetrasomes, 66% ($n = 49$) of the assembled modified tetrasomes were found to disassemble in the course of the measurements, regardless of the NAP1/histone ratio employed (Figure 5.S9 of the Supplementary Information), indicating their decreased stability. A destabilizing effect of the 10-fold higher concentration of crowding agents compared to our previous studies on tetrasomes [48, 49] seems unlikely given the observation that under the same conditions, untreated tetrasomes did not disassemble (Figure 5.S10a of the Supplementary Information).

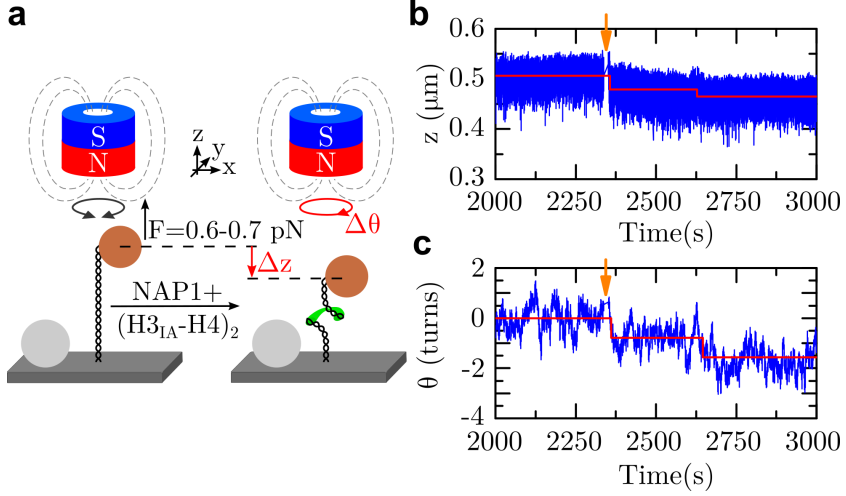


Figure 5.2: Experimental configuration. **a** The assembly and structural dynamics of $(\text{H3}_{\text{IA}}\text{-H4})_2$ tetrasomes were studied using FOMT [50]. A single DNA molecule (black) is tethered between the lower cover glass (dark gray) of a flow cell and a micron-sized paramagnetic bead (brown) that is subject to a constant force exerted by a permanent magnet (blue/red) of cylindrical geometry above the flow cell. The bead is free to rotate in the x, y -plane, which allows direct measurement of the twist in the DNA molecule in addition to its length. Non-magnetic beads (light gray) adhered to the surface are used as reference to correct for drift. Flushing in of $(\text{H3}_{\text{IA}}\text{-H4})_2$ tetramers pre-incubated with the chaperone NAP1 results in the assembly of the modified tetrasomes, which is reflected in the decrease of the molecule's length Δz (red arrow) and linking number $\Delta \theta$ (red circular arrow). **b,c** Partial time traces of a DNA molecule's length z (in μm , (b)) and linking number θ (in turns, (c)) simultaneously following the assembly of two $(\text{H3.3}_{\text{IA}}\text{-H4})_2$ tetrasomes after flushing in the histone/chaperone complexes (indicated by orange arrows). The assembly of the modified tetrasomes happened in the form of consecutive, distinct steps that were detected using a custom-written step-fitting algorithm (red lines) (see Section 5.2 and Supplementary Information)). Here, the two tetrasomes induced two simultaneous steps in both DNA length and linking number with the sizes $\Delta z = 28 \pm 8 \text{ nm} / \Delta \theta = -0.8 \pm 0.3$ turns, and $\Delta z = 15 \pm 8 \text{ nm} / \Delta \theta = -0.8 \pm 0.3$ turns, respectively (errors are 1 STD determined from the values of all experiments as described in the main text and Figure 3c,d).

While multiple IA-treated tetrasomes mostly assembled simultaneously as reflected in large steps, their disassembly mainly occurred in a one-by-one fashion, indicating proper formation of individual complexes rather than aggregates (Figure 5.3b). A possible reason for this behavior could be a cooperative binding mechanism that leads to a simultaneous or faster assembly of individual IA-treated tetrasomes than we can experimentally resolve. The several individual changes in DNA length $\Delta z_{dis-/ass}$ ($N = 71$) and linking number $\Delta \theta_{dis-/ass}$ upon tetrasome assembly or disassembly ($N = 71$) also follow a linear relation with a slope of $\Delta z_{dis-/ass} / \Delta \theta_{dis-/ass} = 26 \pm 4$ nm/turn (95% confidence interval for estimated values from a linear fit). Similar to the total changes, some of the changes in DNA linking number showed the opposite sign compared to those expected from the change in DNA length, indicating the assembly or disassembly of right-handed tetrasomes. Such data ($n = 14$) were likewise excluded from the fit.

Combining the absolute values from all measurements with (H3.1_{IA}-H4)₂ and (H3.3_{IA}-H4)₂ tetrasomes for improved statistics yielded a mean change in DNA length of $\Delta z_{dis-/ass} = 28 \pm 8$ nm ($n = 49$) and a mean change in linking number of $\Delta \theta_{dis-/ass} = 1.0 \pm 0.3$ turns ($n = 61$) upon the assembly or disassembly of IA-treated tetrasomes (Figure 5.3c,d). The individual distributions and results of the changes for the two types of tetrasomes are shown in Figures 5.S11 and 5.S12 of the Supplementary Information. The mean values were determined from the data within the corresponding resolution limits, the contour length (50 nm) of nucleosomal DNA and the number of turns (1.7 turns) that it is wrapped around the histone octamer. Considering the above observed linear relation between the changes in DNA length and linking number, the mean values yield a ratio of $\Delta z_{dis-/ass} / \Delta \theta_{dis-/ass} = 28 \pm 12$ nm/turn, which is in good agreement with the results obtained from the linear fits to the two different data sets above.

Overall, these values agree well with previous studies in which tetrasomes were characterized as intermediates during un- and refolding of complete nucleosomes [34–37] or by direct measurements [39, 40, 43–45, 47–49]. The linear dependency between the key quantities characterizing the structure of the modified tetrasomes further suggests that their conformation is independent of their number being assembled on a DNA molecule, as we previously observed for untreated tetrasomes as well. These results show that IA-treated tetrasomes assembled properly in our assay with a very similar structure to untreated tetrasomes.

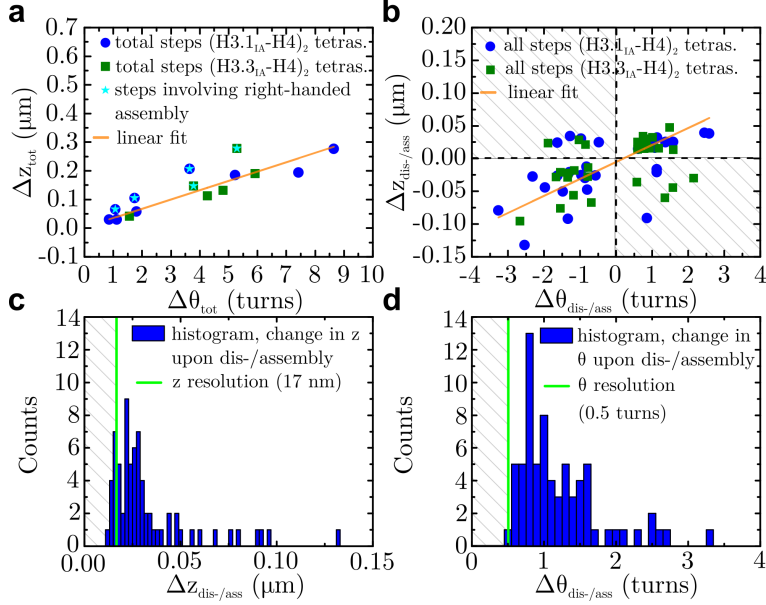
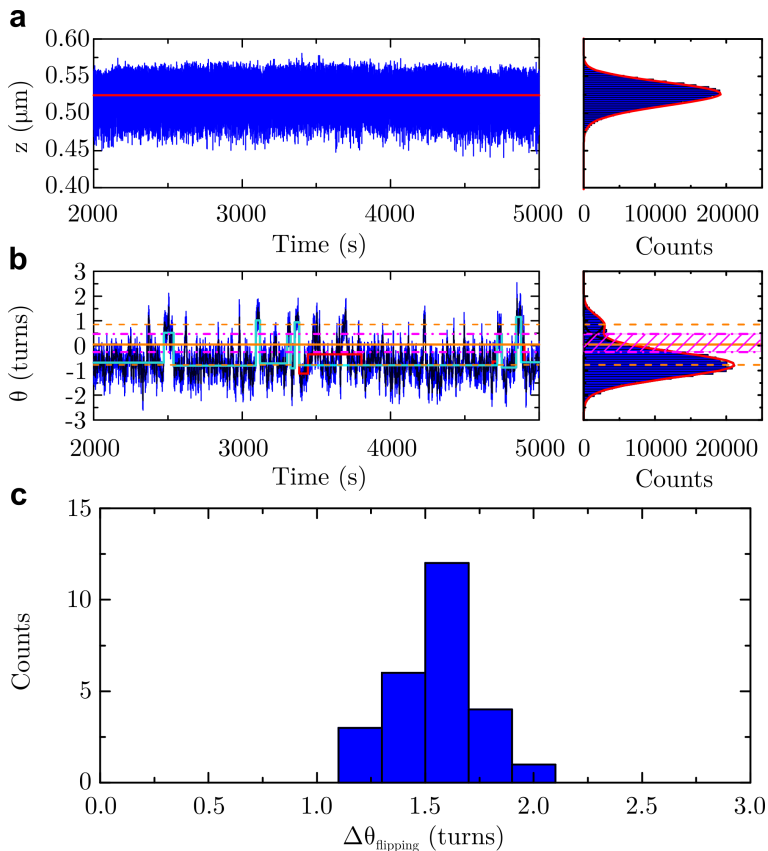


Figure 5.3: Changes in DNA length and linking number upon dis-/assembly of IA-treated tetrasomes. **a** Total changes in DNA length Δz_{tot} (in μm) upon assembly of different numbers of $(\text{H3.1}_{\text{IA}}\text{-H4})_2$ (blue circles) or $(\text{H3.3}_{\text{IA}}\text{-H4})_2$ tetrasomes (dark green squares) in several experiments plotted against their corresponding total change in DNA linking number $\Delta\theta_{tot}$ (in turns) ($N = 15$). A linear fit (orange solid line) yielded a slope of $\Delta z_{tot}/\Delta\theta_{tot} = 33 \pm 6 \text{ nm/turn}$ (95% confidence interval for estimated values). Data involving right-handed assembly (cyan stars, $n = 5$) were excluded from the fit (see main text). **b** Changes in DNA length $\Delta z_{dis-/ass}$ (in μm) upon dis-/assembly of IA-treated tetrasomes plotted against their corresponding change in DNA linking number $\Delta\theta_{dis-/ass}$ (in turns) ($N = 71$). A linear fit yielded a slope of $\Delta z_{dis-/ass}/\Delta\theta_{dis-/ass} = 26 \pm 4 \text{ nm/turn}$ (95% confidence interval for estimated values). Data involving right-handed dis-/assembly (shaded areas, $n = 14$) were excluded from the fit (see main text). **c** Histogram of the changes in DNA length $\Delta z_{dis-/ass}$ (blue bars) upon dis-/assembly of IA-treated tetrasomes plotted together with the mean spatial resolution based on 1 STD (17 nm, green line). The mean change in length of $\Delta z_{dis-/ass} = 28 \pm 8 \text{ nm}$ was determined from the data within the range bounded by the resolution limit (shaded area) and the DNA contour length wrapped in a full nucleosome (50 nm) ($n = 49$). **(d)** Histogram of the changes in DNA linking number $\Delta\theta_{dis-/ass}$ plotted together with the mean spatial resolution based on 1 STD (0.5 turns, green line). The mean change in linking number of $\Delta\theta_{dis-/ass} = 1.0 \pm 0.3$ turns was determined from the data within the range bounded by the resolution limit (shaded area) and the number of turns the DNA is wrapped around the histone core in a full nucleosome (1.7 turns) ($n = 61$).

5.3.2 IA-treated tetrasomes have reduced tendency towards handedness flipping

To observe tetrasome behavior after assembly over an extended period of time, the FOMT experiments were carried out for several hours. As mentioned above, most modified tetrasomes were observed to disassemble in the course of the experiments, unlike untreated tetrasomes [48, 49]. On average, (H3.1_{IA}-H4)₂ tetrasomes were found to disassemble within 2499 ± 415 s (1 SEM, Figure 5.S7 of the Supplementary Information). Therefore, the structural dynamics of tetrasomes was analyzed in partial traces with states of stable binding between two subsequent assembly and/or disassembly events. Quite unexpectedly, since IA-modification was previously reported to block the structural transition of tetrasomes [44], we found IA-treated tetrasomes to be dynamic in terms of their handedness. While the DNA length remained constant (Figure 5.4a), the linking number of a DNA molecule loaded with a tetrasome continuously fluctuated between two states corresponding to a left-handed superhelix, like in the full nucleosome, and a right-handed conformation of DNA wrapping (Figure 5.4b). Such handedness flipping was observed in 86% ($n = 12$) of the analyzed partial traces ($N = 14$) with (H3.1_{IA}-H4)₂ tetrasomes. (H3.3_{IA}-H4)₂ tetrasomes were found to flip in 50% ($n = 10$) of the analyzed partial traces ($N = 20$). The associated change in tetrasome structure was quantified by the difference between the means of the corresponding number of Gaussian distributions fitted to the linking number data that show flipping ($N = 26$). On average, the change in DNA linking number associated with flipping $\Delta\theta_{flipping}$ equalled 1.6 ± 0.2 turns (Figure 5.4c), which exactly corresponds to the values obtained for the two types of tetrasomes individually (Figure 5.S13 of the Supplementary Information). This value further agrees well with that determined previously for untreated tetrasomes and reaffirms our observation that IA-treated tetrasomes assembled into proper complexes. Nevertheless, the considerable remaining fractions of the analyzed partial traces did not show such handedness flipping. This indicates the existence of another, rather metastable population/state induced upon IA-modification. Along these lines, we also observed that the linking number data of multiple loaded IA-treated tetrasomes never showed the number of states that would be expected, if they all flipped simultaneously. At most three states were observed in 14% ($n = 2$) of the analyzed traces deduced from (H3.1_{IA}-H4)₂ tetrasomes, and in 10% ($n = 2$) of the analyzed traces obtained with (H3.3_{IA}-H4)₂ tetrasomes. This implies that usually only one, but not necessarily the same tetrasome exhibited handedness

5 Conformations and Dynamics of Modified Tetrasomes



flipping. Additionally, in 43% of the data from experiments with $(\text{H3.1}_{\text{IA}}\text{-H4})_2$ tetrasomes, the lowest linking number state did not correspond to the value expected for all tetrasomes being in the left-handed conformation. While not observed for $(\text{H3.3}_{\text{IA}}\text{-H4})_2$ tetrasomes, this phenomenon indicates that some $(\text{H3.1}_{\text{IA}}\text{-H4})_2$ tetrasomes also stably dwelled in the right-handed state. From the DNA length and the corresponding linking number values, we determined that 18% ($n=6$) of all assembled $(\text{H3.1}_{\text{IA}}\text{-H4})_2$ tetrasomes ($N=33$) in the considered traces stably remained in the right-handed conformation.

Overall, these results show that IA-modification does not fully prevent tetrasomes from changing their handedness. Nonetheless, our findings clearly indicate that IA-treated tetrasomes have a reduced tendency towards flipping, which might arise from the incorporated IA molecules.

Figure 5.4: Handedness flipping of IA-treated tetrasomes. **a** Partial time trace of a DNA molecule’s length z (in μm) after the assembly of a $(\text{H3.1}_{\text{IA}}\text{-H4})_2$ tetrasome. The DNA length stays constant over time, as can be seen both from the fit to the time trace (*red line*) by the custom-written step-fitting algorithm and its histogram on the right panel. The data for the histogram was fitted by a gamma function (*red line* in histogram) after mirroring at the x-axis and offsetting to positive values (see Supplementary Information). **b** The corresponding part of the time trace of the same DNA molecule’s linking number θ (in turns). This shows spontaneous fluctuations between a predominantly occupied left-handed state and a less occupied right-handed state with a mean of $\theta_{\text{left}} = -0.77 \pm 0.01$ turns and $\theta_{\text{right}} = +0.86 \pm 0.06$ turns (95% confidence intervals for estimated values; *orange dashed lines*), respectively, as can be seen both from the fit to the time trace (*red line*) by the custom-written step-fitting algorithm and its histogram on the right panel. The data for the histogram were fit to two Gaussian functions (*black lines* in histogram) underlying the full profile (*red line* in histogram). For dwell time analysis, the time trace was smoothed (*black*) before categorizing the data into the two states based on a threshold (*orange solid line*) set at the average value of the means determined from the unfiltered data (*orange dashed lines*). The threshold was further extended to a zone (*magenta striped area*) bounded by 1 STD from the corresponding means (*magenta dashed-dotted lines*). Alternatively, the dwell times in the step plateaus from the step-fitting algorithm were analyzed after manual correction to obtain a better match to the data (*cyan solid line*). **c** Histogram of the changes in linking number upon handedness flipping of IA-treated tetrasomes. The data have a mean value of $\Delta\theta_{\text{flipping}} = 1.6 \pm 0.2$ turns ($N = 26$).

This would support the idea that a potential rotation of the two H3-H4 tetramers against each other at the H3-H3 interface is the mechanistic requirement enabling handedness flipping. The simultaneous flipping of multiple tetrasomes might be hindered by the increased stability of individual complexes in a cooperative setting. The differing behavior and statistics for $(\text{H3.1}_{\text{IA}}\text{-H4})_2$ and $(\text{H3.3}_{\text{IA}}\text{-H4})_2$ tetrasomes might result from subtle differences in their structure upon IA-incorporation. Similar to the case of tetrasome stability, the 10-fold higher concentration of crowding agents compared to our previous studies on tetrasomes [48, 49] is unlikely to affect tetrasome flipping, as untreated tetrasomes assembled in the same conditions did flip as previously observed (Figure 5.S10b of the Supplementary Information).

5.3.3 IA-treatment impacts the conformational plasticity of tetrasomes

The presence of non-flipping tetrasomes described above indicates that the H3-H3 interface of the histone tetramer plays an important role in tetrasome flexibility. However, since most IA-treated tetrasomes still exhibited handedness flipping, we looked more closely into its dynamics to obtain a more detailed picture of this process.

For this purpose, the linking number traces ($N = 4$) of a single loaded, flipping (H3.1_{IA}-H4)₂ tetrasome were first analyzed in terms of the times that it spent in each state (dwell times). The underlying data analysis is described in Section 5.2 and the resulting mean dwell times of a (H3.1_{IA}-H4)₂ tetrasome in the left-handed and right-handed conformation are shown in Figure 5.5a,b, respectively. These values, and those determined in a separate analysis based on the dwell times from the step-fitting algorithm, together with the results obtained for an untreated (H3.1-H4)₂ tetrasome from the re-analysis of the partial traces of an earlier experiment [48] are summarized for comparison in Table 5.1. While the total dwell times for each type of tetrasome varied depending on the smoothing, which in the case of the step-fitting algorithm is caused by missed events, their ratio was essentially not affected. This result suggests a reliable analysis that allows the direct comparison of the total dwell times obtained for an untreated tetrasome and an IA-treated tetrasome with the same settings, as well as their ratios.

Table 5.1: Results of the dwell time analysis. The dwell times $\tau_{D,left}$ in the left-handed state and $\tau_{D,right}$ in the right-handed state were obtained as described in Section 5.2.

Sample	Time average in filtering (s)	$\tau_{D,left}$ (s)	$\tau_{D,right}$ (s)	$\frac{\tau_{D,left}}{\tau_{D,right}}$
(H3.1-H4) ₂	3.4 (N = 340)	177 +15/-12*	16 ± 1**	11 ± 1*
tetrasomes	18.4 (N = 1840)	366 +51/-39*	29 +4/-3**	13 ± 2*
(H3.1 _{IA} -H4) ₂	3.4 (N = 340)	105 +8/-7**	24 ± 2**	4 ± 0*
tetrasomes	18.4 (N = 1840)	244 +32/-25**	52 +6/-5**	5 ± 1*
	Step fitting algorithm	288 +41/-32**	71 +10/-7**	4 ± 1*

*Errors calculated by error propagation

**Errors correspond to 68% confidence interval for estimated values from fits

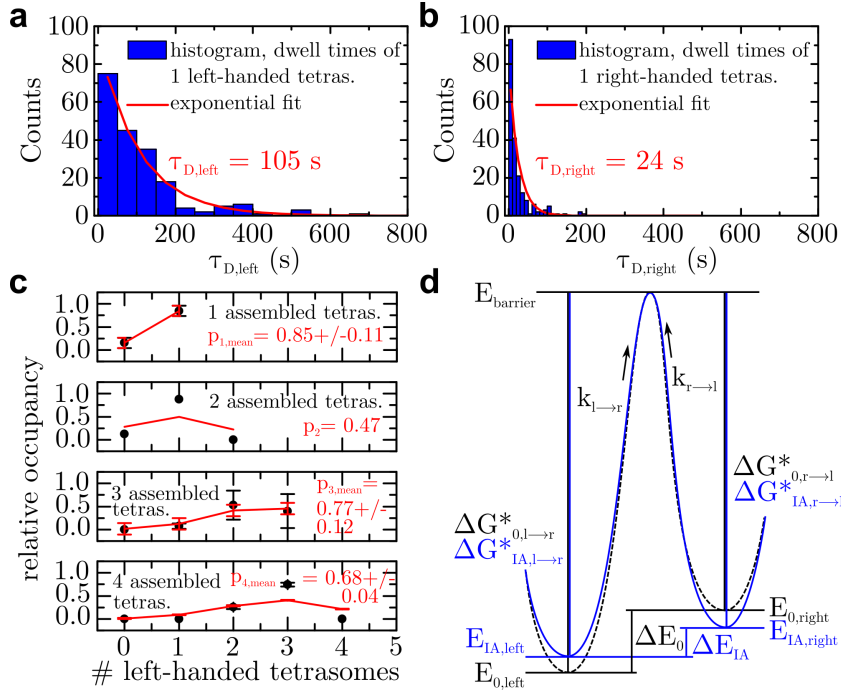
Overall, a (H3.1_{IA}-H4)₂ tetrasome dwelled 1.5 ± 0.3 times shorter in the left-handed state compared to an untreated (H3.1-H4)₂ tetrasome, while the opposite was the case for the right-handed state with a likewise longer dwell time. This indicates that left-handed and right-handed (H3.1_{IA}-H4)₂ tetrasomes are energetically less and more stable, respectively, than their untreated counterparts, while the transition barrier between the two states remains essentially unaffected. The overall impact of IA-treatment is clearly illustrated by the 3 ± 1 -fold decrease of the left-handed versus right-handed dwell time ratio, which suggests a change in the free energy difference between the two states of (H3.1_{IA}-H4)₂ and untreated (H3.1-H4)₂ tetrasomes.

The free energy difference between the two states can be determined from the ratio of the respective dwell times by computing $\Delta E = -k_B T \ln(\tau_{D, \text{right}}/\tau_{D, \text{left}})$. This calculation yields a value of $\Delta E_{IA} = 1.5 \pm 0.1 k_B T$, which is considerably different from the values resulting from dwell time analyses for an untreated (H3.1-H4)₂ tetrasome, i.e., the previously reported value $\Delta E_0 = 2.6 \pm 0.8 k_B T$ (Ref. [48]) or the corresponding value $\Delta E_0 = 2.4 \pm 0.1 k_B T$ determined via our updated analysis algorithm. Thus, the cumulative change in the free energy difference between the left-handed and right-handed state of IA-treated and unmodified tetrasomes by $\Delta E_0 - \Delta E_{IA} = 1.1 \pm 0.3 k_B T$ is consistent with the 3 ± 1 -fold difference in the dwell time ratio.

For validation purposes, the same linking number data were also analyzed in terms of the probability for a (H3.1_{IA}-H4)₂ tetrasome to occupy either the left-handed or right-handed state. This was achieved by considering the peak areas of the fitted Gaussian distributions (Figure 5.4b) whose relative ratios give the probabilities p and $1-p$ to occupy the corresponding states. By this means, a single flipping (H3.1_{IA}-H4)₂ tetrasome was found to obtain the left-handed conformation with an average probability of $p_{av} = 0.85 \pm 0.11$ ($N = 4$), corresponding to an average probability of $1-p_{av} = 0.15 \pm 0.11$ for occupying the right-handed conformation. Likewise, the free energy difference between the two states of $\Delta E_{IA} = 1.7 \pm 0.7 k_B T$ which is deduced from the ratio of the probabilities according to $\Delta E = -k_B T \ln((1-p)/p)$ is similar to the value obtained from the dwell time ratio above.

Alternatively, the free energy difference of the two states was also calculated from the probabilities of all data sets including multiple assembled (H3.1_{IA}-H4)₂ tetrasomes ($N = 12$) by fitting to a binomial distribution (Figure 5.5c). In this approach, the probabilities based on the relative peak area ratios of the Gaussian distributions for each data set with varying number of assembled tetrasomes were assigned to their corresponding

5 Conformations and Dynamics of Modified Tetrasomes



states in terms of the number of tetrasomes being in the left-handed state. Non-observed states were assigned a probability of zero. These data were fit to a binomial distribution with the number of assembled tetrasomes, i.e., the expected number of states being fixed, and the probability of a tetrasome to have the left-handed conformation treated as the free parameter.

Averaging over all obtained values yields a mean probability of $p_{av} = 0.76 \pm 0.15$ of a $(\text{H3.1}_{\text{IA}}\text{-H4})_2$ tetrasome to occupy the left-handed state. This value corresponds to a free energy difference between the two states of $\Delta E = 1.2 \pm 0.6 k_B T$ which agrees well with the values determined from

Figure 5.5: Kinetics and energetics of IA-treated (H3.1-H4)₂ tetrasomes. **a** Histogram of the dwell times of a single (H3.1_{IA}-H4)₂ tetrasome in the left-handed state obtained from linking number time traces smoothed by averaging over $N = 340$ data points, corresponding to a time average of 3.4 s, using a moving average filter. An exponential fit (*red line*) yielded a mean dwell time of $\tau_{D,left} = 105 \pm 8/-7$ s (68% confidence interval for estimated values). **b** Histogram of the dwell times of a single (H3.1_{IA}-H4)₂ tetrasome in the right-handed state obtained from the same linking number data as described in (a). An exponential fit (*red line*) yielded a mean dwell time of $\tau_{D,right} = 24 \pm 2$ s (68% confidence interval for estimated values). **c** Relative occupancies of the left-handed states obtained from the ratios of the mean peak areas of the linking number distributions for different numbers of assembled, flipping (H3.1_{IA}-H4)₂ tetrasomes. Data sets displaying the same number of assembled tetrasomes were averaged (*black circles*), if applicable, and plotted together with a corresponding binomial curve (*red line*) generated using the mean value of the probabilities obtained from a binomial fit to each data set. Data sets displaying different number of assembled tetrasomes are presented in separate panels. Non-occupied states were assigned to the value of 0 relative occupancy. A mean probability for a (H3.1_{IA}-H4)₂ tetrasome to occupy the left-handed state of $p_{left} = 0.76 \pm 0.15$ was determined by averaging over all individual data sets. **d** Energy diagram of untreated (*black*) and (H3.1_{IA}-H4)₂ tetrasomes (*blue*) based on the values determined from the dwell times and the linking number distributions. While the free energy of left-handed (H3.1_{IA}-H4)₂ tetrasomes $E_{IA,left}$ is slightly higher, that of right-handed (H3.1_{IA}-H4)₂ tetrasomes $E_{IA,right}$ is slightly less by the same extent than the respective levels for untreated tetrasomes, $E_{0,left}$ and $E_{0,right}$. Likewise, the free energy difference ΔE_{IA} between the two states of (H3.1_{IA}-H4)₂ tetrasomes is less than that for untreated tetrasomes, ΔE_0 . The energy barriers for the transitions between the two states with the rates $k_{l \rightarrow r}$ and $k_{r \rightarrow l}$ are, respectively, decreased and increased for IA-treated tetrasomes ($\Delta G_{IA,l \rightarrow r}^*$ and $\Delta G_{IA,r \rightarrow l}^*$) compared to the barriers for untreated tetrasomes, $\Delta G_{0,l \rightarrow r}^*$ and $\Delta G_{0,r \rightarrow l}^*$.

the two other approaches above. An untreated (H3.1-H4)₂ tetrasome, however, was previously found to occupy the left-handed conformation with a probability of $p_{av} = 0.90 \pm 0.08$ (Ref. [48]) corresponding to a free energy difference between the two states of $\Delta E_0 = 2.3 \pm 0.8 k_B T$ (Ref. [48]). Taken together, the results from different analysis approaches consistently indicate a decrease in the free energy difference between the states of left-handed and right-handed DNA wrapping in (H3.1_{IA}-H4)₂ versus (H3.1-H4)₂ tetrasomes by $1 k_B T$. For a (H3.3_{IA}-H4)₂ tetrasome, only the latter approach by fitting all probability data ($N = 10$) to a binomial fit was used (Figure 5.S14 of the Supplementary Information),

because the structural dynamics of (H3.3-H4)₂ tetrasomes was previously observed to be very similar to (H3.1-H4)₂ tetrasomes and no dwell time data are available for direct comparison [49]. On average, a mean probability of $p_{av} = 0.88 \pm 0.08$ was found for a (H3.3_{IA}-H4)₂ tetrasome to be in the left-handed state, which corresponds to a difference in free energy between the two states of $\Delta E_{IA} = 2.0 \pm 0.7 k_B T$. In contrast to the observation with (H3.1_{IA}-H4)₂ tetrasomes above, these values agree well with those obtained previously for untreated (H3.3-H4)₂ tetrasomes ($p_{av} = 0.91 \pm 0.03$ and $\Delta E = 2.3 \pm 0.4 k_B T$ (Ref. [49])). The differing results for (H3.3_{IA}-H4)₂ tetrasomes and (H3.1_{IA}-H4)₂ tetrasomes, as also observed for their flipping behavior, might arise from subtle structural differences upon IA-incorporation. However, it was also observed that the handedness dynamics of (H3.3-H4)₂ tetrasomes was slightly stimulated by the presence of NAP1, in contrast to (H3.1-H4)₂ tetrasomes [48, 49]. In our experiments, NAP1 was present in solution throughout the measurements due to the observed trend of enhanced disassembly of IA-treated tetrasomes upon flushing out free proteins. Therefore, the mean probability and free energy difference for (H3.3_{IA}-H4)₂ tetrasomes might also be smaller than the obtained value and similar to that determined for (H3.1_{IA}-H4)₂ tetrasomes.

Overall, these results indicate that IA-modification influences the stability of and the kinetics between the two tetrasome conformations. The shorter dwell time in the left-handed state suggests its decreased stability, while the right-handed conformation with a dwell time increased to the same extent is more stable compared to untreated tetrasomes. These effects are also reflected by corresponding differences in the probabilities of finding an IA-treated tetrasome in a certain state. Thus, the IA-treatment results in a decrease of the free energy difference between the two states.

5.4 Discussion and Conclusion

Since four decades, chromatin research continues to reveal various aspects of the structure, function, and dynamics of the nucleosome as the fundamental DNA-protein complex in increasing detail. The chemically, force-, or torque-induced partial or full removal of H2A/H2B dimers by changes in buffer conditions, mechanical manipulation, or by genome-processing enzymes such as the RNAP [59–61], makes subnucleosomal structures a topic of great interest. As stable intermediates, tetrasomes were investigated early on by biochemical approaches [42, 43]. These pioneering experiments demonstrated the high affinity of the (H3-H4)₂ tetramers for either negatively or positively supercoiled DNA, resulting in mutually

convertible tetrasome conformations of a left-handed superhelix, like in the full nucleosome, or a right-handed DNA wrapping, respectively. Additional studies have suggested that this transition in tetrasome handedness results from the spontaneous reorientation of the $(\text{H3-H4})_2$ tetramer at the H3-H3 interface [44–47]. Our previous studies of the assembly and structural dynamics of tetrasomes at the single-molecule level have confirmed the existence of two handedness states and revealed their dynamic nature [48, 49]. The tetrasomes were observed to continuously flip between a predominant left-handed and a less occupied right-handed conformation. However, these studies did not directly investigate the underlying mechanism of this phenomenon.

In this work, we sought to address this issue by interfering with the potential flexibility of the histone tetramer at the H3-H3 interface and monitoring the effects at the single-molecule level. We have investigated the NAP1-mediated assembly and structural dynamics of individual $(\text{H3.1-H4})_2$ and $(\text{H3.3-H4})_2$ tetrasomes modified with IA at the single cysteine at position 110 of the H3 histones in real time using FOMT [50]. In biochemical analyses of bulk tetrasome assemblies, this modification was previously found to block the handedness flipping of tetrasomes by potentially generating a steric hindrance at the H3-H3 interface of the histone tetramers [44]. The IA-treated histone $((\text{H3}_{\text{IA}}\text{-H4})_2)$ tetramers had been reported to only form inherently left-handed tetrasomes lacking the structural transition to the right-handed conformation. In agreement with this biochemical study, IA-treated tetrasomes assembled with a similar structure to untreated tetrasomes in our assay, which indicates the formation of proper complexes. However, in contrast to untreated tetrasomes, we observed IA-treated tetrasomes to disassemble in the course of the experiments, which suggests their decreased stability, possibly due to changes in their properties upon IA-incorporation. In the previous biochemical analyses, IA-treated tetramers have also been found to exhibit a low affinity to relaxed circular DNA templates and modified tetrasomes migrated faster on a gel than untreated tetrasomes. However, unlike the observation of only left-handed IA-treated tetrasomes in that study, we found $(\text{H3}_{\text{IA}}\text{-H4})_2$ tetramers to also form right-handed tetrasomes. The varying results likely arise from the use of different approaches: single-molecule experiments, performed in highly diluted conditions, are known to be more sensitive than bulk assays, especially in terms of revealing transient intermediates and the dynamics of biomolecules. Another reason for this discrepancy could be the difference in the topology of the employed DNA constructs, which might be critical. The different topological restriction of tethered linear DNA fragments being subject to (low) force in our assay and of super-

coiled circular DNA molecules employed in the biochemical analyses might bias tetrasome assembly. Likewise, apart from right-handed assembly, we also observed IA-treated tetrasomes to exhibit spontaneous changes in their handedness. However, while their structural rearrangement upon handedness flipping was very similar to that of untreated tetrasomes, the kinetics were found to be different.

The different kinetics and energetics between IA-treated and untreated tetrasomes are shown by the schematic energy diagram presented in Figure 5.5d, based on the here obtained results. Setting the barrier energy (E_{barrier}) to the same value for a common reference, the free energy of left-handed IA-treated tetrasomes ($\Delta E_{IA, \text{left}}$) is by a small amount higher than that for untreated tetrasomes ($\Delta E_{0, \text{left}}$), as reflected in the 1.5-fold decrease in the corresponding dwell time $\tau_{D, \text{left}}$. Conversely, the 1.5-fold increase in the dwell time $\tau_{D, \text{right}}$ indicates a likewise lower free energy of right-handed IA-treated tetrasomes. These differences indicate that IA-treated tetrasomes are slightly less stable in the left-handed state and slightly more stable in the right-handed conformation than untreated tetrasomes due to the incorporated IA molecules. This effect might also play the central role in the 3-fold decreased ratio of the dwell times for IA-treated tetrasomes, which corresponds to a change in the free energy difference between the two states of $1 k_B T$ compared to untreated tetrasomes, as determined from three different approaches. Knowing the transition rates $k_{l \rightarrow r}$ and $k_{r \rightarrow l}$, related to the corresponding dwell times $\tau_{D, \text{left}}$ and $\tau_{D, \text{right}}$ by $k = 1/\tau$, the height of the respective transition barriers can be calculated according to $\Delta G^* = -k_B T \ln(k/k_0)$ with the rate k_0 for spontaneous transitions in tetrasome structure at zero force. Considering a rate of $k_0 \sim 10^7 \text{ s}^{-1}$ based on the value of $\sim 3 \cdot 10^6 \text{ s}^{-1}$ previously estimated for spontaneous structural transitions of full nucleosomes [62], the energy barrier for the transition from the left-handed to the right-handed state can be estimated to $\Delta G_{0, l \rightarrow r}^* \sim 21.3 k_B T$ for untreated, and to $\Delta G_{IA, l \rightarrow r}^* \sim 20.8 k_B T$ for (H3.1_{IA}-H4)₂ tetrasomes. The same calculation gives an estimate of $\Delta G_{0, r \rightarrow l}^* \sim 18.9 k_B T$ and $\Delta G_{IA, r \rightarrow l}^* \sim 19.3 k_B T$ for the transition from the right-handed to the left-handed state for untreated and (H3.1_{IA}-H4)₂ tetrasomes, respectively. The results consistently indicate that the energies of the two states are altered, while the energy barrier for the structural transition of tetrasomes is essentially unaffected. On the whole, our findings show that the IA-treatment did not affect the overall structural properties of tetrasomes but had some impact on their stability, flexibility, and dynamics. The unexpected occurrence of continuous handedness flipping and assembly of IA-treated tetrasomes into the right-handed conformation indicate that the incorporation of the IA

molecules does not fully prevent these dynamics. Our results are directly comparable to our previous studies of untreated tetrasomes, as the same technique and essentially the same conditions have been used (Table 5.2). Based on the observations in other single-molecule assays [63], we do not expect such low volume concentrations ($<1\%$) of crowding agents to have a significant impact on the kinetics and energetics of the biological system under study. For this reason, we conclude that the observed changes in the energetics and flipping kinetics of tetrasomes are due to the IA-treatment. The results suggest that IA-modification enhances the conformational plasticity of tetrasomes, while their structural dynamics is affected to a lesser extent. Considering the very low forces of 0.6-0.7 pN employed in our experiments, possible contributions from other phenomena, such as DNA flexibility, cannot be excluded.

Table 5.2: Summary of the properties of IA-treated and untreated tetrasomes for comparison.

Quantity	(H3.1-H4) ₂ tetrasomes	(H3.1 _{IA} -H4) ₂ tetrasomes	(H3.3-H4) ₂ tetrasomes	(H3.3 _{IA} -H4) ₂ tetrasomes
$\Delta z_{dis-/ass}$ (nm)	$24 \pm 3^*$	29 ± 8	$25 \pm 6^{**}$	26 ± 8
$\Delta \theta_{dis-/ass}$ (turns)	$0.73 \pm 0.05^*$	1.1 ± 0.3	$0.8 \pm 0.2^{**}$	1.0 ± 0.3
$\Delta \theta_{flipping}$ (turns)	$1.7 \pm 0.1^*$	1.6 ± 0.2	$1.7 \pm 0.1^{**}$	1.6 ± 0.2
$\tau_{D,left}$ (s)	$177 \pm 15/-12$	$105 \pm 8/-7$	—	—
$\tau_{D,right}$ (s)	16 ± 1	24 ± 2	—	—
ΔE ($k_B T$) (dwell times)	2.4 ± 0.1	1.5 ± 0.1	—	—
ΔE ($k_B T$) (binomial fits)	$2.3 \pm 0.8^*$	1.2 ± 0.6	$2.3 \pm 0.4^{**}$ ($1.6 \pm 0.8^{**}$)	2.0 ± 0.7
ΔE ($k_B T$) (peak-area ratios)	—	1.7 ± 0.7	—	—

*values taken from our previous study of (H3.1-H4)₂ tetrasomes [48]

**values taken from our previous study of (H3.3-H4)₂ tetrasomes [49]

In a broader context, our previous and current findings suggest the handedness dynamics of tetrasomes as an intrinsic and tunable mechanism of chromatin to regulate the impact of supercoiling on the genome at

the nucleosomal level. Although tetrasomes have not yet been observed *in vivo*, their existence seems quite likely based on *in vivo* studies that have reported higher exchange and mobility of H2A and H2B histones compared to histones H3 and H4 [64–66], as well as the involvement of chaperones or remodelers that specifically target histones H2A and H2B [67, 68]. Interestingly, these observations were made in transcriptionally active chromatin, indicating an important role of subnucleosomal structures during genome-processing by RNAP exerting forces and torques on the DNA [51]. The same would be expected for other key cellular processes such as replication and DNA repair [69, 70]. Subnucleosomal structures could facilitate and regulate these processes, especially due to their intrinsic dynamics which could further be adjusted by histone core modifications altering DNA-histone or histone-histone interactions [52]. Next to collecting more evidence for the existence of subnucleosomal structures, the key and challenging task will be to identify their structural, functional, and dynamic properties in molecular detail in order to advance our understanding of the mechanisms underlying chromatin structure and dynamics.

5.5 Supplementary Information

Supplementary materials and methods

MS experiments with IA-treated histones

Protein bands were excised from SDS-PAGE gels and digested with trypsin from porcine pancreas (Sigma-Aldrich) as previously described in Ref. [71]. Tryptic digests were analyzed using an UltiMate 3000 nano-HPLC system (Thermo Scientific by Thermo Fisher Scientific, Waltham, MA, United States) coupled to a Q Exactive HF mass spectrometer (Thermo Scientific) equipped with a Nanospray Flex ionization source. The peptides were separated on a homemade fritless fused-silica microcapillary column (75 μm i.d. \times 280 μm o.d. \times 10 cm length) packed with 3 μm reversed-phase C18 material (Reprosil, Ammerbuch-Entringen, Germany). Solvents for HPLC were 0.1% formic acid (solvent A) and 0.1% formic acid in 85% acetonitrile (solvent B). The gradient profile was as follows: 0–2 min, 4% B; 2–55 min, 4–50% B; 55–60 min, 50–100% B, and 60–65 min, 100% B. The flow rate was 250 nl/min. The Q Exactive HF mass spectrometer was operated in the data dependent mode by selecting the top 20 most abundant isotope patterns with charge >1 from the survey scan with an isolation window of 1.6 mass-to-charge ratio (m/z). Survey full scan MS spectra were acquired

from 300 to 1750 m/z at a resolution of 60,000 with a maximum injection time (IT) of 120 ms, and automatic gain control (AGC) target $1e6$. The selected isotope patterns were fragmented by higher-energy collisional dissociation (HCD) with a normalized collision energy of 28 at a resolution of 15,000 with a maximum IT of 120 ms, and AGC target $5e5$.

Data analysis was performed using Proteome Discoverer 1.4.1.14 (Thermo Scientific) with the search engine Sequest. The raw files were searched against the *Drosophila melanogaster* database extracted from the Uniprot database. Precursor and fragment mass tolerances were set to 10 ppm and 0.02 Da, respectively, and up to two missed cleavages were allowed. Carbamidomethylation of cysteine and oxidation of methionine were set as variable modifications. Peptide identifications were filtered at 1% false discovery rate. Quantification of modified and unmodified H3.1 and H3.3 peptides was performed by summing over the respective areas under the curve (AUC) (Figure 5.S2c,d below). The underlying HPLC chromatograms and MS2-spectra are shown in Figures 5.S3 and 5.S4 below, respectively.

Salt-dialysis reconstitution of tetrasomes

For the reconstitution of untreated tetrasomes, either 0.2 μg , 0.3 μg or 0.4 μg H3.3-H4 histones were mixed with 700 ng of the 3.25 kbp linear DNA construct. Either 0.125 μg , 0.15 μg or 0.175 μg IA-treated H3.3-H4 (H3.3_{IA}-H4) histones were mixed with 700 ng DNA for the assembly of IA-treated tetrasomes. The samples were prepared in 50 μl high-salt buffer containing 2 M NaCl (J.T. Baker, Phillipsburg, NJ, United States), 10 mM Tris(hydroxymethyl)amino-methane-HCl (Tris-HCl, pH 7.4; Sigma-Aldrich, St. Louis, MO, United States), 1 mM EDTA (Sigma-Aldrich), and 1 mM DTT (Sigma-Aldrich).

Tetrasome assembly was then induced by dialyzing the samples placed in 200 ml high-salt buffer against 920 ml of a buffer containing 10 mM Tris-HCl, 1 mM EDTA, and 1 mM DTT using a multi-channel peristaltic pump (ISMATEC by Cole-Parmer, Wertheim, Germany) at a flow rate of 800 $\mu\text{l}/\text{min}$ over 19 h at 4°C. The resulting products were checked by electrophoresis on a pre-run 0.7%-agarose gel loaded with 70 ng or 140 ng sample and run in $0.1\times$ Tris-Borate-EDTA buffer (TBE; Promega) at 80 V for 3 h at RT. The samples on the gel were visualized by post-staining with Ethidium Bromide (Promega) for 30 min and imaged using a gel imager (ChemiDoc MP, Bio-Rad, Hercules, CA, United States) (Figure 5.S5a below).

The best products of each reconstitution reaction were also diluted to

concentrations resembling the conditions in single-molecule experiments and analyzed by native gel electrophoresis to determine the effects of high dilutions. For this purpose, the pre-run 0.7% agarose gel was loaded with 0.4 ng of bare DNA and either 0.14 ng, 0.28 ng, or 0.56 ng of each of the two samples and run at 80 V for 3 h at RT. DNA was visualized by Sybr Gold (Invitrogen by Thermo Fisher Scientific) staining for 30 min on the gel imaged using a variable mode laser scanning imager (Typhoon TRIO, GE Healthcare, Chicago, IL, United States). The image was taken using the basic settings with the filter 488/520 BP 40 and +3 mm focal depth, and the variable settings set to high sensitivity at 550 PMT with a pixel size of 100 μm (Figure 5.S5b below).

Flow cell assembly and preparation for single-molecule experiments

The lower coverglass was coated with 2.5 μl of a 0.1% solution of nitrocellulose (Invitrogen) dissolved in pentyl acetate solution (Sigma Aldrich). One flow cell was used for each experiment. The flow cell was prepared by first incubating for 1 h with 100 μl of amine-coated polystyrene beads (1 μm diameter, Polysciences, Warrington, PA, United States) diluted by 1:2500 or 1:5000 in a buffer containing 100 mM NaCl, 10 mM Tris-HCl, and 1 mM EDTA (TE buffer). Unbound beads were then washed out with 300-500 μl TE buffer. Subsequently, the flow cell was put on a heat-plate for 100-120 s at 100°C to melt down the bound polystyrene beads for stable adhesion to the nitrocellulose-coated surface. After subsequent rinsing with 300-500 μl buffer, the flow cell was washed and incubated overnight with 100 μl of a 0.1 mg/ml solution of anti-digoxigenin antibody fragments (Roche) dissolved in PBS (Sigma-Aldrich). The next day, the flow cell was washed with 300-500 μl TE buffer and passivated with 100 μl of a 20 mg/ml BSA solution (New England Biolabs, Ipswich, MA, United States) diluted 1:1 in TE buffer.

Thus functionalized, the flow cell was then prepared for tethering of DNA constructs by washing with 500-1000 μl TE buffer containing 0.015% Triton-X (Sigma-Aldrich; TE-TX buffer). 0.2 or 0.4 μl of a solution with superparamagnetic beads (0.5 μm diameter, Ademtech, Pessac, France) were washed three times in 10 μl of TE-TX buffer, then mixed and incubated for 10 min with 0.4 or 0.8 μl of a DNA solution diluted 1:100 from the stock solution with a DNA concentration of 16 ng/ μl . Upon a subsequent dilution by 1:100, 100 μl of the DNA/bead solution was flushed into the flow cell and incubated for 2-3 h for tethering to the functionalized coverglass. Unbound tethers were flushed out with at least 2 ml buffer for

a clean flow cell to start the experiment.

MT hardware

The hardware of the MT setup used in this study has been detailed previously [72]. In brief, the flow cell containing the sample is illuminated from the top by a light-emitting diode (LED; Lumitronix, Hechingen, Germany). The transmitted light is collected by a 100x oil-immersion objective (Olympus, Tokyo, Japan) and directed onto a CMOS camera (Teledyne Dalsa, Waterloo, Canada) operated at an acquisition rate of 100 Hz. By this means of video microscopy, the bead's position is tracked with nanometer accuracy using a custom-written tracker software [73]. In this FOMT-based study, the bead is subject to a magnetic field generated by a cylindrical permanent magnet stacked of three ring-shaped magnets (Supermagnete, Gottmadingen, Germany) and positioned between the flow cell and the LED. The DNA tethers were aligned with the magnet axis by manually and/or electronically positioning the custom-built sample stage using linear actuators of sub-micrometer precision (Physik Instrumente, Karlsruhe, Germany).

Data analysis

The recorded, raw time traces of the bead's lateral position in x , y , and vertical position in z were converted into the corresponding time traces of the linking number and the length of the tethered DNA molecule, respectively, as described in [50]. The time windows in which proteins were flushed in, and so the bead was subject to fluid flow, were cut out before the subsequent quantitative analysis of the traces, which was performed as briefly described in Section 5.2.

In the determination of the steps coinciding in both time traces, a maximum time difference of 18.4 s, deduced from autocorrelation analysis of the bead's rotational fluctuations (Figure 5.S6 below), was tolerated between the steps. By this means, 43% ($n = 33$) of all identified coinciding steps ($N = 76$) were detected automatically, while 63% ($n = 48$) were determined after manually correcting misidentified steps to better match the data.

The sizes of all thus determined steps were further compared against the mean spatial resolution, essentially corresponding to the experimental measurement error. The time traces contain intrinsic time-correlated fluctuations that result from the (dominant) thermal motion of the tethered beads and hardware-inherent noise. These values supported a more reliable interpretation of the fitted steps, as those with sizes below the mean spatial

resolution might also be the result of experimental drift or artifacts by the step-fitting algorithm due to the high noise in the time traces. Therefore, steps coinciding in both time traces of individual measurements were considered to have been induced by tetrasome assembly, regardless of their size. The mean spatial resolution was calculated for both quantities by averaging over the STDs from the functions fitted to their time trace profiles. In general, the length data was fitted by a gamma function after mirroring at the x -axis to compensate for the slight skew of the data towards smaller values, possibly due to attractive bead-surface interactions. As the spatial resolution in one experiment, the average of the STDs from gamma fits to three (in one case two) different parts of the longest durations between two subsequent steps were considered. The linking number data was fitted to a corresponding number of Gaussian functions. Here, the spatial resolution in one experiment was determined by the STD from the fit of a single Gaussian function to the data in the initial part of the time trace, before proteins were flushed in.

In the employed dwell time analysis for a more detailed picture of the handedness dynamics, the traces were filtered by averaging over either a number $N = 340$ or $N = 1840$ data points which, based on the acquisition rate of 100 Hz, correspond to a time average of 3.4 s or 18.4 s, respectively, in agreement with the results from the autocorrelation analysis of the bead's rotational fluctuations (Figure 5.S6 below). This approach ensured the decoupling of the beads' thermal motion from the flipping dynamics of the tetrasomes. The extent of the filtering proved to be very critical due to its high impact on the overall results such that no preference could be made between the two approaches for an explicit statement about the total dwell times. By extending the threshold into a zone, only linking number changes upon flipping that were greater than this threshold zone were considered, while mostly events in the noisy, undefined region at the overlap of the two states were disregarded by adding their dwell times to that in the current state up to that point. Likewise, detected events with dwell times shorter than the mean characteristic time of the bead's rotational fluctuations (bead response time) of 3.4 s (Figure 5.S6 below) were corrected for in a last step.

In the separate analysis of the recorded dwell times in the plateaus of the steps fitted by the step-fitting algorithm, some of the flipping events were missed and steps introduced which do not match the data very well, although the algorithm was allowed to overfit to detect as many states as possible (Figure 5.4b). Such steps were manually corrected for a better match to the data and a more reliable dwell time analysis. The mean dwell times were determined by an exponential fit to the combined data

sets assigned to the left-handed ($N = 65$) and right-handed state ($N = 64$) and, if applicable, cut off at the mean dissociation time reduced by 1 SEM (Figure 5.S7 below), i.e. 2084 s.

In the re-analysis of the partial traces from an earlier experiment with untreated (H3.1-H4)₂ tetrasomes presented in [48], the resulting mean dwell time for the left-handed state was multiplied by a factor of three to obtain the life time for a single left-handed tetrasome, as three independent tetrasomes were assembled on the DNA molecule here. Since a second tetrasome only flipped with relative occurrences of 2.7% and 0.7% in two of the partial time traces, all data assigned to the right-handed state was considered as flipping events of one tetrasome.

Supplementary tables

Table 5.S1. The sequences of the primers used to generate the DNA constructs. Lowercases indicate the specific overhangs at the BsaI sites.

Primers	Primer Sequences
1	5'-CTGCGGTCTCGtaggCCTCAGCGACGCAGGGGACCTGCAGG
2	5'-CTGCGGTCTCGtcaaTGCCGTTGTAACCGGTCATC
3	5'-CCATCTTGGTCTCCcctaCGCTCTAGAACTAGTGGATCCCC
4	5'-CCATCTTGGTCTCCttgaCGCTCTAGAACTAGTGGATCCCC
5	5'-GACCGAGATAGGGTTGAGTG

Supplementary figures



Figure 5.S1. Details of the DNA construct used in this study. a Schematic depiction of the 1.97 kbp linear DNA fragment (*light purple*) generated from a pBluescript (pBlue) 2,3 plasmid by PCR with primers 1 and 2. Shorter, either biotin- (Bio, *black*) or digoxigenin-coated (Dig, *red*) fragments (handles) of 643 bp generated by primers 3 and 4, respectively, in combination with primer 5, were each ligated via *Bsa*I sites to either end. For details on the preparation of the DNA constructs, see Section 5.2 and Table 5.S1 above. **b** Sequence of the main DNA segment.

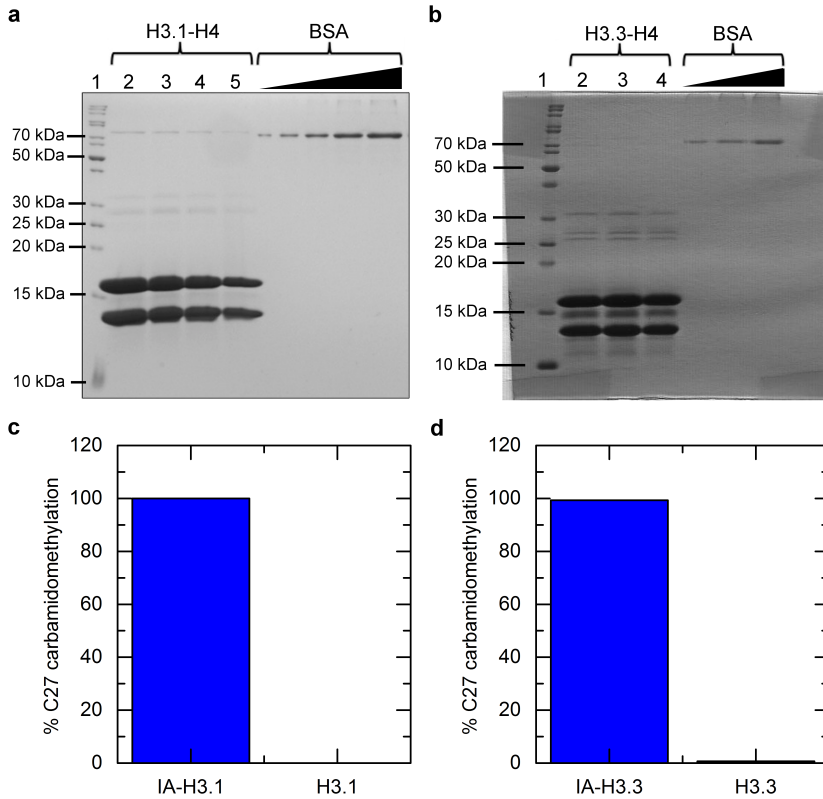


Figure 5.S2. Purified and IA-treated histones. **a, b** Protein gels stained with Coomassie blue showing H3.1-H4 and H3.3-H4 histones, respectively, before (lanes 2) and after dialysis into a buffer suitable for the IA-treatment (lanes 3), as well as after the treatment (lane 4 in (a), not shown in (b)) and after another dialysis to remove IA (lane 5 in (a), lane 4 in (b)). The total concentrations of histones in the equimolar samples were estimated to 2 $\mu\text{g}/\mu\text{l}$ and 280 $\text{ng}/\mu\text{l}$, respectively, from BSA standards (subsequent lanes with 50 ng , 100 ng , 200 ng , 400 ng , 600 ng in (a), and 100 ng , 200 ng , 400 ng in (b)). **c, d** MS analysis of IA-treated histones H3.1 (H3.1_{IA}) and H3.3 (H3.3_{IA}), respectively, showing complete (100%, (c)) or near complete ((d), 99.3%) conversion of the cysteine residues into carbamidomethyl-cysteine. Values were calculated from the sum of the respective areas under the curve (AUC) of C27-containing peptides with or without carbamidomethylation.

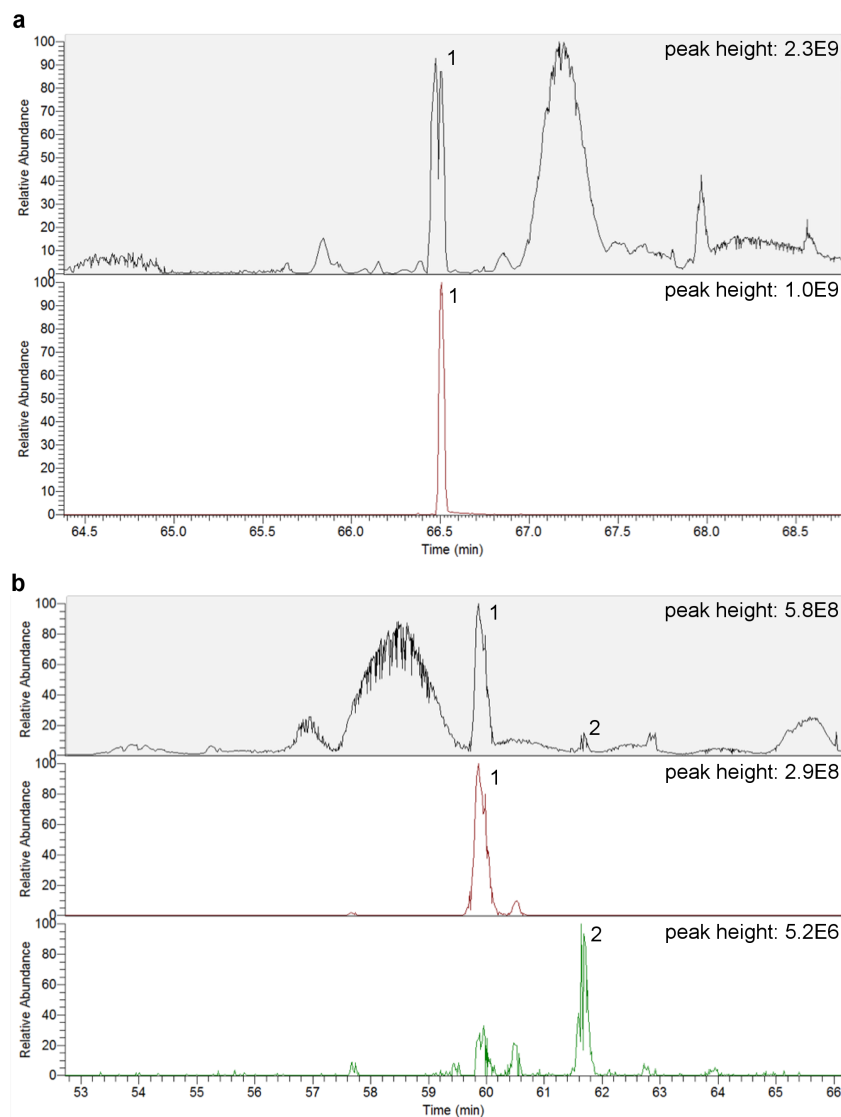


Figure 5.S3. HPLC chromatograms. **a** Base peak (top) and extracted ion chromatogram (bottom) of H3.1 digest. Only the carbamidomethylated peptide spanning amino acids 85-116 (peak 1) was found. **b** Base peak (top) and extracted ion chromatograms (middle, bottom) of H3.3 digest. Peak 1 corresponds to the carbamidomethylated peptide 85-116, while peak 2 depicts the unmodified peptide.

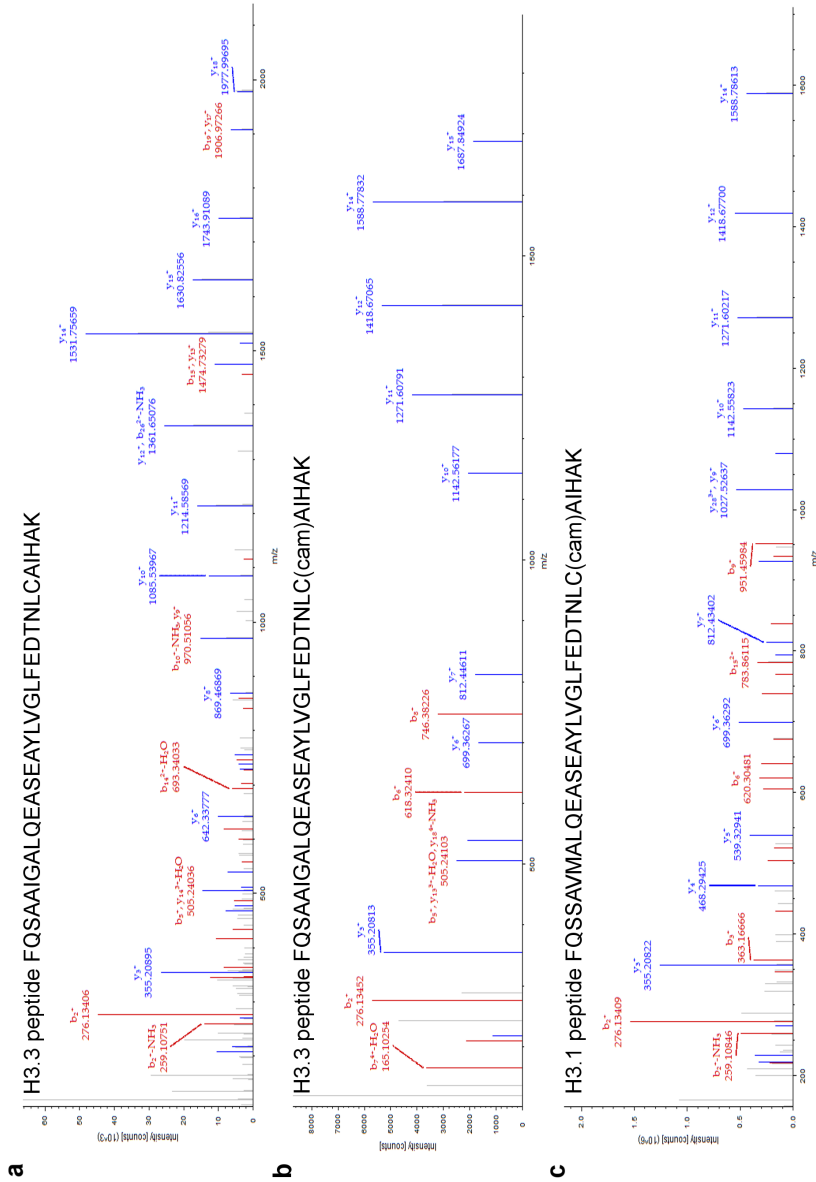


Figure 5.S4. MS2-spectra of the histone H3 peptides. a, b MS2-spectra of the unmodified (a) and carbamidomethylated (b) histone H3.3 peptide spanning amino acids 85-116. **c** MS2-spectrum of the carbamidomethylated histone H3.1 peptide 85-116.

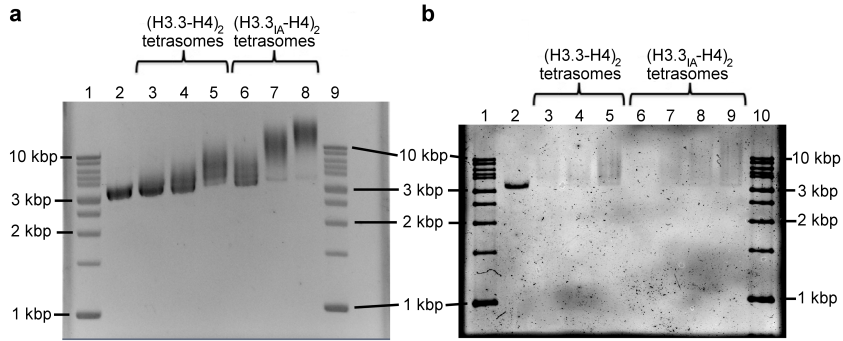


Figure 5.S5. Untreated and (H3.3_{IA}-H4)₂ tetrasomes reconstituted via salt-dialysis. **a** 0.7%-agarose gel of reconstitution products using three different concentrations of untreated (lanes 3-5) and (H3.3_{IA}-H4)₂ tetrasomes (lanes 6-8) and a 3.25 kbp long linear DNA fragment (lane 2). Increasing amounts of untreated H3.3-H4 histones (0.2 μ g, 0.3 μ g, 0.4 μ g in lanes 3-5) or H3.3_{IA}-H4 histones (0.125 μ g, 0.15 μ g, 0.175 μ g in lanes 6-8) were loaded onto 700 ng DNA. After reconstitution via salt-dialysis, 70 ng (lanes 2 and 3) or 140 ng (lanes 4-8) of DNA assembled into tetrasomes were loaded onto the gel and stained with ethidium bromide. Lanes 1 and 9 contain the DNA size marker. **b** 0.7%-agarose gel showing different dilutions of lanes 5 and 7 from (a) stained with Sybr Gold. The degrees of dilution (1:1000, 1:500, and 1:250 in lanes 3-5 and 7-9, respectively) correspond to conditions used in single-molecule experiments. The shift of the DNA smears towards reduced molecular weights indicates at least partial disassembly upon dilution. Lanes 1 and 10 contain the DNA size marker.

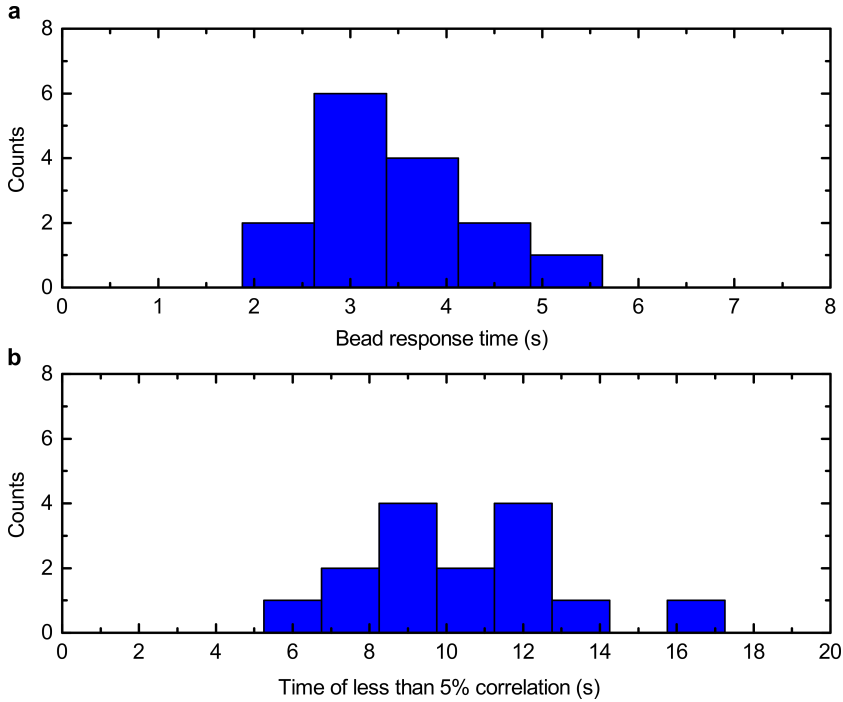


Figure 5.S6. Characteristic times of the measured fluctuations in the linking number of bare DNA molecules. **a** Histogram of the bead response times for a 1.97 kbp DNA segment tethered to a small paramagnetic bead (diameter of 500 nm). The response times are determined from autocorrelation analysis of the DNA linking number time traces measured in FOMT experiments [50]. Knowledge of the bead's response time, characterizing its thermal motion, is critical for both the identification of coinciding steps in the time traces of DNA length and linking number upon tetrasome assembly or disassembly, and for the dwell time analysis. The data yielded a mean value of $\tau_c = 3.4 \pm 0.9$ s. **b** Histogram of the first times at which the autocorrelation is below 5%, showing a mean value of $\tau_c = 10.3 \pm 2.7$ s. This mean value plus three STDs ($\tau_c = 18.4$ s) was employed as an upper cutoff for the time difference between assembly or disassembly steps in both quantities to be identified as coinciding. These values also provided the filtering time scales for the time traces subjected to dwell time analysis (see Supplementary Materials and Methods above).

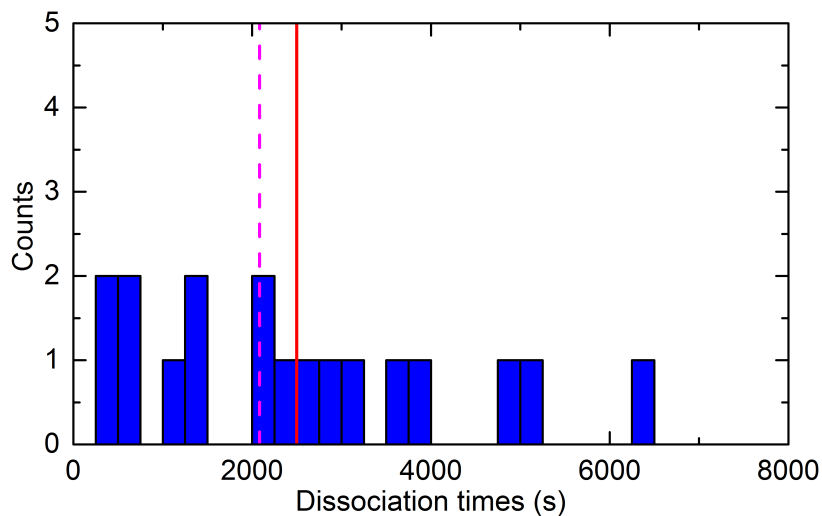


Figure 5.S7. Distribution of the dissociation times for (H3.1_{IA}-H4)₂ tetrasomes. IA-treated (H3.1-H4)₂ tetrasomes were found to disassemble at different times during the experiments. These dissociation times can be critical for the study of the dynamics, but they are distributed broadly: the mean value of 2499 s (red line) with a STD of ± 1763 s is poorly defined. Therefore, the mean value subtracted by 1 SEM (= 415 s) at 2084 s (*dashed magenta line*) is considered, e.g. in the dwell time analysis.

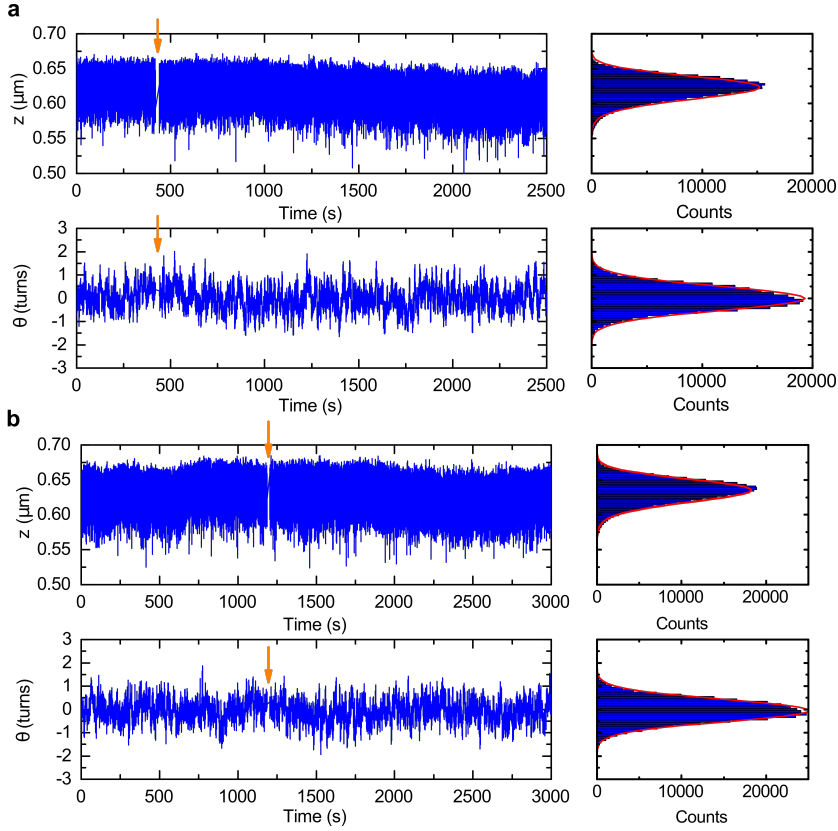


Figure 5.S8. Example traces with the individual proteins. **a** Time traces of length z (in μm , upper panel) and linking number θ (in turns, lower panel) of a DNA molecule before and after flushing in (*orange arrows*) $(\text{H3.1IA-H4})_2$ tetramers without pre-incubation with NAP1 under the standard conditions in this study (see Section 5.2). As the singly peaked mirrored gamma (due to the slight skew of the data to smaller values) and normal distributions (*red*) indicate, the histone tetramers do not assemble into tetrasomes in the absence of NAP1. **b** Time traces of DNA length z (upper panel) and linking number θ (lower panel) of a DNA molecule before and after flushing in (*orange arrows*) only NAP1 proteins under the standard conditions in this study. As the singly peaked mirrored gamma (due to the slight skew of the data to smaller values) and normal distributions (*red*) indicate, NAP1 alone does not interact with the DNA molecule.

5 Conformations and Dynamics of Modified Tetrasomes

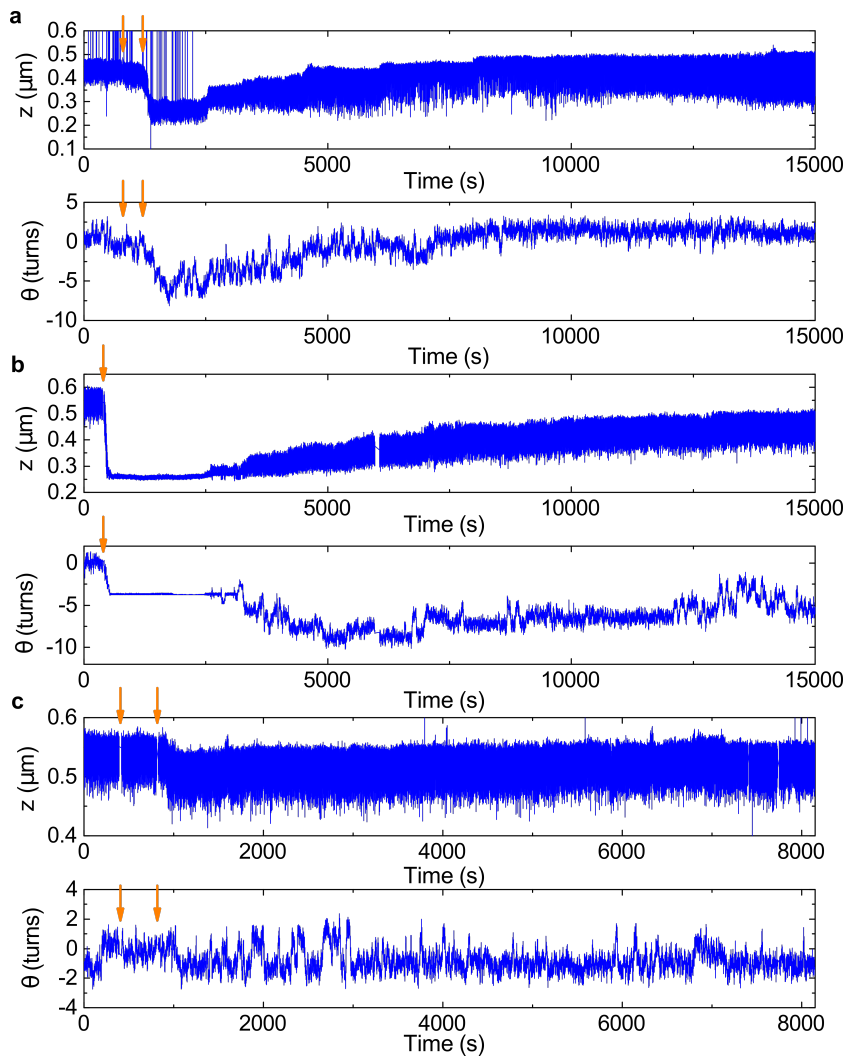


Figure 5.S9. Example traces with different ratios of IA-treated histones and NAP1. **a** Time traces of length z (in μm , upper panel) and linking number θ (in turns, lower panel) of an initially bare DNA molecule with $(\text{H3.3}_{\text{IA}}\text{-H4})_2$ tetrasomes assembled after flushing in (*orange arrows*) 108 nM $\text{H3.3}_{\text{IA}}\text{-H4}$ histones pre-incubated with 192 nM NAP1, i.e. in a ratio of 1:1.8. Initially (up to about 2000 s), the z position is not very well tracked, which results in some spikes, but does not affect the overall signal. As indicated by the stepwise increases in DNA length and linking number, the modified tetrasomes also disassembled under these conditions. **b** Time traces of DNA length z and linking number θ of an initially bare DNA molecule with $(\text{H3.3}_{\text{IA}}\text{-H4})_2$ tetrasomes assembled after flushing in (*orange arrows*) 127 nM $\text{H3.3}_{\text{IA}}\text{-H4}$ histones incubated with 192 nM NAP1, i.e. in a ratio of 1:1.5. Here, the modified tetrasomes even disassembled from a fully assembled DNA molecule. While the assembly of the multiple tetrasomes in both (a) and (b) happened simultaneously in the form of large steps, they mainly disassembled in a one-by-one fashion, indicating the formation of proper individual complexes (see main text and Figure 5.3b). **c** Time traces of DNA length z and linking number θ of an initially bare DNA molecule with $(\text{H3.1}_{\text{IA}}\text{-H4})_2$ tetrasomes after flushing in (*orange arrows*) 100 nM $\text{H3.1}_{\text{IA}}\text{-H4}$ histones incubated with 113 nM NAP1, i.e. in a ratio of 1:1.1. Here, the modified tetrasome did not disassemble over the total measurement time, while it exhibited the same handedness dynamics, within error, as quantified by analyzing the dwell times in the step plateaus from the step-fitting algorithm ($\tau_{D,\text{left}} = 326\text{ s}$ and $\tau_{D,\text{right}} = 79\text{ s}$, see Section 5.2, and Table 5.1).

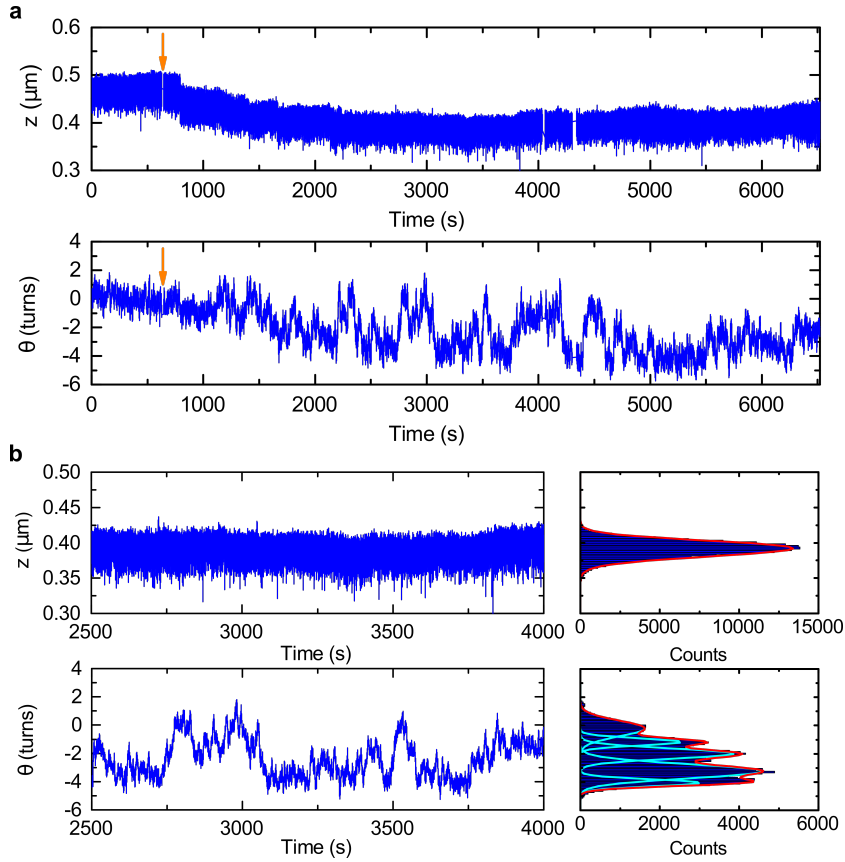


Figure 5.S10. Example time traces with untreated tetrasomes in the same buffer conditions as the IA-treated tetrasomes. **(a)** Time traces of length z (in μm , upper panel) and linking number θ (in turns, lower panel) of an initially bare DNA molecule with $(\text{H3.3-H4})_2$ tetrasomes assembled after flushing in (*orange arrows*) $(\text{H3.3-H4})_2$ tetramers pre-incubated with NAP1 under the standard conditions in this study (see Section 5.2). The untreated tetrasomes do not disassemble during the experiment. **(b)** Partial time traces from (a) to illustrate the handedness dynamics of the untreated tetrasomes. While the DNA length z stays constant (upper panel), the linking number θ (lower panel) is observed between several discrete levels. The four assembled tetrasomes occupy five states whose populations were fit to normal distributions (individual fits in *cyan*; sum of all fits in *red*).

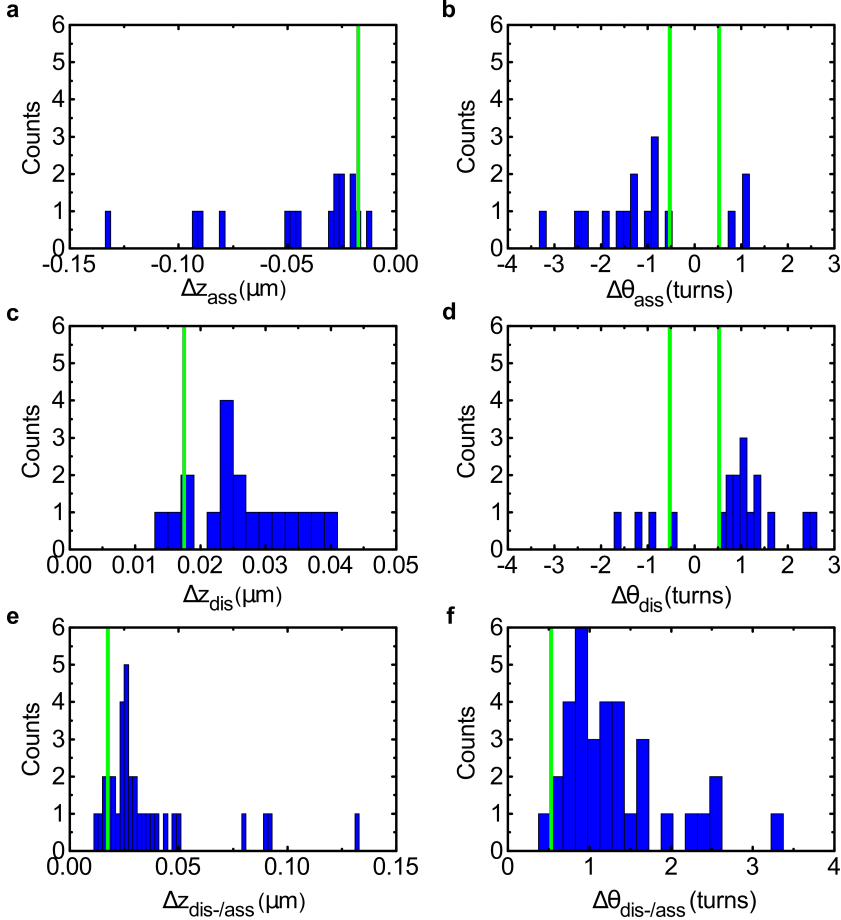


Figure 5.S11. Changes in DNA length and linking number upon assembly and disassembly of $(\text{H3.1IA-H4})_2$ tetrasomes. **a** Histogram of changes in DNA length Δz (in μm) upon assembly, **c** upon disassembly, and **e** upon both assembly and disassembly of $(\text{H3.1IA-H4})_2$ tetrasomes. The mean spatial resolution based on 1 STD ($=18\text{ nm}$) is indicated by the *green line*. **b** Histogram of changes in DNA linking number $\Delta\theta$ upon assembly, **d** upon disassembly, and **f** both upon assembly and disassembly of $(\text{H3.1IA-H4})_2$ tetrasomes. The mean spatial resolution based on 1 STD (0.5 turns) is indicated by the *green line*. The absolute values of the combined data (panels **e**) and **f**, $N=34$) yielded mean values of $\Delta z_{\text{dis-}/\text{ass}} = 29 \pm 8\text{ nm}$ ($n=24$) and $\Delta\theta_{\text{dis-}/\text{ass}} = 1.1 \pm 0.3\text{ turns}$ ($n=27$) obtained from the data within the range bounded by the resolution limit (*green lines*) and the DNA contour length wrapped in a full nucleosome (50 nm) and the number of turns it is wrapped around the histone core (1.7 turns), respectively.

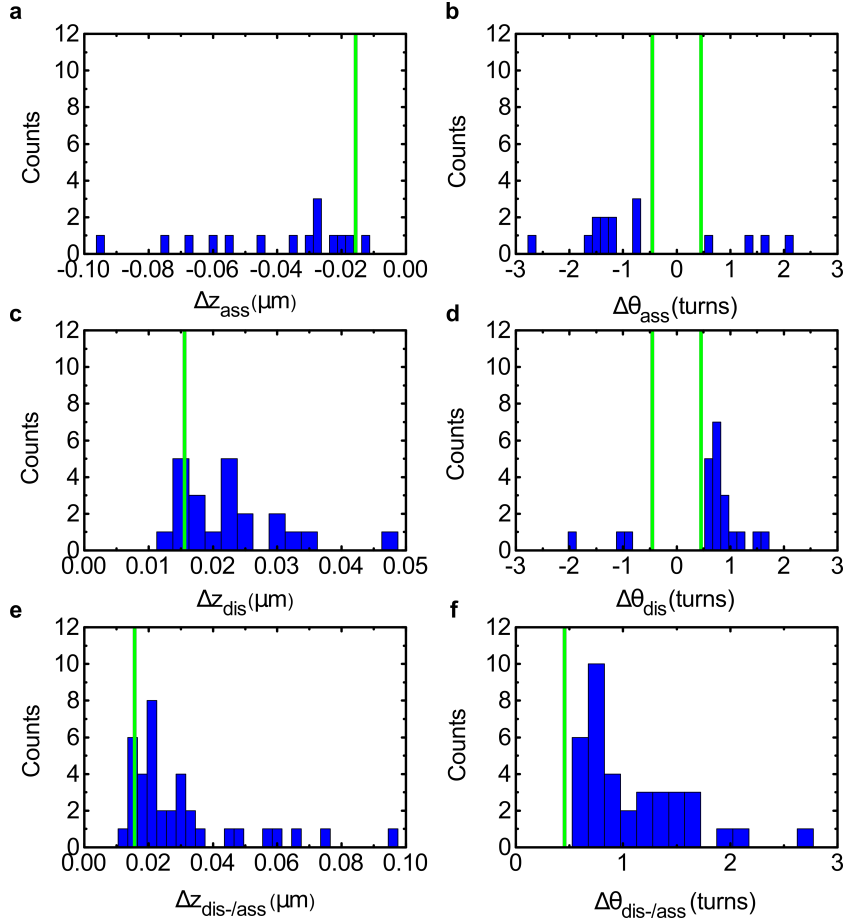


Figure 5.S12. Changes in DNA length and linking number upon assembly and disassembly of (H3.3_{IA}-H4)₂ tetrasomes. **a** Histogram of the changes in DNA length Δz (in μm) upon assembly, **c** upon disassembly, and **e** both assembly and disassembly of (H3.3_{IA}-H4)₂ tetrasomes. The mean spatial resolution based on 1 STD (16 nm) is indicated by the *green line*. **b** Histogram of changes in DNA linking number $\Delta\theta$ (in turns) upon assembly, **d** upon disassembly, and **f** both assembly and disassembly of (H3.3_{IA}-H4)₂ tetrasomes. The mean spatial resolution based on 1 STD (0.5 turns) is indicated by the *green line*. The absolute values of the combined data (panels (e) and (f), $N = 37$) yielded mean values of $\Delta z_{\text{dis-}/\text{ass}} = 26 \pm 8 \text{ nm}$ ($n = 27$) and $\Delta\theta_{\text{dis-}/\text{ass}} = 1.0 \pm 0.3 \text{ turns}$ ($n = 34$) obtained from the data within the range bounded by the resolution limit (*green lines*) and the DNA contour length wrapped in a full nucleosome (50 nm) and the number of turns it is wrapped around the histone core (1.7 turns), respectively.

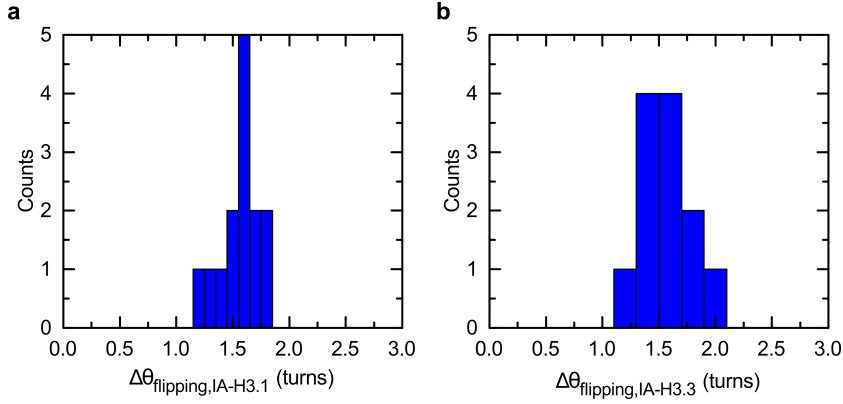


Figure 5.S13. Change in linking number upon handedness flipping of IA-treated tetrasomes. **a** Histogram of the changes in linking number $\Delta\theta_{flipping}$ (in turns) upon the handedness flipping of $(H3.1_{IA}-H4)_2$ tetrasomes. The data has a value of $\Delta\theta_{flipping} = 1.6 \pm 0.2$ turns. **b** Histogram of the changes in linking number upon the handedness flipping of $(H3.3_{IA}-H4)_2$ tetrasomes. The data has a mean value of $\Delta\theta_{flipping} = 1.6 \pm 0.2$ turns.

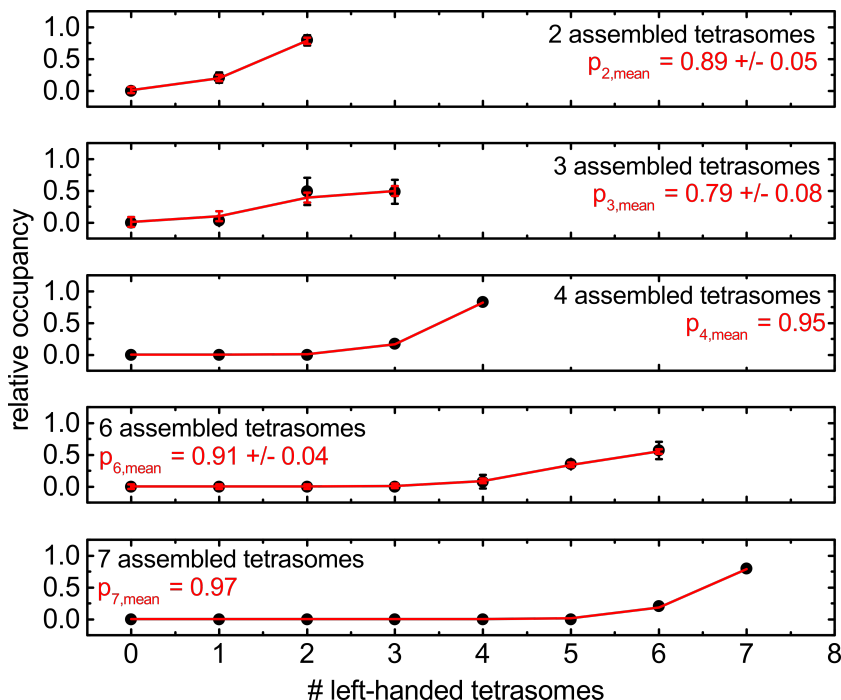


Figure 5.S14. Probability of a $(\text{H3.3}_{\text{IA}}\text{-H4})_2$ tetrasome occupying the left-handed state. Relative occupancies are obtained from the ratios of the mean peak areas of the linking number distributions for different numbers of assembled, flipping $(\text{H3.3}_{\text{IA}}\text{-H4})_2$ tetrasomes. Data sets displaying the same number of assembled tetrasomes were averaged (black circles), if applicable, and plotted together with a corresponding binomial curve (red line) generated using the mean value of the probabilities obtained from a binomial fit to each data set. Data sets displaying different number of assembled tetrasomes are presented in separate panels. Non-occupied states were assigned to the value of 0 relative occupancy. A mean probability of a $(\text{H3.3}_{\text{IA}}\text{-H4})_2$ tetrasome occupying the left-handed state of $p_{\text{left}} = 0.88 \pm 0.08$ was determined by averaging over all individual data sets.

5.6 References

- [1] R. D. Kornberg. *Science* **184**, 868 (1974).
- [2] A. L. Olins and D. E. Olins. *Science* **183**, 330 (1974).
- [3] P. Oudet, M. Gross-Bellard, and P. Chambon. *Cell* **4**, 281 (1975).

- [4] T. J. Richmond, J. T. Finch, B. Rushton, D. Rhodes, and A. Klug. *Nature* **311**, 532 (1984).
- [5] K. Luger, A. W. Mäder, R. K. Richmond, D. F. Sargent, and T. J. Richmond. *Nature* **389**, 251 (1997).
- [6] C. A. Davey, D. F. Sargent, K. Luger, A. W. Mäder, and T. J. Richmond. *J. Mol. Biol.* **319**, 1097 (2002).
- [7] A. Klug, D. Rhodes, J. Smith, J. T. Finch, and J. O. Thomas. *Nature* **287**, 509 (1980).
- [8] G. Arents, R. W. Burlingame, B. C. Wang, W. E. Love, and E. N. Moudrianakis. *Proc. Natl. Acad. Sci. U.S.A.* **88**, 10148 (1991).
- [9] S. E. Polo and G. Almouzni. *Curr. Opin. Genet. Dev.* **16**, 104 (2006).
- [10] J. K. Tyler. *Eur. J. Biochem.* **269**, 2268 (2002).
- [11] A. Lusser, D. L. Urwin, and J. T. Kadonaga. *Nat. Struct. Mol. Biol.* **12**, 160 (2005).
- [12] A. Lusser and J. T. Kadonaga. *Nat. Methods* **1**, 19 (2004).
- [13] S. Khorasanizadeh. *Cell* **116**, 259 (2004).
- [14] B. Li, M. Carey, and J. L. Workman. *Cell* **128**, 707 (2007).
- [15] O. J. Rando and H. Y. Chang. *Annu. Rev. Biochem.* **78**, 245 (2009).
- [16] G. E. Zentner and S. Henikoff. *Nat. Struct. Mol. Biol.* **20**, 259 (2013).
- [17] R. K. McGinty and S. Tan. *Chem. Rev.* **115**, 2255 (2015).
- [18] O. Ordu, A. Lusser, and N. H. Dekker. *Biophys. Rev.* **8**, 33 (2016).
- [19] G. Li, M. Levitus, C. Bustamante, and J. Widom. *Nat. Struct. Mol. Biol.* **12**, 46 (2005).
- [20] W. J. A. Koopmans, A. Brehm, C. Logie, T. Schmidt, and J. van Noort. *J. Fluoresc.* **17**, 785 (2007).
- [21] A. Miyagi, T. Ando, and Y. L. Lyubchenko. *Biochemistry* **50**, 7901 (2011).
- [22] S. Wei, S. J. Falk, B. E. Black, and T. H. Lee. *Nucleic Acids Res.* **43**, e111 (2015).

- [23] T. T. Ngo and T. Ha. *Nucleic Acids Res.* **43**, 3964 (2015).
- [24] G. D. Bowman and M. G. Poirier. *Chem. Rev.* **115**, 2274 (2015).
- [25] C. R. Clapier and B. R. Cairns. *Annu. Rev. Biochem.* **78**, 273 (2009).
- [26] P. B. Talbert and S. Henikoff. *Nat. Rev. Mol. Cell Biol.* **11**, 264 (2010).
- [27] P. B. Talbert and S. Henikoff. *Nat. Rev. Mol. Cell Biol.* **18**, 115 (2017).
- [28] A. J. Andrews and K. Luger. *Annu. Rev. Biophys.* **40**, 99 (2011).
- [29] B. Sollner-Webb, R. D. Camerini-Otero, and G. Felsenfeld. *Cell* **9**, 179 (1976).
- [30] M. Bina-Stein and R. T. Simpson. *Cell* **11**, 609 (1977).
- [31] T. H. Eickbush and E. N. Moudrianakis. *Biochemistry* **17**, 4955 (1978).
- [32] F. Dong and K. E. van Holde. *Proc. Natl. Acad. Sci. U.S.A.* **88**, 10596 (1991).
- [33] S. Jackson, W. Brooks, and V. Jackson. *Biochemistry* **33**, 5392 (1994).
- [34] B. D. Brower-Toland, C. L. Smith, R. C. Yeh, J. T. Lis, C. L. Peterson, and M. D. Wang. *Proc. Natl. Acad. Sci. U.S.A.* **99**, 1960 (2002).
- [35] G. J. Gemmen, R. Sim, K. A. Haushalter, P. C. Ke, J. T. Kadonaga, and D. E. Smith. *J. Mol. Biol.* **351**, 89 (2005).
- [36] S. Mihardja, A. J. Spakowitz, Y. L. Zhang, and C. Bustamante. *Proc. Natl. Acad. Sci. U.S.A.* **103**, 15871 (2006).
- [37] M. A. Hall, A. Shundrovsky, L. Bai, R. M. Fulbright, J. T. Lis, and M. D. Wang. *Nat. Struct. Mol. Biol.* **16**, 124 (2009).
- [38] V. Böhm, A. R. Hieb, A. J. Andrews, A. Gansen, A. Rocker, K. Toth, K. Luger, and J. Langowski. *Nucleic Acids Res.* **39**, 3093 (2011).
- [39] R. Vlijm, J. S. J. Smitshuijzen, A. Lusser, and C. Dekker. *PLoS One* **7**, e46306 (2012).
- [40] A. J. Katan, R. Vlijm, A. Lusser, and C. Dekker. *Small* **11**, 976 (2015).

- [41] T. Elbel and J. Langowski. *J. Phys. Condens. Matter* **27**, 064105 (2015).
- [42] V. Jackson. *Biochemistry* **34**, 10607 (1995).
- [43] A. Hamiche, V. Carot, M. Alilat, F. De Lucia, M. F. O'Donohue, B. Revet, and A. Prunell. *Proc. Natl. Acad. Sci. U.S.A.* **93**, 7588 (1996).
- [44] A. Hamiche, and H. Richard-Foy. *J. Biol. Chem.* **273**, 9261 (1998).
- [45] M. Alilat, A. Sivolob, B. Revet, and A. Prunell. *J. Mol. Biol.* **291**, 815 (1999).
- [46] A. Sivolob and A. Prunell. *J. Mol. Biol.* **295**, 41 (2000).
- [47] A. Sivolob, F. De Lucia, M. Alilat, and A. Prunell. *J. Mol. Biol.* **295**, 55 (2000).
- [48] R. Vlijm, M. Lee, J. Lipfert, A. Lusser, C. Dekker, and N. H. Dekker. *Cell Rep.* **10**, 216 (2015).
- [49] R. Vlijm, M. Lee, O. Ordu, A. Boltengagen, A. Lusser, N. H. Dekker, and C. Dekker. *PLoS One* **10**, e0141267 (2015).
- [50] J. Lipfert, M. Wiggin, J. W. J. Kerssemakers, F. Pedaci, and N. H. Dekker. *Nat. Commun.* **2**, 439 (2011).
- [51] C. Lavelle. *Curr. Opin. Genet. Dev.* **25**, 74 (2014).
- [52] P. Tessarz and T. Kouzarides. *Nat. Rev. Mol. Cell Biol.* **15**, 703 (2014).
- [53] C. R. Clapier, S. Chakravarthy, C. Petosa, C. Fernandez-Tornero, K. Luger, and C. W. Muller. *Proteins* **71**, 1 (2008).
- [54] L. Favrot, D. H. Lajiness, and D. R. Ronning. *J. Biol. Chem.* **289**, 25031 (2014).
- [55] K. Luger, T. J. Rechsteiner, and T. J. Richmond. *Methods Enzymol.* **304**, 3 (1999).
- [56] K.-M. Lee and G. Narlikar. *Current Protocols in Molecular Biology* by John Wiley & Sons, Inc. (2001).
- [57] J. W. J. Kerssemakers, E. L. Munteanu, L. Laan, T. L. Noetzel, M. E. Janson, and M. Dogterom. *Nature* **442**, 709 (2006).

- [58] J. Lipfert, G. M. Skinner, J. M. Keegstra, T. Hensgens, T. Jager, D. Dulin, M. Köber, Z. Yu, S. P. Donkers, F. C. Chou, R. Das, and N. H. Dekker. *Proc. Natl. Acad. Sci. U.S.A.* **111**, 15408 (2014).
- [59] J. L. Workman and R. E. Kingston. *Annu. Rev. Biochem.* **67**, 545 (1998).
- [60] S. J. Petesch and J. T. Lis. *Trends Genet.* **28**, 285 (2012).
- [61] S. S. Teves, C. M. Weber, and S. Henikoff. *Trends Biochem. Sci.* **39**, 577 (2014).
- [62] A. Bancaud, G. Wagner, N. Conde e Silva, C. Lavelle, H. Wong, J. Mozziconacci, M. Barbi, A. Sivolob, E. Le Cam, L. Mouawad, J. L. Viovy, J. M. Victor, and A. Prunell. *Mol. Cell* **27**, 135 (2007).
- [63] N. F. Dupuis, E. D. Holmstrom, and D. J. Nesbitt. *Proc. Natl. Acad. Sci. U.S.A.* **111**, 8464 (2014).
- [64] B. W. Baer and D. Rhodes. *Nature* **301**, 482 (1983).
- [65] H. Kimura and P. R. Cook. *J. Cell Biol.* **153**, 1341 (2001).
- [66] C. Thiriet and J. J. Hayes. In: Laurent, B. C. *Chromatin Dynamics in Cellular Function*. Springer, Berlin, Heidelberg (2006).
- [67] D. Reinberg and R. J. Sims. *J. Biol. Chem.* **281**, 23297 (2006).
- [68] M. Bruno, A. Flaus, C. Stockdale, C. Rencurel, H. Ferreira, and T. Owen-Hughes. *Mol. Cell* **12**, 1599 (2003).
- [69] L. J. Benson, Y. L. Gu, T. Yakovleva, K. Tong, C. Barrows, C. L. Strack, R. G. Cook, C. A. Mizzen, and A. T. Annunziato. *J. Biol. Chem.* **281**, 9287 (2006).
- [70] O. Gursoy-Yuzugullu, N. House, and B. D. Price. *J. Mol. Biol.* **428**, 1846 (2016).
- [71] A. Sobieszek, O. S. Matusovsky, T. V. Permyakova, B. Sarg, H. Lindner, N. S. Shelud'ko. *Arch. Biochem. Biophys.* **454**, 197 (2006).
- [72] Z. Yu, D. Dulin, J. Cnossen, M. Köber, M. M. van Oene, O. Ordu, B. A. Berghuis, T. Hensgens, J. Lipfert, and N. H. Dekker. *Rev. Sci. Instrum.* **85**, 123114 (2014).
- [73] J. P. Cnossen, D. Dulin, and N. H. Dekker. *Rev. Sci. Instrum.* **85**, 103712 (2014).

6 Structural Dynamics of Tetrasomes Depend on the Underlying DNA Sequence and Ambient Conditions

The genome of eukaryotes is hierarchically organized into protein-DNA assemblies for essential compaction in the nucleus. Nucleosomes, consisting of a stretch of DNA that is first wrapped around a (H3-H4)₂ tetramer into tetrasomes and then completed by two H2A/H2B dimers, constitute the basic unit of eukaryotic chromatin. This fundamental assembly, together with the (H3-H4)₂ tetrasome as an intermediate, is highly dynamic due to different mechanisms involving numerous factors. However, the influence of the underlying DNA sequence and ambient conditions on nucleosomal structures and dynamics is not fully understood. We have recently shown that tetrasomes spontaneously change the direction of their DNA wrapping between a left-handed and a right-handed conformation. Here, we have investigated the impact of DNA sequence and different buffer conditions on tetrasome structure and dynamics using FOMT. These factors did not affect the overall tetrasome structure, but significantly impacted the handedness dynamics in terms of the tendency towards flipping. The results show that the DNA sequence and different ambient conditions distinctly influence the conformational plasticity of tetrasomes. This suggests tetrasome dynamics as an intrinsic and tunable mechanism of chromatin for gene regulation during vital genomic processes such as transcription, replication, and repair at the subnucleosomal level.

The contents of this chapter will be submitted in a manuscript by O. Ordu, A. Lusser, and N. H. Dekker.

6.1 Introduction

The nucleosome is the basic complex of chromatin in eukaryotic cells [1–3] and comprises 147 bp of DNA wrapped around a disk-shaped assembly of eight histone proteins in 1.7 turns [4–6]. The histone octamer consists of two copies of two types of heterodimers, one of which is formed by histones H3 and H4, and the other by histones H2A and H2B [7, 8]. During nucleosome formation, the two H3-H4 dimers assemble onto the DNA first into a tetrasome which is subsequently completed to the full complex by binding of the two H2A/H2B dimers [9]. The resulting compaction limits the accessibility of the genome for essential cellular processes, such as transcription, replication and repair. Hence, this primary function of nucleosomes also assigns them a key role in gene regulation and renders them an important object of research to understand the functioning and viability of cells.

As proven powerful tools for characterizing biological systems at the molecular level, single-molecule techniques have provided significant insights into the structure and especially the dynamics of nucleosomes [10]. They have revealed the intrinsically dynamic nature of nucleosomes in the form of ‘breathing’, i.e. the transient un- and rewinding of the nucleosomal DNA ends [11–14]. Recently, nucleosomes were also found to ‘gap’ by transiently opening and closing the two turns of nucleosomal DNA along the direction of the superhelical axis [63]. Furthermore, the structure, stability and dynamics of nucleosomes are regulated chemically by post-translational modifications [16], chaperones [17], and ATP-dependent remodelers [18]. Besides these specific mechanisms, the nucleosome composition and dynamics can be altered by forces and torques generated by genome-processing molecular motors [19, 20]. Under such external effects, including changes in the ambient conditions, nucleosomes have also been found to reorganize into different (sub)structures [21].

In this context, tetrasomes consisting of about 80 bp of DNA bound to the (H3-H4)₂ tetramer have been observed as viable intermediates in several studies [22–34] (Figure 6.S1a of the Supplementary Information). Surprisingly, next to the more intuitive left-handed complex based on the left-handed nucleosome, also tetrasomes with a right-handed DNA wrapping have been identified [35–40]. We have recently found that tetrasomes switch spontaneously between the prevalent state of left-handed, and the less adopted conformation of right-handed DNA wrapping [41–43] (Figure 6.S1b of the Supplementary Information).

Besides these numerous mechanisms, the sequence of the nucleosomal DNA has also been suggested to play an important role for the structural and

dynamic properties of nucleosomes [44]. By impacting the mechanical properties of the nucleosomal DNA, the sequence may induce or alter specific DNA-histone interactions. This prospect has led to the identification and design of various nucleosomal DNA sequences [45]. The high-affinity Widom 601-sequence [46] in particular has become a well-established template for the formation and positioning of stable nucleosomes, including in *in vitro* single-molecule assays [12, 14, 15, 29–31, 47–63]. Several experimental and theoretical studies increasingly indicate the importance of the mechanical properties of the underlying DNA for the structure and dynamics of nucleosomes [64]. However, more systematic studies to investigate the direct effect of DNA sequence on (sub)nucleosomal structures and dynamics are required.

In this work, we have studied the structure and handedness dynamics of single canonical (H3.1-H4)₂ tetrasomes assembled onto DNA molecules containing one high-affinity 601-sequence [46] (‘601-tetrasomes’) in real time using FOMT [65]. For direct comparison, we have performed the experiments in the same buffer conditions as in our previous study with canonical tetrasomes assembled onto DNA molecules of a random sequence [41]. To also investigate the effects of ambient conditions, we have performed measurements in various buffer conditions, including those employed in previous studies on chromatin fibers [66, 67]. Neither factor affected the structural properties of the tetrasomes, but both significantly impacted their flipping kinetics. These findings suggest that the underlying DNA sequence and ambient conditions are important factors influencing (sub)nucleosomal dynamics. Consequently, they also play a considerable role in the associated regulation of the genome during DNA-templated processes. Furthermore, our results point out that findings obtained using nucleosome-positioning sequences must be interpreted in the context of the specific ambient conditions.

6.2 Materials and Methods

6.2.1 Preparation of DNA molecules

In all experiments, tetrasome assembly was performed on linear dsDNA fragments of 1.96 kbp length containing a single 601-sequence of 147 bp in their center. The two ends of these main DNA fragments were ligated to a digoxigenin-coated (Roche Diagnostics, Basel, Switzerland) and a biotin-coated (Roche Diagnostics) double-stranded fragment (handle) of 643 bp length, respectively, for immobilization and tethering. The schematics,

sequence, and preparation of the DNA molecules are described in Figure 6.S2, together with Table 6.S1 of the Supplementary Information. Further details on the handles have been described in Ref. [43].

6.2.2 Expression and purification of proteins

The recombinant canonical *Drosophila* histones H3.1-H4 and NAP1 chaperones were expressed and purified as described in Ref. [41] and Ref. [43]. While NAP1 has been identified as a chaperone for histones H2A and H2B *in vivo* [68], it has been found to also interact with histones H3 and H4 and prevent histone aggregation *in vitro* [32, 41, 42, 69–72].

6.2.3 Preparation of histones and tetrasome assembly

Individual 601-tetrasomes were assembled and measured in real time by means of single-molecule experiments in three buffers with varying compositions of core components employed in different previous studies [41–43, 66, 67] (Table 6.1). To allow for direct comparison to our previous study [41], the protein samples were prepared in a similar way. 51 nM of an equimolar solution of H3.1-H4 histones were incubated – either without or with 192 nM NAP1 – on ice for 30 min. The incubation buffers were the same as the measurement buffers (Table 6.1), except for buffer A. In that case, the incubation buffer contained 10-fold higher concentrations of 0.25% (w/v) PEG and 0.25% (w/v) PVA, and 0.1% (w/v) BSA, as employed in our previous study [41]. The incubated protein solutions were then diluted by at most 1:5000, and 100 μ l of the diluted solution were flushed into the flow cell to assemble a single tetrasome in real time. About 60 s after assembly, 100–300 μ l of measurement buffer was flushed through the flow cell to remove free proteins and to prevent assembly of more tetrasomes without losing the already assembled tetrasome and/or tether.

The details of the sample and flow cell preparation for such single-molecule experiments have been described in Ref. [43]. The deviating concentrations and volumes of the DNA and magnetic bead solutions used in this work are stated in Table 6.S2 of the Supplementary Information. Five (out of $N=20$) experiments were performed by resuming the measurement on a tetrasome that did not disassemble during the preceding experiment for improved statistics with the employed low-throughput technique. Two of such experiments involved an exchange between the similar buffers B and C (Table 6.1) with 300–500 μ l of the respective measurement buffer. In one of these two experiments a second measurement was resumed in buffer

C on a tetrasome assembled before in buffer B, in the other the reverse procedure was employed.

Table 6.1: The composition of the measurement buffers.

Measurement buffers	Buffer components
A	25 mM HEPES-KOH (pH 7.5) (Sigma-Aldrich, St. Louis, MO, United States), 0.1 mM EDTA (Sigma-Aldrich), 50 mM KCl (Merck, Darmstadt, Germany), 0.01% (w/v) BSA (Sigma-Aldrich), 0.025% (w/v) PEG (Sigma-Aldrich), 0.025% (w/v) PVA (Sigma-Aldrich)
B	10 mM HEPES (pH 7.5), 100 mM KCl, 0.2% (w/v) BSA, 0.1% (w/v) Tween-20, 10 mM NaN_3
C	10 mM HEPES (pH 7.5), 100 mM KCl, 0.2% (w/v) BSA, 0.1% (w/v) Tween-20, 10 mM NaN_3 , 2 mM MgCl_2

6.2.4 MT instrumentation

The assembly and dynamics of an individual tetrasome was monitored by directly measuring the length and angular position, i.e. the linking number, of a single DNA molecule in each experiment using FOMT [65]. The hardware of the used magnetic tweezers setup has been detailed in Ref. [43]. For each experiment, the exerted force was calibrated at 0.6-0.7 pN. All experiments were performed at room temperature (22 °C) for up to 10 h.

6.2.5 Data analysis

The analysis of the acquired data was performed using custom-written scripts with built-in functions in Matlab (Mathworks, Natick, MA, United States). An improved version of the custom-written step-finder algorithm described in Ref. [73] was used to detect stepwise changes in the time traces of the DNA length and DNA linking number. Subsequently, these fits were analyzed to identify simultaneous steps in both the DNA length

and DNA linking number within a time window of 19.1 s (see below), resulting from the assembly or disassembly of a tetrasome (Figure 6.1b and Figure 6.S3 of the Supplementary Information). With this approach, 48% ($n=13$) of all such steps ($N=27$) were automatically identified, while the remaining 52% ($n=14$) were corrected manually to better match the data. The sizes of these common changes in DNA length ($N=27$) and DNA linking number ($N=27$) were finally retrieved as the basic quantities characterizing the structure of the tetrasomes (Tables 6.S3 and 6.S4 of the Supplementary Information). For a reliable interpretation, these step sizes were also compared to the respective mean spatial resolutions determined from the STDs of the time trace profiles in all experiments by averaging (Figure 6.1c,d, Figures 6.S4 and 6.S5 of the Supplementary Information).

The dynamics of tetrasome structure in terms of handedness flipping was separately analyzed in the parts of the time traces with a stable baseline in DNA length and DNA linking number (Figure 6.2a and Figure 6.S6 of the Supplementary Information). The change in DNA linking number upon flipping was determined by fitting a double Gaussian function to the DNA linking number data ($N=23$; Figure 6.2b, Table 6.S9 of the Supplementary Information) and calculating the difference between the mean values. The probability for a tetrasome to occupy one of the two states was calculated from the relative ratio of the corresponding peak-areas of the two Gaussian fits (Table 6.S14 of the Supplementary Information).

The handedness dynamics of the single, flipping (H3.1-H4)₂ tetrasomes was further analyzed in terms of the times spent in the left-handed or right-handed state of DNA wrapping using another custom-written algorithm based on [74] and a threshold zone set at 1 STDs from the mean values of the two Gaussian distributions around their average (Figure 6.2a and Figure 6.S6 of the Supplementary Information). The details of the dwell time analysis have been described in Ref. [43]. Here, the corresponding DNA linking number data of the time traces of sufficiently long duration (>1600 s) were smoothed by filtering over $N=330$ ($N=1910$) points corresponding to a time average of $\tau_{short} = 3.3$ s ($\tau_{long} = 19.1$ s). These time scales were obtained from autocorrelation analysis of the bead's angular fluctuations as described in Ref. [65] and Ref. [43] (Figure 6.S7 of the Supplementary Information). The mean dwell time in each state was then determined by combining all data sets obtained in the same buffer conditions and fitting an exponential function (Table 6.2, Figure 6.3a,b, Figures 6.S8 and 6.S9 of the Supplementary Information). For reasons of direct comparison, we also performed the same dwell time analysis with the same settings on the partial time traces ($N=6$) of one of our earlier experiments published in Ref. [41] ($N=159$ ($N=63$) for 3.3 s (19.1 s) time averaging for the

left-handed state; $N=161$ ($N=63$) for 3.3 s (19.1 s) time averaging for the right-handed state).

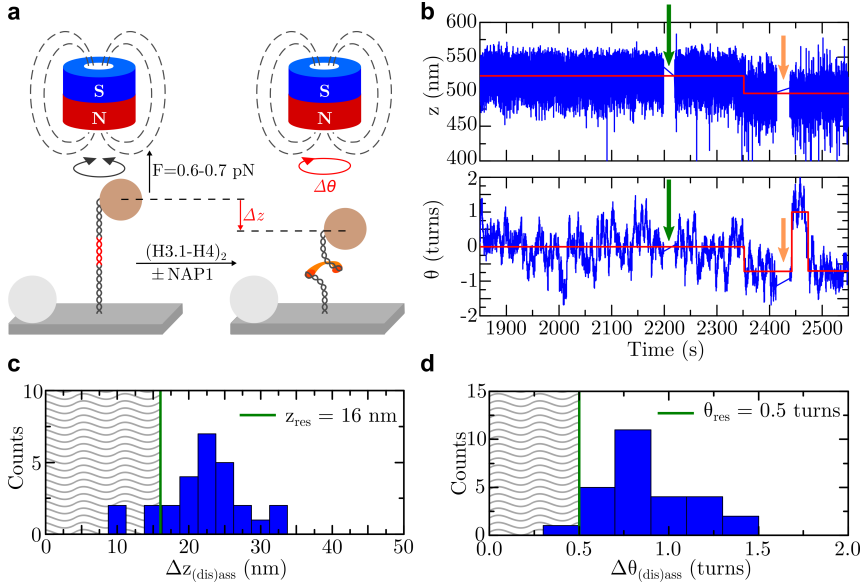
Further details of the data analysis have been described in Ref. [43]. The significance of the similarity between the structural quantities obtained in the different conditions was assessed by respective unpaired two-sample t-tests (Tables 6.S5-6.S8 and 6.S10 of the Supplementary Information). The results for the dwell times obtained in the different conditions were checked for similarity by respective Wilcoxon rank-sum tests (Tables 6.S11-6.S13 of the Supplementary Information). Finally, we note that the times measured in this study are an upper boundary due to the finite bead response time. The errors stated on the reported mean values correspond to 1 STD from the underlying distributions, unless indicated otherwise.

6.3 Results and Discussion

6.3.1 The structural properties of tetrasomes are unaffected by the underlying DNA sequence and ambient conditions

Tetrasome assembly was recorded in real time by tracking the length z and linking number θ of individual DNA molecules containing a 601-sequence at their center using FOMT [65]. A single immobilized DNA molecule is tethered to a magnetic bead that is subject to constant force applied by a cylindrical permanent magnet allowing its free rotation in the (x,y) -plane (Figure 6.1a). The formation of a ‘601-tetrasome’ upon flushing in either $(\text{H3.1-H4})_2$ tetramers alone (‘self-loaded’) or in complex with NAP1 chaperones upon pre-incubation (‘NAP1-loaded’) resulted in a simultaneous step-like change in both the length z and linking number θ of the DNA molecule (Figure 6.1b, Figure 6.S3 of the Supplementary Information). The applied force was set to 0.6-0.7 pN to compare to our previous study of $(\text{H3.1-H4})_2$ tetrasomes assembled on DNA molecules with a random sequence [41]. The experiments were further performed in buffers with a varying composition of core components (see Table 6.1) employed in different previous studies [41–43, 66, 67]. By this means, we investigated potential effects of altered ambient conditions on tetrasome structure and dynamics.

In contrast to our observation in previous experiments with DNA molecules of a random sequence [41–43], histone tetramers alone were found to as-



semble onto DNA molecules with a centered 601-sequence. Since the experimental conditions were otherwise identical, this observation likely arises from the presence of the high-affinity 601-sequence. Therefore, we also assembled single 601-tetrasomes without NAP1 chaperones in about half ($n=11$) of the experiments ($N=20$) (Figure 6.S3 of the Supplementary Information). All individual values obtained upon tetrasome assembly are given in Table 6.S3 of the Supplementary Information. In agreement with our previous studies [41–43], we did not observe NAP1 chaperones alone to interact with DNA molecules containing a 601-sequence at their center in any of the buffer conditions (Figure 6.S10 of the Supplementary Information).

Under the highly diluted conditions required for the controlled assembly of a single tetrasome (see Section 6.2), we observed in 40% ($n=8$) of all experiments ($N=20$) that tetrasomes disassembled within an average time of 3364 ± 765 s (1 SEM; Figure 6.S11 of the Supplementary Information). Disassembly was observed for both NAP1-loaded and self-loaded 601-tetrasomes in all buffer conditions, which excludes the destabilizing effect of NAP1 and/or specific ambient conditions. All individual values obtained upon tetrasome disassembly are listed in Table 6.S4 of the Supplementary Information.

Figure 6.1: Formation of single 601-tetrasomes in real time. **a** Experimental assay based on FOMT [65]. A single DNA construct (*black*) containing a 601-sequence (*red*) for tetrasome positioning at its center is immobilized on the coverslip (*light blue*) and tethered to a superparamagnetic bead (*light brown*) at the other end. A permanent cylindrical magnet (*dark blue/red*) above the flow cell, whose axis is precisely aligned with the DNA tether, exerts a constant force (F) on the bead while allowing its free rotation in the (x,y) -plane, indicated by the black circular arrow. This enables the direct measurement of the DNA molecule's length z and linking number θ , which are changed by Δz and $\Delta\theta$ upon the assembly of a tetrasome (*orange*), indicated by the *red straight* and *circular arrow*, respectively. Tetrasome assembly is induced by flushing in either $(H3.1-H4)_2$ tetramers alone or pre-incubated histone/NAP1 complexes. Non-magnetic beads attached to the surface serve as reference for drift correction. This figure is adapted from Ref. [43]. **b** Partial time traces of the length z (in nm, panel above) and the linking number θ (in turns, panel below) of a DNA molecule with a centered 601-sequence before and upon the assembly of a $(H3.1-H4)_2$ tetrasome. Assembly was achieved by either flushing in $(H3.1-H4)_2$ tetramers alone or together with NAP1 upon pre-incubation (*green arrows*). The formation of a tetrasome simultaneously decreased both quantities in the form of a step identified using a step-finder algorithm (*red lines*) (see Section 6.2). About 60 s after assembly, free proteins were flushed out with measurement buffer (*orange arrows*) to prevent further histone binding. In this particular experiment, the tetrasome was assembled from NAP1/histone complexes in buffer A (see Table 6.1). Corresponding partial time traces of a DNA molecule before and upon the assembly of a 601-tetrasome from histone tetramers alone is likewise shown in Figure 6.S3 of the Supplementary Information. **c** Histogram of the change in DNA length upon assembly and disassembly $\Delta z_{(dis)ass}$ (in nm) of single $(H3.1-H4)_2$ tetrasomes ($N=27$) in all buffers (see Table 6.1) shown together with the mean spatial resolution corresponding to the average 1 STD (16 nm, *green line*) from all experiments. Data beyond the resolution limit (*corrugated area*) was excluded to determine the mean change of $\Delta z_{(dis)ass} = 23 \pm 5$ nm ($n=25$). **d** Histogram of the change in DNA linking number upon assembly and disassembly $\Delta\theta_{(dis)ass}$ (in turns) of single $(H3.1-H4)_2$ tetrasomes ($N=27$) in all buffers (see Table 6.1) shown together with the mean spatial resolution corresponding to the average 1 STD (0.5 turns, *green line*) from all experiments. Data beyond the resolution limit (*corrugated area*) were excluded to determine the mean change of $\Delta\theta_{(dis)ass} = 0.9 \pm 0.2$ turns ($n=26$). The separate distributions of the changes upon assembly or disassembly are shown in Figures 6.S4 and 6.S5 of the Supplementary Information, respectively. All individual values are given in Tables 6.S3 and 6.S4 of the Supplementary Information.

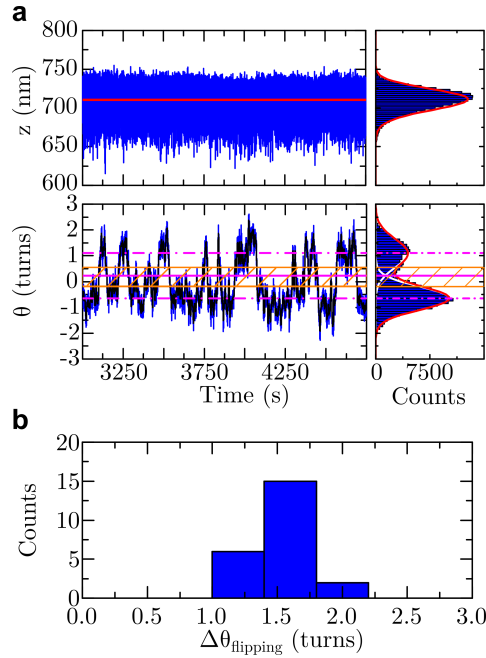


Figure 6.2: The structural dynamics of single 601-tetrasomes. **a** Partial time traces of the length z (in nm, panel above) and the linking number θ (in turns, panel below) of another DNA molecule after the assembly of a $(\text{H3.1-H4})_2$ tetrasome in buffer A (see Table 6.1) upon flushing in histone tetramers only. As indicated from the fit by the step-finder algorithm to the time trace (*red line*, left panel) and the fit of a mirrored gamma function (*red line* in histogram plot, right panel) to the skewed data, the DNA length stays constant. The DNA linking number spontaneously fluctuates, i.e. ‘flips’, between two states identified by fitting two Gaussian functions (*white lines* in histogram plot, right panel) underlying the full profile (*red line* in histogram plot, right panel). The two states correspond to a prevalent left-handed and a less adopted right-handed conformation of DNA wrapping with the respective mean linking numbers $\theta_{\text{left}} = -0.65 \pm 0.02$ turns and $\theta_{\text{right}} = +1.10 \pm 0.04$ turns (*dashed-dotted magenta lines*, 95% confidence level for estimated values). These structural dynamics were quantified in terms of the dwell times in the two states based on a threshold zone (*shaded orange area*) set by 1 STD from each mean value (*orange solid lines*) around their average (*solid magenta line*) (see Section 6.2). Corresponding partial time traces of a DNA molecule upon the assembly of a 601-tetrasome from histone/NAP1 complexes is likewise shown in Figure 6.S6 of the Supplementary Information. **b** Histogram of the change in DNA linking number $\Delta\theta_{\text{flipping}}$ (in turns) upon flipping of single $(\text{H3.1-H4})_2$ tetrasomes in their handedness of DNA-wrapping in all buffers (see Table 6.1). The data yields a mean value of $\Delta\theta_{\text{flipping}} = 1.6 \pm 0.2$ turns ($N=23$). The individual values are given in Table 6.S9 of the Supplementary Information.

Due to their similarity based on respective t-tests (see Tables 6.S5-6.S8 of the Supplementary Information), the results from all experiments ($N=20$) were combined for improved statistics. The absolute changes in DNA length and DNA linking number upon assembly and disassembly of single 601-tetrasomes ($N=27$) yielded a mean value of $\Delta z_{(dis)ass} = 23 \pm 5$ nm ($n=26$) and $\Delta \theta_{(dis)ass} = 0.9 \pm 0.2$ turns ($n=25$), respectively (Figure 6.1c,d). The separate distributions of the changes upon assembly or disassembly are shown in Figures 6.S4 and 6.S5 of the Supplementary Information, respectively. These results are in excellent agreement with values reported in other studies involving tetrasomes [27–30, 32, 33, 36–43]. Overall, our findings indicate that (H3.1-H4)₂ tetramers adopt the same particular structure, regardless of the underlying DNA sequence and ambient conditions.

To investigate the time-dependent behavior of 601-tetrasomes, the FOMT measurements were continued over several hours after assembly. Like tetrasomes assembled on DNA with a random sequence [41–43], the stably bound 601-tetrasomes also exhibited spontaneous dynamics in the handedness of their DNA wrapping. The length of the DNA molecules stayed constant, while their linking number spontaneously fluctuated, i.e. flipped, between two states (Figure 6.2a and Figure 6.S6 of the Supplementary Information). Based on the negative and positive mean values of the respective DNA linking numbers, the states correspond to a left-handed and right-handed conformation of DNA wrapping. As observed with tetrasomes on DNA with a random sequence [41–43], the left-handed structure is more prevalent than the right-handed state for 601-tetrasomes. The difference between the two mean values describes the change in tetrasome structure induced by these handedness dynamics. All individual values are summarized in Table 6.S9 of the Supplementary Information. The results from all experiments were combined for improved statistics due to their similarity based on respective t-tests (see Table 6.S10 of the Supplementary Information). The results yielded a mean change in DNA linking number upon flipping of $\Delta \theta_{flipping} = 1.6 \pm 0.2$ turns ($N=23$) (Figure 6.2b). This value is in excellent agreement with our previous studies [41–43]. The consistent results indicate that the DNA sequence and ambient conditions do not affect the structural rearrangement of tetrasomes associated with the flipping dynamics.

6.3.2 The kinetics of the flipping in tetrasome handedness are altered by the underlying DNA sequence and ambient conditions

For a more detailed picture, we examined the handedness dynamics of the single 601-tetrasomes in terms of the times spent in each of the two states (see Section 6.2, Figure 6.2a and Figure 6.S6 of the Supplementary Information). The distributions and mean values of the dwell times in the different buffer conditions (see Table 6.1) are shown in Figure 6.3a,b and Figures 6.S8 and 6.S9 of the Supplementary Information. Table 6.2 summarizes the results for both 601-tetrasomes and tetrasomes assembled on DNA with a random sequence, including the values obtained from dwell time analysis using another time averaging for filtering (see Section 6.2).

The impact of the underlying DNA Sequence

Remarkably, the underlying DNA sequence significantly affected the dwell times of tetrasomes in both states, as assessed by respective Wilcoxon rank-sum tests (see Tables 6.S11-6.S13 of the Supplementary Information). The average time a NAP1-loaded 601-tetrasome spent in the left-handed (right-handed) state in buffer A is 4.9 ± 0.5 (2.0 ± 0.3) times shorter (longer) than the dwell times of a NAP1-loaded (H3.1-H4)₂ tetrasome assembled on DNA with a random sequence in the same buffer A (Table 6.2). These results surprisingly indicate that NAP1-loaded 601-tetrasomes are less stable in the left-handed state than tetrasomes assembled on DNA with a random sequence, while the opposite is the case for the right-handed conformations (6.S13 of the Supplementary Information). Since the experimental conditions were the same in both studies except for the DNA sequence, these effects likely arise from the presence of the 601-sequence and/or NAP1.

In fact, a self-loaded 601-tetrasome was found to dwell 2.5 ± 0.2 times longer in the left-handed conformation than a NAP1-loaded 601-tetrasome, while its dwell time in the right-handed state was only slightly increased. These different results (see Tables 6.S11-6.S13 of the Supplementary Information) indicate that NAP1 forms 601-tetrasomes that are considerably less stable in the left-handed state, while the right-handed conformation remains essentially unaffected. Possibly, NAP1 does not accurately position histone tetramers onto the high-affinity 601-sequence. In fact, it has been reported that nucleosomes are not preferably located on the 601-sequence *in vivo*, indicating that it does not necessarily assemble stable nucleosomes in the cellular environment despite its high affinity for histones *in vitro* [75].

In particular, this observation suggests that nucleosome formation and positioning is not dominated by intrinsically strong interactions between histones and DNA. The presence of chaperones, nucleosome assembly factors and/or remodelers in specific ambient conditions may affect the formation, positioning, and/or stability of nucleosomes. Accordingly, the combination of the 601-sequence with NAP1 in certain buffer conditions *in vitro* could also result in more dynamic tetrasomes than those assembled on DNA with a random sequence (Table 6.2).

Table 6.2: Dwell times of tetrasomes. Results for the times $\tau_{D,left}$ and $\tau_{D,right}$ a tetrasome dwelled in the left-handed and right-handed conformation, respectively. The underlying analysis is described in Section 6.2 and detailed in Ref. [43].

Sample	Time average in filtering (s)	$\tau_{D,left}$ (s) [buffer type]	$\tau_{D,right}$ (s) [buffer type]
NAP1-loaded (H3.1-H4) ₂ tetrasomes [in buffer A]	3.3 (N = 330)	183 (+15/-12)*	14 (± 1)**
	19.1 (N = 1910)	417 (+60/-48)*	34 (+5/-4)**
NAP1-loaded (H3.1-H4) ₂ tetrasomes on 601-DNA	3.3 (N=330)	37 (± 8)** [A] 62 (± 3)** [B] 141 (+11/-10)** [C]	28 (+2/-1)** [A] 33 (± 1)** [B] 30 (± 2)** [C]
	19.1 (N = 1910)	67 (+5/-4)** [A] 121 (+8/-7)** [B] 231 (+24/-20)** [C]	48 (+4/-3)** [A] 64 (± 4)** [B] 44 (+5/-4)** [C]
self-loaded (H3.1-H4) ₂ tetrasomes on 601-DNA	3.3 (N=330)	93 (+7/-6)** [A] 175 (± 11 /-10)** [B] 93 (± 4)** [C]	34 (+3/-2)** [A] 27 (± 2)** [B] 19 (± 1)** [C]
	19.1 (N = 1910)	164 (+18/-15)** [A] 344 (+33/-28)** [B] 194 (+12/-11)** [C]	58 (+6/-4)** [A] 50 (+5/-4)** [B] 36 (± 2)** [C]

*Errors calculated by error propagation

**Errors correspond to 68% confidence interval for estimated values from fits

In support of this prospect, we found self-loaded 601-tetrasomes to exhibit a 2.0 ± 0.2 (2.4 ± 0.3) times shorter (longer) mean dwell time in the left-handed (right-handed) state than NAP1-loaded tetrasomes on DNA with a random sequence (Table 6.2 and Table 6.S13 of the Supplementary Information). These results indicate that self-loaded 601-tetrasomes are also considerably less (more) stable in the left-handed (right-handed) state than NAP1-loaded tetrasomes on DNA with a random sequence. Comparison of the otherwise identical experimental conditions suggests that this effect likely arises from the presence of the 601-sequence within the specific ambient conditions.

In fact, in the same *in vivo* study mentioned above, it was also observed that histone localization on the 601-sequence depends on the context of the enclosing sequence [75]. In a recent *in vitro* study at the single-molecule level, the force-induced unwrapping of 601-nucleosomes was further reported to occur in an asymmetric manner due to base-pair differences in the two halves of the 601-sequence [63]. This effect is suggested to arise from the related differences in the local flexibility of the nucleosomal DNA. Along these lines, it also seems possible that the base-pair sequence and the local flexibility of the DNA adjacent to the 601-sequence influences the structure, dynamics and stability of nucleosomes. This scenario seems even more likely in our assay involving DNA molecules with a centered 601-sequence, which are in total 3.25-kbp long and tethered at a very low force. Therefore, the 601-sequence might form more dynamic tetrasomes based on its particular location within our DNA molecule, due to specific influences from the adjacent base-pair sequences and/or the buffer conditions affecting its overall properties.

The impact of the ambient conditions

Accordingly, we observed a different behavior of 601-tetrasomes in the other buffers B and C (see Table 6.1) from the 601-tetrasomes assembled in buffer A. More specifically, NAP1-loaded (self-loaded) 601-tetrasomes dwelled 1.7 ± 0.1 (1.9 ± 0.1) times longer in the left-handed state in buffer B compared to buffer A. The average dwell time in the right-handed conformation was only affected slightly (Table 6.2 and Figure 6.S8, Tables 6.S9 and 6.S12 of the Supplementary Information). In buffer C, a NAP1-loaded 601-tetrasome dwelled 2.3 ± 0.2 times longer in the left-handed conformation compared to buffer B, while the mean dwell time in the right-handed state did not change (Table 6.2 and Figure 6.S9, Tables 6.S11 and 6.S12 of the Supplementary Information). Remarkably, the average time a self-loaded 601-tetrasome spent in the left-handed (right-handed)

state is, however, 1.5 ± 0.1 (1.6 ± 0.1) times shorter than a NAP1-loaded 601-tetrasome in the same buffer C. These values are also 1.9 ± 0.1 (1.4 ± 0.1) times smaller than the dwell times of a self-loaded 601-tetrasome in the left-handed (right-handed) state in buffer B.

In comparison, the results indicate that both NAP1-loaded and self-loaded 601-tetrasomes are similarly more stable in the left-handed state in buffer B compared to buffer A. A NAP1-loaded 601-tetrasome becomes even more stable in the left-handed state in buffer C (which only differed from buffer B by the presence of magnesium). The right-handed conformation remains essentially unaffected. However, both conformations are similarly less stable for self-loaded 601-tetrasomes compared to NAP1-loaded 601-tetrasomes in the same buffer C.

Overall, these results show a considerable effect of the buffer conditions on the flipping kinetics of tetrasomes. A possible explanation for the different results in buffer A is the presence of the synthetic crowding agents, PEG and PVA, which were not present in buffers B and C. These agents may interact differently with DNA molecules containing the high-affinity 601-sequence due to altered properties compared to DNA constructs with a random sequence. In fact, PEG has been both theoretically and experimentally shown to induce concentration- and sequence-dependent compaction of single DNA molecules in aqueous solution [76]. The same study also reported a similar effect of the salt concentration. Buffer B does not contain synthetic crowding agents but a twice higher salt concentration than buffer A, which might altogether affect the properties of the DNA molecules and histones.

Given that buffers B and C only differ by the addition of magnesium, the distinct results suggest a critical role for magnesium in tetrasome flipping, possibly due to the associated increase in ionic strength. This may affect the properties of the DNA molecule and its interaction with the histone tetramer based on physical characteristics, such as electrostatic screening. In fact, magnesium ions have been reported to cause aggregation of DNA molecules [77, 78] or nucleosomes [79], and to induce chromatin compaction [80–82] *in vitro*. A direct impact of magnesium on histone loading by NAP1 can be excluded, because the experiment in buffer C was performed on a tetrasome assembled by NAP1 previously in buffer B (see Section 6.2). The differing results for NAP1-loaded and self-loaded tetrasomes might result from a NAP1-induced change in tetrasome location due to the altered environment and DNA properties, as discussed above.

6.3.3 The effects of the underlying DNA sequence and ambient conditions is revealed in the energetics of tetrasomes

The distinct effects of the 601-sequence and the different buffers on tetrasome structure and dynamics become more evident when looking at their energetics. The ratio of the dwell times in the two states can be used to calculate the difference between their free energies according to $\Delta E_{\text{dwell-times}} = -k_B T \ln(\tau_{D,\text{right}}/\tau_{D,\text{left}})$. The obtained results are summarized together with the values of the other characteristic quantities determined for (H3.1-H4)₂ tetrasomes in Table 6.3. Alternatively, the free energy differences were also calculated from the ratio of the probabilities $p_{\text{left}} = p$ and $p_{\text{right}} = 1 - p$ for a tetrasome to be in the respective conformations according to $\Delta E_{\text{peak-areas}} = -k_B T \ln((1 - p)/p)$. The probability values were determined from the relative ratio between the peak-areas in the double-Gaussian distribution of the same linking number data (see Section 6.2 and Table 6.S14 of the Supplementary Information). The results from the two approaches are in good agreement within error-bars, but the energy differences calculated from the dwell times are considered as more reliable due to the larger sample size (Table 6.3).

The dwell times $\tau_{D,\text{left}}$ and $\tau_{D,\text{right}}$ are further related to the respective transition rates $k_{l \rightarrow r}$ and $k_{r \rightarrow l}$ between the two conformations by $k = 1/\tau$. Assuming an equal transition rate between the two conformations at zero force of $k_0 \sim 10^7 \text{s}^{-1}$ [43], the height of the energy barriers ΔG^* for the transitions can also be estimated according to $\Delta G^* = -k_B T \ln(k/k_0)$. This allows to assess the impact of the underlying DNA sequence and/or ambient conditions on the dynamic nature of the tetrasomes in general.

In comparison, the energy differences ΔE between the left-handed and right-handed conformation of 601-tetrasomes are overall considerably smaller than the value determined for tetrasomes assembled on DNA with a random sequence (Table 6.3). The changes in the energy difference range from $\Delta \Delta E \sim 1.3 k_B T$ to $\Delta \Delta E \sim 0.7 k_B T$. Such decrease in energy difference reflects a realignment of both states to similar energies, corresponding to a shift of the equilibrium condition towards the right-handed conformation. These results strongly suggest a critical role of the DNA sequence for the conformational dynamics of tetrasomes by possibly inducing subtle changes in their structure. As discussed above, we have not observed such differences in the overall structural properties of the tetrasomes in our assay. However, they have a significant impact on the stability of the conformations and, hence, the kinetics of the structural dynamics.

Table 6.3: Quantified properties of tetrasomes for comparison.

Quantity	(H3.1-H4) ₂ tetrasomes	(H3.1-H4) ₂ tetrasomes on 601-DNA
$\Delta z_{(dis)ass}$ (nm)	24 (± 3)*	23 (± 5)
$\Delta \theta_{(dis)ass}$ (turns)	0.73 (± 0.05)*	0.9 (± 0.2)
$\Delta \theta_{flipping}$ (turns)	1.7 (± 0.1)*	1.6 (± 0.2)
$\tau_{D,left}$ (s) (NAP1-loaded// <u>self-loaded</u>) [buffer type]	183 (+15/-12) ⁺ [A]	37// <u>93</u> [A]** 62// <u>175</u> [B]** 141// <u>93</u> [C]**
$\tau_{D,right}$ (s) (NAP1-loaded// <u>self-loaded</u>) [buffer type]	14 (± 1) [A]	28// <u>34</u> [A]** 33// <u>27</u> [B]** 30// <u>19</u> [C]**
$\Delta E_{dwell-times}$ ($k_B T$) (NAP1-loaded// <u>self-loaded</u>) [buffer type]	2.6 (± 0.1) ⁺ [A]	0.3 \pm 0.1// <u>1.0 \pm 0.1</u> [A] ⁺ 0.3 \pm 0.1// <u>1.9 \pm 0.1</u> [B] ⁺ 1.5 \pm 0.1// <u>1.6 \pm 0.1</u> [C] ⁺
$\Delta E_{peak-areas}$ ($k_B T$) (NAP1-loaded// <u>self-loaded</u>) [buffer type]	-	0.9 \pm 0.7// <u>1.1 \pm 0.2</u> [A] ⁺ 1.4 \pm 0.8// <u>2.1 \pm 0.2</u> [B] ⁺ 1.7 — // <u>1.6 \pm 0.4</u> [C] ⁺

*Values taken from Ref. [41]

**The corresponding errors, excluded here for clarity, can be retrieved from Table 6.2

⁺Errors calculated by error propagation

The changes induced in the energetics of the tetrasomes by the incorporation of the 601-sequence are represented in the schematic energy diagram shown in the *left panel* of Figure 6.3c. The barrier energy $E_{barrier}$ is set to the same value as a common reference point. Based on the results from our dwell time analysis (Table 6.2 and Figure 6.3a,b), the left-handed state of a NAP1-loaded 601-tetrasome is considerably less stable with a respectively higher free energy E than a NAP1-loaded tetrasome assembled on a DNA molecule of random sequence in the same buffer A. The same effect is induced in the right-handed conformation, but to a lesser extent. The assembly of (H3.1-H4)₂ tetramers without NAP1 results in a more stable left-handed conformation for 601-tetrasomes, while the right-handed state is essentially unaffected. However, self-loaded 601-tetrasomes are still considerably less stable in the left-handed state than NAP1-loaded tetrasomes assembled on DNA with a random sequence. Additionally, the

6 Structural Dynamics of 601-Tetrasomes

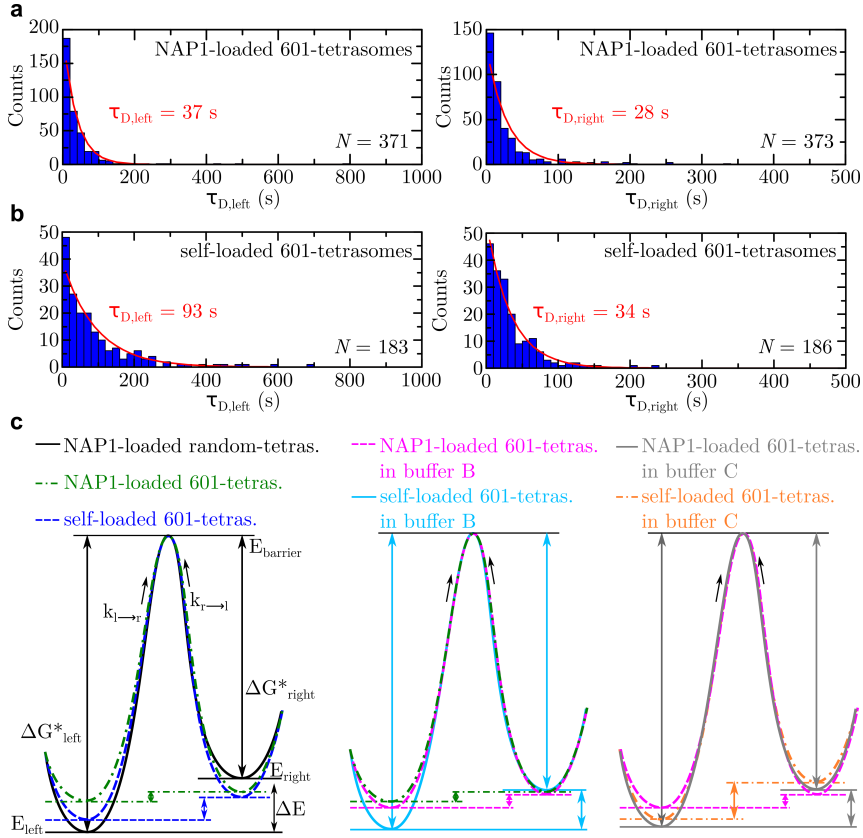


Figure 6.3: Energetics and kinetics of single 601-tetrasomes. **a** Histograms of the times a single NAP1-loaded (H3.1-H4)₂ tetrasome on a DNA molecule with a centered 601-sequence (‘NAP1-loaded 601-tetrasome’) dwelled in the left-handed (*left panel*) and right-handed (*right panel*) conformation in buffer A (see Tables 6.1 and 6.2). These data were obtained by dwell time analysis of the DNA linking number time traces filtered by averaging over 3.3 s ($N=330$) (see Section 6.2, Figure 6.2a and Figure 6.S7 of the Supplementary Information). Exponential fits (*red lines*) yielded a mean dwell time of $\tau_{D,left} = 37 \pm 2$ s ($N=371$) and $\tau_{D,right} = 28 + 2/-1$ s ($N=373$), respectively (68% confidence level for estimated values). **b** Histograms of the dwell times of a single (H3.1-H4)₂ tetrasome loaded on a DNA molecule with a centered 601-sequence without NAP1 (‘self-loaded tetrasomes’) in the left-handed (*left panel*) and right-handed conformation (*right panel*). Exponential fits (*red lines*) yielded a mean dwell time of $\tau_{D,left} = 93 + 7/-6$ s ($N=183$) and $\tau_{D,right} = 34 + 3/-2$ s ($N=186$), respectively (68% confidence level for estimated values). **c** Schematic energy diagrams of single 601-tetrasomes in all buffer conditions based on the dwell time values and the probabilities obtained from the linking number distributions (see Tables 6.2

and 6.3, Tables 6.S9-S12 and S14, and Figures 6.S8 and 6.S9 of the Supplementary Information). The *left panel* illustrates the energy levels for a NAP1-loaded (H3.1-H4)₂ tetrasome on a DNA-molecule with a random sequence ('random-tetrasomes'; *solid black lines*) and either NAP1-loaded (*green dashed-dotted lines*) or self-loaded (*blue dashed lines*) 601-tetrasome in buffer A (see Table 6.1). The free energy of a left-handed NAP1-loaded random-tetrasome (E_{left}) is considerably lower than that of a left-handed 601-tetrasome, while the reverse is the case for the right-handed conformation (E_{right}). The NAP1-mediated loading of a 601-tetrasome results in a considerably less stable left-handed conformation with a respectively higher free energy than self-loaded 601-tetrasomes. Accordingly, the free energy differences (ΔE) between the two conformations of the 601-tetrasomes are considerably decreased compared to random tetrasomes. Likewise, the energy barriers ΔG_{left}^* and ΔG_{right}^* for the transitions between the two states with the corresponding rates $k_{l \rightarrow r}$ and $k_{r \rightarrow l}$ are respectively altered for 601-tetrasomes compared to the transition energies for a random tetrasome. The *middle panel* illustrates the considerably lower free energy of a left-handed self-loaded 601-tetrasome (*cyan solid lines*) in buffer B compared to that of a left-handed NAP1-loaded 601-tetrasome in the same buffer B (*dashed magenta lines*) or buffer A, while the right-handed conformations are essentially unaffected. Accordingly, the free energy difference between the two states of the self-loaded 601-tetrasomes in buffer B is considerably increased as is the barrier height for the transition from the left-handed to the right-handed state. The *right panel* illustrates the considerably lower free energy of a left-handed NAP1-loaded tetrasome in buffer C (*gray solid lines*) compared to that of a left-handed self-loaded 601-tetrasome in the same buffer C (*orange dashed-dotted lines*) and a NAP1-loaded 601-tetrasome in buffer B, while the right-handed conformation is essentially unaltered compared to the latter. Both conformations become considerably less stable by the same extent for self-loaded tetrasomes in the same buffer C. Accordingly, the free energy difference between the two states of the NAP1-loaded and self-loaded 601-tetrasomes remains unchanged.

estimated barrier height of the transition from the left-handed and right-handed conformation is appreciably decreased by $\Delta \Delta G_{left}^* \sim 1.6 k_B T$ for NAP1-loaded 601-tetrasomes ($\Delta G_{left}^* \sim 19.7 k_B T$) compared to NAP1-loaded tetrasomes on DNA of a random sequence ($\Delta G_{left}^* \sim 21.3 k_B T$). The barrier height for the opposite transition is essentially unaffected. This result indicates that the combination of the 601-sequence and NAP1 form tetrasomes with an increased handedness dynamics, i.e. with an increased tendency to flip to the right-handed conformation.

Different ambient conditions also distinctly affect the energetics of tetrasomes. The resulting changes in the buffers B and C are likewise visualized in schematic energy diagrams shown in the *middle* and *right panel* of

Figure 6.3c, respectively. The underlying results from the dwell time analysis are summarized in Table 6.2 and shown Figures 6.S8 and 6.S9 of the Supplementary Information, respectively. The energy differences between the left-handed and right-handed states of 601-tetrasomes are listed in Table 6.3 together with other characteristic quantities.

The values indicate that buffer B induces changes in NAP1-loaded 601-tetrasomes, which increase the energy difference between the two states by about a factor of two compared to buffer A. The same effect is also observed for self-loaded tetrasomes. With an increase by about a factor of three, the differences between NAP1-loaded and self-loaded 601-tetrasomes in the same buffer B are even more appreciable. These changes are mainly related to the increased stability of the left-handed conformation for tetrasomes in buffer B, as assessed by the dwell time analysis discussed above. In particular, the barrier heights for the transition from the left-handed to the right-handed state show an appreciable difference by $\Delta\Delta G_{left}^* \sim 1.1 k_B T$ between NAP1-loaded ($\Delta G_{left}^* \sim 20.2 k_B T$) and self-loaded tetrasomes ($\Delta G_{left}^* \sim 21.3 k_B T$) in buffer B. This result indicates that tetrasomes assembled in buffer B, which does not contain synthetic crowding agents and a higher salt concentration compared to buffer A, have a decreased tendency to flip to the right-handed state.

Buffer C induces a considerable change in the energetics of NAP1-loaded tetrasomes compared to buffers A and B, likely due to the presence of magnesium. Here, the main influence is also an increased stability of the left-handed conformation, as indicated by the corresponding change in the dwell times discussed before. This change is further reflected in an appreciable increase of the barrier height for the transition of the NAP1-loaded tetrasomes in buffer C ($\Delta G_{left}^* \sim 21.1 k_B T$) from the left-handed and right-handed state by $\Delta\Delta G_{left}^* \sim 0.9 k_B T$ compared to NAP1-loaded tetrasomes in buffer B ($\Delta G_{left}^* \sim 20.2 k_B T$). This result indicates that NAP1-loaded tetrasomes are less likely to flip to the right-handed conformation in buffer C than in buffer B.

Remarkably, the energy difference between the two conformations of self-loaded tetrasomes in buffer C is essentially the same as for NAP1-loaded tetrasomes, while the dwell times are equally decreased for both states (Table 6.3). This result indicates that both conformations of self-loaded tetrasomes are less stable by the same extent in buffer C, likely due to the presence of magnesium. Hence, in this case, the buffer conditions impact the dynamic nature of tetrasomes by increasing both transition rates, i.e. their tendency to flip between both conformations.

6.4 Conclusion

In summary, we did not observe any effect of the 601-sequence and different ambient conditions on the overall structural properties of the tetrasomes (Table 6.3). Likewise, tetrasomes exhibit spontaneous handedness dynamics with the same associated change in DNA linking number irrespective of the DNA sequence and buffer conditions. However, our analysis of the dwell times in both states (Table 6.2) reveals that the 601-sequence and different buffer conditions have a significant impact on the kinetics and energetics of the tetrasomes (Table 6.3). Mainly the inherent left-handed conformation of tetrasomes is affected, while the right-handed state remains essentially unaltered. The presence of the 601-sequence decreases the stability of the left-handed state compared to tetrasomes assembled on DNA with a random sequence. The same impact is observed for NAP1, i.e. NAP1-loaded 601-tetrasomes have an increased tendency to adopt the right-handed conformation compared to self-loaded 601-tetrasomes. These effects are enhanced in buffers without synthetic crowding agents and a higher salt/ion concentration, except for self-loaded 601-tetrasomes. In the presence of magnesium, both conformations of self-loaded 601-tetrasomes are less stable by the same extent compared to NAP1-loaded 601-tetrasomes, corresponding to an overall increased structural dynamics. Taken together, the results demonstrate that the underlying DNA sequence and ambient conditions have a significant impact on the conformational plasticity of tetrasomes.

In the broader context, our previous [41–43] and present findings suggest tetrasomes as viable intermediates with intrinsic structural dynamics that can serve as a potential mechanism for gene regulation at the subnucleosomal level. The ability of tetrasomes to dynamically switch between two conformations with opposite directions of DNA wrapping may facilitate vital DNA-templated processes such as transcription, replication and repair. In particular, the impact of forces and torques exerted by genome-processing enzymes could be reduced without full but partial disassembly of nucleosomes. This mechanism may further be tuned by histone modifications, the underlying DNA sequence and ambient conditions. Changes in these critical factors can affect these subnucleosomal dynamics by altering the DNA and/or histone properties and, hence, their interactions. Such changes may involve chemical modifications, salt concentration, cations, chaperones, active assembly factors and/or remodeling enzymes. In this context, our findings explicitly show that results from experiments with nucleosome-positioning sequences require careful interpretation considering the specific ambient conditions in the employed assay.

6.5 Supplementary Information

Supplementary Tables

Table 6.S1. The sequences of the primers used to make the main DNA fragments. The specific overhangs at the *BsaI* sites are indicated by the lowercases.

Primers	Primer Sequences
1	5'-CCATCTGGTCTCCtcaaatcctgttaccagtggctgctgcc
2	5'-CCATCTGGTCTCCtaggtgttgagatccagttcgatgtaacc
3	5'-CCATCTGGTCTCCttgaCGCTCTAGAACTAGTGGATCCCCC
4	5'-CCATCTGGTCTCCcctaCGCTCTAGAACTAGTGGATCCCCC
5	5'-GACCGAGATAGGGTTGAGTG

Table 6.S2. Concentrations and volumes of the DNA and bead solution used in this work. The remaining details of the flow cell and sample preparation have been described in Ref. [43].

Sample	Concentrations and volumes for tethering
DNA molecules (Figure 6.S2)	Stock concentration: $c_{stock} = 45 \text{ ng}/\mu\text{l}$ 0.2 μl of 1:300 dilution from stock solution
superparamagnetic beads (0.5- μm diameter, Adem- tech, Pessac, France)	0.2 μl or 0.3 μl from stock solution

Table 6.S3. Summary of the assembly events. Sizes of the step-like change in DNA length Δz_{ass} (in nm) and $\Delta\theta_{ass}$ (in turns) upon the assembly of one tetrasome as obtained in the different buffer conditions. The compositions of the buffers are stated in Table 6.1.

Buffers	Δz_{ass} (nm)	$\Delta\theta_{ass}$ (turns)	mean Δz_{ass} (\pm STD, nm)	mean $\Delta\theta_{ass}$ (\pm STD, turns)
Buffer A	-21	-1.0		
<i>with NAP1</i>	-23	-1.2		
	-25	-0.7	-23 (± 2)*	-1.0 (± 0.3)**
without NAP1	-23	-0.8		
	-10	-0.8		
	-23	-1.3		
	-28	-0.5	-25 (± 3)*	-1.0 (± 0.3)**
<i>overall means</i>			-24 (± 3)*	-1.0 (± 0.2)**
Buffer B	-16	-1.3		
<i>with NAP1</i>	-16	-1.0		
	-24	-1.0		
	-16	-0.9		
	-33	-0.7	-21 (± 7)	-1.0 (± 0.2)
without NAP1	-23	-0.9	—	—
<i>overall means</i>			-21 (± 7)	-1.0 (± 0.2)
Buffer C	-24	-0.6		
without NAP1	-27	-0.7		
	-19	-0.8		
	-16	-1.2	-22 (± 5)	-0.8 (± 0.2)
TOTAL MEANS			-22 (± 5)*	-0.9 (± 0.2)**

*excluding the value $\Delta z_{ass} = -10$ nm beyond the mean resolution in z ($z_{res} = \pm 16$ nm)

**excluding the value $\Delta\theta_{ass} = -0.5$ (-0.46) turns beyond the mean resolution in θ ($\theta_{res} = \pm 0.5$ (0.47) turns)

Table 6.S4. Summary of the disassembly events. Sizes of the step-like change in DNA length Δz_{disass} (in nm) and $\Delta\theta_{disass}$ (in turns) upon the disassembly of one tetrasome as obtained in the different buffer conditions. The compositions of the buffers are stated in Table 6.1.

Buffers	Δz_{disass} (nm)	$\Delta\theta_{disass}$ (turns)	mean Δz_{disass} (\pm STD, nm)	mean $\Delta\theta_{disass}$ (\pm STD, turns)
Buffer A	<i>31</i>	<i>0.7</i>		
<i>with NAP1</i>	<i>19</i>	<i>0.5</i>	<i>25 (± 8)</i>	<i>0.6 (± 0.1)</i>
without NAP1	23	0.6		
	20	0.9		
	25	-1.1	23 (± 3)	0.9 (± 0.2)**
overall means			24 (± 5)	0.8 (± 0.2)**
Buffer B	<i>11</i>	<i>0.9</i>		
<i>with NAP1</i>	<i>25</i>	<i>0.7</i>		
	<i>25</i>	<i>1.2</i>	<i>25 (± 0)*</i>	<i>0.9 (± 0.2)</i>
without NAP1	33	0.7	—	—
overall means			28 (± 5)*	0.9 (± 0.2)
Buffer C	22	0.6	—	—
without NAP1				
TOTAL MEANS			-25 (± 5)*	0.8 (± 0.2)**

*excluding the value $\Delta z_{disass} = 11$ nm beyond the mean resolution in z ($z_{res} = \pm 16$ nm)

**considering the absolute value from the single right-handed disassembly observed ($\Delta\theta_{disass} = -1.1$ turns)

Table 6.S5. Results of the unpaired two-sample t-tests on the changes in DNA length Δz upon tetrasome assembly or disassembly. The h-value of h=0 (h=1) indicates that the data sets (do not) originate from independent, normally distributed random samples with equal means and equal but unknown variances at 5% significance level. The p-values essentially correspond to the probabilities for the similarity between the two data sets. The values in normal font depict the results for the assembly data only, while values in *italic* font depict the results for the disassembly data only.

Buffers +/-NAP1	A+	B+	C+*	A-	B-**	C-(**)
A+	—	<i>h=0</i> <i>p=0.98</i>	—	<i>h=0</i> <i>p=0.65</i>	<i>h=0</i> <i>p=0.59</i>	<i>h=0</i> <i>p=0.79</i>
B+	h=0 p=0.68	—	—	<i>h=0</i> <i>p=0.34</i>	<i>h=1</i> <i>p=0.02</i>	<i>h=0</i> <i>p=0.05</i>
C+*	—	—	—	—	—	—
A-	h=0 p=0.57	h=0 p=0.49	—	—	<i>h=0</i> <i>p=0.08</i>	<i>h=0</i> <i>p=0.75</i>
B-**	h=0 p=0.98	h=0 p=0.83	—	h=0 p=0.72	—	<i>h=NaN</i> <i>p=NaN</i>
C-(**)	h=0 p=0.59	h=0 p=0.94	—	h=0 p=0.37	h=0 p=0.78	—

*neither assembly nor disassembly data available

**data sets contain one value

(**)disassembly data set contains one value

Table 6.S6. Results of the unpaired two-sample t-tests on the changes in DNA length Δz upon tetrasome assembly and disassembly. The h-value of h=0 indicates that the data sets originate from independent, normally distributed random samples with equal means and equal but unknown variances at 5% significance level. The p-values essentially correspond to the probabilities for the similarity between the two data sets.

Buffers +/- <i>NAP1</i>	A+	B+	C+*	A-	B-**	C-**
A+	h=0 p=0.70	h=0 p=0.37	— —	h=0 p=0.84	h=0 p=0.07	h=0 p=0.62
B+	h=0 p=0.56	h=0 p=0.52	— —	h=0 p=0.74	h=0 p=0.23	h=0 p=0.96
C+*	—	—	—	—	—	—
A-	h=0 p=0.90	h=0 p=0.85	— —	h=0 p=0.48	h=0 p=0.14	h=0 p=0.48
B-**	h=0 p=0.87	h=0 p=0.09	— —	h=0 p=0.92	h=NaN p=NaN	h=NaN p=NaN
C-**	h=0 p=0.50	h=0 p=0.36	— —	h=0 p=0.70	h=0 p=0.11	h=0 p=0.98

*no data available

**data sets contain one value

Table 6.S7. Results of the unpaired two-sample t-tests on the changes in DNA linking number $\Delta\theta$ upon tetrasome assembly or disassembly. The h-value of h=0 indicates that the data sets originate from independent, normally distributed random samples with equal means and equal but unknown variances at 5% significance level. The p-values essentially correspond to the probabilities for the similarity between the two data sets. The values in normal font depict the results for the assembly data only, while values in *italic* font depict the results for the disassembly data only.

Buffers +/- <i>NAP1</i>	A+	B+	C+*	A-	B-**	C-(**)
A+	—	<i>h=0</i> <i>p=0.18</i>	—	<i>h=0</i> <i>p=0.31</i>	<i>h=0</i> <i>p=0.72</i>	<i>h=0</i> <i>p=0.97</i>
B+	h=0 p=0.98	—	—	<i>h=0</i> <i>p=0.75</i>	<i>h=0</i> <i>p=0.45</i>	<i>h=0</i> <i>p=0.35</i>
C+*	—	—	—	—	—	—
A-	h=0 p=0.94	h=0 p=0.94	—	—	<i>h=0</i> <i>p=0.63</i>	<i>h=0</i> <i>p=0.50</i>
B-**	h=0 p=0.71	h=0 p=0.62	—	h=0 p=0.76	—	<i>h=NaN</i> <i>p=NaN</i>
C-(**)	h=0 p=0.38	h=0 p=0.27	—	h=0 p=0.44	h=0 p=0.85	—

*neither assembly nor disassembly data available

**data sets contain one value

(**)disassembly data set contains one value

Table 6.S8. Results of the unpaired two-sample t-tests on the changes in DNA linking number $\Delta\theta$ upon tetrasome assembly and disassembly. The h-value of h=0 indicates that the data sets originate from independent, normally distributed random samples with equal means and equal but unknown variances at 5% significance level. The p-values essentially correspond to the probabilities for the similarity between the two data sets.

Buffers +/- <i>NAP1</i>	A+	B+	C+*	A-	B-**	C-**
A+	h=0 p=0.19	h=0 p=0.79	— —	h=0 p=0.60	h=0 p=0.46	h=0 p=0.37
B+	h=0 p=0.09	h=0 p=0.76	— —	h=0 p=0.52	h=0 p=0.30	h=0 p=0.21
C+*	—	—	—	—	—	—
A-	h=0 p=0.22	h=0 p=0.87	— —	h=0 p=0.67	h=0 p=0.51	h=0 p=0.42
B-**	h=0 p=0.40	h=0 p=0.78	— —	h=0 p=0.97	h=NaN p=NaN	h=NaN p=NaN
C-**	h=0 p=0.42	h=0 p=0.49	— —	h=0 p=0.73	h=0 p=0.75	h=0 p=0.59

*no data available

**data sets contain one value

Table 6.S9. Summary of the flipping events. Sizes of the change in DNA linking number $\Delta\theta_{flipping}$ (in turns) upon the flipping of an assembled tetrasome as obtained in the different buffer conditions. The compositions of the buffers are stated in Table 6.1.

Buffers	$\Delta\theta_{flipping}$ (turns) with <i>NAP1</i>	$\Delta\theta_{flipping}$ (turns) without <i>NAP1</i>	mean $\Delta\theta_{flipping}$ (\pm STD, turns)
Buffer A	1.8	1.6	
	1.0	1.6	
	1.8	1.7	
	—	1.3	
	—	1.3	
	—	1.3	
<i>overall means</i>	1.5 (± 0.4)	1.5 (± 0.2)	1.5 (± 0.3)
Buffer B	1.6	1.0	
	1.8	1.0	
	1.8	1.7	
	1.7	1.7	
	1.7	—	
	1.3	—	
	1.2	—	
	1.7	—	
<i>overall means</i>	1.6 (± 0.2)	1.5 (± 0.4)	1.5 (± 0.3)
Buffer C	1.7	1.7	
	—	1.7	
	—	1.7	
	—	1.7	
	—	1.7	
<i>overall means</i>	—	1.7 (± 0.0)	1.7 (± 0.0)
Total MEAN			1.6 (± 0.2)

Table 6.S10. Results of the unpaired two-sample t-tests on the changes in DNA linking number $\Delta\theta_{\text{flipping}}$ upon tetrasome flipping. The h-value h=0 indicates that the data sets originate from independent, normally distributed random samples with equal means and equal but unknown variances at 5% significance level. The p-values essentially correspond to the probabilities of the similarity between the two data sets.

Buffers + or -NAP1	A+	B+	C+*	A-	B-	C-
A+	—	h=0 p=0.79	h=0 p=0.73	h=0 p=0.97	h=0 p=0.89	h=0 p=0.42
B+		—	h=0 p=0.57	h=0 p=0.62	h=0 p=0.60	h=0 p=0.29
C+*			—	h=0 p=0.31	h=0 p=0.63	h=0 p=0.47
A-				—	h=0 p=0.83	h=0 p=0.05
B-					—	h=0 p=0.26

*data sets contain one value

Table 6.S11. Results of the Wilcoxon rank-sum tests on the dwell times of a 601-tetrasome in the left-handed or right-handed conformation. A h-value of h=0 (h=1) indicates that the data sets – obtained from filtering by averaging over 3.3 s [N=330] – (do not) originate from independent, continuously distributed random samples with equal medians at 5% significance level. The p-values essentially correspond to the probabilities for the similarity between the two data sets. Unlike the t-test, this test does not assume normal distributions and is therefore applicable to the exponentially distributed dwell time data (see Figure 6.3a,b, and Figures 6.S8 and 6.S9). The values in normal font depict the results for the left-handed data only, while values in *italic* font depict the results for the right-handed data only.

Buffers + or - <i>NAP1</i>	A+	B+	C+	A-	B-	C-
A+	—	<i>h=1</i> <i>p=5.6</i> <i>·10⁻⁸</i>	<i>h=1</i> <i>p=8.6</i> <i>·10⁻⁶</i>	<i>h=1</i> <i>p=2.1</i> <i>·10⁻⁵</i>	<i>h=1</i> <i>p=0.02</i>	<i>h=0</i> <i>p=0.37</i>
B+	h=1 p=1.9 ·10 ⁻³	—	<i>h=0</i> <i>p=0.93</i>	<i>h=0</i> <i>p=0.79</i>	<i>h=1</i> <i>p=8.4</i> <i>·10⁻³</i>	<i>h=1</i> <i>p=6.1</i> <i>·10⁻¹⁶</i>
C+	h=1 p=1.6 ·10 ⁻³⁷	h=1 p=1.9 ·10 ⁻²⁵	—	<i>h=0</i> <i>p=0.78</i>	<i>h=1</i> <i>p=0.02</i>	<i>h=1</i> <i>p=8.1</i> <i>·10⁻¹⁰</i>
A-	h=1 p=3.9 ·10 ⁻¹⁴	h=1 p=3.5 ·10 ⁻⁷	h=1 p=1.2 ·10 ⁻⁶	—	<i>h=1</i> <i>p=0.03</i>	<i>h=1</i> <i>p=4.2</i> <i>·10⁻⁹</i>
B-	h=1 p=3.7 ·10 ⁻⁴⁶	h=1 p=2.6 ·10 ⁻³³	h=0 p=0.64	h=1 p=3.8 ·10 ⁻⁸	—	<i>h=1</i> <i>p=1.5</i> <i>·10⁻⁴</i>
C-	h=1 p=1.6 ·10 ⁻³³	h=1 p=6.6 ·10 ⁻¹⁸	h=1 p=3.0 ·10 ⁻⁹	h=0 p=0.64	h=1 p=2.5 ·10 ⁻¹²	—

Table 6.S12. Results of the Wilcoxon rank-sum tests on the dwell times of a 601-tetrasome in the left-handed and right-handed conformation. A h-value of h=0 (h=1) indicates that the data sets – obtained from filtering by averaging over 3.3 s [N=330] – (do not) originate from independent, continuously distributed random samples with equal medians at 5% significance level. The p-values essentially correspond to the probabilities for the similarity between the two data sets. Unlike the t-test, this test does not assume normal distributions and is therefore applicable to the exponentially distributed dwell time data (see Figure 6.3a,b, and Figures 6.S8 and 6.S9).

Buffers + or -NAP1	A+	B+	C+	A-	B-	C-
A+	h=1 p=1.6 $\cdot 10^{-5}$	h=0 p=0.51	h=0 p=0.63	h=0 p=0.47	h=0 p=0.07	h=1 p=2.8 $\cdot 10^{-10}$
B+	h=1 p=7.0 $\cdot 10^{-12}$	h=1 p=2.4 $\cdot 10^{-3}$	h=1 p=0.02	h=0 p=0.05	h=1 p=7.0 $\cdot 10^{-6}$	h=1 p=9.7 $\cdot 10^{-22}$
C+	h=1 p=5.4 $\cdot 10^{-46}$	h=1 p=2.8 $\cdot 10^{-42}$	h=1 p=8.5 $\cdot 10^{-31}$	h=1 p=4.4 $\cdot 10^{-28}$	h=1 p=1.1 $\cdot 10^{-39}$	h=1 p=1.4 $\cdot 10^{-62}$
A-	h=1 p=2.1 $\cdot 10^{-22}$	h=1 p=3.2 $\cdot 10^{-15}$	h=1 p=1.5 $\cdot 10^{-11}$	h=1 p=2.2 $\cdot 10^{-10}$	h=1 p=2.9 $\cdot 10^{-17}$	h=1 p=2.6 $\cdot 10^{-32}$
B-	h=1 p=3.1 $\cdot 10^{-57}$	h=1 p=1.4 $\cdot 10^{-53}$	h=1 p=2.6 $\cdot 10^{-35}$	h=1 p=3.2 $\cdot 10^{-32}$	h=1 p=2.5 $\cdot 10^{-47}$	h=1 p=4.3 $\cdot 10^{-80}$
C-	h=1 p=2.5 $\cdot 10^{-52}$	h=1 p=1.9 $\cdot 10^{-40}$	h=1 p=2.2 $\cdot 10^{-23}$	h=1 p=1.6 $\cdot 10^{-19}$	h=1 p=3.2 $\cdot 10^{-37}$	h=1 p=2.4 $\cdot 10^{-89}$

Table 6.S13. Results of the Wilcoxon rank-sum tests on the dwell times of a 601-tetrasome in the left-handed and right-handed conformation in buffer A. A h -value of $h=0$ ($h=1$) indicates that the data sets – obtained from filtering by averaging over 3.3 s [$N=330$] – (do not) originate from independent, continuously distributed random samples with equal medians at 5% significance level. The p -values essentially correspond to the probabilities for the similarity between the two data sets. Unlike the t -test, this test does not assume normal distributions and is therefore applicable to the exponentially distributed dwell time data (see Figure 6.3a,b, and Figures 6.S8 and 6.S9). Values in *italic* font depict the results for the left-handed states only, while underlined values depict the results for the right-handed states only. Values in normal font represent the results for the left-handed with the right-handed states.

Buffer A +/-NAP1	random* tetras. +NAP1	601- tetras. +NAP1	601- tetras. -NAP1	random* tetras. +NAP1	601- tetras. +NAP1	601- tetras. -NAP1
random* tetras. +NAP1	—	$h=1$ $p=6.8$ $\cdot 10^{-7}$	$h=1$ $p=7.0$ $\cdot 10^{-3}$	$h=1$ $p=2.2$ $\cdot 10^{-21}$	$h=1$ $p=1.5$ $\cdot 10^{-14}$	$h=1$ $p=8.7$ $\cdot 10^{-5}$
601- tetras. +NAP1		—	$h=1$ $p=3.9$ $\cdot 10^{-14}$	$h=1$ $p=1.9$ $\cdot 10^{-12}$	$h=1$ $p=1.6$ $\cdot 10^{-5}$	$h=0$ $p=0.74$
601- tetras. -NAP1			—	$h=1$ $p=3.6$ $\cdot 10^{-26}$	$h=1$ $p=2.1$ $\cdot 10^{-22}$	$h=1$ $p=2.2$ $\cdot 10^{-10}$
random* tetras. +NAP1				—	<u>$h=1$</u> <u>$p=5.9$</u> <u>$\cdot 10^{-4}$</u>	<u>$h=1$</u> <u>$p=5.7$</u> <u>$\cdot 10^{-12}$</u>
601- tetras. +NAP1					—	<u>$h=1$</u> <u>$p=2.1$</u> <u>$\cdot 10^{-5}$</u>

*data sets obtained by dwell time analysis of the linking number data from our previous study with (H3.1-H4)₂ tetrasomes assembled on DNA with a random sequence [41].

Table 6.S14. Probabilities for a 601-tetrasome to occupy the left-handed and right-handed conformation in the different buffer conditions. The respective values p and q ($=1 - p$) were obtained from the relative ratio between the peak-areas of the two Gaussian functions fitted to the linking number data (see Section 6.2, Figure 6.2A, and Figure 6.S6).

Buffers	p <i>with NAP1</i>	q <i>with NAP1</i>	p without NAP1	q without NAP1
Buffer A	<i>0.86</i>	<i>0.14</i>	0.72	0.28
	<i>0.51</i>	<i>0.49</i>	0.80	0.20
	<i>0.73</i>	<i>0.27</i>	0.73	0.27
	—	—	0.80	0.20
	—	—	0.71	0.29
	<i>0.70 (± 0.18)</i>	<i>0.30 (± 0.18)</i>	0.75 (± 0.05)	0.25 (± 0.05)
Buffer B	<i>0.83</i>	<i>0.17</i>	0.90	0.10
	<i>0.92</i>	<i>0.08</i>	0.86	0.14
	<i>0.83</i>	<i>0.17</i>	0.90	0.10
	<i>85</i>	<i>0.15</i>	—	—
	<i>46</i>	<i>0.54</i>	—	—
	<i>90</i>	<i>0.10</i>	—	—
	<i>81</i>	<i>0.19</i>	—	—
	<i>0.80 (± 0.15)</i>	<i>0.20 (± 0.15)</i>	0.89 (± 0.02)	0.11 (± 0.02)
Buffer C	<i>0.86</i>	<i>0.14</i>	0.90	0.10
	—	—	0.85	0.15
	—	—	0.74	0.26
	—	—	0.85	0.15
	—	—	0.83 (± 0.07)	0.17 (± 0.07)
	<i>overall means</i>			

Supplementary Figures

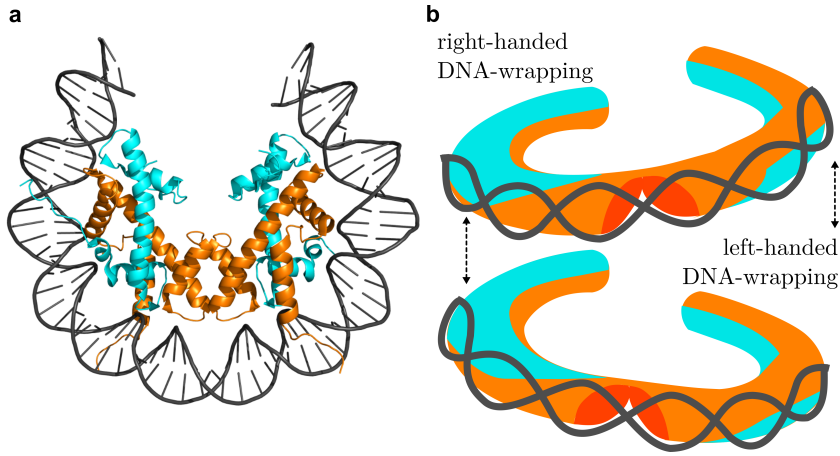


Figure 6.S1. Schematic depiction of tetrasome structure and dynamics. **a** Top view on about 80 bp of DNA (*dark gray*) bound to a tetrameric protein core consisting of the histones H3 (*orange*) and H4 (*cyan*). This image was created by modifying the structural data of the *Drosophila* nucleosome from the RCSB PDB with the identification code 2PYO [83] using the PyMOL Molecular Graphics System, Version 1.8 Schrödinger, LLC. **a** Representation of the two tetrasome conformations with the DNA wrapped in either a left-handed or a right-handed superhelix. Tetrasomes were observed to spontaneously flip between these two states [41–43]. This image is adapted from Ref. [43].

6 Structural Dynamics of 601-Tetrasomes

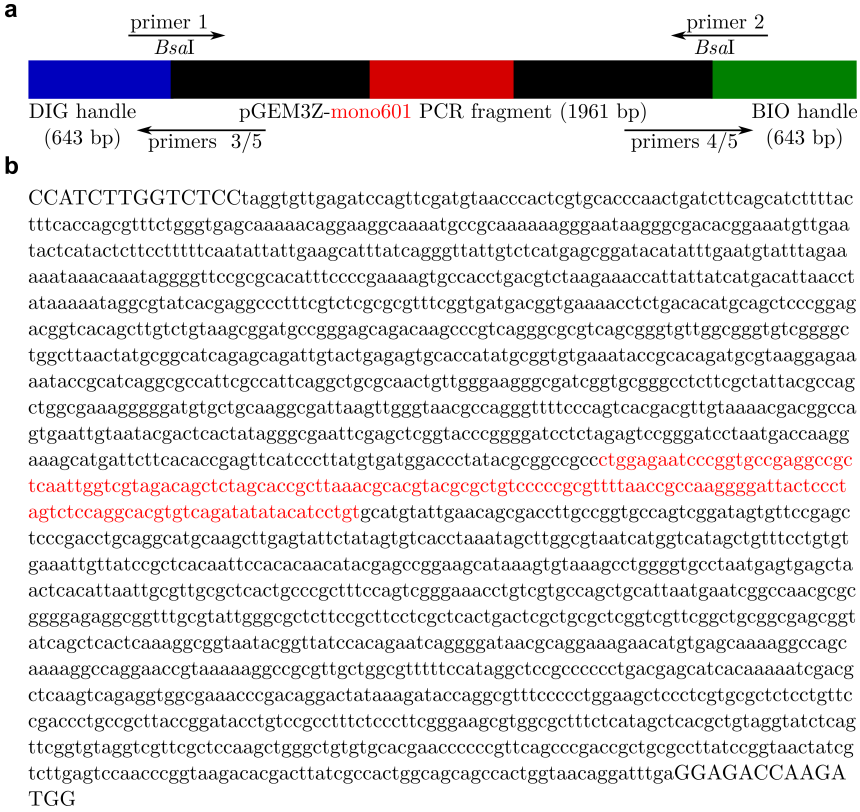


Figure 6.S2. Specifications of the DNA molecule used in this work.
a Schematics of the 1.96 kbp linear DNA fragments (*black*) prepared from a pGEM3Z plasmid containing a single 601-sequence (*red*) in the center (pGEM3Z-mono601) by PCR with primers 1 and 2 (see Table 6.S1). These main fragments were ligated to a shorter digoxigenin-coated (DIG, *blue*) fragment (handle) at one end and to a biotin-coated (BIO, *green*) handle at the other end via *BsaI* sites. The handles were generated by combinations of primer 5 with primer 3 and 4, respectively (see Table 6.S1). **b** Sequence of the main DNA fragment containing a single 601-sequence (*red*) in the center.

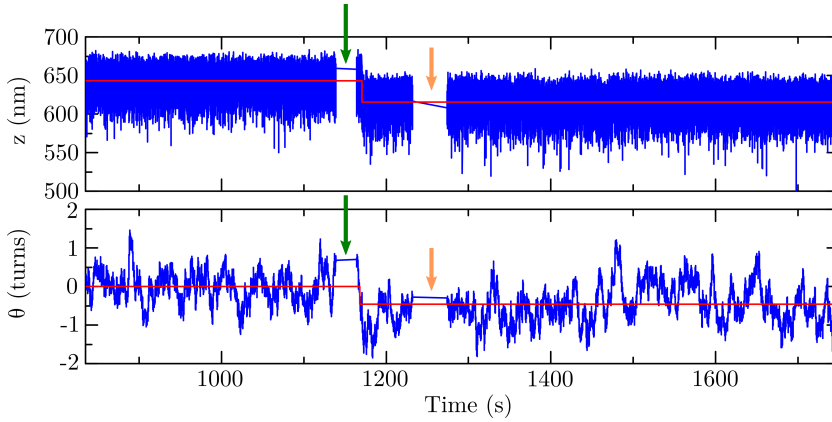


Figure 6.S3. Assembly of a single self-loaded 601-tetrasome. Partial time traces of the length z (in nm, panel above) and the linking number θ (in turns, panel below) of a DNA molecule with a centered 601-sequence before and upon the assembly of a $(\text{H3.1-H4})_2$ tetrasome without NAP1 in buffer A (see Table 6.1). The formation of a tetrasome simultaneously decreased both quantities in the form of a step identified using a step-finder algorithm (*red lines*) (see Section 6.2). About 60 s after assembly, free proteins were flushed out with measurement buffer (*orange arrows*) to prevent further histone binding.

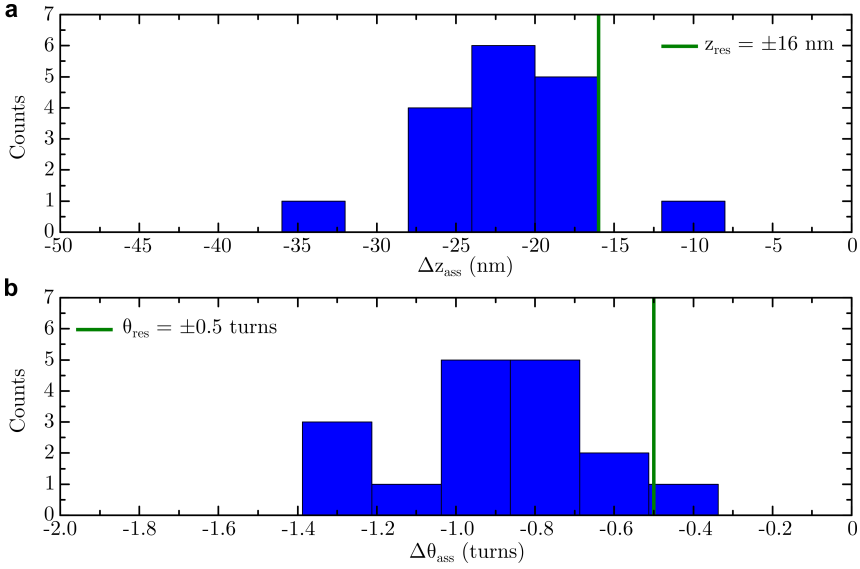


Figure 6.S4. Changes in DNA length and DNA linking number upon assembly of single 601-tetrasomes. **a** Histogram of changes in DNA length Δz_{ass} (in nm) upon tetrasome assembly in all buffer conditions (see Table 6.S3). The *green line* depicts the mean spatial resolution based on 1 average STD (± 16 nm) determined from all experiments (see Section 6.2). The data within resolution yielded a mean value of $\Delta z_{ass} = -22 \pm 5$ nm. **b** Histogram of changes in DNA linking number $\Delta \theta_{ass}$ upon tetrasome assembly in all buffer conditions (see Table 6.S3). The *green line* indicates the mean spatial resolution based on 1 average STD (± 0.5 turns) determined from all experiments (see Section 6.2). The data within resolution yielded a mean value of $\Delta \theta_{ass} = -0.9 \pm 0.2$ turns.

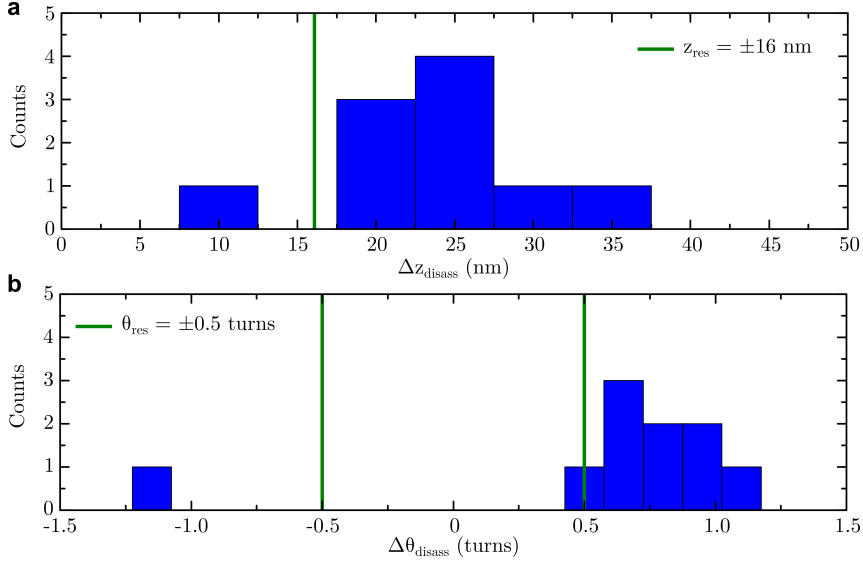


Figure 6.S5. Changes in DNA length and DNA linking number upon disassembly of single 601-tetrasomes. **a** Histogram of changes in DNA length Δz_{disass} (in nm) upon tetrasome disassembly in all buffer conditions (see Table 6.S4). The *green line* depicts the mean spatial resolution based on 1 average STD (± 16 nm) determined from all experiments (see Section 6.2). The data within resolution yielded a mean value of $\Delta z_{disass} = 25 \pm 5$ nm. **b** Histogram of changes in DNA linking number $\Delta \theta_{disass}$ upon tetrasome disassembly in all buffer conditions (see Table 6.S4). The *green line* indicates the mean spatial resolution based on 1 average STD (± 0.5 turns) determined from all experiments (see Section 6.2). The data within resolution yielded a mean value of $\Delta \theta_{disass} = 0.8 \pm 0.2$ turns (considering the absolute value of the single negative value indicating right-handed disassembly).

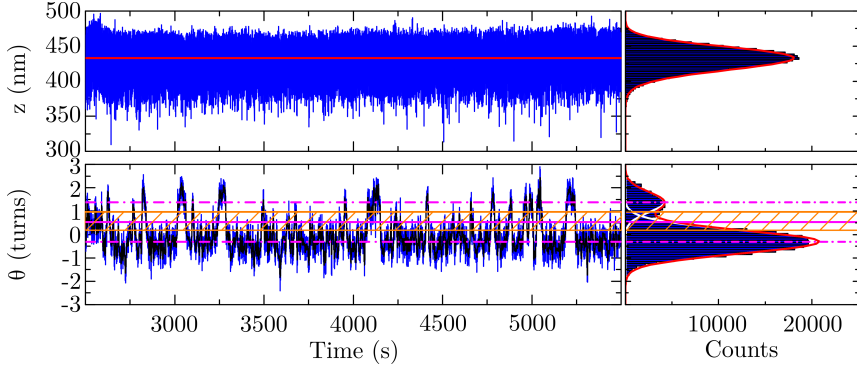


Figure 6.S6. Flipping of a single NAP1-loaded 601-tetrasome. Partial time traces of the length z (in nm, panel above) and the linking number θ (in turns, panel below) of a DNA molecule after the assembly of a $(\text{H3.1-H4})_2$ tetrasome in buffer A (see Table 6.1) upon flushing in histone tetramers only. As indicated from the fit by the step-finder algorithm to the time trace (*red line, left panel*) and the fit of a mirrored gamma function (*red line in histogram plot, right panel*) to the skewed data, the DNA length stays constant. The DNA linking number spontaneously fluctuates, i.e. ‘flips’, between two states identified by fitting two Gaussian functions (*white lines in histogram plot, right panel*) underlying the full profile (*red line in histogram plot, right panel*). The two states correspond to a prevalent left-handed and a less adopted right-handed conformation of DNA wrapping with the respective mean linking numbers $\theta_{\text{left}} = -0.31 \pm 0.01$ turns and $\theta_{\text{right}} = +1.38 \pm 0.06$ turns (*dashed-dotted magenta lines*, 95% confidence level for estimated values). These structural dynamics were quantified in terms of the dwell times in the two states based on a threshold zone (*shaded orange area*) set by 1 STD from each mean value (*orange solid lines*) around their average (*solid magenta line*) (see Section 6.2).

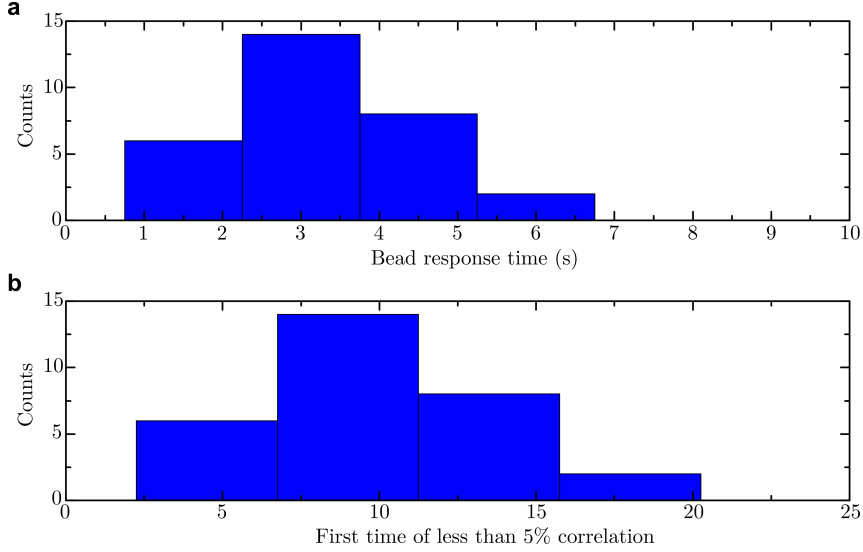


Figure 6.S7. Characteristic times of the bead's angular fluctuations. **a** Histogram of the response times of the superparamagnetic bead (Table 6.S2) tethered by a 1.96 kbp DNA fragment (Figure 6.S1). The response times are obtained by autocorrelation analysis of the DNA linking number time traces from FOMT measurements as described in Ref. [65]. Several measurements ($N=30$) yielded a mean value of $\tau_c = 3.3 \pm 1.0$ s. **b** Histogram of the first times at which the correlation amounts to less than 5%. The data ($N=30$) resulted in a mean value of $\tau_{c,5\%} = 9.8 \pm 3.1$ s. This mean value plus three times its STD ($\tau_{c,long} = 19.1$ s) was used as an upper boundary for the time difference between steps in the DNA length and DNA linking number time traces to be considered as coinciding.

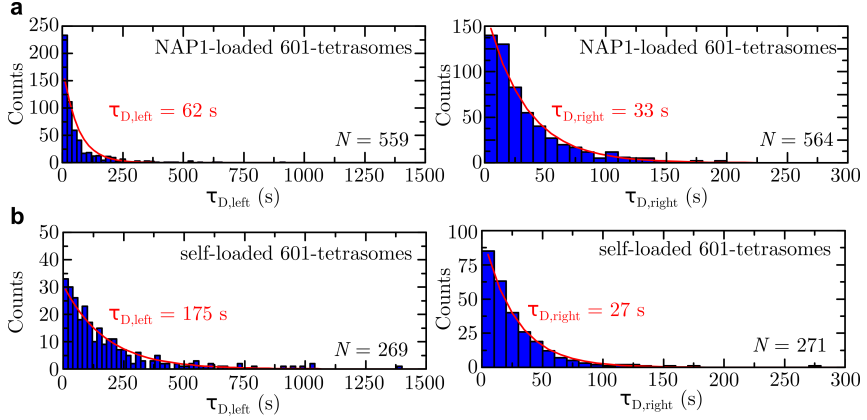


Figure 6.S8. Dwell times of 601-tetrasomes in buffer B. **a** Histograms of the times a single NAP1-loaded (H3.1-H4)₂ tetrasome on a DNA molecule with a centered 601-sequence ('NAP1-loaded 601-tetrasome') dwelled in the left-handed (*left panel*) and right-handed (*right panel*) conformation in buffer B (see Table 6.2). These data were obtained by dwell time analysis of the DNA linking number traces filtered by averaging over 3.3 s ($N=330$) (see Section 6.2, Figure 6.2a, and Figure 6.S7). Exponential fits (*red lines*) yielded a mean dwell time of $\tau_{D,left} = 62 \pm 3$ s ($N=559$) and $\tau_{D,right} = 33 \pm 1$ s ($N=564$) (68% confidence level for estimated values), respectively. **b** Histograms of the dwell times of a single (H3.1-H4)₂ tetrasome loaded on a DNA molecule with a centered 601-sequence without NAP1 ('self-loaded 601-tetrasomes') in the left-handed (*left panel*) and right-handed (*right panel*) conformation. Exponential fits (*red lines*) yielded a mean dwell time of $\tau_{D,left} = 175 +11/-10$ s ($N=269$) and $\tau_{D,right} = 27 \pm 2$ s ($N=271$) (68% confidence level for estimated values), respectively.

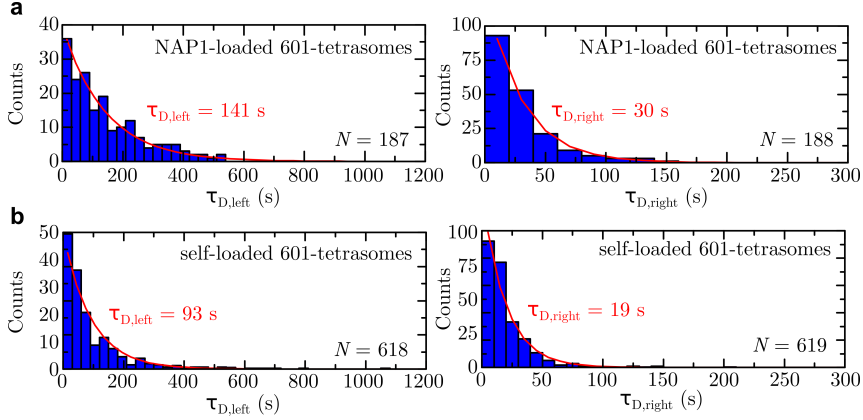


Figure 6.S9. Dwell times of 601-tetrasomes in buffer C. **a** Histograms of the times a single NAP1-loaded (H3.1-H4)₂ tetrasome on a DNA molecule with a centered 601-sequence (‘NAP1-loaded 601-tetrasome’) dwelled in the left-handed (*left panel*) and right-handed (*right panel*) conformation in buffer C (see Table 6.2). These data were obtained by dwell time analysis of the DNA linking number traces filtered by averaging over 3.3 s ($N=330$) (see Section 6.2, Figure 6.2a, and Figure 6.S7). Exponential fits (*red lines*) yielded a mean dwell time of $\tau_{D,left} = 141 \pm 11/-10$ s ($N=187$) and $\tau_{D,right} = 30 \pm 2$ s ($N=188$) (68% confidence level for estimated values), respectively. **b** Histograms of the dwell times of a single (H3.1-H4)₂ tetrasome loaded on a DNA molecule with a centered 601-sequence without NAP1 (‘self-loaded 601-tetrasomes’) in the left-handed (*left panel*) and right-handed (*right panel*) conformation. Exponential fits (*red lines*) yielded a mean dwell time of $\tau_{D,left} = 93 \pm 4$ s ($N=618$) and $\tau_{D,right} = 19 \pm 1$ s ($N=619$) (68% confidence level for estimated values), respectively.

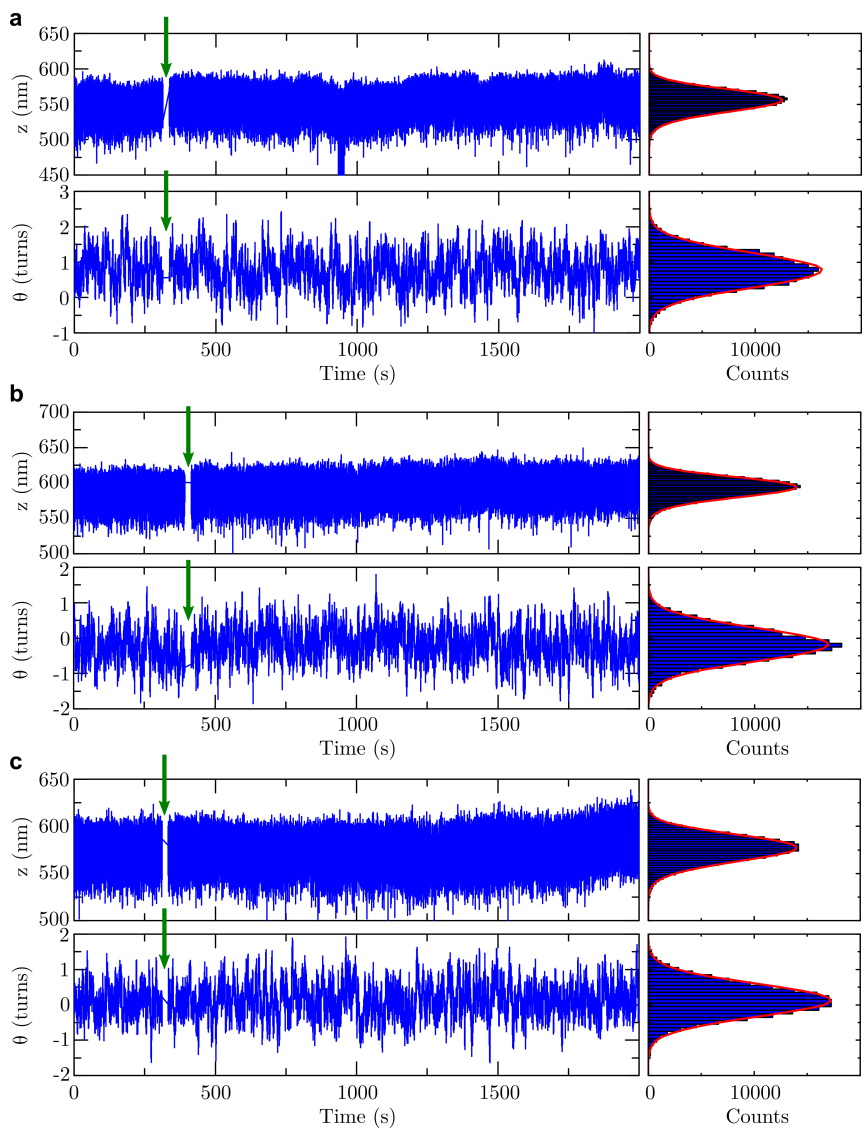


Figure 6.S10. Experiments with NAP1 only. **a** Time traces of the length z (in nm, panel above) and the linking number θ (in turns, panel below) of a DNA molecule before and after flushing in (*green arrows*) only NAP1 chaperones under the standard conditions of this study in buffer A (see Section 6.2 and Table 6.1). **b** Time traces of the length z (panel above) and the linking number θ (panel below) of a DNA molecule before and after flushing in (*green arrows*) only NAP1 chaperones under the standard conditions of this study in buffer B (see Section 6.2 and Table 6.1). **c** Time traces of the length z (panel above) and the linking number θ (panel below) of a DNA molecule before and after flushing in (*green arrows*) only NAP1 chaperones under the standard conditions of this study in buffer C (see Section 6.2 and Table 6.1). As the respective singly peaked mirrored gamma (due to the slight skew of the data to smaller values) and normal distributions (*red*) indicate, NAP1 proteins alone do not interact with the DNA molecule.

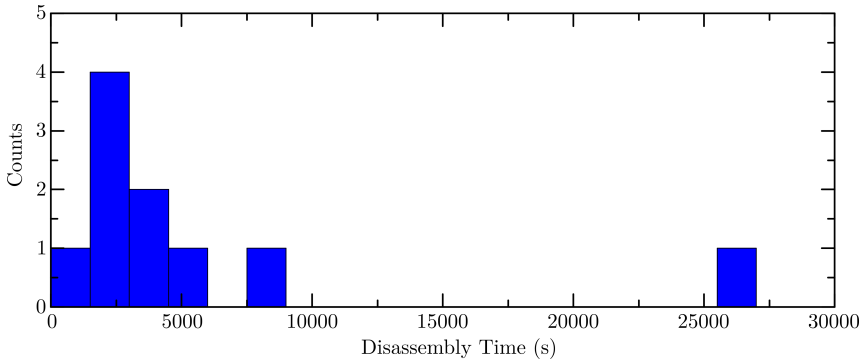


Figure 6.S11. Distribution of the disassembly times for 601-tetrasomes. In 40% ($n=8$) of all experiments ($N=20$), the single 601-tetrasomes were observed to disassemble in the course of the measurements at different times (Table 6.S4 and Figure 6.S5). The data yielded a mean value of $\tau_{disass} = 3364 \pm 765$ s (1 SEM due to broadness). The longest disassembly time at 26487 s was excluded from this calculation, as it is even longer than the mean duration $t_m = 22665 \pm 3141$ s (1 SEM) of the measurements. The dissociation times can be critical with regard to the study of the dynamics, but are much longer than the time scales of the relevant dynamics such as the dwell times investigated in this study (see Section 6.2 and Figure 6.3a,b, and Figures 6.S8 and 6.S9).

6.6 References

- [1] R. D. Kornberg. *Science* **184**, 868 (1974).
- [2] A. L. Olins and D. E. Olins. *Science* **183**, 330 (1974).
- [3] P. Oudet, M. Gross-Bellard, and P. Chambon. *Cell* **4**, 281 (1975).
- [4] T. J. Richmond, J. T. Finch, B. Rushton, D. Rhodes, and A. Klug. *Nature* **311**, 532 (1984).
- [5] K. Luger, A. W. Mäder, R. K. Richmond, D. F. Sargent, and T. J. Richmond. *Nature* **389**, 251 (1997).
- [6] C. A. Davey, D. F. Sargent, K. Luger, A. W. Mäder, and T. J. Richmond. *J. Mol. Biol.* **319**, 1097 (2002).
- [7] A. Klug, D. Rhodes, J. Smith, J. T. Finch, and J. O. Thomas. *Nature* **287**, 509 (1980).
- [8] G. Arents, R. W. Burlingame, B. C. Wang, W. E. Love, and E. N. Moudrianakis. *Proc. Natl. Acad. Sci. U.S.A.* **88**, 10148 (1991).
- [9] S. E. Polo and G. Almouzni. *Curr. Opin. Genet. Dev.* **16**, 104 (2006).
- [10] O. Ordu, A. Lusser, and N. H. Dekker. *Biophys. Rev.* **8**, 33 (2016).
- [11] G. Li, M. Levitus, C. Bustamante, and J. Widom. *Nat. Struct. Mol. Biol.* **12**, 46 (2005).
- [12] W. J. A. Koopmans, A. Brehm, C. Logie, T. Schmidt, and J. van Noort. *J. Fluoresc.* **17**, 785 (2007).
- [13] A. Miyagi, T. Ando, and Y. L. Lyubchenko. *Biochemistry* **50**, 7901 (2011).
- [14] S. Wei, S. J. Falk, B. E. Black, and T. H. Lee. *Nucleic Acids Res.* **43**, e111 (2015).
- [15] T. T. Ngo and T. Ha. *Nucleic Acids Res.* **43**, 3964 (2015).
- [16] G. D. Bowman and M. G. Poirier. *Chem. Rev.* **115**, 2274 (2015).
- [17] Z. A. Gurard-Levin, J. P. Quivy, and G. Almouzni. *Annu. Rev. Biochem.* **83**, 487 (2014).
- [18] C. R. Clapier and B. R. Cairns. *Annu. Rev. Biochem.* **78**, 273 (2009).

- [19] C. Lavelle, E. Praly, D. Bensimon, E. le Cam, and V. Croquette. *FEBS J.* **278**, 3596 (2011).
- [20] C. Lavelle. *Curr. Opin. Genet. Dev.* **25**, 74 (2014).
- [21] A. J. Andrews and K. Luger. *Annu. Rev. Biophys.* **40**, 99 (2011).
- [22] B. Sollner-Webb, R. D. Camerini-Otero, and G. Felsenfeld. *Cell* **9**, 179 (1976).
- [23] M. Bina-Stein and R. T. Simpson. *Cell* **11**, 609 (1977).
- [24] T. H. Eickbush and E. N. Moudrianakis. *Biochemistry* **17**, 4955 (1978).
- [25] F. Dong and K. E. van Holde. *Proc. Natl. Acad. Sci. U.S.A.* **88**, 10596 (1991).
- [26] S. Jackson, W. Brooks, and V. Jackson. *Biochemistry* **33**, 5392 (1994).
- [27] B. D. Brower-Toland, C. L. Smith, R. C. Yeh, J. T. Lis, C. L. Peterson, and M. D. Wang. *Proc. Natl. Acad. Sci. U.S.A.* **99**, 1960 (2002).
- [28] G. J. Gemmen, R. Sim, K. A. Haushalter, P. C. Ke, J. T. Kadonaga, and D. E. Smith. *J. Mol. Biol.* **351**, 89 (2005).
- [29] S. Mihardja, A. J. Spakowitz, Y. L. Zhang, and C. Bustamante. *Proc. Natl. Acad. Sci. U.S.A.* **103**, 15871 (2006).
- [30] M. A. Hall, A. Shundrovsky, L. Bai, R. M. Fulbright, J. T. Lis, and M. D. Wang. *Nat. Struct. Mol. Biol.* **16**, 124 (2009).
- [31] V. Böhm, A. R. Hieb, A. J. Andrews, A. Gansen, A. Rocker, K. Toth, K. Luger, and J. Langowski. *Nucleic Acids Res.* **39**, 3093 (2011).
- [32] R. Vlijm, J. S. J. Smitshuijzen, A. Lusser, and C. Dekker. *PLoS One* **7**, e46306 (2012).
- [33] A. J. Katan, R. Vlijm, A. Lusser, and C. Dekker. *Small* **11**, 976 (2015).
- [34] T. Elbel and J. Langowski. *J. Phys. Condens. Matter* **27**, 064105 (2015).
- [35] V. Jackson. *Biochemistry* **34**, 10607 (1995).

- [36] A. Hamiche, V. Carot, M. Alilat, F. De Lucia, M. F. O'Donohue, B. Revet, and A. Prunell. *Proc. Natl. Acad. Sci. U.S.A.* **93**, 7588 (1996).
- [37] A. Hamiche, and H. Richard-Foy. *J. Biol. Chem.* **273**, 9261 (1998).
- [38] M. Alilat, A. Sivolob, B. Revet, and A. Prunell. *J. Mol. Biol.* **291**, 815 (1999).
- [39] A. Sivolob and A. Prunell. *J. Mol. Biol.* **295**, 41 (2000).
- [40] A. Sivolob, F. De Lucia, M. Alilat, and A. Prunell. *J. Mol. Biol.* **295**, 55 (2000).
- [41] R. Vlijm, M. Lee, J. Lipfert, A. Lusser, C. Dekker, and N. H. Dekker. *Cell Rep.* **10**, 216 (2015).
- [42] R. Vlijm, M. Lee, O. Ordu, A. Boltengagen, A. Lusser, N. H. Dekker, and C. Dekker. *PLoS One* **10**, e0141267 (2015).
- [43] O. Ordu, L. Kremser, A. Lusser, and N.H. Dekker. *J. Chem Phys.* **148**, 123323 (2018).
- [44] J. Widom. *Q. Rev. Biophys.* **34**, 269 (2001).
- [45] E. N. Trifonov and R. Nibhani. *Biopolymers* **103**, 432 (2015).
- [46] P.T. Lowary and J. Widom. *J. Mol. Biol.* **276**, 19 (1998).
- [47] A. Shundrovsky, C. L. Smith, J. T. Lis, C. L. Peterson, and M. D. Wang. *Nat. Struct. Mol. Biol.* **13**, 549 (2006).
- [48] T. R. Blosser, J. G. Yang, M. D. Stone, G. J. Narlikar, and X. Zhuang. *Nature* **462**, 1022 (2009).
- [49] A. Gansen, A. Valeri, F. Hauger, S. Felekyan, S. Kalinin, K. Toth, J. Langowski, and C. A. Seidel. *Proc. Natl. Acad. Sci. U.S.A.* **106**, 15308 (2009).
- [50] M. Kruithof, F. T. Chien, A. Routh, C. Logie, D. Rhodes, and J. van Noort. *Nat. Struct. Mol. Biol.* **16**, 534 (2009).
- [51] C. Hodges, L. Bintu, L. Lubkowska, M. Kashlev, and C. Bustamante. *Science* **325**, 626 (2009).
- [52] J. Jin, L. Bai, D. S. Johnson, R. M. Fulbright, M. L. Kireeva, M. Kashlev, and M. D. Wang. *Nat. Struct. Mol. Biol.* **17**, 745 (2010).

- [53] L. Bintu, M. Kopaczynska, C. Hodges, L. Lubkowska, M. Kashlev, and C. Bustamante. *Nat. Struct. Mol. Biol.* **18**, 1394 (2011).
- [54] L. Bintu, T. Ishibashi, M. Dangkulwanich, Y. Y. Wu, L. Lubkowska, M. Kashlev, and C. Bustamante. *Cell* **151**, 738 (2012).
- [55] A. H. Mack, D. J. Schlingman, R. P. Ilagan, L. Regan, and S. G. J. Mochrie. *J. Mol. Biol.* **423**, 687 (2012).
- [56] J. A. North, J. C. Shimko, S. Javaid, A. M. Mooney, M.A. Shoffner, S. D. Rose, R. Bundschuh, R. Fishel, J. J. Ottesen, and M. G. Poirier. *Nucleic Acids Res.* **40**, 10215 (2012).
- [57] S. Deindl, W. L. Hwang, S. K. Hota, T. R. Blosser, P. Prasad, B. Bartholomew, and X. Zhuang. *Cell* **152**, 442 (2013).
- [58] M. Y. Sheinin, M. Li, M. Soltani, K. Luger, and M. D. Wang. *Nat. Commun.* **4**, 2579 (2013).
- [59] W. L. Hwang, S. Deindl, B. T. Harada, X. Zhuang. *Nature* **512**, 213 (2014).
- [60] T. Ishibashi, M. Dangkulwanich, Y. Coello, T. A. Lionberger, L. Lubkowska, A. S. Ponticelli, M. Kashlev, and C. Bustamante. *Proc. Natl. Acad. Sci. U.S.A.* **111**, 3419 (2014).
- [61] Y. Luo, J. A. North, S. D. Rose, M. G. Poirier. *Nucleic Acids Res.* **42**, 3017 (2014).
- [62] M. Brehove, T. Wang, J. North, Y. Luo, S. J. Dreher, J. C. Shimko, J. J. Ottesen, K. Luger, and M. G. Poirier. *J. Biol. Chem.* **290**, 22612 (2015).
- [63] T. T. Ngo, Q. Zhang, R. Zhou, J. G. Yodh, and T. Ha. *Cell* **160**, 1135 (2015).
- [64] B. Eslami-Mosallam, H. Schiessel, and J. van Noort. *Adv. Colloid Interface Sci.* **232**, 101 (2016).
- [65] J. Lipfert, M. Wiggin, J. W. J. Kerssemakers, F. Pedaci, and N. H. Dekker. *Nat. Commun.* **2**, 439 (2011).
- [66] H. Meng, K. Andresen, and J. van Noort. *Nucleic Acids Res.* **43**, 3578 (2015).

- [67] A. Kaczmarczyk, A. Allahverdi, T. B. Brouwer, L. Nordenskiöld, N. H. Dekker, and J. van Noort. *J. Biol. Chem.* **292**, 17506 (2017).
- [68] J. Zlatanova, C. Seebart, and M. Tomschik. *FASEB J.* **21**, 1294 (2007).
- [69] T. Fujii-Nakata, Y. Ishimi, A. Okuda, and A. Kikuchi. *J. Biol. Chem.* **267**, 20980 (1992).
- [70] T. Nakagawa, M. Bulger, M. Muramatsu, and T. Ito. *J. Biol. Chem.* **276**, 27384 (2001).
- [71] J. Mazurkiewicz, J. F. Kepert, and K. Rippe. *J. Biol. Chem.* **281**, 16462 (2006).
- [72] A. J. Andrews, X. Chen, A. Zevin, L. A. Stargell, and K. Luger. *Mol. Cell* **37**, 834 (2010).
- [73] J. W. J. Kerssemakers, E. L. Munteanu, L. Laan, T. L. Noetzel, M. E. Janson, and M. Dogterom. *Nature* **442**, 709 (2006).
- [74] J. Lipfert, G. M. Skinner, J. M. Keegstra, T. Hensgens, T. Jager, D. Dulin, M. Köber, Z. Yu, S. P. Donkers, F. C. Chou, R. Das, and N. H. Dekker. *Proc. Natl. Acad. Sci. U.S.A.* **111**, 15408 (2014).
- [75] R. Perales, L. Zhang, and D. Bentley. *Mol. Cell. Biol.* **31**, 3485 (2011).
- [76] V. V. Vasilevskaya, A. R. Khokhlov, Y. Matsuzawa, and K. Yoshikawa. *J. Chem. Phys.* **102**, 6595 (1995).
- [77] I. Koltover, K. Wagner, and C. R. Safinya. *Proc. Natl. Acad. Sci. U.S.A.* **97**, 14046 (2000).
- [78] X. Qui, K. Andresen, L. W. Kwok, J. S. Lamb, H. Y. Park, and L. Pollack. *Phys. Rev. Lett.* **99**, 038104 (2007).
- [79] M. de Frutos, E. Raspaud, A. Leforestier, and F. Livolant. *Biophys. J.* **81**, 1127 (2001).
- [80] F. Thoma, T. Koller, and A. Klug. *J. Cell Biol.* **83**, 403 (1979).
- [81] M. d’Erme, G. Yang, E. Sheagly, F. Palitti, and C. Bustamante. *Biochemistry* **40**, 10947 (2001).
- [82] V. A. T. Huynh, P. J. J. Robinson, and D. Rhodes. *J. Mol. Biol.* **345**, 957 (2005).

- [83] C. R. Clapier, S. Chakravarthy, C. Petosa, C. Fernandez-Tornero, K. Luger, and C. W. Muller. *Proteins* **71**, 1 (2008).

Summary

The entire blueprint of all living things is encoded in their genomes, which consist of DNA strands. The genome of a complex organism like ourselves can be several meters long. One of the miracles of nature is that such DNA molecules can be stored in the micron-sized nucleus of eukaryotic cells. For this purpose, the relatively large genome of eukaryotes has to be tightly packed while still remaining accessible for vital cellular processes such as replication, transcription, and repair. This is achieved by the organization of the eukaryotic genome into a hierarchical nucleoprotein assembly termed chromatin. Its fundamental unit is the nucleosome, which comprises a short piece of DNA wrapped around a disk-shaped core of eight histone proteins in a left-handed superhelix. As such, nucleosomes constitute the first level of DNA compaction and are assigned a key role in the regulation of the genome to maintain the proper functioning and viability of eukaryotic cells. Hence, detailed knowledge of this fascinating complex is crucial for understanding fundamental processes of life. This thesis deals with investigations of the structure and dynamics of a nucleosomal substructure called tetrasome at the single-molecule level.

About four decades of research have provided invaluable insights into the structure, function, and dynamics of nucleosomes. It is becoming increasingly clear that nucleosomes are not static, but instead dynamic, both intrinsically and extrinsically. As we review in the **Introduction** and **Chapter 3**, their dynamic features have been particularly revealed by the observation and manipulation of individual complexes at the molecular level in real time. In such single-molecule studies, nucleosomes have been found to transiently un- and rewrap at the DNA ends, or to temporarily open the wrapped DNA along the superhelical axis. In addition, nucleosomes are subject to the concerted interplay of numerous external mechanisms, such as remodeling, chemical modifications of the DNA and histones, or forces and torques exerted by genome-processing enzymes. All of these processes affect the structure, function, and dynamics of nucleosomes. In this context, nucleosomes have also been observed to organize into substructures lacking two or four histone proteins. One key subnucleosomal complex, the tetrasome, acts as an intermediate in nucleosome assembly and disassembly and has been the research topic of

this thesis.

Tetrasomes consist of a shorter stretch of DNA wrapped around a horseshoe-shaped core of four histone proteins. They have been observed to predominantly wrap the DNA in a left-handed superhelix, just like the full nucleosome, or in a right-handed manner. Recent single-molecule experiments have revealed that tetrasomes spontaneously switch between these two conformations, which suggests a potential mechanism for gene regulation at the subnucleosomal level. The availability of two tetrasome conformations with opposite DNA wrapping directions may buffer against the impact of forces and torques exerted by genome-processing enzymes without the complete disassembly of the histones. In this thesis, we have presented our research on the properties of these structural dynamics of tetrasomes using state-of-the-art magnetic tweezers experiments.

In **Chapter 2**, we describe various measurement principles of different magnetic tweezers configurations and the corresponding experimental procedures. Conventional magnetic tweezers use video-microscopy to track the positions of biomolecule-tethered beads from which the molecules' length and the applied force are deduced, while also allowing the application of torque. With novel magnetic tweezers techniques, such as the freely-orbiting magnetic tweezers or (electro-)magnetic torque tweezers, it is further possible to measure the twist or torque stored in the molecules.

In **Chapter 4**, we report our observation of similar structural dynamics for tetrasomes containing a transcription-related variant of one of the histone proteins. Remarkably, we found that the tetrasome conformations and dynamics change upon chemical modification of the histone core, as described in **Chapter 5**. Overall, such tetrasomes had a reduced tendency towards changing their handedness, while a small but non-negligible fraction even assembled into right-handed complexes. Single modified tetrasomes that still exhibited handedness dynamics were less stable in the left-handed state and more stable in the right-handed conformation by the same extent, indicating their altered conformational plasticity. Furthermore, our study presented in **Chapter 6** demonstrated that the conformational plasticity of tetrasomes depends on the underlying DNA sequence and ambient conditions. We observed that the handedness dynamics of tetrasomes assembled on a nucleosome-positioning sequence varies for different buffer conditions and in the presence or absence of a chaperone. Altogether, our results suggest that the structural dynamics of tetrasomes in terms of their handedness constitutes a potential intrinsic mechanism of chromatin for regulating the genome at the subnucleosomal level. This mechanism may further be tuned by modifications of the histone core, the underlying DNA sequence, and/or ambient conditions.

In a general context, our findings indicate that tetrasomes may be a key player in the structure and functioning of chromatin.

Overall, the research presented in this thesis provides new insights into chromatin organization, which promotes the exploration of a still obscure field of research on subnucleosomal structures and dynamics. Together with the observation of different substructures under various conditions in other studies, the intriguing results obtained here for tetrasomes demonstrate the highly complex nature of chromatin, involving components below the nucleosomal level. The continuous improvements of measurement techniques and assays promise increasing opportunities to study and characterize subnucleosomal structures both *in vitro* and *in vivo*. This will advance our understanding of this fundamental nucleoprotein complex and help us to combine different pieces of a big puzzle around the key question of how the genome is organized into a meaningful picture.

Samenvatting

De hele blauwdruk van alle levende wezens ligt opgeslagen in hun genomen, die uit DNA-strengen bestaan. Het genoom van een hoger ontwikkeld organisme zoals wij kan enkele meters lang zijn. Een van de wonderen van de natuur is dat zulke DNA-moleculen bewaard kunnen worden in de eukaryotische celkern van micrometer-afmeting. Hiervoor moet het relatief grote genoom dicht worden ingepakt, terwijl het nog steeds beschikbaar moet blijven voor essentiële cellulaire processen zoals replicatie, transcriptie en herstel. Dit wordt bereikt door de organisatie van het eukaryotische genoom in een hiërarchisch samenstel van verschillende eiwitten en DNA, dat chromatine wordt genoemd. De fundamentele bouwsteen van chromatine is het nucleosoom, dat een kort stuk van DNA omvat, dat als een linkshandige superhelix om een schijfvormige kern van acht histon-eiwitten is gewikkeld. Als zodanig vormen nucleosomen de eerste stap van de compacte DNA-structuur en spelen zij een sleutelrol bij de regulatie van het genoom om de goede werking en levensvatbaarheid van eukaryotische cellen te onderhouden. Daarom is gedetailleerde kennis van dit fascinerende samenstel doorslaggevend om fundamentele levensprocessen te kunnen begrijpen. Dit proefschrift behandelt onderzoeken over de structuur en dynamica van een substructuur van nucleosomen, die tetrasoom wordt genoemd, op het niveau van enkele moleculen.

Ongeveer vier decennia aan onderzoek hebben inzichten van onschatbare waarde in de structuur, functie en dynamica van nucleosomen opgeleverd. Het wordt in toenemende mate duidelijk dat nucleosomen niet statisch zijn, maar juist dynamisch, zowel op een intrinsieke als extrinsieke manier. Zoals uiteengezet in de **Inleiding** en **Hoofdstuk 3**, zijn hun dynamische kenmerken vooral door de observatie en manipulatie van individuele samenstellen op moleculair niveau in echte tijd ontdekt. In dergelijke onderzoeken van enkele moleculen is vermeld dat nucleosomen kortstondig aan hun einden opengaan of tijdelijk het gewikkelde DNA langs de as van de superhelix openen. Daarnaast zijn nucleosomen onderworpen aan het gecoördineerde samenspel van talrijke externe mechanismen zoals vervorming, chemische modificatie van het DNA en de histonen, of krachten en draaimomenten, die door enzymen op het genoom worden uitgeoefend. Al deze processen beïnvloeden de structuur, functie en dynamica van

nucleosomen. In dit verband is het ook gebleken dat nucleosomen zich in substructuren kunnen organiseren, waarin twee of vier histonen ontbreken. Een belangrijke substructuur van het nucleosoom, het tetrasoom, doet zich voor als een tussenstructuur van de vorming en afbreking van nucleosomen en is het onderwerp van onderzoek in dit proefschrift geweest.

Tetrasomen bestaan uit een korter stuk DNA, dat om een hoefijzervormige kern van vier histonen is gewikkeld. Het is gebleken dat tetrasomen het DNA voornamelijk in een linkshandige superhelix wikkelen, zoals het hele nucleosoom, of op een rechtshandige manier. Recente onderzoeken van enkele moleculen hebben onthuld dat tetrasomen spontaan tussen deze twee structuren wisselen, wat op een mogelijk mechanisme voor genregulatie op het niveau onder het nucleosoom wijst. De beschikbaarheid van twee structuren met de wikkeling van het DNA in tegengestelde richtingen zou tegen de invloeden van uitgeoefende krachten en draaimomenten door enzymen, die op het genoom werken, beschermen zonder de volledige afbreking van de histonen. In dit proefschrift is ons onderzoek over de kenmerken van deze structurele dynamica van tetrasomen met gebruik van de modernste experimenten met magnetische pincetten gepresenteerd.

In **Hoofdstuk 2** zijn diverse metingsprincipes van verschillende configuraties van magnetische pincetten en de bijbehorende experimentele procedures beschreven. De traditionele magnetische pincetten gebruiken video-microscopie om de posities van aan een biomolecuul vastgebonden kralen te volgen, waaruit de lengte van de moleculen en de uitgeoefende kracht bepaald kunnen worden, hoewel ook de uitoefening van draaimomenten mogelijk is. Met nieuwere methoden van magnetische pincetten zoals de freely-orbiting magnetic tweezers of de (electro-)magnetic torque tweezers is het mogelijk om ook de in de moleculen bewaarde draai of het draaimoment te meten.

In **Hoofdstuk 4** zijn onze vaststellingen van de vergelijkbare structurele dynamica van tetrasomen gemeld, die een met transcriptie verbonden variant van een van de histonen bevatten. Opmerkelijk veranderden de structuren en dynamica van tetrasomen na een chemische modificatie van de histon-kern, zoals beschreven in **Hoofdstuk 5**. Algemeen hadden zulke tetrasomen een verminderde neiging om de handigheid te wisselen, terwijl een kleine maar niet te verwaarlozen fractie zelfs de rechtshandige structuur vormden. Individuele gemodificeerde tetrasomen, die de dynamica in hun handigheid vertoonden, waren minder stabiel in de linkshandige structuur en in dezelfde mate meer stabiel in de rechtshandige structuur, wat een veranderde vervormbaarheid aanduidt. Verder demonstreerde ons in **Hoofdstuk 6** voorgestelde onderzoek dat de vervormbaarheid van tetrasomen afhankelijk is van de onderliggende DNA-sequentie en

de omgevingsfactoren. De dynamica in de handigheid van tetrasomen, die door een specifieke sequentie voor de positionering van nucleosomen zijn gevormd, varieerde voor verschillende buffercondities en de aan- of afwezigheid van een chaperon. In totaal wijzen onze bevindingen erop dat de structurele dynamica van tetrasomen wat hun handigheid betreft een mogelijk intrinsiek mechanisme van chromatine is voor de regulatie van het genoom op het niveau onder het nucleosoom. Dit mechanisme kan worden aangepast door de modificaties van de histon-kern, de onderliggende DNA-sequentie en/of de omgevingsfactoren. In een algemene context duiden onze inzichten erop dat tetrasomen een belangrijke speler voor de structuur en werking van chromatine zijn.

Samenvattend geeft het in dit proefschrift voorgestelde onderzoek nieuwe inzichten in de organisatie van chromatine, wat de verkenning van een nog steeds obscuur gebied van onderzoek over substructuren van nucleosomen en hun dynamica stimuleerd. Samen met de observatie van verschillende substructuren onder diverse condities in andere onderzoeken, openbaren de hier verkregen resultaten de hoogst ingewikkelde natuur van chromatine, die onderdelen van nucleosomen bevat. De voortdurende verbeteringen van metingsmethoden beloven betere mogelijkheden om substructuren van nucleosomen zowel *in vivo* als *in vitro* te onderzoeken en te karakteriseren. Dit gaat ons begrip van dit fundamentele samenstel uit DNA en eiwitten bevorderen, en ons helpen om verschillende delen van een puzzel over de sleutelvraag hoe het genoom is georganiseerd in een duidelijk beeld samen te voegen.

Acknowledgments

Physicists are usually seen as generalists with outstanding problem-solving skills and a very high frustration tolerance. During my PhD studies, I got to understand much better where this comes from. It was a long, tough, but also a very interesting and joyful time. I have grown a lot in a professional context and, more importantly, as a person thanks to many people who have been an essential part of this journey in many different ways and to whom I would like to express my gratitude.

First of all, I would like to thank my supervisor Nynke Dekker for taking me on as a PhD student in her lab. I have learned a lot both professionally and personally from working with you and feel very well prepared for the future. This is extendable to the whole Nynke Dekker Lab and the Department of Bionanoscience: thank you all for a stimulating environment and an instructive time with a lot of insightful and interesting discussions, nice conversations, and good experiences – both at work and outside work! I want to say special thanks to our secretaries, especially Dijana, Emmylou, and Jolijn, for all their help with administrative issues! Likewise, I would like to thank Belen for all her support with lab-related administration, proofreading manuscripts, as well as scientific and personal discussions – you are a big enrichment for the lab!

I am very grateful to Mina who introduced me to the lab work at the very beginning. She taught me how to make flow cells, prepare samples, and use magnetic tweezers, and much more. Since we had a similar attitude and way of working, the knowledge transfer went fast and smooth so that I could then quickly start working on another joined project about nucleosome assembly and dynamics with the Cees Dekker Lab and the Alexandra Lusser Lab. In this context, I would also like to thank Rifka who introduced me to the handling of the histone proteins and data analysis, and to Cees and Alexandra for insightful discussions. When both Mina and Rifka moved on to take the next steps in their careers, I had a great foundation to continue exploring the structure and dynamics of tetrasomes. This would not have been possible without the various DNA constructs that Theo prepared based on his great knowledge of biochemistry and experience with biochemical methods, which he was always happy to share – many thanks to you, also for proofreading the Dutch translation of my summary!

Acknowledgments

At this point, I would also like to acknowledge Anastasiya Boltengagen and Alexandra Wille from the Alexandra Lusser Lab for preparing the histone proteins, and Leopold Kremser for characterizing the chemically modified histones using mass spectrometry.

Regarding the magnetic tweezers hardware, software and data analysis, I had very helpful discussions with Richard, Mariana, Zhongbo, Jan, David, Maarten, Jelmer, Jordi, Margreet, and Jacob, which I highly appreciated. In particular, I want to thank Jacob for providing me with the improved version of his step-fitting algorithm. Also, the help of Jelle and Dimitri was essential for building, customizing and maintaining setups and parts – thank you so much for your always immediate availability, your work, and for your time, which we also spent in nice conversations! Furthermore, I had several insightful discussions with Kaley and Sam on biophysical issues – thanks to both of you, also for reviewing my English summary! In general, I had a nice time with all lab members both at work and outside work – many thanks to my so far mentioned colleagues, as well as to Artur, Filip, Louis, Sumit, Seungkyu, Josko, Fatemeh, Humberto, Florian, Sriram, Ayşen, Charl, Roy, Peter, Eugen, Yera, Ilyong, Bojk, and Laura for the fruitful discussions and nice conversations about work and life, as well as the fun we had together! Richard and Mariana quickly became a lot more than just colleagues – I am deeply grateful to both of you for your close friendship, continuous support and encouragement; I would have not made it without having you around during and outside work, which was always a lot of fun! The same holds for Artur who soon became a very good friend as well, then a regular office mate, and in the end also one of my paranymphs – thank you so much for everything and best of luck with writing your thesis!

Speaking about office mates, I want to thank Bojk and Sriram for a warm welcome at the very beginning and a nice atmosphere with discussions about science, research, and life. Sriram, I want to thank you for being a good friend and for showing me the benefits of staying calm in stressful situations! At those times, we had the luxury of having additional space with a free desk which Laura could temporarily use during her internship with magnetic tweezers under my supervision – thank you very much for your great work which sped things up during the setup upgrade! Later on, Ayşen joined the office and we quickly became friends, not only due to our common Turkish background, but mainly because of the way she is – thank you so much for readily sharing your scientific knowledge and expertise, as well as your personal experiences and thoughts about everything! Our continuous exchange might have been a bit overwhelming for Florian who joined us later, with his counterbalancing quite nature but also interesting

perspectives that he added to our discussions and conversations at the right moments – I wish you all the best with your PhD studies! After the move to the new building, I had the nice experience of sharing the new office with two people from another lab before the rearrangement into lab-specific groups again, when Louis and Sumit took the chairs of Thijs and Luuk, which also involved the temporary visits of Filip and Seungkyu – many thanks to all of you for all the fun moments with interesting discussions and nice conversations about work and life, also including some tabletop soccer once in a while!

Together with Thijs and Luuk, I would also like to thank several other people from other labs for a great time with both work-related and personal discussions, nice conversations at the coffee tables or during lunch, and all the fun at work and outside work: Malwina, Mohamed, Viktorija, Laura, Jetty, Mathia, Stanley, Pawel, Alicia, Pauline, Natalia, Louis, Esengül, Eve, Vanessa, Dominik, Victor, Behrouz, Marek, and Michela who receives my special thanks for also having been an essential part of my wedding day as one of the witnesses! From the Department of Quantum Nanoscience, I likewise want to thank Olya for her friendship – it was an honor to be one of the witnesses on your wedding day!

I also got to know many other people outside TU Delft, with whom I had great exchange about work and personal matters. This involves many people from the Biological and Soft Matter Physics group at Leiden University: Sara, Kirsten, Thomas, Redmar, Klaas, Wim, Maria, Nelli, Olga, Patrick, Noémie, Babette, Wietske, Hedde, Stefano, Lena, Emrah and Veer – thank you all so much for the great and fun times we spent together! The same holds for many people from the Lorentz Institute: Marco, Sasha, Cameron, Vincenzo, Aurelio, and especially the whole Carlo Beenakker group. As the most awesome theoretical physics group I have ever met, Michal, Mark, Nicandro, Nikolay, Slava, Tom, Yaroslav, Xavi, Lizzy, Jimmy, Brian, Bernard, Denis, Cosma, and Timo quickly became good friends – many thanks to all of you for everything and special thanks to Brian and Denis for having been witnesses on my wedding day! Gamze and Konstantin from the Institute of Chemistry, I got to know at a later stage but we have collected a lot of memories by now – thank you so much for the great times we spent together! I have further met and worked with several great people in the Casimir PhD platform: Marije, Vincent, Jelmer, Bob, Mickael, Lena, Sara, Julia, Kirsten, Floris, Koen, Nicole, and Gesa – many thanks to all of you for the nice and creative environment with fruitful discussions that yielded great ideas for improving the professional and personal development of our peers. In particular, Gesa became a very good friend over time and finally also my other paranymp – thank

Acknowledgments

you so much for openly sharing your experiences and thoughts in all the interesting and deep discussions about work and life, as well as the fun times we spent together, especially at soccer!

Soccer has always played a key role in my life and I am very glad that I got the opportunity to join different groups during this period as well: many thanks to all players of Real RKC/Kavli Warriors, FC Tutor, and Ariston'80 in Delft, and LA FC, Wonders of the World, Sunday International, and the Friday soccer group in Leiden for the fun matches and nice chats!

Furthermore, I feel very glad to have lived in a really nice neighborhood with great neighbors. I have had great conversations about life, sports, and work with Aldjia and Andrew – many thanks for sharing your experiences and thoughts about everything! Alpita and Paul have also been interested in the details of my work – my special thanks to both of you, also for proofreading the Dutch translation of my summary!

I am deeply grateful to Carmen and Beate, my long-term close friends from high school times with whom I share endless memories and who I can always count on – thank you so much for being there for me over all these years! Likewise, I am very thankful to my close friends from my studies in Karlsruhe, Ewa, Max, Caro, and Tobi – many thanks for your continuous friendship, support and encouragement during this long journey, and special thanks to you, Ewa, for making my wedding day so special as a witness!

My deepest gratitude I want to express to my whole family, especially to my parents, my brother, my by now husband Paul, and my parents-in-law – I would have never made it without your endless love, trust, confidence, support, and encouragement! Everything I have achieved is thanks to the opportunities and freedom you trustfully gave me for doing what I wanted to do and how I wanted to do it!

Overall, I am looking back on an unforgettable period of my life, which shaped me both professionally and especially as a person with many interesting and instructive encounters, new friendships, and precious memories!

Orkide ORDU,
Leiden, August 2018

Curriculum Vitae

Orkide ORDU

- 5 June 1987 Born in Heilbronn-Neckargartach, Germany
- 1997 - 2006 Secondary school education at the Justinus-Kerner-Gymnasium Weinsberg, Germany
General qualification for university entrance (Abitur)
- 2006 - 2012 Studies of physics (Diplomstudiengang) at the Karlsruhe Institute of Technology (KIT), Germany
Degree: Diplom-Physikerin
Thesis: Characterization of Protein Adsorption onto Iron-Platinum Nanoparticles by Two-Focus Fluorescence Spectroscopy and Atomic Force Microscopy
Supervisor: Prof. Dr. G. Ulrich Nienhaus
- 2009 - 2010 Academic year within the Erasmus program at the Royal Institute of Technology (KTH) in Stockholm, Sweden
- 2013 - 2018 PhD research at the Department of Bionanoscience, Delft University of Technology (TUD), The Netherlands
Thesis: Dissecting the Nucleosome: Single-Molecule Studies of Subnucleosomal Structure and Dynamics
Promotor: Prof. Dr. Nynke H. Dekker

List of Publications

- **O. Ordu**, A. Lusser, and N.H. Dekker. *Structural Dynamics of Tetrasomes Depend on Underlying DNA Sequence and Ambient Conditions*. manuscript in preparation [Chapter 6]
- **O. Ordu**, L. Kremser, A. Lusser, and N.H. Dekker. *Modification of the Histone Tetramer at the H3-H3 Interface Impacts Tetrasome Conformations and Dynamics*. J. Chem. Phys. **148**, 123323 (2018). [Chapter 5]
- **O. Ordu**, A. Lusser, and N.H. Dekker. *Recent Insights from In Vitro Single-Molecule Studies into Nucleosome Structure and Dynamics*. Biophys. Rev. **8**, 33 (2016). [Chapters 1 and 3]
- R. Vlijm, M. Lee, **O. Ordu**, A. Boltengagen, A. Lusser, N.H. Dekker, and C. Dekker. *Comparing the Assembly and Handedness Dynamics of (H3.3-H4)₂ Tetrasomes to Canonical Tetrasomes*. PLoS One **10**, e0141267 (2015). [Chapter 4]
- Z. Yu, D. Dulin, J. Cnossen, M. Köber, M.M. van Oene, **O. Ordu**, B.A. Berghuis, T. Hensgens, J. Lipfert, and N.H. Dekker. *A Force Calibration Standard for Magnetic Tweezers*. Rev. Sci. Instrum. **85**, 123114 (2014).
- J. Lipfert, M. Lee, **O. Ordu**, J.W.J. Kerssemakers, and N.H. Dekker. *Magnetic Tweezers for the Measurement of Twist and Torque*. J. Vis. Exp. **87**, e51503 (2014). [Chapter 2]

